



# UDP-glucose pyrophosphorylase (UGP) : import dans les glycosomes et implication dans la biosynthèse glycosomale et cytosolique des sucres nucléotidiques chez *Trypanosoma brucei*

Oriana Villafraz

## ► To cite this version:

Oriana Villafraz. UDP-glucose pyrophosphorylase (UGP) : import dans les glycosomes et implication dans la biosynthèse glycosomale et cytosolique des sucres nucléotidiques chez *Trypanosoma brucei*. Microbiologie et Parasitologie. Université de Bordeaux, 2020. Français. NNT : 2020BORD0215 . tel-03118553

**HAL Id: tel-03118553**

**<https://theses.hal.science/tel-03118553>**

Submitted on 22 Jan 2021

**HAL** is a multi-disciplinary open access archive for the deposit and dissemination of scientific research documents, whether they are published or not. The documents may come from teaching and research institutions in France or abroad, or from public or private research centers.

L'archive ouverte pluridisciplinaire **HAL**, est destinée au dépôt et à la diffusion de documents scientifiques de niveau recherche, publiés ou non, émanant des établissements d'enseignement et de recherche français ou étrangers, des laboratoires publics ou privés.

Thèse présentée pour obtenir le grade de

DOCTEUR  
DE L'UNIVERSITÉ DE BORDEAUX

École Doctorale Sciences de la Vie et de la Santé  
Microbiologie - Immunologie

Par **Oriana Villafranz**

**UDP-glucose pyrophosphorylase (UGP) : import  
dans les glycosomes et implication dans la  
biosynthèse glycosomale et cytosolique des sucres  
nucléotidiques chez *Trypanosoma brucei***

Sous la direction de : Frédéric Bringaud

**Membres du jury:**

Président: Dr. Sébastien Mongrand

Rapporteur: Pr. Wolfgang Schliebs

Rapporteur: Pr. Mick Urbaniak

Examineur: Pr. Paul Michels

Directeur de thèse: Dr. Frédéric Bringaud

Soutenue le 4 décembre 2020

## Résumé

*Trypanosoma brucei*, un protiste responsable de la Trypanosomose Humaine Africaine, également connue sous le nom de la maladie du sommeil, est transmis par la mouche tsé-tsé (*Glossina* sp.). La découverte d'organites de type peroxysome spécialisés dans la glycolyse, appelés glycosomes, a soulevé un certain nombre de questions sur le rôle de cet organite dans la biologie des trypanosomes. Plusieurs voies métaboliques présentes dans le cytosol d'autres eucaryotes, comme la glycolyse et la biosynthèse des sucres nucléotidiques, sont compartimentées dans les glycosomes. Les raisons et les avantages de la présence des enzymes glycolytiques dans l'organite ont été largement discutés, mais la fonctionnalité et le rôle des voies de biosynthèse des sucres nucléotidiques glycosomales ne sont pas connus. Notre étude s'est focalisée sur l'UDP-glucose pyrophosphorylase (UGP), une enzyme impliquée dans la synthèse de l'UDP-glucose (UDP-Glc). Sur la base de la double localisation glycosomale et cytosolique de l'UGP mise en évidence ici à l'aide de plusieurs techniques de localisation subcellulaire, nous avons abordé deux questions en utilisant comme modèle les formes procycliques de *T. brucei* présentes dans l'insecte vecteur. La première est liée au mécanisme d'import de l'UGP dans les glycosomes, car cette protéine ne possède aucun signal d'adressage aux peroxysomes de type PTS1 ou PTS2. Nous avons montré que l'UGP est importée dans les glycosomes par "piggybacking" en s'associant à la phosphoénolpyruvate décarboxylase (PEPCK) possédant un signal d'adressage PTS1. Les interactions entre l'UGP et la PEPCK ont été montrées *in situ* et l'identification des régions impliquées dans ces interactions ont été identifiées. Nos résultats suggèrent que le complexe UGP-PEPCK est formé de manière transitoire lors de son import dans les glycosomes nouvellement produits et compétents pour l'import des protéines. La seconde question concerne le rôle de l'UGP dans les glycosomes. Nous avons montré que l'UGP est essentielle à la croissance des trypanosomes et que les voies métaboliques glycosomales et cytosoliques dont l'UGP fait partie sont fonctionnelles. En effet, des mutants viables contenant l'UGP exclusivement dans les glycosomes ou dans le cytosol sont viables et produisent des quantités similaires d'UDP-Glc. La raison d'être de la production glycosomale d'UDP-Glc par l'UGP reste inconnue, mais elle n'est probablement pas liée aux réactions de glycosylation, étant donné qu'aucune glycosyltransférase n'a été détectée dans l'organite.

Un autre aspect de ce travail concerne le rôle des intermédiaires du cycle de l'acide tricarboxylique (TCA) dans le métabolisme mitochondrial des formes procycliques. Dans le tractus digestif de son insecte vecteur, les trypanosomes dépendent de la proline pour alimenter leur métabolisme énergétique. Cependant, la disponibilité d'éventuelles autres sources de carbone pouvant être utilisées par le parasite est actuellement inconnue. Nous avons montré que les intermédiaires du cycle TCA, *i.e.* succinate, malate et  $\alpha$ -cétoglutarate, stimulent la croissance des formes procycliques incubées dans un milieu contenant 2 mM de proline, concentration se situant dans la gamme des quantités mesurées dans l'intestin de la mouche. De plus, le développement de nouvelles approches ont permis d'étudier une branche peu explorée du cycle TCA convertissant le malate en  $\alpha$ -cétoglutarate, précédemment décrite comme peu ou pas utilisée par le parasite, quelles que soient les quantités de glucose disponibles. L'activité de cette branche suggère qu'un cycle TCA complet peut être mis en œuvre dans les formes procycliques et probablement dans les autres formes parasitaires de l'insecte. Nos données élargissent le potentiel métabolique des trypanosomes et ouvrent la voie vers une meilleure compréhension du métabolisme de ce parasite dans divers organes de la mouche tsé-tsé, où il évolue.

**Mot clés :** *Trypanosoma brucei*; formes procycliques; glycosome; "piggybacking"; UDP-glucose; mitochondrie; cycle TCA; métabolisme du glucose et de la proline



## Abstract

*Trypanosoma brucei*, a protist responsible for human African trypanosomiasis, also known as sleeping sickness, is transmitted by the tsetse fly (*Glossina* sp.). The discovery of peroxisome-related organelles specialised in glycolysis called glycosomes, has raised a number of questions about the role of this organelle in the biology of trypanosomes. Several metabolic pathways present in the cytosol of eukaryotes, like glycolysis and sugar nucleotides biosynthesis, are compartmentalised within glycosomes. While the reasons and advantages of having glycolytic enzymes compartmentalised in the organelle have been extensively discussed, little is proposed for sugar nucleotides biosynthetic pathways. This study is focused on the UDP-glucose pyrophosphorylase (UGP), an enzyme involved in the synthesis of UDP-glucose (UDP-Glc). Based on the UGP's dual glycosomal and cytosolic localisation evidenced here by using several subcellular localisation techniques, we addressed two questions using as a model the procyclic form of *T. brucei* present in the insect vector. The first question is related to the mechanism of UGP import into glycosomes, since this protein lacks any known peroxisomal targeting signal (PTS1 and PTS2). We demonstrated that UGP is imported into the organelle by piggybacking on the glycosomal PTS1-containing phosphoenolpyruvate carboxykinase (PEPCK). Interactions between UGP and PEPCK were shown *in situ* and the interacting regions were identified. Our data suggest that the complex UGP-PEPCK is formed transiently to facilitate the import of UGP and that it is detected in newly formed import-competent glycosomes. The second question concerns the role of UGP in glycosomes. We demonstrated that UGP is essential for the growth of trypanosomes and that mutants containing UGP exclusively in the glycosomes or in the cytosol still produce UDP-Glc at similar levels and are viable, which implies that the glycosomal and cytosolic metabolic pathways involving UGP are functional. The glycosomal function of UDP-Glc is currently unknown and probably not related to glycosylation reactions since no glycosyltransferases have been detected in the organelle.

Another aspect of this work concerns the role of tricarboxylic acid (TCA) cycle intermediates in the mitochondrial metabolism of the procyclic trypanosomes. In the midgut of its insect vector, trypanosomes rely on proline to feed their energy metabolism. However, the availability of other potential carbon sources that can be used by the parasite is currently unknown.

We showed that TCA cycle intermediates, *i.e.* succinate, malate and  $\alpha$ -ketoglutarate, stimulate growth of procyclic trypanosomes incubated in medium containing 2 mM proline, which is in the range of the amounts measured in the midgut of the fly. In addition, we have implemented new approaches to study cell growth and metabolic pathways in order to investigate mitochondrial metabolism. These new tools have allowed us to study a poorly explored branch of the TCA cycle converting malate to  $\alpha$ -ketoglutarate, which was previously described as non-functional or little used in the parasite, regardless of the glucose levels available. The discovery of this branch reveals that a full TCA cycle can operate in procyclic trypanosomes and probably in the other trypanosome forms present in the fly. Our data broaden the metabolic potential of trypanosomes and pave the way for a better understanding of the parasite's metabolism in various organ systems of the tsetse fly, where it evolves.

**Keywords:** *Trypanosoma brucei*; procyclic forms; glycosome; piggybacking; UDP-glucose; mitochondria; TCA cycle; glucose and proline metabolism

---

**Laboratoire de Microbiologie Fondamentale et Pathogénicité - UMR5234**

146, Rue Leo Saignat, 33076 Bordeaux Cedex (France)

## Acknowledgements

I would like to express my sincere gratitude to Dr. Frédéric Bringaud for letting me be part of this incredible Laboratory, for his kind supervision, consistent support and guidance during my PhD. It has been a great honour to work with you and to learn from you.

I am also grateful to the LabEx ParaFrap PhD Program for its financial support and for organising remarkable workshops that let me grow both professionally and personally. A special thanks to the members of my thesis committee Dr. Sébastien Mongrand, Pr. Wolfgang Schliebs, Pr. Mick Urbaniak and Pr. Paul Michels for reviewing my thesis and participating in my defence.

I acknowledge all members of the iMET Team for their constant support and encouragement. I feel I have all the more reason to extend my thanks to Erika, Sarah and Simone, for their invaluable advice, for being always there and making me feel home. A very special thanks to Nico, Corinne and Magali for their contribution to this thesis project, for being always kind and willing to help me. To Stefan for training me at the very beginning of this journey. Thanks also to Manu, Loïc, Chloé, Magamba, Yoann and Pauline for their support and helpful discussions during the Lab meetings. To Rodolpho for giving me a helping hand during his stay in Bordeaux. Thank you to all members of the MFP, UMR 5234 for their assistance and support, specially to Dr. Mélanie Bonhivers, Nicolas Landrein and Doranda who have usefully contributed to my work.

I extend my gratitude to all the people who collaborated on this project. To Marc Biran, for his invaluable contribution with analyses of NMR spectra, to Jean-William Dupuy, Hanna Kulyk, Dr. Edern Cahoreau, Dr. Jean-Charles Portais, Dr. Michael Boshart, Dr. Ariel Silber, Dr. Alena Zíková, Dr. Michael Barrett, Dr. Daniel Inaoka and the members of the GlycoNov network for their constructive discussions.

Finally, many thanks to my family and all my friends for their continuous encouragement and love.

## CONTENTS

Résumé.....	ii
Abstract.....	iv
Acknowledgements .....	vi
<b>1. INTRODUCTION.....</b>	<b>2</b>
1.1 Trypanosomes .....	2
1.2. Human African Trypanosomiasis (HAT).....	6
1.2.1. Diagnosis, Prevention and Treatment.....	6
1.2.2. Challenges for HAT elimination .....	8
a) Drug resistance .....	8
b) Human and animal reservoirs .....	10
1.3. Animal African Trypanosomiasis (AAT).....	12
1.4. <i>Trypanosoma brucei</i> : a remarkable biological model.....	14
1.4.1. Life cycle and transmission.....	14
1.4.2. Cell architecture.....	18
1.4.4. Gene expression and regulation .....	18
1.4.5. Cell surface.....	22
a) VSG.....	22
b) Procyclins.....	24
c) Other surface glycoproteins.....	26
d) GPI anchors .....	26
1.5. Intermediate and energy metabolism.....	28
1.5.1. Bloodstream vs procyclic, an overview .....	30
1.5.2. Energy metabolism of PCF.....	31
a) Glucose metabolism.....	31
b) Glycerol metabolism.....	39
c) Proline metabolism and TCA cycle.....	39
d) Metabolism of other amino acids.....	44
e) Respiratory chain and mitochondrial ATP production.....	44
1.5.3. Energy metabolism of BSF .....	46
a) Glucose metabolism.....	50
b) Mitochondrial metabolism and ATP production .....	51
1.6. Glycosomes .....	57
1.6.1. Morphology and composition .....	57
1.6.1. Origin and evolution.....	59
1.6.2. Biogenesis and dynamics .....	59
1.7. Piggybacking.....	67
1.8. Glycobiology .....	73
1.8.1. Sugar nucleotide biosynthesis .....	73
1.8.2. UDP-glucose pyrophosphorylases.....	79
1.9. Aims.....	82

<b>2. RESULTS PART I: Glycosomal import of UDP-glucose pyrophosphorylase and its functionality in glycosomal and cytosolic UDP-glucose producing pathways.....</b>	<b>83</b>
2.1. Abstract.....	86
2.2. Introduction .....	87
2.3. Results.....	91
a) UDP-glucose pyrophosphorylase (UGP) has a dual glycosomal and cytosolic localisation .....	91
b) PEPCK-dependent import of UGP into glycosomes.....	93
c) Production and analysis of UGP-MYC and TY-PEPCK tagged cell lines ...	95
d) UGP interacts with PEPCK in some glycosomes .....	99
e) Determination of critical parts for PEPCK-UGP interaction .....	101
f) The UGP protein is essential for <i>T. brucei</i> .....	107
g) Targeting a recombinant UGP exclusively to the glycosomes.....	109
h) Expression of the glycosomal rUGP-GPDH rescues the lethality of the <i>RNAi</i> UGP mutant .....	111
i) The $\Delta ugp/^{EXP}$ rUGP-GPDH cell line is viable.....	113
j) The glycosomal and cytosol UGP-containing pathways are functional.....	115
2.4. Supplementary results .....	121
2.5. Discussion .....	123
<b>3. RESULTS PART II. Analysis of TCA intermediates and metabolites excreted from glucose metabolism as alternative carbon sources .....</b>	<b>130</b>
3.1. Abstract.....	132
3.2. Introduction .....	133
3.3. Results.....	139
a) Procyclic trypanosomes can re-metabolise end products excreted from glucose degradation .....	139
b) Succinate, pyruvate and alanine are metabolised in the presence of glucose or proline .....	141
c) TCA cycle intermediates stimulate growth of the PCF in <i>in vivo</i> -like conditions .....	145
d) The TCA cycle is used to metabolise malate in procyclic trypanosomes .	149
e) Metabolism of $\alpha$ -ketoglutarate in the presence of proline.....	151
f) $\alpha$ -Ketoglutarate rescued the growth defect of the <i>RNAi</i> PROD <i>H</i> .i and <i>RNAi</i> AAT.i mutants.....	155
g) $\alpha$ -Ketoglutarate is toxic if not metabolised at a high rate.....	157
3.4. Supplementary results .....	163
3.5. Discussion .....	166
<b>4. GENERAL DISCUSSION AND PERSPECTIVES .....</b>	<b>171</b>
4.1. Overview Part I: UDP-glucose pyrophosphorylase (UGP) .....	171
4.2. <i>T. brucei</i> UGP features .....	171
4.3. Functions of UDP-glucose .....	173

4.4. The UGP-PEPCK interaction, a new way to study import of glycosomal proteins .....	175
4.5. Is piggybacking a rule or an exception? .....	176
4.6. Overview Part II: Alternative carbon sources for PCF .....	177
4.7. PCF trypanosomes metabolise carbon sources other than glucose and proline .....	177
4.8. Unravelling new mitochondrial capabilities.....	178
4.9. Role of metabolites in trypanosomes differentiation.....	178
<b>5. MATERIALS AND METHODS.....</b>	<b>180</b>
5.1. Materials .....	180
5.1.1. Trypanosomes .....	180
5.1.2. Plasmids and bacteria .....	180
5.2. Methods .....	182
5.2.1. Molecular biology .....	182
a) Cloning and sequencing .....	182
b) DNA purification .....	184
- Plasmid DNA .....	184
- Genomic DNA.....	184
5.2.2. Cell biology .....	184
a) Growth of <i>T. brucei</i> : curves and alamar blue assays .....	184
b) Transfection .....	186
c) Inhibition of gene expression by RNA interference (RNAi) .....	188
d) Production of null mutants.....	190
e) Expression of tagged proteins.....	190
- Endogenous tagging.....	190
- Over-expression .....	192
- Glycosomal recombinant UGP proteins.....	194
5.2.3. Biochemistry .....	194
a) Differential centrifugation.....	194
b) Digitonin permeabilization .....	196
c) Cell fractionation by hypotonic lysis.....	196
e) Blue-native PAGE (BN-PAGE) .....	196
f) SDS-PAGE and Western Blots .....	198
g) Enzymatic activity assays.....	198
5.2.4. Imaging .....	200
a) Immunofluorescence Microscopy .....	200
b) Proximity Ligation Assay (PLA) .....	200
5.2.5. Proteomics and metabolomics.....	201
a) Label-free quantitative proteomics .....	201
b) Mass spectrometry analyses of intracellular metabolites by IC-HRMS ....	202
c) Analysis of excreted end products by proton NMR.....	202
<b>REFERENCES.....</b>	<b>204</b>

## LIST OF FIGURES

Figure 1.1. Classification of <i>Trypanosoma</i> species. ....	1
Figure 1.2. Morphology and phylogeny of kinetoplastids, diplomonads, and euglenids. .....	3
Figure 1.3. Trypanosomes of mammals. ....	5
Figure 1.4. Progress in the elimination of HAT. ....	7
Figure 1.5. Morphological characteristics of <i>T. brucei</i> , <i>T. congolense</i> and <i>T. vivax</i> bloodstream form. ....	11
Figure 1.6. Life cycle of <i>T. brucei</i> . ....	13
Figure 1.7. Life cycle stages of <i>T. b. brucei</i> within the tsetse fly. ....	15
Figure 1.8. Morphology of <i>Trypanosoma brucei</i> . ....	17
Figure 1.9. Gene expression mechanisms in kinetoplastids. ....	19
Figure 1.10. The dynamic Variant Surface Glycoprotein (VSG) coat of <i>T. brucei</i> bloodstream forms. ....	21
Figure 1.11. Surface glycocalyx of <i>T. brucei</i> procyclic cells. ....	23
Figure 1.12. Developmental expression of major surface glycoproteins. ....	25
Figure 1.13. The GPI biosynthetic pathway of <i>T. brucei</i> . ....	27
Figure 1.14. ATP production in PCF and BSF trypanosomes. ....	29
Figure 1.15. Intermediate metabolism of PCF trypanosomes in glucose rich conditions. ....	33
Figure 1.16. [U- <sup>13</sup> C] enrichment of key glycolytic intermediates from proline, glycerol or glucose. ....	35
Figure 1.17. Proline metabolism of PCF trypanosomes in glucose-depleted conditions. ....	38
Figure 1.18. Respiratory chain of <i>T. brucei</i> . ....	43
Figure 1.19. F <sub>0</sub> F <sub>1</sub> -ATP synthase/ATPase complex in <i>T. brucei</i> mitochondria. ....	45
Figure 1.20. Glucose and glycerol aerobic metabolism of BSF trypanosomes. ....	48
Figure 1.21. Mitochondrial morphology and proteome of PCF and BSF .....	49
Figure 1.22. Glycosomal metabolic pathways – Part 1 .....	53
Figure 1.23. Structure and distribution of glycosomes. ....	56
Figure 1.24. A proposed metabolic model and peroxisome remodeling during evolution in Euglenozoa. ....	58
Figure 1.25. Glycosome biogenesis in <i>Trypanosoma brucei</i> . ....	62
Figure 1.26. Mechanisms for peroxisome formation in mammalian cells. ....	64
Figure 1.27. Proliferation of glycosomes. ....	66
Figure 1.28. Piggyback import model of peroxisomal matrix proteins. ....	68
Figure 1.29. Biosynthesis of UDP-Glc, UDP-Gal, UDP-GlcNAc, GDP-Man and GDP- Fuc in <i>T. brucei</i> . ....	74
Figure 1.30. 3D structure of TbUGP in complex with UDP-Glc. ....	78
Figure 1.31. Sequence alignments of UGP orthologues. ....	80
Figure 2.32. UGP has a dual localisation in PCF and BSF. ....	90
Figure 2.33. UGP import into glycosomes depends on the PTS1-containing protein PEPCK. ....	94

Figure 2.34. Production of UGP-MYC and TY-PEPCK tagged cell lines.....	96
Figure 2.35. UGP interacts transiently with PEPCK. ....	98
Figure 2.36. Analysis of UGP oligomerization in native gel. ....	100
Figure 2.37. The N-terminal 123 residues of UGP are required for import into the glycosomes. ....	102
Figure 2.38. PCR analysis to confirm endo-tagging at the <i>UGP</i> locus. ....	103
Figure 2.39. A 34-residues peptide of PEPCK is required for glycosomal import of UGP. ....	104
Figure 2.40. Production and functional analyses of <i>RNAi</i> UGP cell lines.....	106
Figure 2.41. Functional analysis of <i>RNAi</i> UGP cell lines in the presence or the absence of glucose.....	108
Figure 2.42. Subcellular localisation of UGP in the presence or the absence of glucose.....	108
Figure 2.43. Expression of a glycosomal recombinant UGP. ....	110
Figure 2.44. Production and functional analyses of $\Delta$ <i>ugp</i> cell lines.....	112
Figure 2.45. Analysis of cell lines expressing UGP in different compartments.....	114
Figure 2.46. PCF produces UDP-Glc in glycosomes and cytosol. ....	116
Figure 2.47. IC-HRMS analyses of intracellular metabolites ....	119
Figure 2.48. Test of anti-UGP antiserum.....	120
Figure 2.49. Sequence alignment of <i>L. major</i> , <i>T. brucei</i> and <i>T. cruzi</i> PEPCK protein sequences.....	120
Figure 2.50. Sequence alignments of UGP orthologues ....	122
Figure 3.51. Proline metabolism of the PCF trypanosomes in the presence of other carbon sources.....	137
Figure 3.52. Kinetic analyses of end products excretion from [U- <sup>13</sup> C]-glucose and proline metabolism. ....	138
Figure 3.53. Proton ( <sup>1</sup> H) NMR analyses of end products excreted from the metabolism of <sup>13</sup> C-enriched succinate, alanine, pyruvate and acetate.....	140
Figure 3.54. <sup>1</sup> H-NMR analyses of end products excreted from the metabolism of <sup>13</sup> C- enriched succinate. ....	142
Figure 3.55. Alamar Blue assays with a series of metabolites. ....	144
Figure 3.56. Succinate, malate and $\alpha$ -ketoglutarate stimulate growth of the PCF..	146
Figure 3.57. <sup>1</sup> H-NMR analyses of end products excreted from the metabolism of malate. ....	148
Figure 3.58. <sup>1</sup> H-NMR analyses of end products excreted from the metabolism of $\alpha$ - ketoglutarate. ....	150
Figure 3.59. Identification of 2-hydroxyglutarate by <sup>1</sup> H-NMR analysis.....	152
Figure 3.60. Growth of the <i>RNAi</i> PROD.H.i mutant is rescued by $\alpha$ -ketoglutarate. ....	154
Figure 3.61. Growth of PCF trypanosomes in low-proline conditions (0.2 mM).....	156
Figure 3.62. $\alpha$ -ketoglutarate is toxic for the $\Delta$ <i>kdh-e2</i> , <i>RNAi</i> SCoAS.i and <i>RNAi</i> SDH.i cell lines.....	159
Figure 3.63. Analysis of the $\Delta$ <i>hgdh</i> mutant.....	162
Figure 3.64. Analysis of <i>RNAi</i> GluDH cell lines.....	164



Figure 3.65. Malate is toxic for the $\Delta$ aco cell line. ....	164
Figure 5.66. Sequence alignment of the recoded <i>UGP</i> sequence ( <i>rUGP</i> ) and native <i>UGP</i> . ....	181
Figure 5.67. UGP knock-down by RNAi in <i>T. brucei</i> . ....	187
Figure 5.68. Production of glycosomal recombinant rUGP proteins. ....	191
Figure 5.69. Principal techniques used for subcellular localisation of proteins. ....	193
Figure 5.70. UGP activity assay. ....	197
Figure 5.71. Duolink® Proximity Ligation Assay reaction. ....	199

## LIST OF TABLES

Table 1.1. Summary of treatment choices for patients with <i>T. gambiense</i> HAT. ....	9
Table 1.2. Effect of proline metabolism and TCA cycle enzymes disruption on PCF growth. ....	40
Table 1.3. Function of peroxins identified in mammals, yeast and <i>T. brucei</i> . ....	60
Table 1.4. Peroxisomal matrix proteins imported as oligomers. ....	70
Table 1.5. Characterised glycosyltransferases from <i>T. brucei</i> . ....	72
Table 1.6. Enzymes of sugar nucleotide biosynthetic pathways. ....	76
Table 2.7. Protein expression levels by label-free mass spectrometry proteomic analysis of glycosomal enriched fractions. ....	92
Table 3.8. Excreted end products from the metabolism of carbon sources in the PCF trypanosomes. ....	161
Table 5.9. PCR primers sequences and features concerning PEPCK mutant cell lines. ....	183
Table 5.10. PCR primers sequences and features concerning UGP mutant cell lines. ....	185
Table 5.11. Mutant cell lines disrupted in expression of enzymes of proline degradation, TCA cycle and acetate production pathways used in this work. ....	189
Table 5.12. Primary and secondary antibodies used for western blot and immunofluorescence analysis. ....	195

Phylum	Class	Subclass	Order	Family	Subfamily	Genus	Subgenus	Species
Euglenozoa	<ul style="list-style-type: none"> <li>Symbiontida</li> <li>Euglenida</li> <li>Diplonemea</li> <li>Kinetoplastea</li> </ul>	<ul style="list-style-type: none"> <li>Prokinetoplastina</li> <li>Metakinetoplastina</li> </ul>	<ul style="list-style-type: none"> <li>Eubodonida</li> <li>Parabodonida</li> <li>Neobodonida</li> <li>Trypanosomatida</li> </ul>	Trypanosomatidae	<ul style="list-style-type: none"> <li>Leishmaniinae</li> <li>Phytomonadinae</li> <li>Strigomonadinae</li> <li>Blechomonadinae</li> <li>Paratrypanosomatinae</li> <li>Trypanosomatinae</li> </ul>	<ul style="list-style-type: none"> <li><i>Leishmania</i></li> <li><i>Trypanosoma</i></li> </ul>	<ul style="list-style-type: none"> <li>Herpetosoma</li> <li>Megatrypanum</li> <li>Schizotrypanum</li> <li>Tejeraia</li> <li>Dunotella</li> <li>Nannomonas</li> <li>Pycnomonas</li> <li>Trypanozoon</li> </ul>	<ul style="list-style-type: none"> <li><i>T. cruzi</i></li> <li><i>T. vivax</i></li> <li><i>T. congolense</i></li> <li><i>T. equiperdum</i></li> <li><i>T. evansi</i></li> <li><i>T. brucei</i></li> </ul>

**Figure 1.1. Classification of *Trypanosoma* species.**

## 1. INTRODUCTION

In this chapter, I describe the biological model used in this thesis: the parasite *Trypanosoma brucei*. Since this parasite causes the sleeping sickness in Africa, a brief description of the diagnosis, prevention and treatment, with special focus on the challenges for the human African trypanosomiasis (HAT) elimination will be done. I explain in detail cellular and metabolic features of particular interest with focus on glycolytic and mitochondrial metabolism. A special section is dedicated to the very important organelle called glycosome, which is key for the development of this thesis. At the end, I present a comparative analysis of UDP-glucose pyrophosphorylases, the enzyme this work is focused on.

### 1.1 Trypanosomes

Trypanosomatids are uniflagellate parasites that belong to the class Kinetoplastea, defined by the presence of mitochondrial DNA organised in a unique and extensively studied structure called kinetoplast (k) which is composed of DNA circles (Shapiro and Englund, 1995; Cayla et al., 2019). Among kinetoplastids, there are free-living and symbiotic organisms in addition to parasitic protists including the well-studied pathogens from *Trypanosoma* and *Leishmania* genera. The most recent classification of the class Kinetoplastea (Figure 1.1) divides it into two groups. The first one is the subclass Prokinetoplastina, which includes an ectoparasite infecting the skin and gills of fishes called *Ichthyobodo* (Robertson, 1985) and the non-photosynthetic symbiont *Perkinsella* that resides inside amoebozoans of the genus *Paramoeba* (Tanifuji et al., 2017). The second subclass of kinetoplastids, Metakinetoplastina, includes three orders of predominantly free-living bodonids (Eubodonida, Parabodonida, and Neobodonida) and the parasitic Trypanosomatida (Moreira, 2004; Simpson et al., 2006; Deschamps et al., 2011; Butenko et al., 2020).

Remarkably, these organisms are considered to have large amounts of organellar DNA (kDNA) with a high structure variability (Figure 1.2). While trypanosomatids kDNA mini and maxicircles are densely packaged, in bodonids and outer groups the kinetoplast is more dispersed (Lukeš et al., 2002).

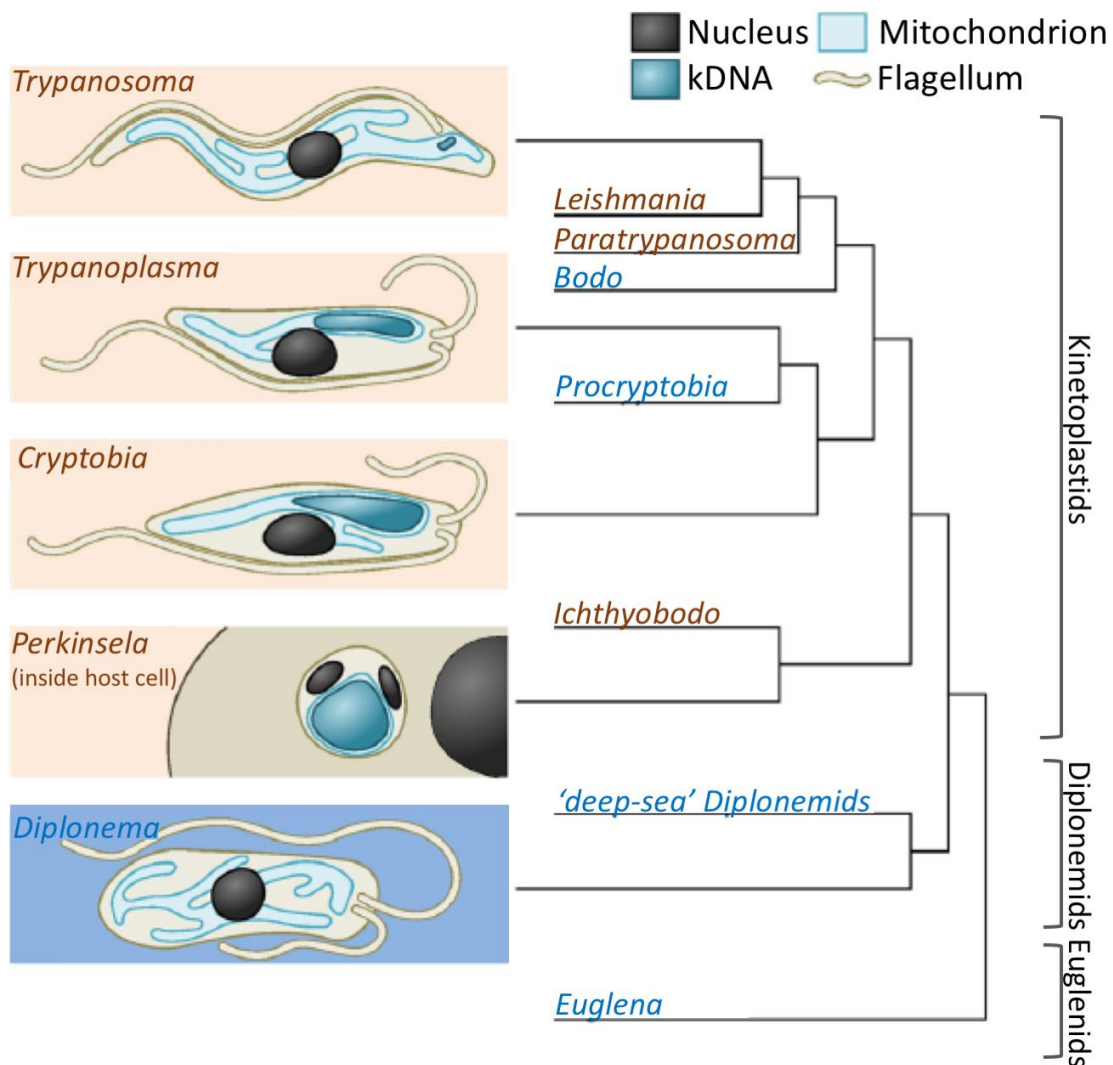
















**Figure 1.2. Morphology and phylogeny of kinetoplastids, diplomonids, and euglenids.**

In the common ancestor shared by diplomonids and kinetoplastids, the organellar DNA content might have increased dramatically soon after the divergence from euglena. Then, *Trypanosoma* may have either undergone massive reduction of its kDNA or has not expanded it to the levels seen in the sister lineages. Cell morphology is shown on the left and a schematic phylogenetic tree is shown on the right. **Brown**: parasitic or endosymbiotic species, **blue**: free-living species (From Lukeš et al., 2018).

It has been recently proposed that the large amounts of kDNA evolved through neutral processes or constructive neutral evolution (CNE), suggesting that it does not represent any adaptive benefit for these organisms (Lukeš et al., 2018). This hypothesis is supported by recent studies performed with the outer group of free-living diplomonids. The authors showed that this abundant and diverse group of organisms has very complex mitochondrial genome architecture, structure and post-transcriptional processes despite the absence of a parasitic lifestyle, which is commonly considered full of peculiarities (Kaur et al., 2020).

Many factors must have participated in the development of parasitism within trypanosomatids. A phylogenomic study recently explored the role of gene gain and gene loss in the development of trypanosomatid genomes. A reduction in complexity of numerous catabolic pathways, macromolecular degradation and ion transport was evidenced, in addition to the gain of gene families involved in host invasion. This work clearly points out the importance of interaction between the protist and the host immune system as a selective pressure that led to the specialization of the parasites cell surface (Jackson et al., 2016).

The trypanosomatid order contains a single family: Trypanosomatidae, which comprises parasites of invertebrates, vertebrates and plants (Maslov et al., 2019). Several species from the genus *Trypanosoma* are of particular medical and veterinary interest (Figure 1.3). This genus is divided in two main groups: stercoraria and salivaria, based on the mode of transmission by their insect vector (Hoare, 1966; Gibson, 2016). The Stercoraria group, represented by the etiological agent of Chagas disease *T. cruzi*, is characterised by transmission through the excretion of faeces (Kaufer et al., 2017). On the other hand, Salivaria group parasites are transmitted by the bite of an infected insect and is represented by *T. vivax*, *T. congolense* and *T. brucei*. The latter is by far the most well studied *Trypanosoma* and the model used in this work. The three *T. brucei* subspecies are transmitted through the bite of an infected tsetse fly. *T. b. gambiense* and *T. b. rhodesiense* infect humans and are the causative agents of Human African Trypanosomiasis (HAT), while *T. b. brucei* infects domestic and wild animals causing the cattle disease nagana, and is unable to infect humans (Hager et al., 1994).

	Species	Main host/Reservoir	Vectors	Disease	Geographical distribution
Stercoraria	<i>T. theileri</i>		Tabanid flies	NP	Worldwide
	<i>T. lewisi</i>		Rat fleas	NP	Worldwide
	<i>T. cruzi</i>		Triatomine bugs	Chagas	Central and South America
Salivaria	<i>T. rangeli</i>		Triatomine bugs	NP	South America
	<i>T. vivax</i>		Tsetse and tabanid flies	Nagana	Sub-Saharan Africa, South America, W. Indies, Mauritius
	<i>T. congolense</i>		Tsetse flies	Nagana	Sub-Saharan Africa
	<i>T. simiae</i>		Tsetse flies	Acute in pigs	Sub-Saharan Africa
	<i>T. godfreyi</i>		Tsetse flies	Mild disease in pigs	Sub-Saharan Africa
	<i>T. suis</i>		Tsetse flies	Acute in piglets	Sub-Saharan Africa
	<i>T. evansi</i>		Tabanid flies, vampire bats	Surra	Worldwide
	<i>T. equiperdum</i>		Veneral contact	Dourine	Worldwide
	<i>T. brucei brucei</i>		Tsetse flies	Nagana	Sub-Saharan Africa
	<i>T. brucei rhodesiense</i>		Tsetse flies	Sleeping sickness	East Africa
	<i>T. brucei gambiense</i>		Tsetse flies	Sleeping sickness	West and Central Africa

**Figure 1.3. Trypanosomes of mammals.**

Hosts, transmission and relation to mammal diseases (adapted from (Gibson, 2016)). Two main groups, stercoraria and salivaria, have been established based on the mode of transmission by their insect vector (Hoare, 1966).

## **1.2. Human African Trypanosomiasis (HAT)**

HAT, also known as sleeping sickness, is a neglected tropical disease that occurs in sub-Saharan Africa and can be fatal if left untreated. There are two forms of the disease, depending on the *T. brucei* subspecies causing the infection. The first one, *T. brucei gambiense*, is the most important one as it is responsible for 98% of cases in western and central Africa. Gambiense HAT progresses slowly causing a chronic infection that can be asymptomatic for years. Secondly, *T. brucei rhodesiense* is responsible for the remaining 2% of cases in eastern and southern Africa. Rhodesiense HAT progresses faster causing an acute infection that can affect the central nervous system within months.

The disease has two stages with a different set of symptoms. In the first or early stage, trypanosomes remain in the blood and lymph system and the patients present mild symptoms like fever, headaches, joint pains and itching. In the second or late stage, parasites are detected in the cerebrospinal fluid and patients can develop disturbed sleep pattern, confusion, sensory disturbances, extreme lethargy, poor condition and, in some severe cases, progression to coma. (Steverding, 2008; Büscher et al., 2017; World Health Organization, 2019). Over the past years, the number of HAT cases has been reduced significantly. The last WHO report in 2019 states that there were less than 1000 cases reported in 2018, targeting elimination of HAT as a public health problem possible by this year (Figure 1.4).

### **1.2.1. Diagnosis, Prevention and Treatment**

There are several approaches to diagnose HAT and the choice depends on the country and available facilities. A serological test is performed first to detect trypanosome-specific antibodies followed by confirmation of parasites present in blood. Finally, the stage of the disease is determined by a lumbar puncture.

Recently introduced rapid tests (Büscher et al., 2013, 2014) and classical card agglutination test for trypanosomiasis (CATT) developed in the late 1970s are the serological tests performed in the field. A new rapid test has been developed with recombinant antigens that showed an increased sensitivity compared to the rapid test made with native antigens, while the specificity was similar (Lumbala et al., 2018).



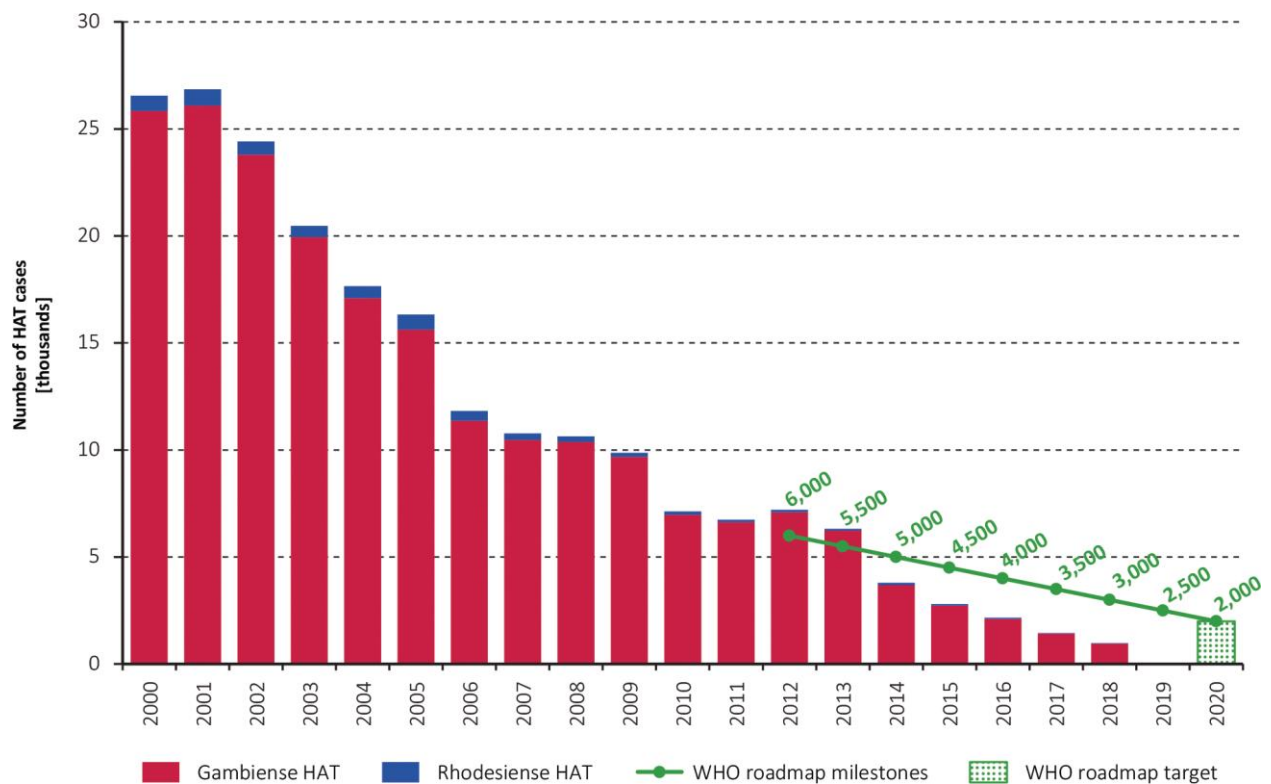


**Figure 1.4. Progress in the elimination of HAT.**

The total number of reported cases of HAT (gambiense and rhodesiense) per year is shown. Less than 1000 cases were reported in 2018, most of which caused by infection with *T. b. gambiense*. HAT was targeted for elimination as a public health problem by this year. A further target is to fully eliminate the occurrence of gambiense HAT (*i.e.* zero cases) within the next ten years. The green line and the green bar show the milestones and target set in the WHO Roadmap for HAT elimination (From Franco et al., 2020).

Combining two or more screening tests seems to be required in order to achieve elimination of HAT since the specificity and sensitivity of individual tests might not be high enough to improve the detection of cases now that the disease prevalence is decreasing (Jamonneau et al., 2015; Lumbala et al., 2018).

In addition to case detection and treatment, the inclusion of vector control is also crucial to achieve HAT elimination. An affordable cost-effective tiny target technology was recently developed consisting of visual devices (blue colour) made with textiles impregnated with the insecticide deltamethrin (Tirados et al., 2015). These 'Tiny Targets' have been successfully used in different regions and represent an effective control strategy of tsetse populations (Courtin et al., 2015; Tirados et al., 2015; Mahamat et al., 2017).

Currently there are six drugs available for the treatment of HAT: pentamidine, suramin, melarsoprol, eflornithine, nifurtimox and fexinidazole. Pentamidine and suramin were the first-line drugs against stage 1 gambiense HAT and rhodesiense HAT, respectively. For the second stage of the disease, a nifurtimox–eflornithine combination therapy (NECT) is used for gambiense HAT, while melarsoprol is restricted to rhodesiense HAT. Recently, the guidelines on therapeutic choices were updated after the approval in 2018 of the new drug fexinidazole (Torreele et al., 2010; Mesu et al., 2018) (Table 1.1). The big advantages of Fexinidazole is that it is orally administered, in contrast to previous treatments, therefore it does not require intravenous or intramuscular infusions which reduces treatment costs and, importantly, is effective against both early and late stages of HAT (World Health Organization, 2019).

### **1.2.2. Challenges for HAT elimination**

Despite the significant reduction of HAT cases, the disease still represents a public health problem in some African countries, especially in the Democratic Republic of the Congo. The factors considered as potential limitations towards elimination of HAT include:

#### **a) Drug resistance**

Melarsoprol resistance is a clear example of widespread drug resistance in HAT patients. Although it represents the only example of clinically relevant drug-resistant parasites (Fairlamb and Horn, 2018), the resistance potential of nifurtimox and

Age, body weight	Clinical examination	Cerebrospinal fluid findings	Treatment		
			1st choice	2nd choice*	Relapse**
< 6 years or <20 kg		≤ 5 WBC/μl, no trypanosomes	Pentamidine	-	NECT
		> 5 WBC/μl or trypanosomes	NECT	Eflornithine	NECT-long
≥ 6 years and ≥ 20 kg	No suspicion of severe HAT	Lumbar puncture not needed	Fexinidazole	Pentamidine (First stage) NECT (Second stage)	NECT
	Suspicion of severe HAT	< 100 WBC/μl	Fexinidazole	Pentamidine (First stage) NECT (Second stage)	NECT
		≥ 100 WBC/μl or failed lumbar puncture	NECT	Fexinidazole	NECT-long or melarsoprol

**Table 1.1. Summary of treatment choices for patients with *T. gambiense* HAT.**

\*2nd choice treatment corresponds to the alternative treatment recommended in cases where the 1st choice treatment is not available or is not appropriate. \*\*Relapse treatment is given in cases of treatment failure.

WBC: White Blood Cells

NECT: nifurtimox–eflornithine combination therapy

NECT-long: nifurtimox (15mg/kg per day) in 3 doses for 10 days, eflornithine (400mg/kg per day) in 2 infusions for 14 days.

(From World Health Organization, 2019)

fexinidazole has already been shown *in vivo* and *in vitro* (Sokolova et al., 2010). Fexinidazole is cross-resistant with nifurtimox which raises questions about a possible selection of resistance to this new drug. However, the progressive reduction of cases could reduce the probability of selecting resistant parasites (Dickie et al., 2020). The search for new treatments is still going on. For instance, clinical trials with an additional oral treatment consisting of only one dose of the drug acoziborole seem promising (Jacobs et al., 2011; Dickie et al., 2020). Furthermore, adenosine analogues showing trypanocidal activity were recently identified. One of these compounds showed to be highly active in both stages of HAT and to not have cross resistance with other drugs, representing a suitable candidate for treatment (Hulpia et al., 2019).

## **b) Human and animal reservoirs**

The importance of asymptomatic infections in serologically positive patients where no trypanosomes are detected in the blood has been recently addressed (Capewell et al., 2019). The authors propose that trypanosomes found in the skin (Caljon et al., 2016; Capewell et al., 2019) and adipose tissue (Trindade et al., 2016) may constitute a crucial reservoir that contributes to transmission. Indeed, a very recent study proved that HAT confirmed and unconfirmed seropositive subjects carry extravascular trypanosomes in their skin, supporting the role of human skin as a reservoir for trypanosomes (Camara et al., 2020). The aparasitaemic cases do not receive any treatment, which might hamper the possibility of eliminating HAT, therefore, a revision of the WHO recommendations was strongly suggested in the light of this new data.

Similar to asymptomatic human infections, the role of animal reservoirs requires further attention. Clearly there is a need to develop more sensitive and specific detection techniques to cope with discordant results produced as a consequence of the low parasitaemia generally observed in *T. b. gambiense* infections. *T. b. gambiense* can infect a variety of domestic animals and wildlife, including cattle and pigs recently identified as potential reservoirs (N'Djetchi et al., 2017). Importantly, a number of animals have been successfully infected with patient-derived *T. b. gambiense* strains. The capacity of these parasites to cycle between animals and tsetse flies without losing infectivity to humans has been shown on several occasions (Büscher et al., 2018).

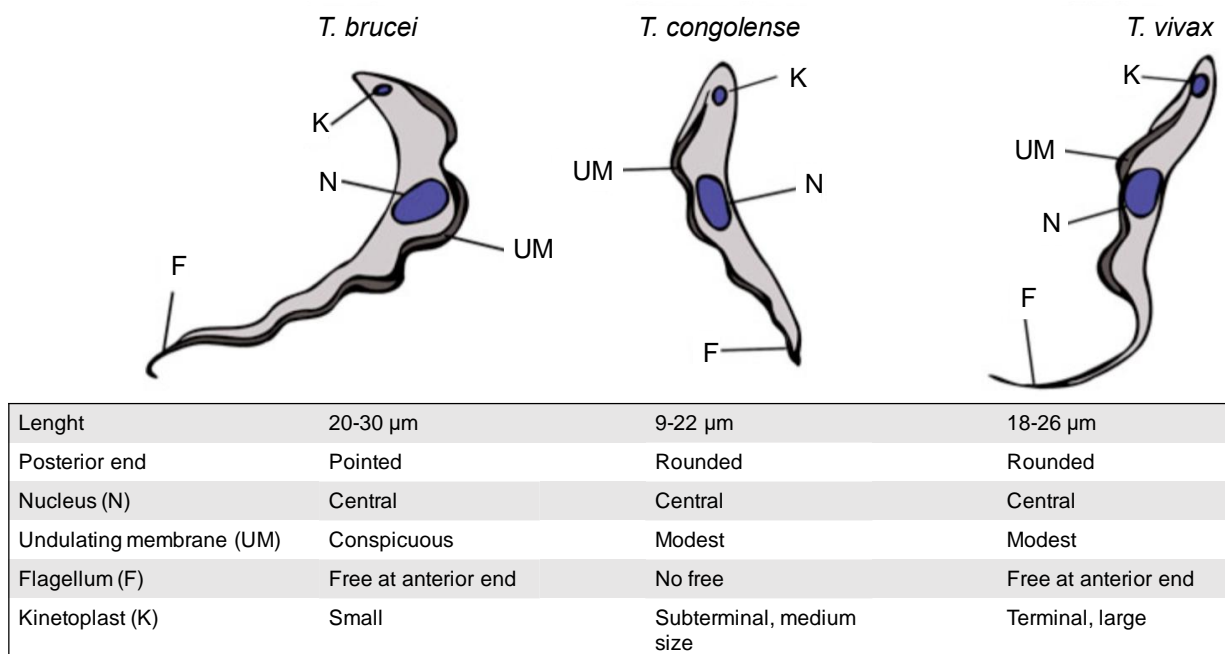


**Figure 1.5. Morphological characteristics of *T. brucei*, *T. congolense* and *T. vivax* bloodstream form.**

*T. brucei* group trypanosomes (*T. b. brucei*, *T. b. evansi*, *T. b. equiperdum*) characteristics are shown (From Giordani et al., 2016).

### 1.3. Animal African Trypanosomiasis (AAT)

AAT also known as nagana is caused by *T. congolense*, *T. vivax* and, to a lesser extent, *T. brucei* spp. The morphological differences between these parasites are shown in Figure 1.5. In addition to tsetse fly, other insects can mechanically transmit *T. vivax* parasites, like tabanid and stable (*Stomoxys* sp) flies, resulting in a wider geographical distribution (Wells, 1972; Jones and Dávila, 2001). The disease is widespread in sub-Saharan Africa and affects valuable domestic livestock including bovines, ovines, caprines, equids, camelids and suids, causing a huge economic and social impact in terms of economic loss. In the absence of treatment, infection with one or more *Trypanosoma* species can lead to acute or chronic disease resulting in weaken animals (Steverding, 2008; Giordani et al., 2016). The compounds diminazene aceturate (DA) and isometamidium chloride (IC) are the most used veterinary trypanocides against AAT. Since the 1960s, resistance to these chemicals has been reported in 17 African countries (Delespaux et al., 2008). Despite the increase of resistance, the treatments are still effective in controlling the parasite and the corresponding disease at an acceptable level (Chitanga et al., 2011).

Interestingly, *T. b. brucei* subspecies as well as *T. congolense* and *T. vivax* are only infectious to animals. The lack of infectivity in humans is due to the trypanolytic activity of a human-specific serum apolipoprotein called Apolipoprotein L-I (APOL-I) which is bound to high-density lipoprotein particles known as trypanolytic factors (TLFs). These particles enter the cell through endocytosis at the flagellar pocket progressing towards the lysosomes. The acidic lysosomal pH induces conformational changes of APOL-I which binds to the lysosomal membrane creating pores that lead to lysis and death of the parasites (Hager et al., 1994; Pays et al., 2006).

In contrast, *T. b. rhodesiense* and *T. b. gambiense* have different ways to escape this trypanolytic activity. *T. b. rhodesiense* expresses a serum-resistance associated protein (SRA) which interacts with APOL-I preventing its insertion in the lysosomal membrane (Van Xong et al., 1998; Stephens et al., 2012). *T. b. gambiense* expresses a specific glycoprotein (TgsGP) whose incorporation into the lysosomal membranes prevents APOL-I insertion (Uzureau et al., 2013).

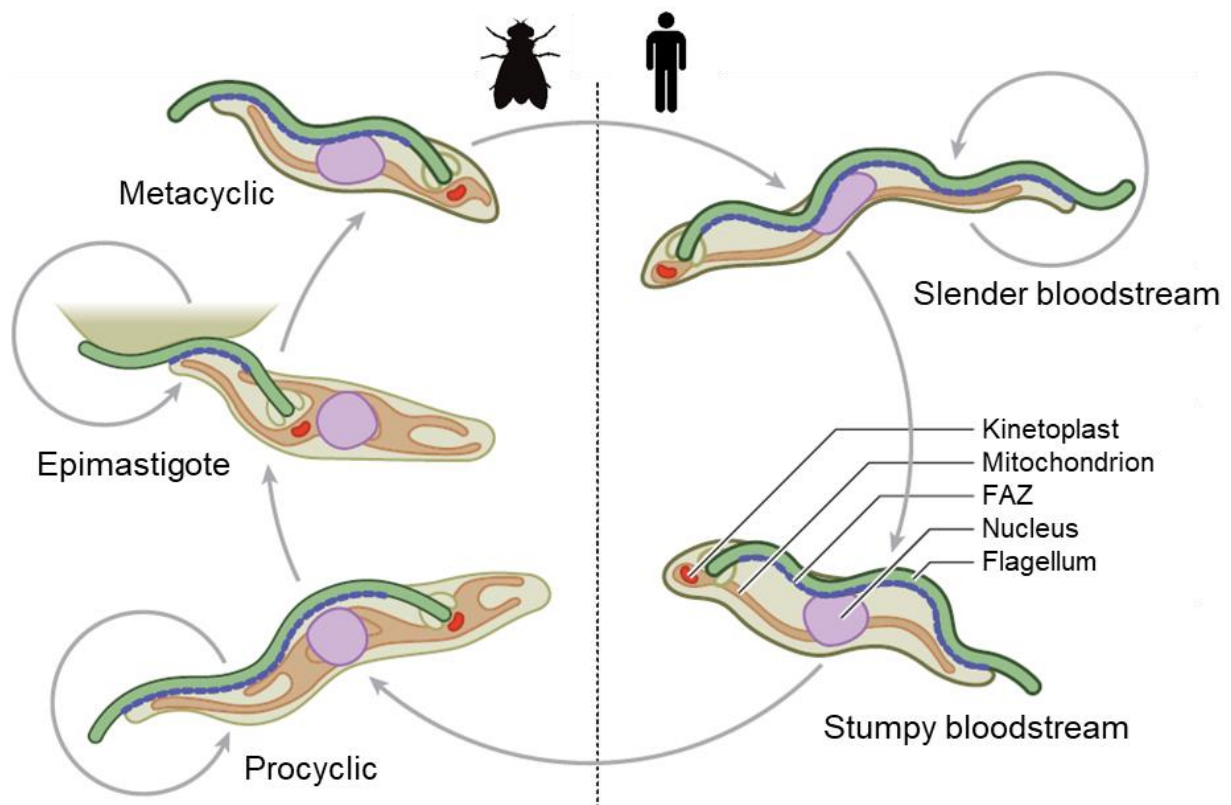


**Figure 1.6. Life cycle of *T. brucei*.**

The five major stages are shown. Circular arrows represent the proliferative capacity of procyclics and epimastigotes in the tsetse fly, as well as slender bloodstream forms in the mammal (From Wheeler et al., 2019).

#### **1.4. *Trypanosoma brucei*: a remarkable biological model**

Several aspects of *T. brucei brucei* biology make it an ideal model for studying trypanosome biology. The genome sequence was published in 2005 (Berriman et al., 2005) and is freely available on TriTrypDB (<http://tritrypdb.org>), a database providing access to genome-scale datasets for kinetoplastid parasites (Aslett et al., 2010).

*T. b. brucei* is not pathogenic for humans and both insect and mammalian stages are relatively easy to culture *in vitro* (Brun and Schönenberger, 1979; Hirumi and Hirumi, 1989). It is also possible to generate different life cycle stages present in the mammals or in the fly using *in vitro* systems (Kolev et al., 2012; Qiu et al., 2018).

A variety of advanced genetic tools have been developed to manipulate *T. brucei*, which can be efficiently transfected by electroporation-based methods. These tools include inducible systems for the regulated ectopic expression of genes, for RNAi mediated knock-down and for the expression of proteins such as Cas9 to use CRISPR-Cas9 technology (Wirtz and Clayton, 1995; Biebinger et al., 1997; Ngô et al., 1998; Bringaud et al., 2000; Beneke et al., 2017; Rico et al., 2018). Up to five drug-resistance markers are available, therefore it is possible to generate mutant cell lines targeting or expressing multiple genes (ten Asbroek et al., 1990; Poon et al., 2012). TrypTag ([http:// tryptag.org](http://tryptag.org)) is another resource available which contains subcellular localisations of over 2000 endogenously-tagged proteins and aims to localise every protein encoded in the genome (Dean et al., 2017). All these characteristics make *T. brucei* an ideal model in fundamental cell biology and applied research looking for drug targets and new potential treatments for HAT.

##### **1.4.1. Life cycle and transmission**

*T. brucei* is transmitted to mammals through the bite of a tsetse fly and has a complex developmental cycle life (Figure 1.6). The mammalian host gets infected when a tsetse fly bite delivers metacyclic trypomastigotes to the bloodstream. Then, growth-arrested metacyclics differentiate into slender forms that proliferate in the blood as well as other fluids and, additionally, accumulate in the interstitial spaces of several tissues like



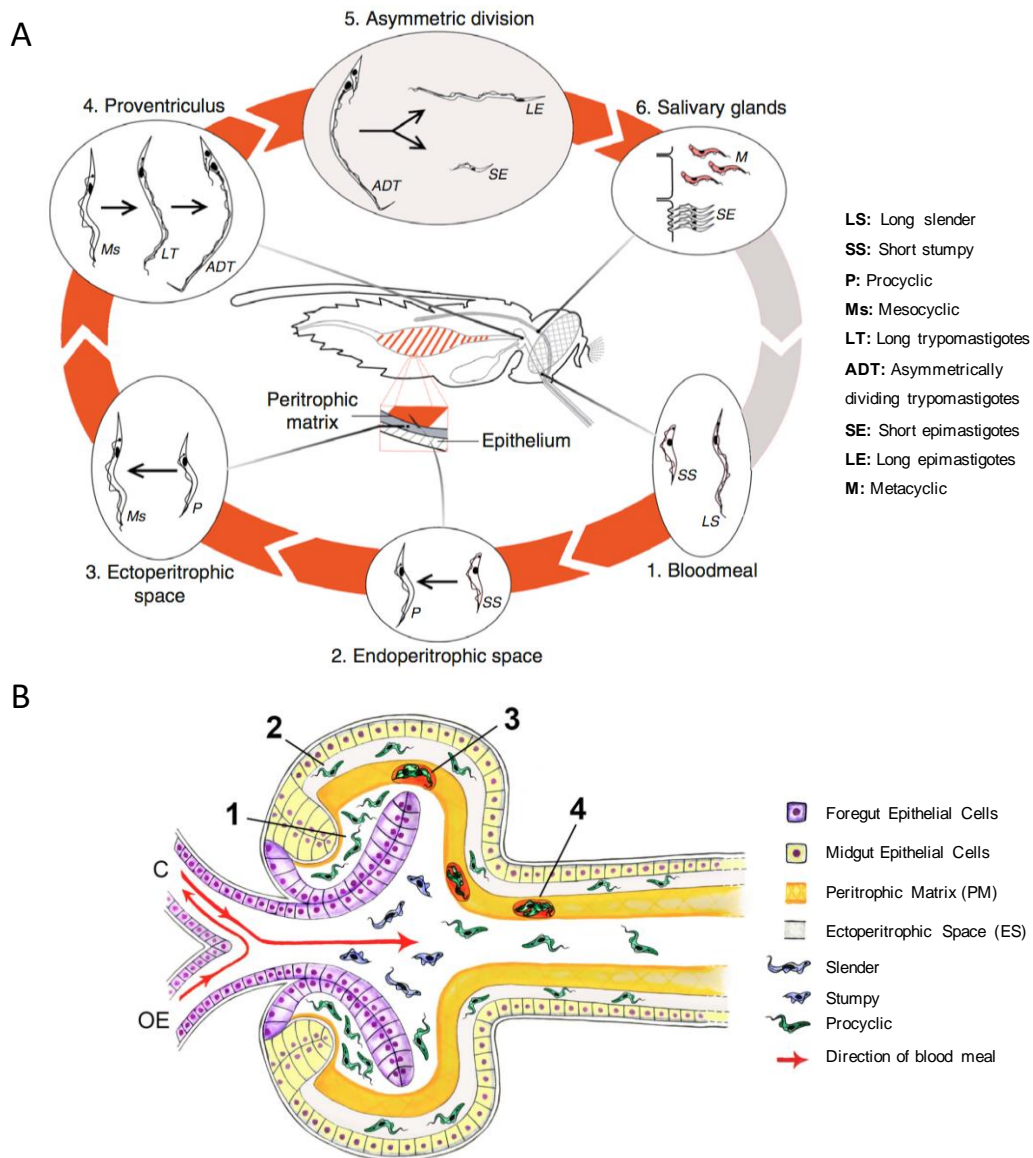


**Figure 1.7. Life cycle stages of *T. b. brucei* within the tsetse fly.**

In panel A, red arrows join life cycle stages within the fly while grey arrows represent transit between insect and mammalian host (Walshe et al., 2009). Panel B shows trypanosomes entering the ectoperitrophic space (ES) *via* the proventriculus of the tsetse fly. Trypanosomes ingested during the blood meal transform into procyclic forms within the proventricular lumen (1) and then migrate to the ES through a more fluid PM in the proventriculus (2). Alternatively, parasites may become trapped between PM layers forming cyst-like bodies (3). These bodies are carried through the midgut as the PM continues to be secreted (4). Blood flow from oesophagus (OE) or crop (C) are represented (From Rose et al., 2020).

skin, visceral adipose tissue and eventually the brain (Langousis and Hill, 2014; Caljon et al., 2016; Capewell et al., 2016; Trindade et al., 2016; Wheeler et al., 2019; Szöör et al., 2020).

Slender bloodstream forms differentiate into the cell-cycle arrested short stumpy form that is pre-adapted for survival in the tsetse fly (Dewar et al., 2018). A quorum sensing-like mechanism involving oligopeptide signals received *via* a transmembrane protein called TbGPR89 triggers differentiation after accumulation of the stumpy-induction factor (SIF) (Rojas et al., 2019).

Bloodstream trypanosomes including slender and stumpy cells are taken up with a blood meal when a tsetse fly bites the infected host. Once in the fly midgut, short stumpy forms differentiate into the proliferative procyclic form that establish a midgut infection. To establish a new infection in mammals, trypanosomes in the fly must reach the salivary glands and be injected within a next blood meal, a journey that includes going through physical barriers (Figure 1.7A). The standard mechanism proposes that trypanosomes penetrate the peritrophic matrix (PM) in the anterior midgut to reach the ectoperitrophic space (ES). This PM is a proteoglycan matrix continuously produced by a specialised region of the anterior midgut that separates the midgut epithelium from the food bolus, protecting the cells of the intestine from mechanical damage, pathogens and toxins (Lehane, 1997).

The trypanosomatid journey has been recently explored using innovative microscopy techniques (Rose et al., 2020). According to this recent model, *T. brucei* procyclics reach the ES after penetrating an immature, freshly secreted PM within the proventriculus (Figure 1.7B). In the proventriculus, parasites go through asymmetric division to generate one long epimastigote and one short epimastigote. Then, epimastigotes go forward to the mouthparts, salivary ducts and ultimately into the salivary glands, where short epimastigotes attach to the gland epithelium, replicate and differentiate into metacyclic trypomastigotes. Finally, metacyclic cells detach from the epithelium and are released to the lumen. These cells are preadapted for transmission and survival in the mammalian host (Tetley and Vickerman, 1985; Vigneron et al., 2020).

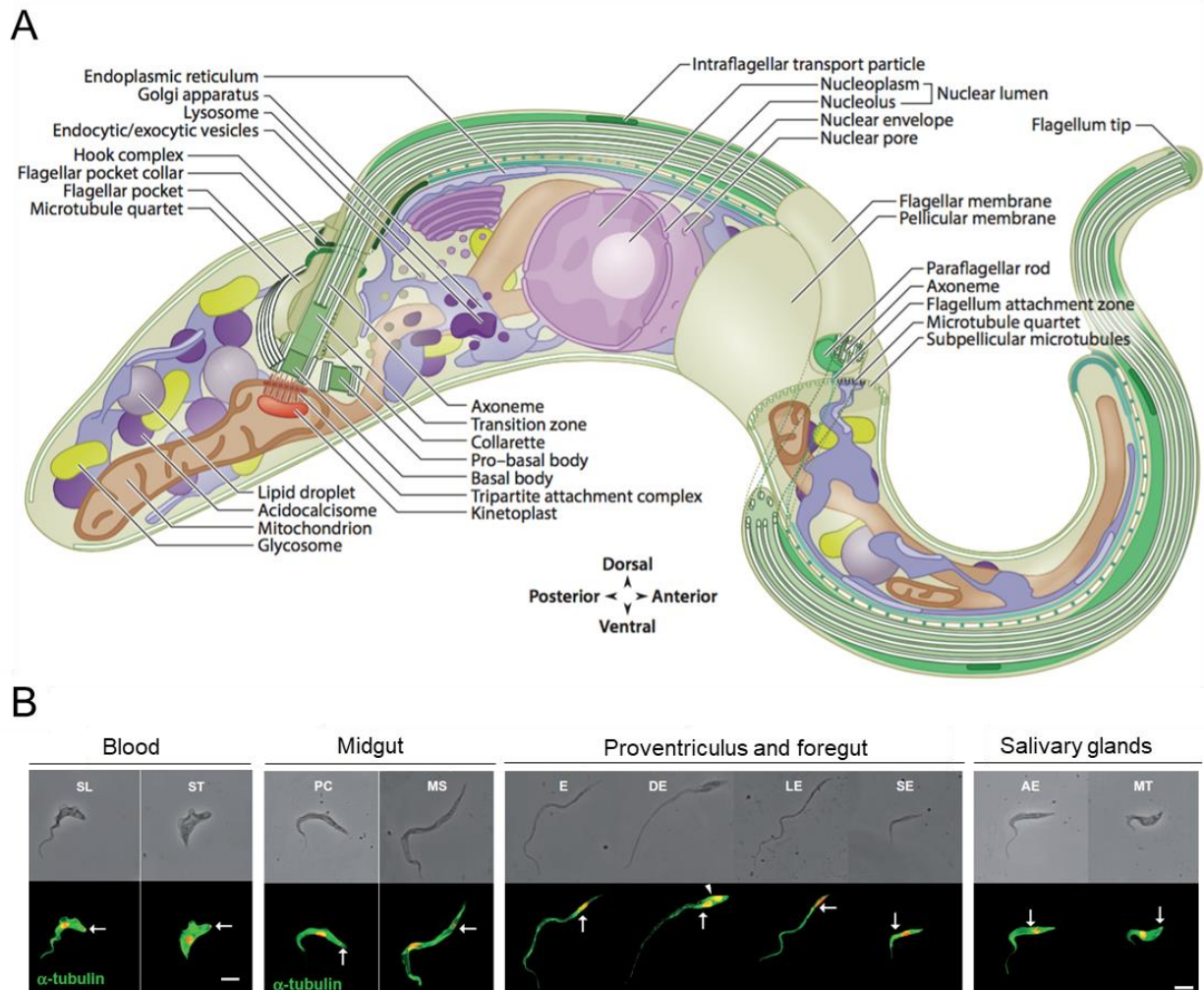


**Figure 1.8. Morphology of *Trypanosoma brucei*.**

Panel A shows the morphology of a procyclic cell based on electron microscopy and tomography. The localisation of organelle components corresponds to reports using fluorescence microscopy of both endogenous fluorescent protein tagging and immunofluorescence (From Wheeler et al., 2019). Morphological changes in trypanosomes during the parasite cycle are shown in panel B. Scale bar: 5  $\mu$ m, old (arrow) and new (arrowhead) basal body positions are indicated, DAPI is in red. SL: slender trypomastigote; ST: stumpy trypomastigote; PC: procyclic trypomastigote; MS: mesocyclic trypomastigote; E: proventricular epimastigote; DE: asymmetrically dividing epimastigote; LE: long epimastigote; SE: short epimastigote; AE: attached epimastigote; MT: metacyclic trypomastigote (From Rotureau et al., 2011).

#### **1.4.2. Cell architecture**

The characteristic shape of *T. brucei* (Figure 1.8A) is defined by its ordered cytoskeleton composed of a packed sub-pellicular microtubule array linked to the plasma membrane (Hemphill et al., 1991). This array of microtubules confers a very pronounced polarity to the cell thanks to its anterior minus ends and posterior plus ends (Robinson et al., 1995).

The single-copy organelles have precise positions within the cell and include the flagellar pocket, flagellum, kinetoplast, mitochondrion and nucleus. The flagellar pocket is an invagination of the plasma membrane where endo and exocytosis take place and where the flagellum emerges onto the cell surface (Overath and Engstler, 2004; Lacomble et al., 2009). The flagellum is attached to the cell body via the flagellum attachment zone (FAZ) composed of a filament and a set of four specialised microtubules originating close to the basal bodies. The distal extremity of the flagellum is free and determines the direction of movement (Robinson et al., 1995).

The mitochondrial genome within the kinetoplast is connected with the basal body where the flagellum originates. The replication of kDNA is coordinated with the cell cycle through the correct segregation of the new and the old basal body (Robinson and Gull, 1991; Ogbadoyi et al., 2003). Like other trypanosomatids, *T. brucei* has a single mitochondrion extended through the whole cell that can adapt during the developmental cycle to take advantage of the different environmental conditions (Priest and Hajduk, 1994).

*T. brucei* has particular peroxisome-related organelles called glycosomes, where the 6-7 first steps of glycolysis are compartmentalised (Opperdoes and Borst, 1977a). This organelle is described in detail in section 1.6. Morphological changes during the parasite cycle are shown in Figure 1.8B.

#### **1.4.4. Gene expression and regulation**

The genome of *T. brucei* has 11 megabase chromosomes (~35 Mb total) containing, with few exceptions, all protein coding genes. In addition, 5 intermediate (200-300 kb) and 60-100 mini-chromosomes (30-150 kb) with functions related to the process of antigenic variation are found. All this genetic information is contained in a nucleus with an approximate diameter of 2.5  $\mu\text{m}$  (Ogbadoyi et al., 2000; Berriman et al., 2005; Ersfeld, 2011).

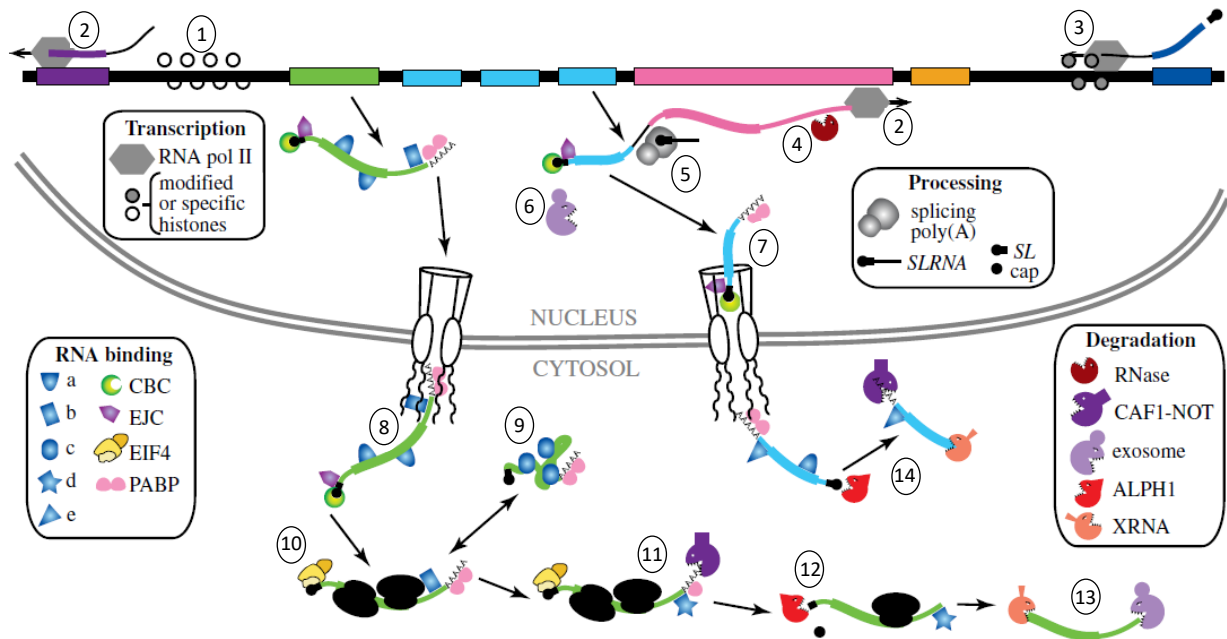


**Figure 1.9. Gene expression mechanisms in kinetoplastids.**

1: Modified histones in an RNA polymerase II initiation region located in a divergent strand-switch intergenic region. 2: RNA polymerase II elongation. 3: RNA polymerase II termination located in a convergent strand-switch intergenic region. 4: Endonuclease cleavage of precursor. 5: Trans-splicing and polyadenylation. 6: Incompletely processed mRNAs can be degraded by the exosome. 7: Export of a completed mRNA, with bound poly(A) binding protein (PABP), exon junction complex (EJC) and nuclear cap-binding complex (CBC). 8: Emergence of a mature mRNA including proteins on the coding region (a) and a specific, stabilizing protein (b) bound to the 3'-untranslated region (3'-UTR). 9: Binding by a silencing or aggregating RNA-binding protein (c) and condensation into granules. 10: Binding of EIF4E, EIF4G and EIF4A, and translation. 11: Protein (b) is replaced by a destabilizing RNA-binding protein (d) and deadenylation starts. 12: Decapping by ALPH1. 13: Degradation by XRNA and the exosome. 14: Rapid decay pathway-immediate decapping promoted by protein (e) (From Clayton, 2019).

Among the unusual aspects that characterise gene expression in trypanosomatids is the fact that the genes are arranged in large multi-gene (polycistronic) transcription units, therefore genes lack individual promoters (Figure 1.9).

The sites of RNA polymerase II initiation located in a divergent strand-switch region (region located between divergent polycistronic transcription units) are epigenetically marked, being enriched in the histone modifications H4K10ac and H3K4me3, the histone variants H2AZ, H2BV and the bromodomain factor BDF3 (Siegel et al., 2009; Wright et al., 2010). Transcription termination is regulated by the histone H3 variant (H3.V) and, in bloodstream forms, the base J ( $\beta$ -D-glucosyl-hydroxymethyluracil). This modified thymidine is the result of a hydroxylation by J-binding proteins JBP1 and JBP2 followed by a glycosylation by the J-associated glucosyl transferase (JGT) (Siegel et al., 2009; Schulz et al., 2016).

RNA polymerase II transcribes most protein-coding genes in polycistronic units that become mature mRNA after two coupled processes: 5' trans-splicing and 3' polyadenylation (Clayton, 2019). Trans-splicing involves addition of a capped 39-nt sequence called 'spliced leader' (SL) at the 5' extremity of all mRNAs. This is performed by the spliceosome, which contains U1, U2, U4, U5, and U6 snRNAs in addition to several proteins (Günzl, 2010). Polyadenylation and trans-splicing are guided by the position of pyrimidine-rich tracts located between these two sites (Clayton and Michaeli, 2011). The polyadenylation complex including a major functional poly(A) polymerase was recently characterised (Koch et al., 2016). RNA polymerase I is responsible for the transcription of ribosomal rDNA, while a modified version transcribes the genes coding for the major surface proteins procyclins and VSG (Günzl et al., 2003).

The extranuclear mitochondrial genome (kDNA) is composed of thousands of minicircles (around 10,000 of 1-kb) and maxicircles (50 of 22-kb) condensed in one structure. Maxicircles encode rRNA and respiratory chain subunits, most of which require post-transcriptional RNA editing to be functional. This RNA editing phenomenon was first discovered in trypanosomes and consists of addition and deletion of uridines (Us) in the pre-mRNA through interaction with guide RNAs (gRNAs) encoded by the minicircles. The editing process involves 1) an endonuclease cleavage of pre-mRNA, 2) addition of Us by a TUTase or deletion by an ExoUase, 3) ligation, 4) repetition until all of the sites specified by the gRNA are edited (Stuart et al., 2005; Hajduk and Ochsenreiter, 2010).



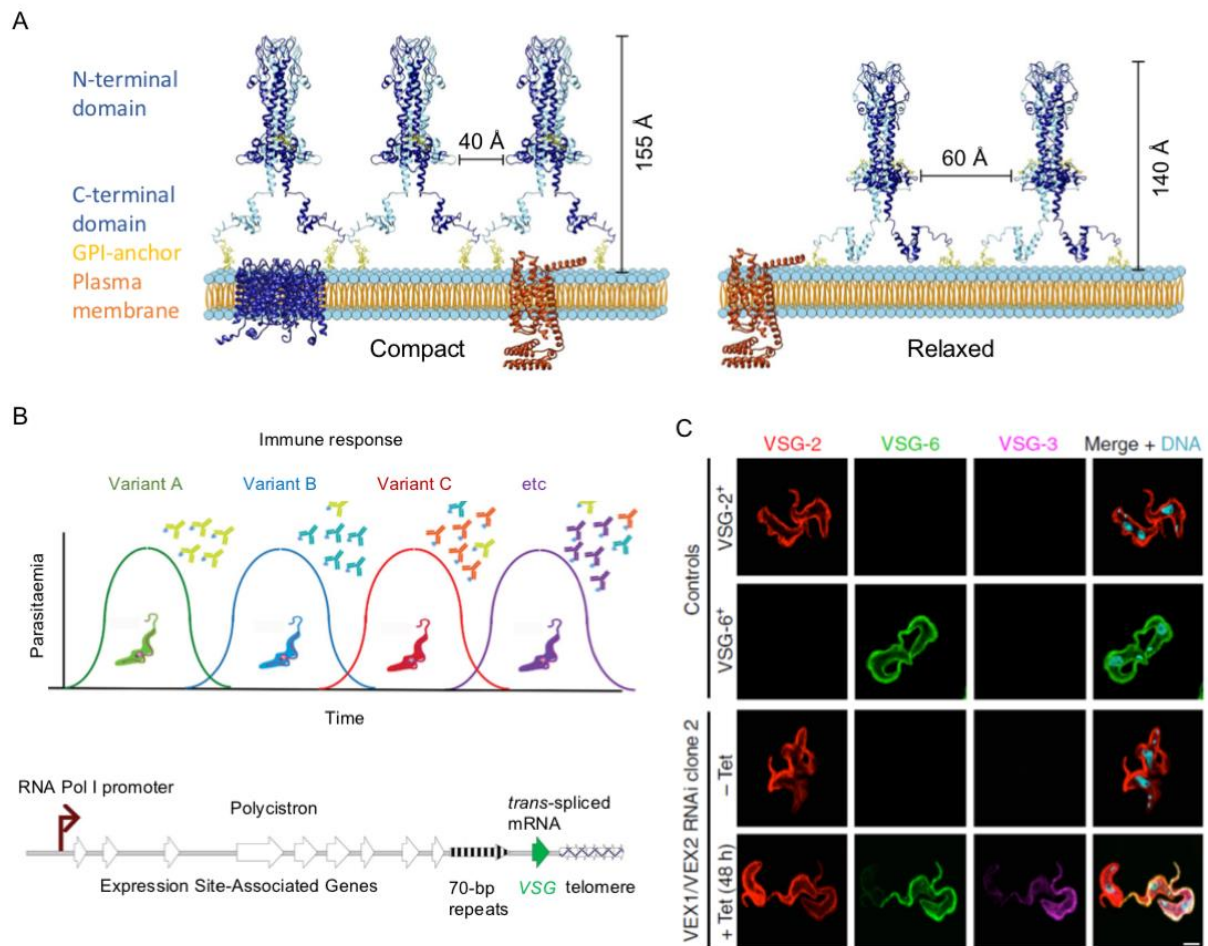


**Figure 1.10. The dynamic Variant Surface Glycoprotein (VSG) coat of *T. brucei* bloodstream forms.**

VSGs are homodimers that are attached to the plasma membrane *via* GPI anchors. The VSGs tightly packed (left) and relaxed conformations (right) are shown in panel A (From Bartossek et al., 2017). The antigenic variation (panel B) depends upon monoallelic and switchable VSG expression (From Horn, 2014). The allelic exclusion that governs the expression of VSG genes is coordinated by the VEX-complex (panel C). Depletion of this complex (VEX1/VEX2 RNAi mutant) yields multi-VSG expression (From Faria et al., 2019).

#### 1.4.5. Cell surface

The surface of *T. brucei* is covered by a dense coat of glycoconjugates forming a protective glycocalyx against the host defence systems that changes depending on the life cycle stage. The bloodstream form (BSF) is coated with a dense layer of variant surface glycoprotein (VSG) (Figure 1.10) while the procyclic form (PCF) is coated with procyclins (Figure 1.11). These families of proteins are anchored to the membrane via GPI anchors (Figure 1.13).

##### a) VSG

VSG is a highly abundant dimeric protein that represents 95% of all BSF surface protein molecules. Its N-terminal domain is connected to the C-terminal domain through a linker region that confers flexibility between domains. VSG can adopt a compact or relaxed conformation (Figure 1.10A) depending on the protein density along the surface and as a response mechanism to changes. Interestingly, VSG forms a mobile and flexible shield that acts as a protective barrier for other less variable or invariant proteins in the plasma membrane to avoid recognition by the immune system (Grunfelder et al., 2002; Horn, 2014; Bartossek et al., 2017).

Given that VSG is immunogenic, the parasites developed an immune evasion strategy involving a switch to express an antigenically distinct VSG, known as antigenic variation (Figure 1.10B). There are three mechanisms of antigenic variation: 1) a coupled transcriptional activation/inactivation of VSG expression site (ES), 2) replacement of the active VSG by homologous recombination and 3) homologous recombination between active and inactive ES (chromosome exchange) (Horn, 2014). Around 300 functionally complete VSG genes are available for expression, in addition to other ~2200 incomplete or partial genes (Cross et al., 2014), but only one VSG gene is transcribed at a time from one of the ~20 telomeric ES until switching. RNA polymerase I is recruited to VSG-ES promoters constituting the expression site body (ESB) (Navarro and Gull, 2001). VSG genes are adjacent to telomeres and most of them are preceded by 70-bp repeats that facilitate recombination and duplication of the genes (Horn, 2014).



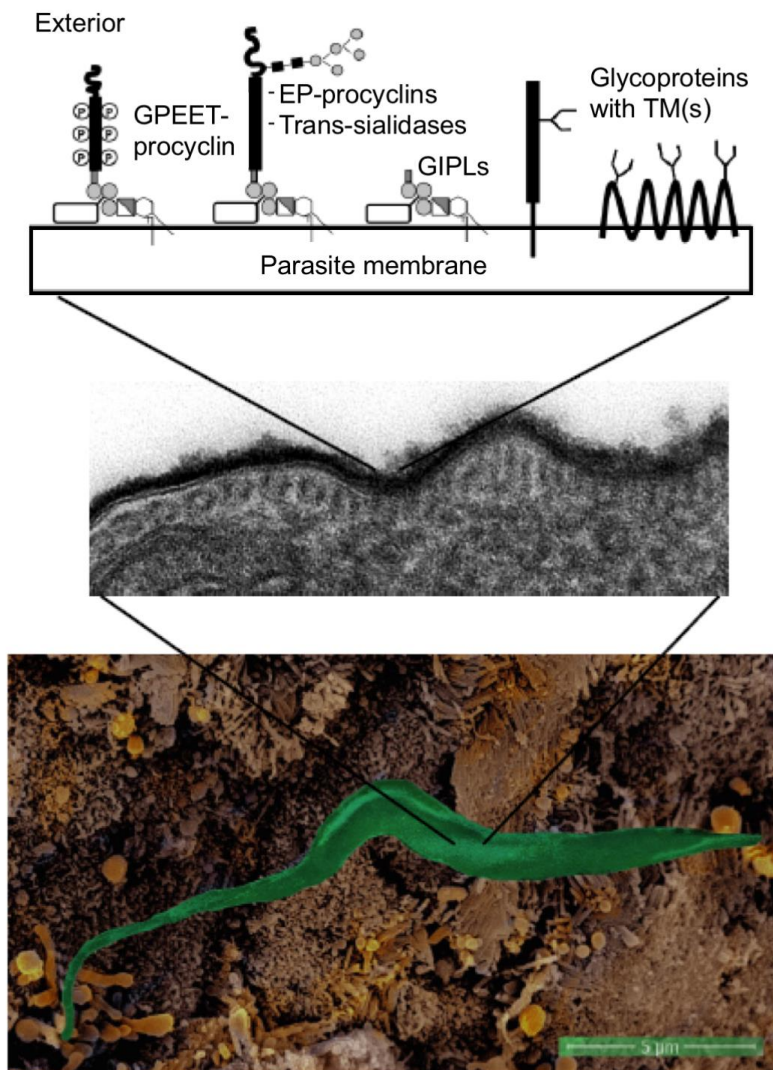


**Figure 1.11. Surface glycocalyx of *T. brucei* procyclic cells.**

A parasite interacting with the cell microvilli in the tsetse fly proventriculus is shown in the bottom panel. Transmission EM showing the surface glycocalyx (central panel). The main surface glycosylphosphatidylinositol (GPI)-anchored (EP- and GPEET-procyclicins and trans-sialidases) and transmembrane (including polytopic) glycoproteins and glycolipids are shown in the top panel. Open rectangles linked to GPI molecules represent side chains. GPIs: glycoinositolphospholipids, or free GPIs (From Rodrigues et al., 2015).

The allelic exclusion mechanism was recently shown to depend on the protein complex VEX1-VEX2 that associates with VSG, promotes transcription and transmits a silencing signal to negatively control transcription of other VSGs (Figure 1.10C). Additionally, it was shown that maintenance of the VEX complex and recruitment of the conserved chromatin assembly factor (CAF-1) during the S-phase allow inheritance of VSG exclusion (Faria et al., 2019).

VSGs can be N-glycosylated with different N-linked oligosaccharides depending on the VSG variant. Type I VSGs contain one N-glycosylation site where oligomannose structures (Man9–5GlcNAc2) are added. Type II VSGs generally have two N-glycosylation sites, one at the C-terminus occupied by a mixture of oligomannose structures similar to those from type II and larger polylactosamine-containing, while the internal site contains small structures like Man4–3GlcNAc2, GlcNAcMan3GlcNAc2 and in some cases, biantennary complex glycans. Type III VSGs have three sites of glycosylation occupied with a combination of oligomannose and complex biantennary glycans (Zamze et al., 1990, 1991; Mehlert, 1998). Additionally, VSGs can be O-glycosylated with a chain of zero to three O-linked hexoses on the top surface of the protein, which can play an immunomodulatory role (Pinger et al., 2018).

## **b) Procyclins**

During differentiation of stumpy to procyclic forms, the VSG molecules are cleaved by a protease and the coat is replaced with procyclic acidic repetitive proteins (PARPs), named procyclins, within hours (Matthews and Gull, 1994). There are two major forms of procyclin, EP and GPEET, which differ in the type of amino acid repeats in their C-terminal domains. EP procyclins have Glu-Pro repeats (Mowatt and Clayton, 1987; Roditi et al., 1987) and GPEET procyclins have Gly-Pro-Glu-Glu-Thr repeats (Mowatt et al., 1989).

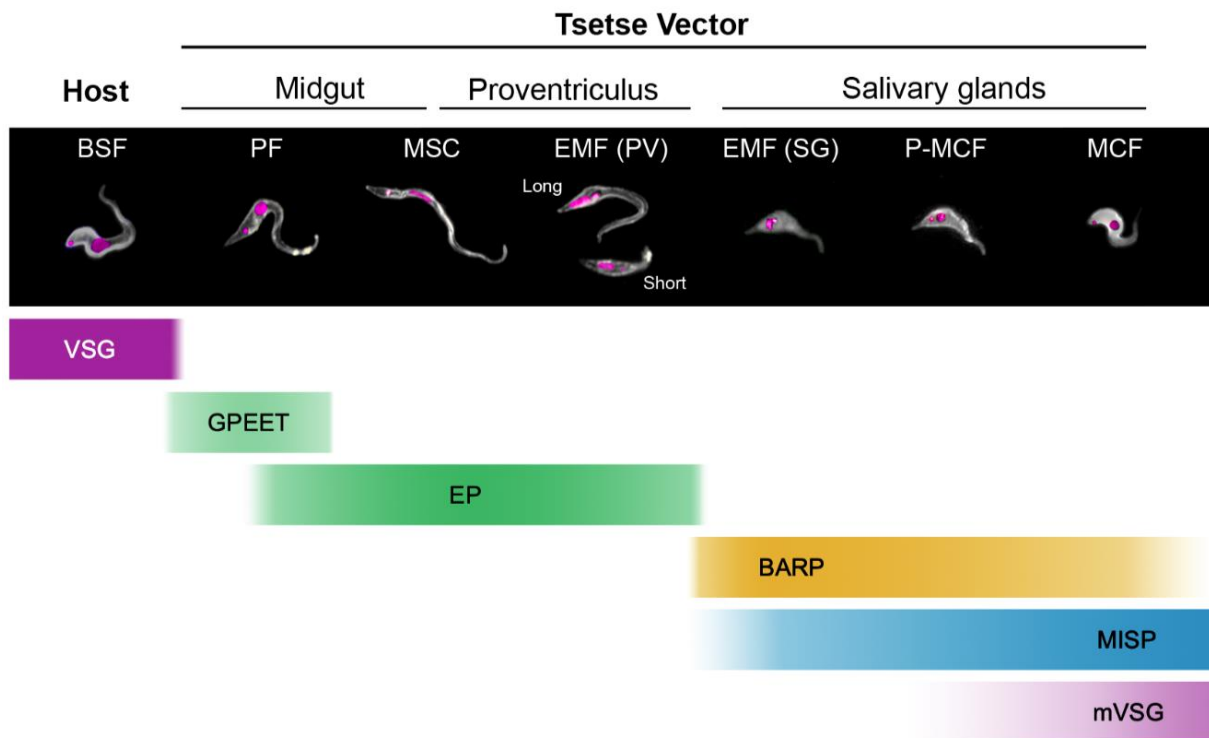


**Figure 1.12. Developmental expression of major surface glycoproteins.**

The top panel shows representative immunostaining images of the parasite stages. Nuclei and kinetoplasts (magenta) and cell surface (white) detected with antibodies corresponding to each surface molecule are highlighted. The bottom bars define the duration and intensity of the protein expression in the corresponding stage. Bloodstream forms (BSF), procyclic forms (PF), mesocyclic forms (MSC), short and long epimastigotes (EMF PV), attached epimastigotes colonising the salivary glands (EMF SG), pre-metacyclic forms (P-MCF) and metacyclic forms (MCF) (From preprint Casas-Sanchez et al., 2018).

There are eight copies of the *PARP* gene sequence per diploid genome encoding three PARP types: two EPs with or without an N-glycosylation site, respectively, and one GPEET with N-glycosylation sites (Mowatt and Clayton, 1987). Both types of procyclins adopt a highly extended rod-like structure (Figure 1.11) and their GPI anchors have an unusual lipid structure and large carbohydrate side chains made of branched polylactosamine repeats. In parasites grown in culture, a trans-sialidase substitutes the  $\beta$ -galactose termini of these side chains with sialic acid present in the fetal calf serum glycoconjugates (Mehlert, 1998). Interestingly, it was shown that the procyclins coating of parasites is not required to establish mature infections and complete the developmental cycle in the fly. However, the mutant analysed in this work lacking all the *PARP* genes showed a 10-fold reduced capacity of transmission and lower prevalence of salivary gland infections than with the wild type, suggesting that alterations of the membrane probably reduce migration and/or adherence of epimastigotes to the salivary glands (Vassella et al., 2009).

### **c) Other surface glycoproteins**

In addition to VSGs and procyclins, *T. brucei* surface has other glycoproteins in minor amounts like the transmembrane invariant surface glycoproteins (ISGs) (Ziegelbauer and Overath, 1992) or transporters, such as the transferrin receptor (TfR) (Mehlert et al., 2012). Epimastigote forms express a different family of GPI-anchored proteins called brucei alanine-rich proteins (BARPs) (Nolan et al., 2000). During metacyclogenesis, this BARP coat is progressively replaced by a novel family of hypothetical proteins called MISPs, which are invariant surface proteins exposed on the surface of metacyclics, along with VSG (Figure 1.12) (Casas-Sánchez et al., 2018). All these proteins are mostly N-glycosylated.

### **d) GPI anchors**

The essentiality of GPI biosynthesis was addressed in bloodstream and procyclic forms by disrupting the *TbGPI10* gene, which codes for a mannose transferase that transfers the third mannose to the forming GPI (Figure 1.13).

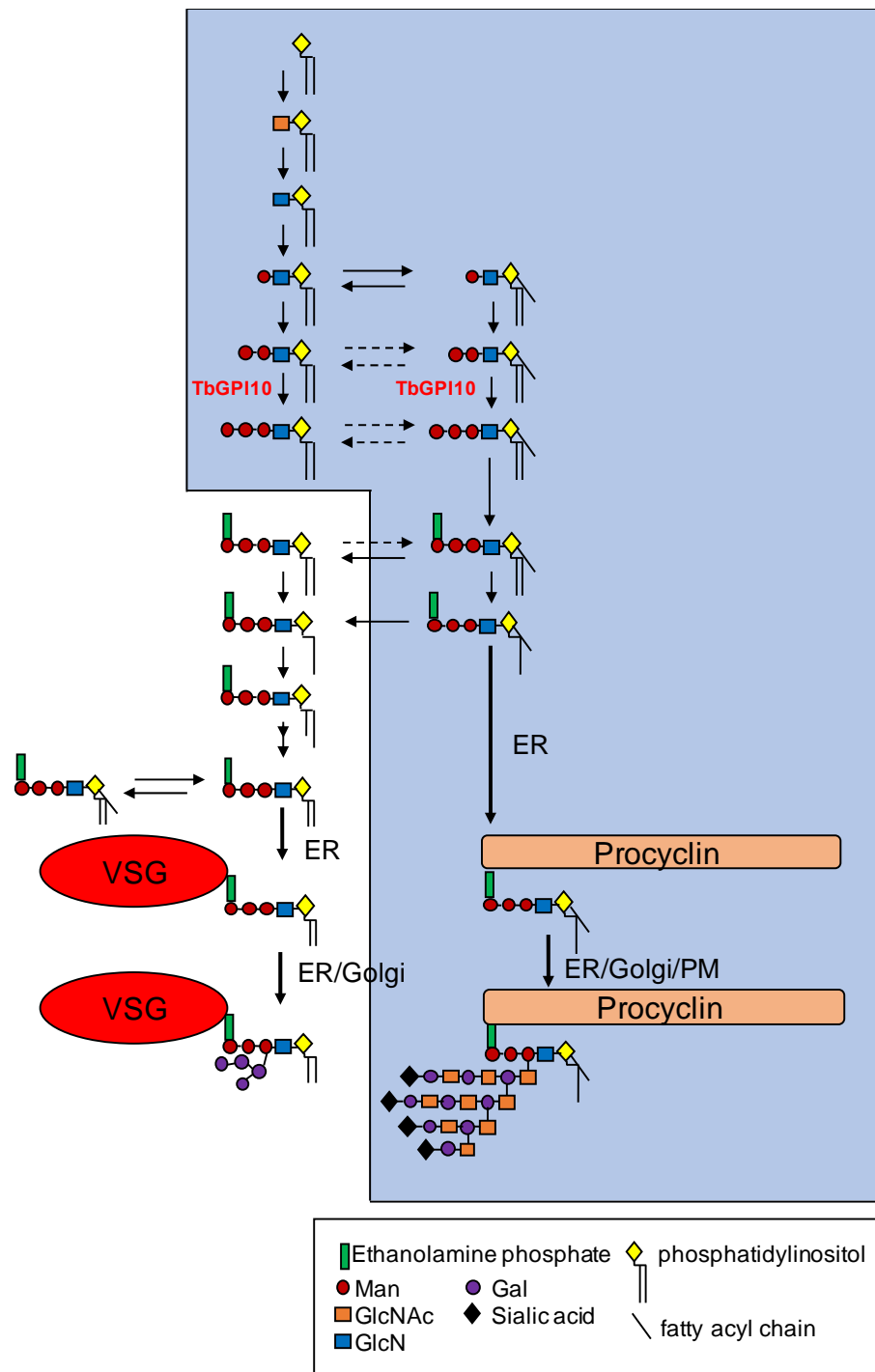


**Figure 1.13. The GPI biosynthetic pathway of *T. brucei*.**

The blue shaded area represents the pathway in procyclic cells and the nonshaded area represents the additional fatty acid remodelling steps (replacement by myristate) and attachment to VSG in bloodstream forms (From Ferguson, 2000).

In BSF, the expression of an extra copy of the *TbGPI10* gene was required for double knock-out cells to be viable, indicating that biosynthesis of GPI anchors is essential for BSF viability. In contrast, mutant PCF cells were able to grow and colonise the tsetse fly midgut, with lower efficiency than wild type cells (Nagamune et al., 2000). This is consistent with the results obtained for procyclin null mutants (Vassella et al., 2009).

*T. brucei* use different GPI structures to anchor VSGs and procyclins in the cell membrane, and the structures of both anchors have been characterised. The complex structure includes a backbone of ethanolamine-phosphate-6Man $\alpha$ 1-2Man $\alpha$ 1-6Man $\alpha$ 1-4GlcNac linked to an inositol phospholipid. In the VSG-GPI anchor, the diacylglycerol moiety suffers fatty-acid remodeling, by replacing the fatty acids by myristate, before transfer to VSG protein, with 1,2-dimyristylglycerol as final lipid (Ferguson et al., 1988). The preassembled GPI membrane anchor is then linked to a pre-VSG C-terminal domain by single-step reaction performed by a multisubunit transamidase complex. Finally, GPI can be glycosylated with branched side chains consisting of a variable number of  $\alpha$ -galactose residues attached to the O-3 position of the mannose residue adjacent to GlcN (Figure 1.13) (Mayor et al., 1992).

In the case of procyclic cells, the structures of procyclins GPEET and EP GPI anchors are very similar, with lipid moiety of 1-stearoyl-2-lyso-glycerol and large complex carbohydrate side chains containing galactose, N-acetylglucosamine and sialic acid. Moreover, the procyclin GPI anchor contains a fatty acid attached to the inositol ring (Field et al., 1991; Ferguson et al., 1993; Bütikofer et al., 1997).

## **1.5. Intermediate and energy metabolism**

*T. brucei* metabolism has been extensively studied due to its peculiar traits and the continuous research of drug targets to develop treatments against HAT. Within the metabolomics approaches currently existing, the two techniques principally used in the majority of references described in the next section are nuclear magnetic resonance (NMR) and mass spectrometry (GC-MS and LC-MS). Indeed, <sup>13</sup>C isotopic profiling strategies by NMR and MS have been applied to study the endo and exometabolome of parental as well as RNAi and null mutant trypanosomes incubated or cultured in the presence of <sup>13</sup>C-enriched carbon sources (Fatarova et al., 2016).

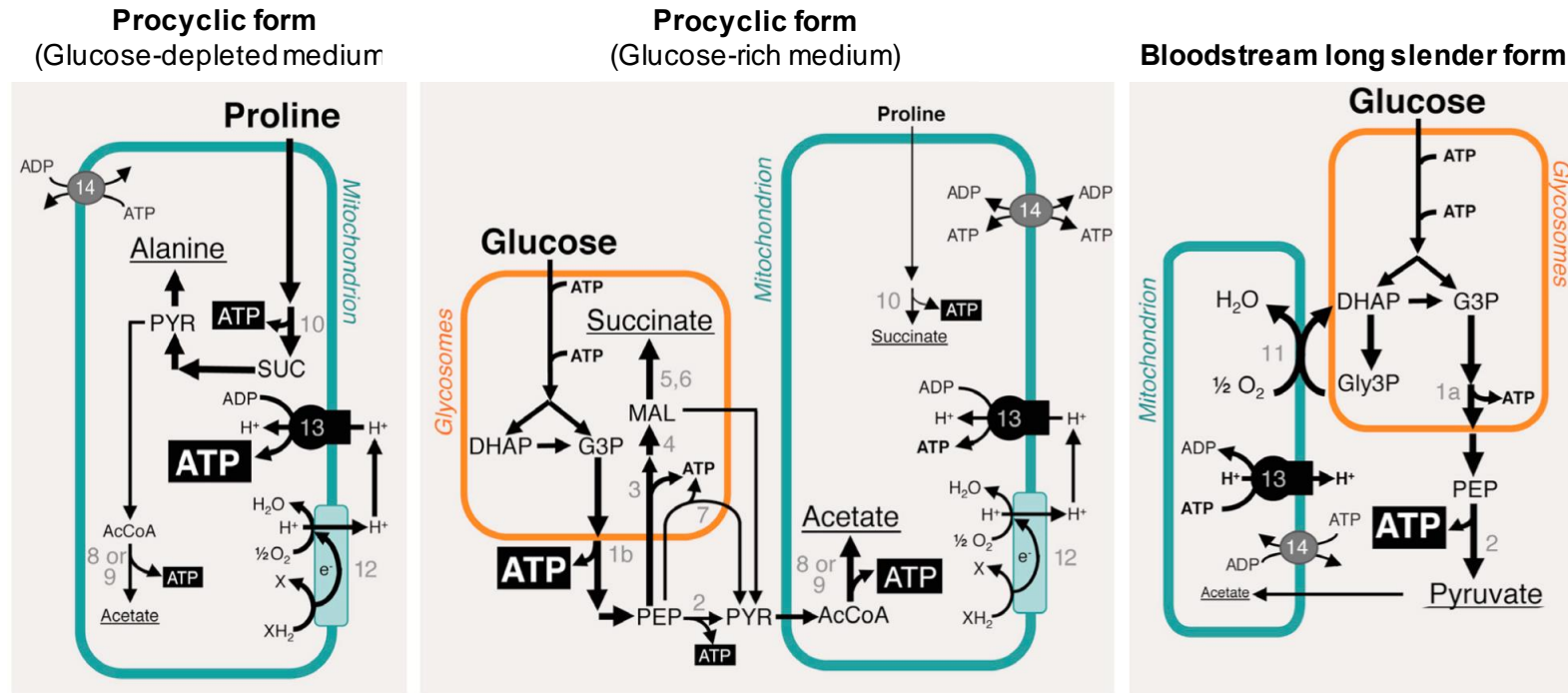


**Figure 1.14. ATP production in PCF and BSF trypanosomes.**

Catabolism of proline and/or glucose is shown. Excreted end products are underlined. Arrows thicknesses represent metabolic flux. Only key enzymes involved in ATP production are indicated here. Mitochondrial production of ATP by succinyl-CoA synthetase is not shown in the right panel (BSF) (From Smith et al., 2017).

**Enzymes:** 1a, glycosomal phosphoglycerate kinase; 1b, cytosolic phosphoglycerate kinase; 2, pyruvate kinase; 3, phosphoenolpyruvate carboxykinase; 4, glycosomal malate dehydrogenase; 5, cytosolic fumarase (for simplification this reaction is placed in the glycosome); 6, glycosomal NADH-dependent fumarate reductase; 7, pyruvate phosphate dikinase; 8, acetate:succinate CoA-transferase; 9, acetyl-CoA thioesterase; 10, succinyl-CoA synthetase; 11, trypanosome alternative oxidase; 12, respiratory chain; 13,  $F_0/F_1$ -ATP synthase; 14, mitochondrial ADP/ATP exchanger. **Abbreviations:** AcCoA, acetyl-CoA A; DHAP, dihydroxyacetone phosphate; G3P, glyceraldehyde 3-phosphate; Gly3P, glycerol 3-phosphate; MAL, malate; PEP, phosphoenolpyruvate; PYR, pyruvate; SUC, succinate

*T. brucei* adapts its metabolism to the available extracellular nutrients encountered during the life cycle within a mammalian host and tsetse fly insect vector. The long-slender bloodstream form mainly catabolises glucose while procyclic forms rely on amino acids metabolism, mostly proline. In the following section, I describe the main metabolic differences between these two life cycle stages.

### **1.5.1. Bloodstream vs procyclic, an overview**

The energy and carbon metabolism of PCF and BSF has been compared in a number of reviews (Bringaud et al., 2006; Michels et al., 2006; Tielens and van Hellemond, 2009; Bringaud, 2012; Creek et al., 2012; Smith et al., 2017). The next few lines highlight the main features of energy metabolism in these two parasitic forms of *T. brucei*. The single mitochondrion, approximately 40 - 60 glycosomes and cytosolic compartment are crucial to understand the differences between bloodstream (BSF) and procyclic (PCF) trypanosomes in terms of energy metabolism. As shown in Figure 1.14, PCF trypanosomes have an elaborate mitochondrion and are able to metabolise amino acids like proline, abundantly present in the fly. In contrast, the BSF mitochondrion is less developed and the parasites have developed a glycolysis-based metabolism from glucose abundantly present in the blood of the mammalian host. The production of ATP in BSF depends on glycolysis, whereof the first seven enzymes are compartmentalised in the glycosomes. The glycosomal membrane is impermeable to large (300 – 400 Da) metabolites, therefore consumption and production of ATP is balanced with no net ATP production inside the organelles. It is in the cytosol where the net ATP production from glycolysis takes place resulting in production and excretion of pyruvate. Besides, relatively low amounts of ATP are generated in the mitochondrion since oxidative phosphorylation does not occur. ATP production in the PCF varies depending on the carbon sources available, as it can be cultured in the presence or the absence of glucose. When glucose is absent, proline is metabolised in the mitochondrion and alanine is excreted as the main end product, in addition to glutamate, succinate and acetate. The reduced cofactors produced during proline metabolism are reoxidised in the respiratory chain and ATP is mainly produced by oxidative phosphorylation, in addition to substrate phosphorylation through the action of the enzyme succinyl-CoA synthetase. However, *in vitro* cultured PCF trypanosomes prefer to use glucose to support their central carbon metabolism. Indeed, in glucose-



rich conditions, proline metabolism is significantly down-regulated and the production of ATP occurs mostly *via* glucose breakdown.

### **1.5.2. Energy metabolism of PCF**

The central metabolic network of PCF is adapted to the metabolism of glucose, glycerol and proline as main carbon sources (Ryley, 1962; Bringaud et al., 2006; Bringaud, 2012; Allmann et al., 2019), in addition to threonine and glutamine (Figure 1.15) (Cross et al., 1975; Millerioux et al., 2013). The potentiality of TCA cycle intermediates as carbon sources has also been described. Among them,  $\alpha$ -ketoglutarate, succinate, malate and fumarate, have been shown to stimulate oxygen consumption of PCF (Ryley, 1962) and  $\alpha$ -ketoglutarate stimulates respiration and sustains mobility of the stumpy forms (Vickerman, 1965; Flynn and Bowman, 1973; Bienen et al., 1993; Dewar et al., 2018). How these TCA cycle intermediates are metabolised and what role, if any, do they have in the insect environment is still an open question. A part of my PhD thesis addresses this question.

#### **a) Glucose metabolism**

PCF parasites have been adapted to *in vitro* axenic culture in the glucose-rich semi-defined SDM79 medium, which contains 6 mM glucose as well as 5 mM of proline. Remarkably, these parasites preferentially consume glucose and down-regulate proline metabolism in the presence of glucose (Lamour et al., 2005).

Glucose uptake is facilitated by two membrane transporters that are differentially expressed during the life cycle. BSF expresses predominantly THT1, a low affinity transporter with high capacity to exploit the high amounts of glucose present in the mammalian serum, while PCF expresses a higher affinity transporter (THT2) (Barrett, 1998). Once in the glycosomes, glucose is phosphorylated by hexokinase (HK). Part of the glucose 6-phosphate feeds 1) the pentose phosphate pathway (PPP) which produces NADPH, involved in protection against oxidative stress, and ribose 5-phosphate, used for nucleotide biosynthesis (Heise and Oppendoes, 1999), as well as 2) biosynthesis of sugar nucleotides (see section 1.8.1).

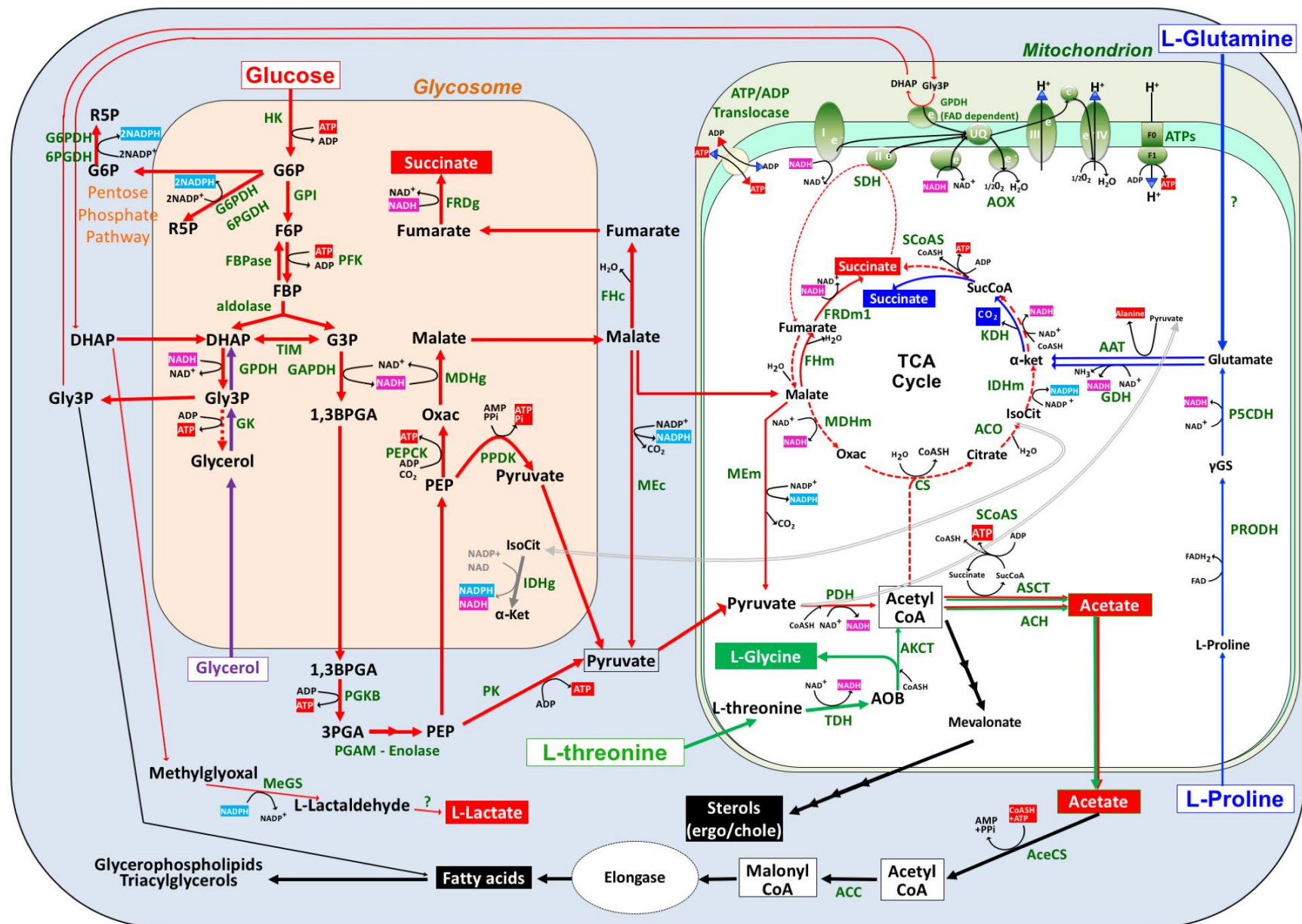


**Figure 1.15. Intermediate metabolism of PCF trypanosomes in glucose rich conditions.**

The colour code of the arrows represents metabolism of glucose (red), glycerol (purple), threonine (green), proline and glutamine (blue). The excreted end products are highlighted in white with colour background corresponding to the carbon sources. Glycosome is represented in red. For the mitochondrion, the matrix is represented in white, the inner membrane in green, the intermembrane space in light green and the outer membrane as a black line. Metabolic steps occurring at the background level or not at all are represented by dotted lines.

**Abbreviations:** 1,3BPGA, 1,3-bisphosphoglycerate; 3PGA, 3-phosphoglycerate; ADP, adenosine diphosphate; AMP, adenosine monophosphate; ATP, adenosine triphosphate; AOB, amino oxobutyrate; C, cytochrome c; CoASH, coenzyme A; DHAP, dihydroxyacetone phosphate; e, electrons; F6P, fructose 6-phosphate; FAD, flavine adenine dinucleotide; FBP, fructose 1,6-bisphosphate; G3P, glyceraldehyde 3-phosphate; G6P, glucose 6-phosphate; Gly3P, glycerol 3-phosphate; IsoCit, isocitrate;  $\alpha$ -ket,  $\alpha$ -ketoglutarate; NAD, nicotinamide adenine dinucleotide; NADP, nicotinamide adenine dinucleotide phosphate; Oxac, oxaloacetate; PEP, phosphoenolpyruvate; Pi, inorganic phosphate; PPi, inorganic pyrophosphate; R5P, ribose 5-phosphate;  $\gamma$ GS, glutamate- $\gamma$ -semialdehyde; SucCoA, succinyl-CoA; UQ, ubiquinone pool.

**Enzymes:** HK, hexokinase; G6PDH, glucose-6-phosphate dehydrogenase; 6PGDH, 6-phosphogluconate dehydrogenase; GPI, glucose 6-phosphate isomerase; PFK, phosphofructokinase; FBPase, fructose-1,6-bisphosphatase; TIM, triose-phosphate isomerase; GPDH, glycerol-3-phosphate dehydrogenase; GK, glycerol kinase; GAPDH, glyceraldehyde-3-phosphate dehydrogenase; PGKB, phosphoglycerate kinase B; PGAM, phosphoglycerate mutase; PK, pyruvate kinase; PEPCK, phosphoenolpyruvate carboxykinase; PPK, pyruvate phosphate dikinase; MDH, malate dehydrogenase (g: glycosomal, m: mitochondrial); FH, fumarase (c: cytosolic, m: mitochondrial); FRD, NADH-dependent fumarate reductase (g: glycosomal, m: mitochondrial); ME, malic enzyme (c: cytosolic, m: mitochondrial); PDH, pyruvate dehydrogenase complex; ASCT, acetate:succinate CoA-transferase; ACH, acetyl-CoA thioesterase; SCoAS, succinyl-CoA synthetase; CS, citrate synthase; ACO, aconitase; IDH, isocitrate dehydrogenase; KDH,  $\alpha$ -ketoglutarate dehydrogenase; SDH, succinate dehydrogenase (respiratory chain complex II); PRODH, L-proline dehydrogenase; P5CDH, pyrroline-5-carboxylate dehydrogenase; AAT, alanine aminotransferase; GDH, glutamate dehydrogenase; TDH, L-threonine dehydrogenase; AKCT, 2-amino-3-ketobutyrate CoA-transferase; AceCS, acetyl-CoA synthetase; ACC, acetyl-CoA carboxylase; MeGS, methylglyoxal reductase; AOX, alternative oxidase; I, II, III, IV, respiratory chain complexes; F<sub>0</sub>F<sub>1</sub>-ATP synthase.

Interestingly, the two glycolytic ATP consuming enzymes, HK and PFK, lack feedback regulation by their products (Nwagwu and Opperdoes, 1982; Michels et al., 2006) which in other organisms prevents the risk of accumulation of hexose phosphates. In trypanosomatids, the glycosomal compartmentalisation of the first glycolytic steps within glycosomes makes feedback regulation of HK and PFK redundant. HK and PFK do not sense the net ATP produced in glycolysis by PYK in the cytosol and ATP consumption and production in the glycosomes are balanced. Therefore, HK and PFK are not undergoing activation by ATP with a risk to exceed the activity of the downstream enzymes (Haanstra et al., 2008, 2014).

The consecutive steps of the pathway lead to production of 1,3-bisphosphoglycerate (1,3BPGA) which is then transferred to the cytosol to be converted in 3-phosphoglycerate (3PGA) by one of the three phosphoglycerate kinase isoforms, PGKB, expressed in PCF (Figure 1.15). The other two proteins are located in the glycosomes. PGKA is expressed in both BSF and PCF at low levels and its role is not clear for *T. brucei* cells (Alexander and Parsons, 1993), while PGKC is only expressed in BSF (Osinga et al., 1985; Colasante et al., 2007).

Up to this point of the pathway, two molecules of ATP have been consumed by HK and PFK, and two molecules of NADH have been produced by GAPDH per molecule of glucose consumed. As stated before, the redox ( $\text{NAD}^+/\text{NADH}$ ) and energy (ATP/ADP) balances need to be maintained within glycosomes. To this end, part of the phosphoenolpyruvate (PEP) produced in the cytosol from 3PGA enters the glycosomes, where it is substrate of both the pyruvate phosphate dikinase (PPDK) and phosphoenolpyruvate carboxykinase (PEPCK) enzymes. In the first case, PEP is converted into pyruvate by PPDK with production of ATP inside glycosomes. In the second case, PEP is converted into oxaloacetate by PEPCK with the concomitant production of ATP followed by regeneration of  $\text{NAD}^+$  by NADH-dependent dehydrogenases. Indeed, oxaloacetate is reduced into malate by the glycosomal malate dehydrogenase which reoxidises NADH. Then, malate leaves the glycosomes to be converted by the cytosolic fumarase (Fhc) into fumarate (Coustou et al., 2006), which enters the glycosome to be reduced to succinate by the NADH-dependent fumarate reductase (FRDg) (Besteiro et al., 2002). This pathway, named “succinic fermentation” contributes to the maintenance of redox balance through reoxidation of

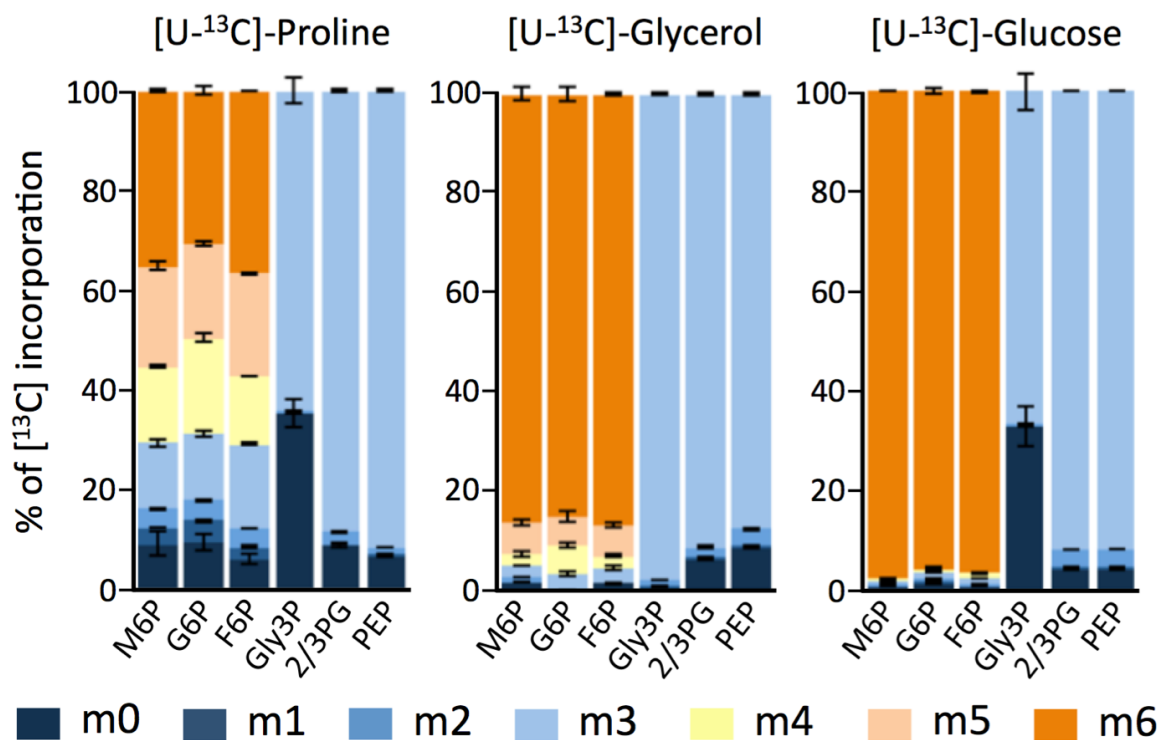


**Figure 1.16.  $[\text{U}-^{13}\text{C}]$  enrichment of key glycolytic intermediates from proline, glycerol or glucose.**

An IC-MS/MS analysis of intracellular metabolites after isotopic labelling with  $[\text{U}-^{13}\text{C}]$ -labelled carbon sources at 2 mM is shown. The percentage of  $^{13}\text{C}$  incorporation is shown for intermediates at 0 to 6 carbon positions (m0 to m6, colour code indicated below). Abbreviations: G6P, glucose 6-phosphate; F6P, fructose 6-phosphate; Gly3P, glycerol 3-phosphate; M6P, mannose 6-phosphate; 2/3PG, 2- or 3-phosphoglycerate (these two metabolites are undistinguished by IC-MS/MS); PEP, phosphoenolpyruvate (From Wagnies et al., 2018).

NADH. Most of the excreted succinate from glucose metabolism is produced by this glycosomal “succinic fermentation”, however a significant part is produced in the mitochondrion from the glycosomally produced malate by the subsequent actions of FHm and FRDm (Coustou et al., 2005).

The PEP produced in the cytosol is also used in the mitochondrial acetate production pathway. This involves production of pyruvate plus ATP in the cytosol catalysed by pyruvate kinase (PK). It is important to notice that disruption of PK activity in cells cultured in glucose conditions is lethal, since this enzyme is crucial for production and maintenance of the cellular ATP levels (Coustou et al., 2003).

Pyruvate produced from PEP is also imported into the mitochondrion where the pyruvate dehydrogenase complex (PDH) produces acetyl-CoA. The oxidation of this glucose-derived acetyl-CoA through the TCA cycle has not been observed in *T. brucei* (van Weelden et al., 2003). In fact, aconitase ( $\Delta$ aco) depleted cells grow at the same rate as WT cells in standard glucose-rich medium and no differences in excreted end products from glucose were observed. Additionally, only negligible amounts of radiolabelled CO<sub>2</sub> coming from WT and  $\Delta$ aco cells incubated with [6-<sup>14</sup>C]-D-glucose were detected (van Weelden et al., 2003). In consequence, no function has been attributed to the oxidative branch of the cycle suggesting that the TCA enzymes do not run as a cycle (van Weelden et al., 2005). The inability of malate and pyruvate to stimulate respiration further supported this notion (Verner et al., 2013). Nevertheless, the functionality of the oxidative branch in other cell cycle stages within the fly or under specific conditions remains to be elucidated. Alternatively, two redundant enzymes, acetyl-CoA thioesterase (ACH) and acetate:succinate CoA-transferase (ASCT) are responsible for acetate production from acetyl-CoA, most of which is ultimately excreted. ASCT also participates in the mitochondrial ATP production through the ASCT/SCoAS cycle (Van Hellemond et al., 1998; Rivière et al., 2004; Millerioux et al., 2012).



**Figure 1.17. Proline metabolism of PCF trypanosomes in glucose-depleted conditions.**

The excreted end products from proline metabolism are highlighted in white with blue background. Glycosome is represented in red. For the mitochondrion, the matrix is represented in white, inner membrane in green, intermembrane space in light green and the outer membrane as a black line. Hypothetical metabolic steps are represented by dotted lines.

**Abbreviations:** 1,3BPGA, 1,3-bisphosphoglycerate; 3PGA, 3-phosphoglycerate; ADP, adenosine diphosphate; AMP, adenosine monophosphate; ATP, adenosine triphosphate; C, cytochrome c; CoASH, coenzyme A; DHAP, dihydroxyacetone phosphate; e, electrons; F6P, fructose 6-phosphate; FAD, flavine adenine dinucleotide; FBP, fructose 1,6-bisphosphate; G3P, glyceraldehyde 3-phosphate; G6P, glucose 6-phosphate; IsoCit, isocitrate;  $\alpha$ -ket,  $\alpha$ -ketoglutarate; NAD, nicotinamide adenine dinucleotide; NADP, nicotinamide adenine dinucleotide phosphate; Oxac, oxaloacetate; PEP, phosphoenolpyruvate; Pi, inorganic phosphate; PPi, inorganic pyrophosphate;  $\gamma$ GS, glutamate- $\gamma$ -semialdehyde; SucCoA, succinyl-CoA; UQ, ubiquinone pool.

**Enzymes:** GPI, glucose-6-phosphate isomerase; FBPase, fructose-1,6-bisphosphatase; TIM, triose-phosphate isomerase; GAPDH, glyceraldehyde-3-phosphate dehydrogenase; PGKB, phosphoglycerate kinase B; PGAM, phosphoglycerate mutase; PK, pyruvate kinase; PEPCK, phosphoenolpyruvate carboxykinase; PPDCK, pyruvate phosphate dikinase; MDH, malate dehydrogenase (g: glycosomal, m: mitochondrial); FH, fumarase (c: cytosolic, m: mitochondrial); FRD, NADH-dependent fumarate reductase (g: glycosomal, m: mitochondrial); ME, malic enzyme (c: cytosolic, m: mitochondrial); PDH, pyruvate dehydrogenase complex; ASCT, acetate:succinate CoA-transferase; ACH, acetyl-CoA thioesterase; SCoAS, succinyl-CoA synthetase; CS, citrate synthase; ACO, aconitase; IDH, isocitrate dehydrogenase; KDH,  $\alpha$ -ketoglutarate dehydrogenase; SDH, succinate dehydrogenase (respiratory chain complex II); PRODH, L-proline dehydrogenase; P5CDH, pyrroline-5-carboxylate dehydrogenase; AAT, alanine aminotransferase; GDH, glutamate dehydrogenase; AOX, alternative oxidase; I, II, III, IV, respiratory chain complexes; F<sub>0</sub>F<sub>1</sub>-ATP synthase.



### **b) Glycerol metabolism**

Glycerol stimulates oxygen uptake, supports growth of PCF cells (Ryley, 1962; van Weelden et al., 2005) and represents an alternative gluconeogenic source when glucose is absent and gluconeogenesis from proline is blocked (Wagnies et al., 2018) (Figure 1.16).

More recently, it has been shown in PCF trypanosomes that glycerol metabolism exerts a catabolic repression over glucose metabolism, since glucose is no longer consumed in the presence of equimolar amounts of glycerol. Indeed, a large excess of GK activity in the glycosomes, which compete with HK for the same glycosomal ATP pool results in a regulation of nutrient utilisation. This new mechanism was called “metabolic contest” (Allmann et al., 2019).

### **c) Proline metabolism and TCA cycle**

In the tsetse fly, glucose is only available during blood meals for a short period of time (Vickerman, 1985), while proline is present (1-2 mM) and synthesized within the insect where it is used for the flight process (Balogun, 1974; Bursell, 1981). Therefore, proline represents the main carbon and energy source used *in vivo* by PCF trypanosomes (Figure 1.17). The optimisation of a glucose-depleted medium for *in vitro* culture opened the door to establish the importance of proline as carbon source (Lamour et al., 2005; Coustou et al., 2008; Wagnies et al., 2018). Remarkably, both proline transport and metabolism are down-regulated in the presence of glucose, since the rate of proline consumption increases up to 6-fold when parasites are cultured in the absence of glucose (Lamour et al., 2005).

Proline is transported into the cells in an active manner by a single transporter ( $K_m = \sim 19 \mu\text{M}$ ) not yet identified (L'Hostis et al., 1993). In the mitochondrion, proline is oxidised to  $\Delta^1$ -pyrroline-5-carboxylate (P5C) by proline dehydrogenase (PRODH), an enzyme encoded by a single gene (Tb927.7.210) that is associated to the inner membrane of the organelle and transfers electrons *via* its FAD cofactor to the electron transport chain. The growth of a knock-down PRODH mutant was shown to be affected only in glucose-depleted conditions (Table 1.2) (Lamour et al., 2005).

Enzymatic step	Cell line	Growth in + Glucose + Proline	Growth in - Glucose + Proline	Reference
PRODHD	<i>RNAi</i> PRODHD.i	WT	Not viable	1
P5CDH	<i>RNAi</i> P5CDH.i	WT	Affected	2
AAT	<i>RNAi</i> AAT.i $\Delta aat$	WT Affected	Affected ND	3
KDH	<i>RNAi</i> KDH-E2.i	WT	ND	4
SCoAS	<i>RNAi</i> SCoAS.i	Arrested	ND	4
SDH	<i>RNAi</i> SDH.i	WT	Not viable	4, 5
FRDg/m	<i>RNAi</i> FRDg/m.i	WT	WT	6, 5
FHc/m	<i>RNAi</i> FHc/m.i	Not viable	Not viable	7, 5
MDH	-	-	-	-
CS	-	-	-	-
ACO	$\Delta aco$	WT	ND	8, 5
IDHm	-	-	-	-
MEEm	<i>RNAi</i> MEEm.i	Arrested	ND	9
MEC/m	<i>RNAi</i> MEC/m.i	Not viable	Not viable	9, 5
PDH	<i>RNAi</i> PDH-E1 <i>RNAi</i> PDH-E2	WT	WT	4, 5
ASCT	<i>RNAi</i> ASCT.i $\Delta asct$	WT WT	ND ND	10
ACH	$\Delta ach$	WT	ND	10
ASCT/ACH	$\Delta ach$ / <i>RNAi</i> ASCT.i	Arrested	ND	10

**Table 1.2. Effect of proline metabolism and TCA cycle enzymes disruption on PCF growth.**

The growth of mutant cell lines was evaluated in glucose-rich or depleted conditions. Growth affected: doubling time strongly increased compared with wild type (WT) cells; Growth arrested: parasites stop dividing but do not die (during growth curve); Not viable: cells die (within 2 weeks); ND: not determined; -: No information available.

References: <sup>1</sup>(Lamour et al., 2005), <sup>2</sup>(Mantilla et al., 2017), <sup>3</sup>(Spitznagel et al., 2009), <sup>4</sup>(Bochud-Allemann and Schneider, 2002), <sup>5</sup>(Coustou et al., 2008), <sup>6</sup>(Coustou et al., 2005), <sup>7</sup>(Coustou et al., 2006), <sup>8</sup>(van Weelden et al., 2003), <sup>9</sup>(Allmann et al., 2013), <sup>10</sup>(Millerioux et al., 2012).

In the next step of the pathway (Figure 1.17), P5C is hydrolysed non-enzymatically to glutamate- $\gamma$ -semialdehyde ( $\gamma$ GS) which is oxidised to glutamate by the NAD-dependent P5C dehydrogenase (P5CDH). This enzyme was recently shown to be essential for PCF growth in glucose-depleted conditions *in vitro* and for infection and survival of parasites in the tsetse midgut, confirming that proline metabolism is required for development and infectivity within the fly (Mantilla et al., 2017).

The glutamate is then used together with pyruvate in a transamination reaction catalysed by alanine aminotransferase (AAT) that produces  $\alpha$ -ketoglutarate ( $\alpha$ -ket) and the final excreted product alanine. This enzyme is essential for PCF even in the presence of glucose (Spitznagel et al., 2009). In *T. cruzi* epimastigotes, glutamate is converted into  $\alpha$ -ket by the glutamate dehydrogenase (GDH) (Cazzulo et al., 1979). The two GDH isoforms (NAD<sup>+</sup> and NADP<sup>+</sup> dependent) can also incorporate NH<sub>3</sub> into  $\alpha$ -ket to produce glutamate (Caldas et al., 1980). Although one gene coding for a GDH has been identified in *T. brucei* BSF, its metabolic role has not been addressed so far (Estévez et al., 1999).

$\alpha$ -ket is then converted into succinyl-CoA by the  $\alpha$ -ketoglutarate dehydrogenase (KDH) complex. This complex is composed of an  $\alpha$ -keto acid dehydrogenase subunit (E1), an acyltransferase subunit (E2) and a dihydrolipoamide dehydrogenase subunit (E3). Interestingly, the subunit E2 is also expressed in BSF trypanosomes, where it plays an essential role in kDNA distribution during cytokinesis (Sykes and Hajduk, 2013). Targeting the E2 subunit by RNAi showed that KDH is not essential for PCF cells grown in standard glucose conditions, however, essentiality has not been addressed in glucose-depleted conditions (Bochud-Allemann and Schneider, 2002).

Succinyl-CoA is converted into succinate by the succinyl-CoA synthetase (SCoAS) with production of ATP by substrate level phosphorylation. Down-regulation of SCoAS expression is lethal for PCF trypanosomes in glucose-rich conditions (Bochud-Allemann and Schneider, 2002). As mentioned above, this enzyme also participates in the ASCT/SCoAS cycle for ATP and acetate production (Van Hellemond et al., 1998; Bochud-Allemann and Schneider, 2002; Mochizuki et al., 2020).

Succinate produced by SCoAS feeds the respiratory chain through succinate dehydrogenase (SDH) with production of fumarate. SDH knock-down cells do not excrete alanine from proline and are not viable in the absence of glucose (Coustou et al., 2008).

The additional presence of a mitochondrial NADH-dependent fumarate reductase (FRDm), which is used to produce succinate from carbohydrate breakdown, is consistent with a previous hypothesis proposing the existence of a FRDm/SDH cycle acting as a NADH dehydrogenase by transferring electrons from NADH to the respiratory chain (Turrens, 1989). The activity of this hypothetical FRDm/SDH cycle has never been demonstrated so far.

Malate is produced from fumarate by the mitochondrial fumarase (FHm), whose down-regulation results in a 3.4- fold decrease of alanine excretion from proline (Coustou et al., 2006). Malate is then converted into pyruvate by three different routes: 1) the mitochondrial malic enzyme (ME<sub>m</sub>), 2) the cytosolic malic enzyme (ME<sub>c</sub>) and 3) a branch that involves MDH<sub>g</sub>, PEPCK and the cytosolic PYK or the glycosomal PPDK (Coustou et al., 2008). The malic enzymes also play key roles in NADPH production in the cytosol and the mitochondrion, but only the mitochondrial isoform is essential for the cells (Allmann et al., 2013).

The pyruvate produced can serve as a substrate for alanine aminotransferase to produce alanine or as described above for the pyruvate dehydrogenase complex (PDH) to produce acetyl-CoA. Production of acetyl-CoA and the acetate from proline metabolism is not essential for the parasites, since knocking down PDH has no effect on their growth (Coustou et al., 2008). As observed under glucose-rich conditions, there is no evidence in the literature that proline-derived acetyl-CoA is further metabolised through the TCA cycle.

These glucose-depleted conditions provided a tool to study gluconeogenesis in this parasite (Wagnies et al., 2018). Thus, it has recently been shown that labelled [U-<sup>13</sup>C]-proline incorporates into key gluconeogenic intermediates of parental cells (Figure 1.16), while this <sup>13</sup>C-incorporation was abolished in the  $\Delta ppdk/\Delta pepck$  double knock-out mutant. This confirmed that production of PEP from pyruvate through PPDK or from malate, through MDH and PEPCK, both contribute to production of glycolytic intermediates from proline (Wagnies et al., 2018).

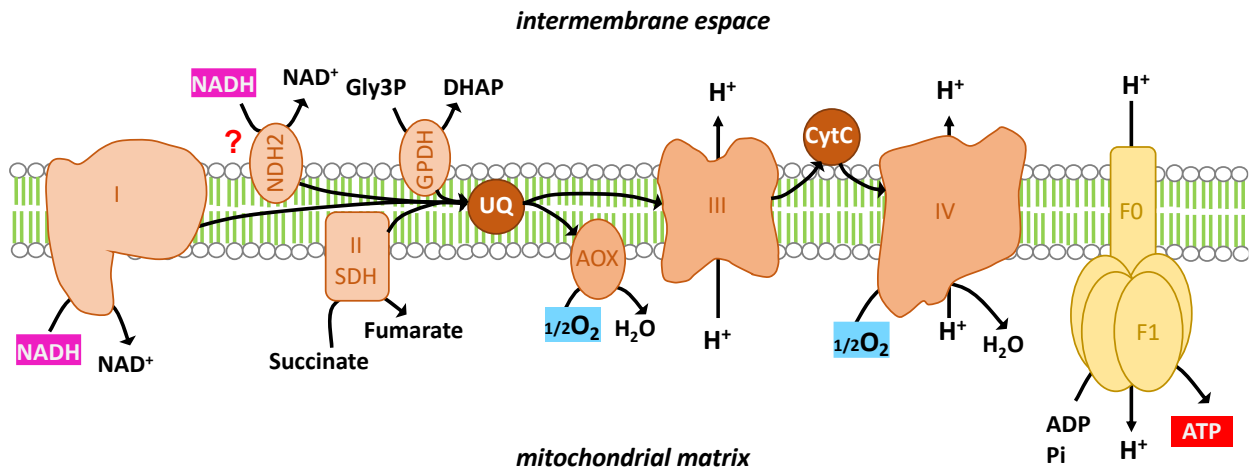


**Figure 1.18. Respiratory chain of *T. brucei*.**

Complex I, complex II - succinate dehydrogenase (SDH), type-II NADH dehydrogenase (NDH<sub>2</sub>) and the FAD-dependent glycerol-3-phosphate dehydrogenase (GPDH) transfer electrons from reduced equivalents to ubiquinone (UQ). Electrons from reduced UQ are then transferred to: 1) complex III, then cytochrome C (CytC) and complex IV to reduce molecular O<sub>2</sub> to H<sub>2</sub>O, or 2) an alternative oxidase (AOX) that catalyses the reduction of O<sub>2</sub> to H<sub>2</sub>O. Electron transfer through complexes III and IV is coupled to H<sup>+</sup> translocation from the mitochondrial matrix to the intermembrane space. The electrochemical proton gradient is used to produce ATP by the F<sub>0</sub>F<sub>1</sub>-ATP synthase. (?) The role of NDH<sub>2</sub> is debated since Verner et al. (2013) and Surve et al. (2017) showed that the enzyme is facing the intermembrane space (see figure) and the matrix (not illustrated here) of the mitochondrion, respectively (From Souza Bombaça et al., 2019).

#### **d) Metabolism of other amino acids**

Threonine is metabolised in the mitochondrion by the consecutive action of L-threonine dehydrogenase (TDH) and 2-amino-3-ketobutyrate CoA-transferase (AKCT), producing equimolar amounts of glycine and acetate (Linstead et al., 1977; Millerioux et al., 2013, 2018). Threonine is similarly consumed in the presence or absence of glucose at relatively high rate, comparable to that of glucose and much higher than that of proline (Cross et al., 1975; Lamour et al., 2005). Threonine is also the preferred carbon source for fatty acid and sterol biosynthesis (Millerioux et al., 2013, 2018). It is important to notice that, unlike proline, threonine cannot support growth of procyclic cells (Lamour et al., 2005).

Glutamine is also consumed by PCF at a similar rate as proline and is metabolised to glutamate by an unidentified enzymatic step (Cross et al., 1975; Coustou et al., 2003; Johnston et al., 2019).

#### **e) Respiratory chain and mitochondrial ATP production**

ATP can be produced by different pathways in the PCF mitochondrion. As mentioned before, SCoAS is essential as it is involved in ATP production by substrate level phosphorylation from proline and glutamine metabolism, as well as by the ASCT/SCoAS cycle coupled to acetate formation. ATP is also produced by oxidative phosphorylation with the respiratory chain complexes coupled to ATP synthase. Together with the ASCT/SCoAS cycle, both pathways supply sufficient mitochondrial ATP for survival and growth of the parasites (Millerioux et al., 2012).

In addition to the classical electron transport chain complexes I, II, III and IV, several enzymes contribute to electron transfer in the membrane of *T. brucei* mitochondria, but not directly to the proton gradient, *i.e.* glycerol-3-phosphate dehydrogenase (GPDH) (Oppenheimer et al., 1977b; Guerra et al., 2006), alternative rotenone-insensitive NADH:Q oxidoreductase (NDH2) (Fang and Beattie, 2002; Verner et al., 2013; Surve et al., 2017) and alternative oxidase (AOX) (Clarkson et al., 1989). Interestingly, trypanosome has the peculiarity of being able to reduce NADH through the respiratory chain without generating a transmembrane proton gradient. Indeed, complex I (NADH:ubiquinone oxidoreductase), which is active but non-essential for PCF or BSF cells (Verner et al., 2011) as well as the plant-like AOX are not involved in proton translocation (Figure 1.18).

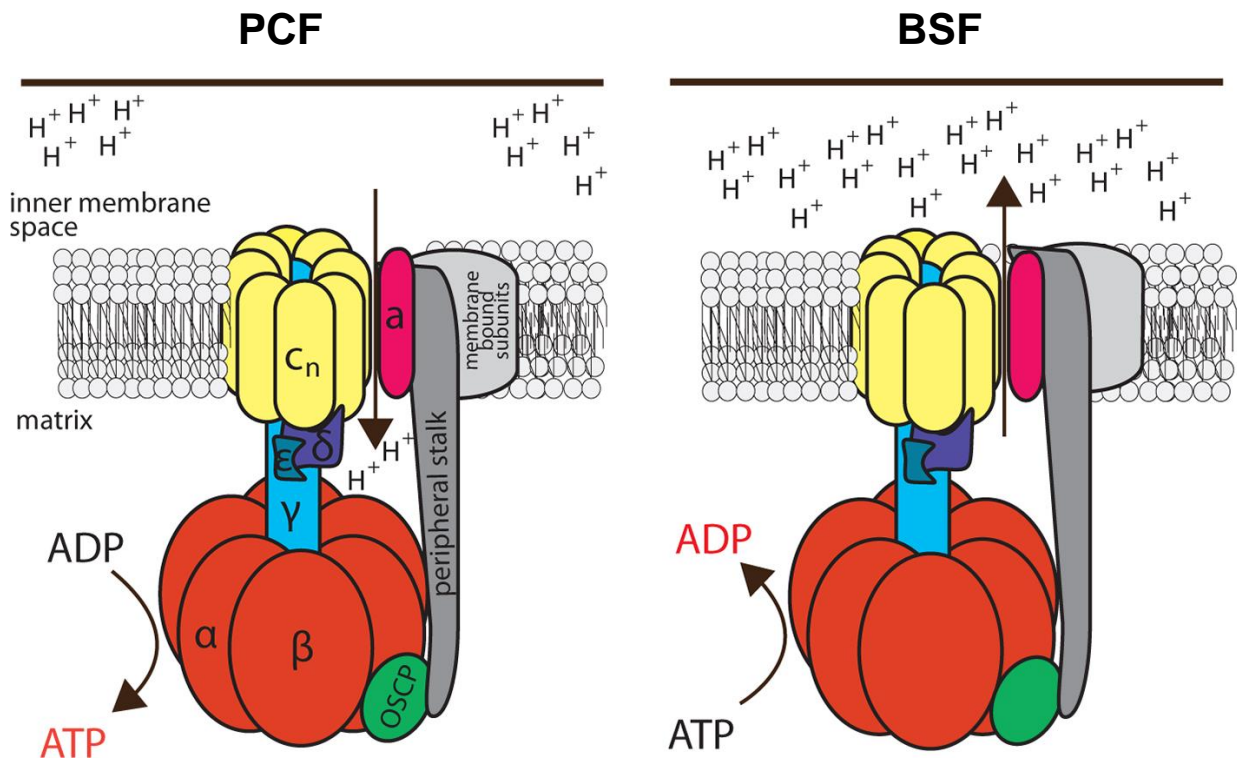


**Figure 1.19. F<sub>0</sub>F<sub>1</sub>-ATP synthase/ATPase complex in *T. brucei* mitochondria.**

In PCF, the F<sub>0</sub>F<sub>1</sub>-ATP synthase couples transmembrane proton transfer with ATP synthesis, while in BSF it works in the reverse direction, hydrolysing ATP to generate the mitochondrial membrane potential ( $\Delta\psi_m$ ) and pH gradient in the absence of canonical cytochrome-containing respiratory complexes.

Orthologues of the coloured subunits ( $\alpha$ ,  $\beta$ ,  $\gamma$ ,  $\delta$ ,  $\epsilon$ , OSCP, a and c) have been annotated in trypanosomes. Homologous of the peripheral stalk b, F6 and d subunits (dark grey) have not been identified in the *T. brucei* genome. Membrane-bound subunits A6L, e, f and g (light grey) are absent in *T. brucei* (From Šubrtová et al., 2015).

Succinate acts as a main substrate for oxidative phosphorylation, with complex II (SDH) loading the respiratory chain with electrons, however SDH is essential only in the absence of glucose (Coustou et al., 2008). Complexes III and IV, which pump protons out of the mitochondrial matrix, are essential for parasite growth since individual knock-down cell lines show decreased membrane potential and oxygen consumption. Interestingly, in these mutant cell lines the electron flow is partially redirected to AOX whose levels increased by 2-fold (Horváth et al., 2005).

Finally, the  $F_0F_1$ -ATP synthase couples transmembrane proton transfer with ATP synthesis (Figure 1.19). Some of the proteins from  $F_0$  and  $F_1$  subunits have been characterised (Zíková et al., 2009). The essentiality of this complex seems to depend on glucose concentrations and strains used. For instance, the EATRO1125 and 427 strains are 1000 times more sensitive to oligomycin in the absence of glucose than in glucose-rich conditions (Lamour et al., 2005) and knocking down the EATRO1125  $F_1$ - $\beta$  subunit is only lethal in glucose-depleted conditions, which suggest that oxidative phosphorylation is exclusively essential in the absence of glucose (Coustou et al., 2008). In contrast, knocking down ATPase subunits is lethal in three different mutants of the 29-13 cell line of the 427 strain in the presence of glucose, suggesting that the ATPase essentiality in these growth conditions is strain dependent (Zíková et al., 2009).

### **1.5.3. Energy metabolism of BSF**

Slender BSF depend on glycolysis for energy metabolism, with a negligible TCA cycle and respiratory chain activity (Figure 1.20). However, recent studies show that metabolism of glucose results in excretion of additional products other than pyruvate, such as acetate, alanine and succinate, and that enzymes involved in their production are essential, suggesting that BSF metabolism is significantly more complex than expected (Spitznagel et al., 2009; Mazet et al., 2013; Creek et al., 2015).

Moreover, it was recently shown that BSF trypanosomes can survive and grow using glycerol instead of glucose as carbon source for ATP production and gluconeogenesis (Kovářová et al., 2018; Pineda et al., 2018). This particularly may be relevant for parasites present in extravascular compartments like the skin and adipose tissue (Caljon et al., 2016; Capewell et al., 2016; Trindade et al., 2016).



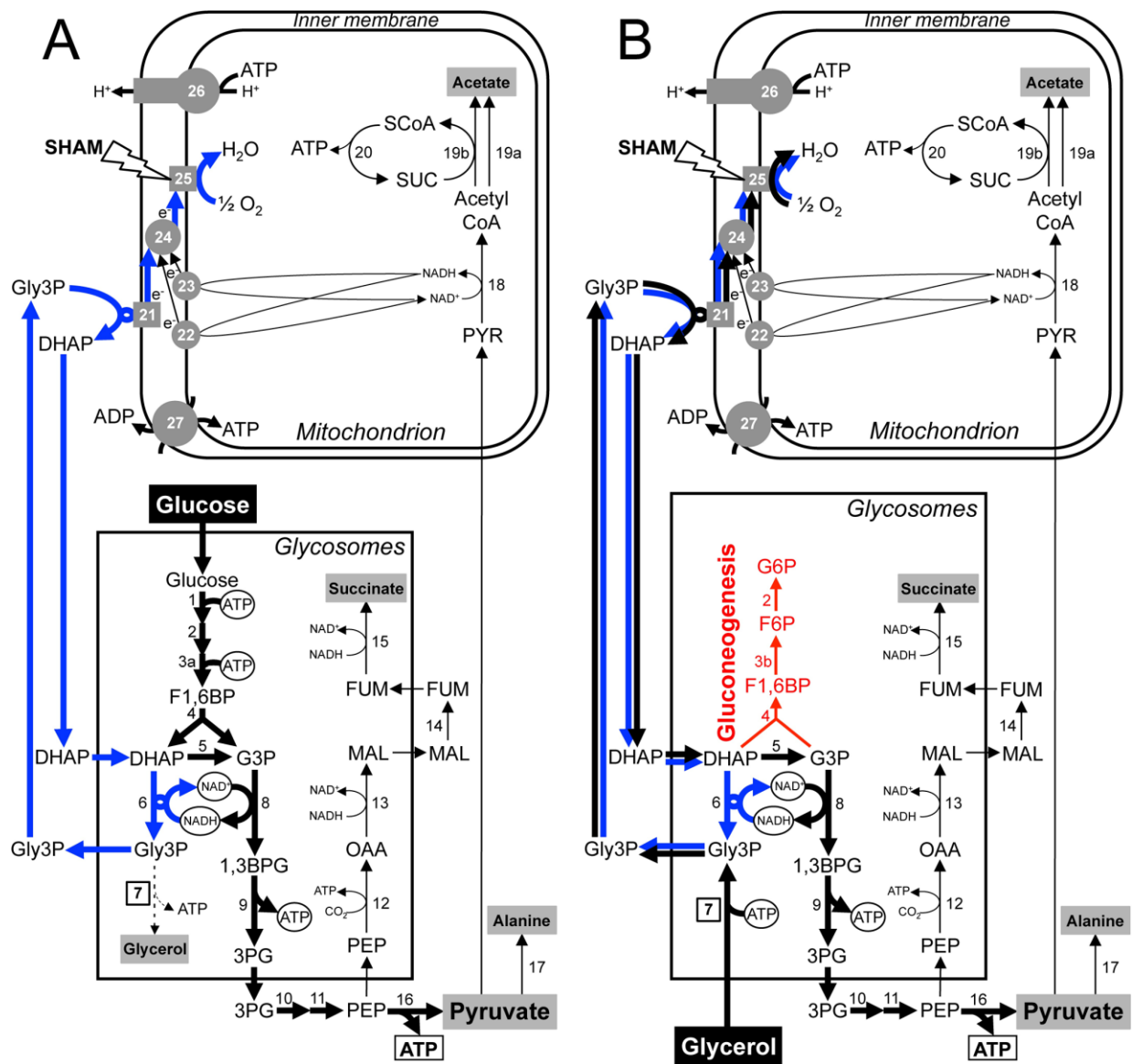


**Figure 1.20. Glucose and glycerol aerobic metabolism of BSF trypanosomes.**

Glucose metabolism in BSF trypanosomes grown in glucose-rich medium (CMM\_Glc) is shown in panel A, while panel B shows glycerol metabolism in the absence of glucose (CMM\_Glyc/GlcNAc). Arrow thickness represents the approximately 10-fold higher metabolic flux in glycolysis (down to pyruvate) compared to that of pathways leading to succinate, acetate and alanine. End products excreted are highlighted in grey. In Panel A, the GK step involved in glycerol production from glucose only under anaerobiosis is represented by dotted lines. The pathway used to maintain the glycosomal redox balance is highlighted by blue arrows. The same pathway is used for conversion of glycerol-derived Gly3P into DHAP (black arrows in panel B). The target of the SHAM metabolic drug (alternative oxidase) is indicated and the gluconeogenesis from glycerol is shown in red (From Pineda et al., 2018).

**Abbreviations:** DHAP, dihydroxyacetone phosphate; e<sup>-</sup>, electrons; FBP, fructose 1,6-bisphosphate; 1,3BPG, 1,3-bisphosphoglycerate; FUM, fumarate; F6P, fructose 6-phosphate; G3P, glyceraldehyde 3-phosphate; G6P, glucose 6-phosphate; Gly3P, glycerol 3-phosphate; MAL, malate; OAA, oxaloacetate; PEP, phosphoenolpyruvate; 3PG, 3-phosphoglycerate; PYR, pyruvate; SCoA, succinyl-CoA; SHAM, salicylhydroxamic acid; SUC, succinate.

**Enzymes:** 1, hexokinase; 2, glucose-6-phosphate isomerase; 3a, phosphofructokinase; 3b, fructose-1,6-bisphosphatase; 4, aldolase; 5, triose-phosphate isomerase; 6, glycerol-3-phosphate dehydrogenase; 7, glycerol kinase; 8, glyceraldehyde-3-phosphate dehydrogenase; 9, phosphoglycerate kinase; 10, phosphoglycerate mutase; 11, enolase; 12, phosphoenolpyruvate carboxykinase; 13, glycosomal malate dehydrogenase; 14, fumarase; 15, NADH-dependent fumarate reductase; 16, pyruvate kinase; 17, L-alanine aminotransferase; 18, pyruvate dehydrogenase complex; 19a, acetyl-CoA thioesterase; 19b, acetate:succinate CoA-transferase; 20, succinyl-CoA synthetase; 21, mitochondrial FAD-dependent glycerol-3-phosphate dehydrogenase; 22, rotenone-sensitive NADH dehydrogenase (complex I of the respiratory chain); 23, rotenone-insensitive NADH dehydrogenase; 24, ubiquinone pool; 25, alternative oxidase (AOX); 26, mitochondrial F<sub>0</sub>/F<sub>1</sub>-ATP synthase; 27, mitochondrial ADP/ATP exchanger.

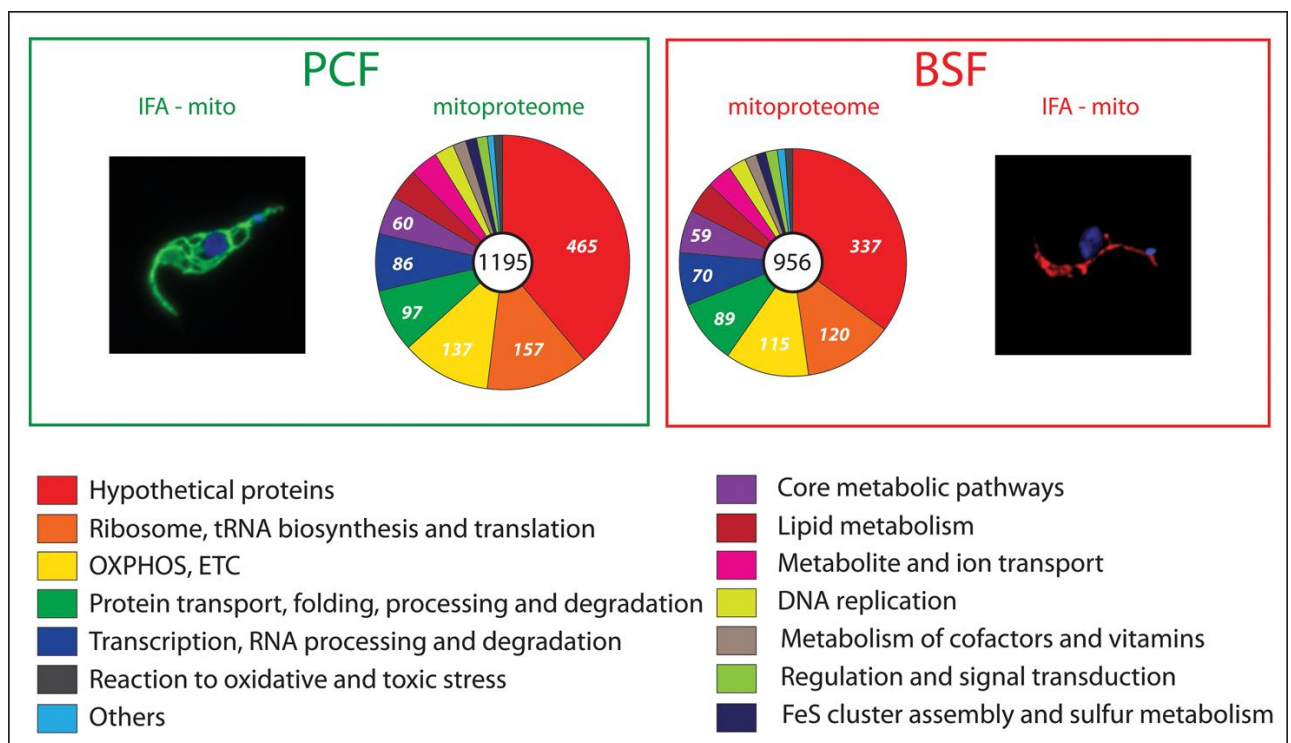


**Figure 1.21. Mitochondrial morphology and proteome of PCF and BSF**

Distribution of mass spectrometry-identified mitochondrial proteins in PCF and BSF trypanosomes in terms of molecular functions. Different colours show different metabolic pathways and categories. The PCF mitochondrion is extensively reticulated and cristae-rich while the BSF organelle has a tube-shaped cristae-poor morphology. IFA-mito: immunofluorescence analysis with the mitochondrial Hsp70 marker (From Zíková et al., 2017).

Finally, an unexpectedly wide range of mitochondrial proteins (80% of those expressed in PCF) was found to be expressed in BSF trypanosomes using proteomic approaches, suggesting that BSF mitochondrion might possess a wider metabolic flexibility (Figure 1.21). BSF and PCF mitochondria may be qualitatively similar but quantitatively very different (Zíková et al., 2017).

#### **a) Glucose metabolism**

BSF trypanosomes have been adapted to *in vitro* axenic culture in the glucose-rich IMDM medium, which contains 10 mM glucose, similar to what is found in the blood of the mammalian host (5 mM glucose). These forms of the parasite generate ATP *via* glycolysis, and the first 7 glycolytic enzymes comprise up to 90% of the total glycosomal protein content (Misset et al., 1986).

As mentioned for PCF, the redox and ATP/ADP balances are maintained inside the glycosomes but in different ways. The NADH produced by the glyceraldehyde-3-phosphate dehydrogenase (GAPDH) is reoxidised by the Gly3P:DHAP (glycerol-3-phosphate: dihydroxyacetone phosphate) shuttle. This shuttle consists of two enzymes: the mitochondrial FAD-dependent glycerol-3-phosphate dehydrogenase (GPDH) and the glycosomal NAD-dependent GPDH (Figure 1.20) (Opperdoes et al., 1977b; Clarkson et al., 1989). The Gly3P produced inside glycosomes from DHAP by the NAD-dependent GPDH is translocated to the mitochondrion where it is reoxidised to DHAP by the FAD-dependent GPDH. This GPDH activity is coupled to AOX by transferring electrons to oxygen *via* the ubiquinone pool (Clarkson et al., 1989). Finally, the DHAP produced by the mitochondrion re-enters the glycosomes to continue the pathway up to production of pyruvate. To maintain the ATP/ADP balance, BSF relies on the PGK activity (PGKC) localised inside the glycosomes which produces ATP, compensating for the two ATP molecules used by HK and PFK in the beginning of glycolysis (Osinga et al., 1985; Colasante et al., 2007).

BSF trypanosomes consume glucose 10 times faster than PCF, resulting in excretion of mainly pyruvate (85% of total products) in addition to alanine (9%), acetate (5%) and succinate (1%) (Mazet et al., 2013). As mentioned above, the pathways leading to production of these three minor end products are essential. For instance, ALAT seems to be essential since attempts to generate a knock-out failed (Spitznagel et al., 2009).

Blocking acetate production from glucose in the *RNAi*PDH-E2 mutant had no effect on parasite viability and growth. Indeed, acetate can also be produced from threonine, as showed by the lethality of the  $\Delta tdh/ RNAi$ PDH.i. cell line. TDH is the first step of the threonine degradation pathway, indicating that production of acetate and/or acetyl-CoA in the mitochondrion is essential for BSF (Mazet et al., 2013).

Finally, the first enzyme of the glycosomal succinate production pathway (PEPCK) is expressed in BSF, though at a much lower level than in PCF. More importantly, down-regulation of PEPCK expression results in reduction of succinate excretion from glucose and growth arrest (Creek et al., 2015).

### **b) Mitochondrial metabolism and ATP production**

BSF trypanosomes lack the conventional cytochrome-mediated respiratory chain (complexes III and IV), relying on the AOX to accept electrons from ubiquinol and reduce oxygen to water. This process is not coupled to proton translocation, so AOX does not participate in the production of mitochondrial membrane potential ( $\Delta\psi_m$ ). The  $F_0F_1$ -ATP synthase/ATPase is responsible for maintaining the  $\Delta\psi_m$  by an ATP hydrolytic activity coupled to proton translocation outside the mitochondrion (Figure 1.19). This ATPase activity is essential for growth of the parasites. The ATP generated from glycolysis is therefore imported into the mitochondrion by an ADP/ATP carrier (AAC) to be mainly used by the ATPase (Nolan and Voorheis, 1992; Schnauffer et al., 2005). Interestingly, the recent production of viable AAC null mutants unable to establish  $\Delta\psi_m$  when supplied with ATP suggests that ATP should be produced by substrate phosphorylation inside the BSF mitochondrion to sustain the reverse ATPase activity. Indeed, the ASCT/SCoAS cycle seems to play this role, since the SCoAS null mutant is 40-times more sensitive to an AAC inhibitor compared to parental cells. Although this mutant is viable, its virulence was reduced in the mouse model (Dolezenova et al., 2019). This once again highlights the unexpected metabolic flexibility and capacity of BSF.



### Figure 1.22. Glycosomal metabolic pathways – Part 1.

Enzymatic reactions are indicated by black arrows. Dashed arrows indicate the absence of experimental proof for the glycosomal activity. Enzymes highlighted in white boxes have no identified glycosomal candidate protein. Grey arrows indicate transport or diffusion processes. Excreted metabolites from glucose degradation are indicated by black boxes. Colour code for pathways: blue,  $\beta$ -oxidation; red, ether-linked lipid synthesis; green, glycolysis/gluconeogenesis; purple, pentose phosphate pathway; brown, trypanothione cascade (From Allman and Bringaud, 2017).

**Abbreviations:**  $\alpha$ KG,  $\alpha$ -ketoglutarate; 1,3BPGA, 1,3-bisphosphoglycerate; 3PGA, 3-phosphoglycerate; 6PGL, 6-phosphogluconolactone; 6PG, 6-phosphogluconate; AOX, alternative oxidase; CoA, coenzyme A; DHAP, dihydroxyacetone phosphate; F1,6BP, fructose 1,6-bisphosphate; F6P, fructose 6-phosphate; Fum, fumarate; G3P, glyceraldehyde 3-phosphate; G6P, glucose 6-phosphate; GAT1, glycosomal ABC transporter 1; Gly3P, glycerol 3-phosphate; isocit, isocitrate; Mal, malate; Oxac, oxaloacetate; P, glycosomal pore; PEP, phosphoenolpyruvate; PPi, pyrophosphate; PPP, pentose phosphate pathway; Rib5P, ribulose 5-phosphate; T[SH]<sub>2</sub>, trypanothione (reduced); TS<sub>2</sub>, trypanothione (oxidised); UQ, ubiquinone pool.

**Enzymes:** 1, hexokinase; 2, glucose-6-phosphate isomerase; 3, phosphofructokinase; 4, fructose-1,6-bisphosphatase; 5, aldolase; 6, triose-phosphate isomerase; 7, glyceraldehyde-3-phosphate dehydrogenase; 8a glycosomal (in BSF) or 8b cytosolic (in PCF) phosphoglycerate kinase; 9, phosphoglycerate mutase and enolase; 10, pyruvate kinase; 11, pyruvate phosphate dikinase; 12, phosphoenolpyruvate carboxykinase; 13, glycosomal malate dehydrogenase; 14, cytosolic CoA (and glycosomal) fumarase; 15, glycosomal NADH-dependent fumarate reductase; 16, glycerol-3-phosphate dehydrogenase; 17, glycerol kinase; 18, FAD-dependent glycerol-3-phosphate dehydrogenase; 19, cytosolic malic enzyme; 20, glucose-6-phosphate dehydrogenase; 21, 6-phosphogluconolactonase; 22, 6-phosphogluconate dehydrogenase; 23, glycosomal isocitrate dehydrogenase; 24, acyl-CoA reductase; 25, DHAP acyltransferase; 26, alkyl-DHAP synthase; 27, acyl/alkyl-DHAP reductase; 28, acyl-CoA dehydrogenase; 29, 2,4-dienoyl reductase; 30 $\alpha$ , 2-enoyl-CoA hydratase/3-hydroxyacyl dehydrogenase; 30 $\beta$ ,  $\beta$ -ketothiolase; 31, trypanothione reductase; 32, tryparedoxin; 33, tryparedoxin peroxidase; 34, acyl-CoA synthetase; 35, adenylate kinase.



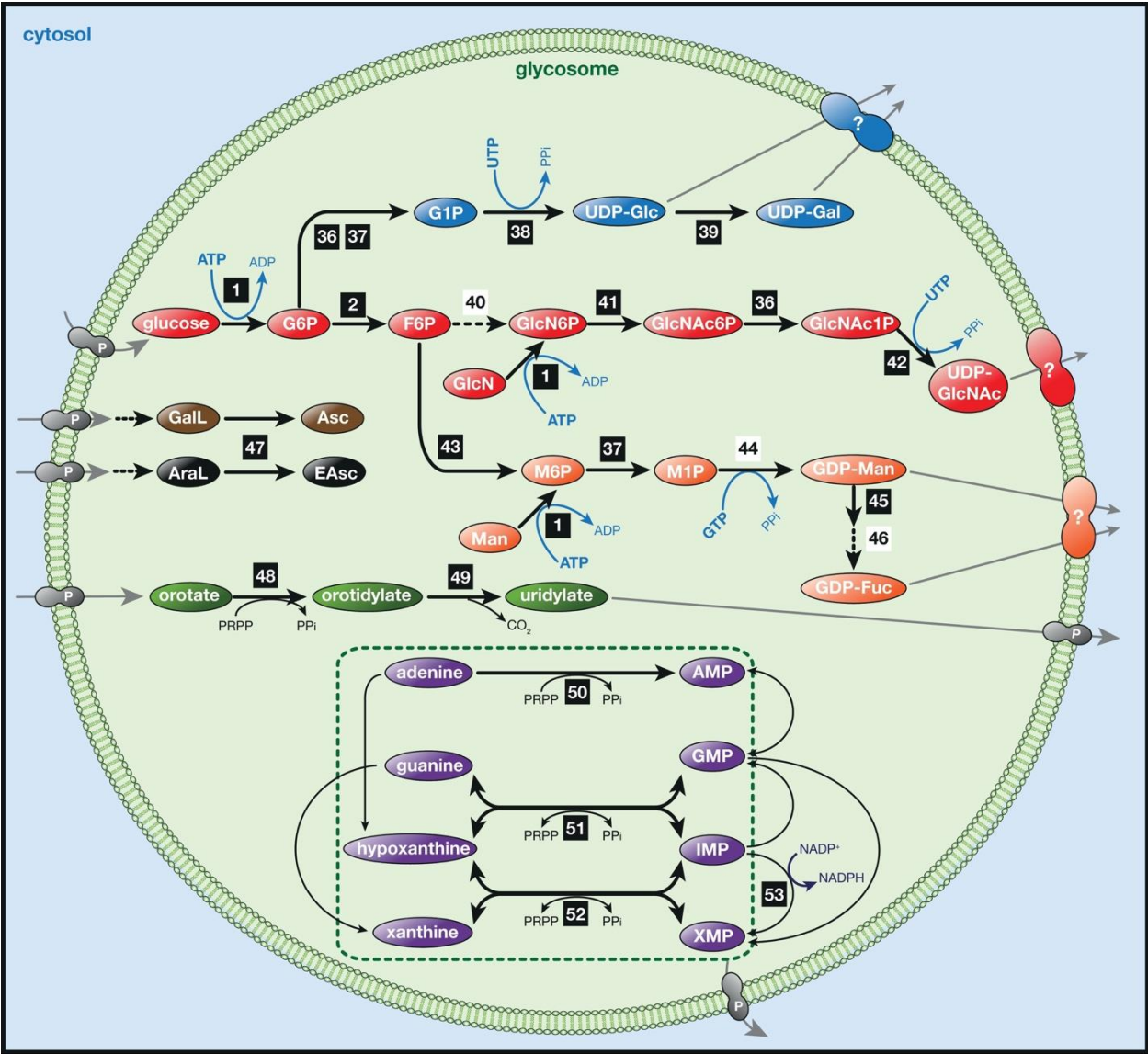




**Fig. 22. Glycosomal metabolic pathways – Part 2.**

Colour code for pathways: blue, synthesis of UDP-glucose and UDP-galactose; red, synthesis of UDP-N-acetyl-glucosamine; orange, synthesis of GDP-mannose and GDP-fucose; brown, synthesis of ascorbate; black synthesis of erythroascorbate; green, pyrimidine synthesis; purple, purine salvage pathway (From Allmann and Bringaud, 2017).

**Abbreviations:** AraL, arabinonolactone; Asc, ascorbate; EAsc, erythroascorbate; Fuc, fucose; G1P, glucose 1-phosphate; GalL, galactonolactone; Gal, galactose; GDP, guanine diphosphate; GlcN, glucosamine; GlcNAc, N-acetyl-glucosamine; GMP, guanine monophosphate; IMP, inosine monophosphate; M1P, mannose 1-phosphate; M6P, mannose 6-phosphate; Man, mannose; PRPP, phosphoribosylpyrophosphate; UDP, uridine diphosphate; XMP, xanthine monophosphate; UTP, uridine triphosphate; XMP, xanthine monophosphate.

**Enzymes:** 36, phosphoacetylglucosamine mutase; 37, phosphomannomutase; 38, UDP-glucose pyrophosphorylase; 39, UDP-galactose 4-epimerase; 40, glucosamine-fructose-6-phosphate aminotransferase; 41, glucosamine-6-phosphate synthase; 42, uridine-acetylglucosamine pyrophosphorylase; 43, phosphomannose isomerase; 44, GDP-mannose pyrophosphorylase; 45, GDP-mannose dehydrogenase; 46, GDP-mannose epimerase/reductase; 47, arabinonolactone oxidase with additional galactonolactone dehydrogenase activity; 48, orotate phosphoribosyltransferase; 49, orotidylate decarboxylase; 50, adenine phosphoribosyltransferase; 51, hypoxanthine-guanine phosphoribosyltransferase; 52, xanthine phosphoribosyltransferase; 53, inosinate dehydrogenase.

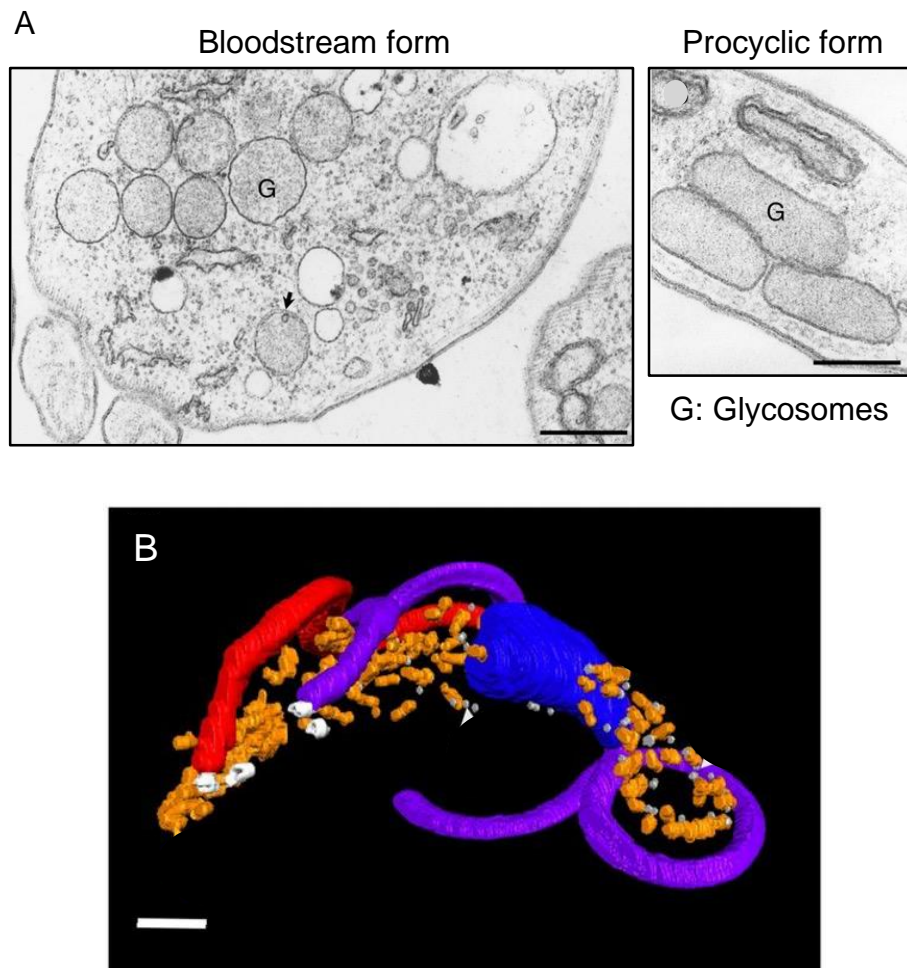


**Figure 1.23. Structure and distribution of glycosomes.**

In panel A, the glycosome ultrastructure by electron micrography is shown. The glycosomes of *T. brucei* BSF are predominantly spherical, while those from PCF are predominantly elongated organelles (From Gualdrón-López et al., 2012a). In B, ultrastructure and distribution of glycosomes (orange) in a BSF trypanosome. Additionally, the flagellum (purple), new flagellum (red) and nucleus (blue) are shown. Scale bar: ~500 nm (From Hughes et al., 2017).

## 1.6. Glycosomes

Glycosomes are peroxisome-related organelles that were firstly described in *T. brucei* (Opperdoes and Borst, 1977a) and later found in several kinetoplastid species (Gualdrón-López et al., 2012a) and in a free-living diplomonid (Morales et al., 2016). As peroxisomes, they are covered by a single phospholipid bilayer, lack nucleic acids and the import of proteins depends on the presence of peroxisomal targeting signals (PTS) that are recognised by peroxins (PEX) (Moyersoen et al., 2004).

### 1.6.1. Morphology and composition

The morphology of *T. brucei* glycosomes is shown in Figure 1.23. These organelles have an average diameter of 0.27 µm and represent 4% of the total cell volume. A 3D reconstruction using electron microscopy techniques (SBF-SEM) showed that glycosomes are distributed throughout the cell body often in clusters. The number of glycosomes in a single BSF cell is around 62-65, which increases up to 120 in dividing cells (Opperdoes et al., 1984; Tetley and Vickerman, 1985; Hughes et al., 2017).

The first six (PCF) or seven (BSF) enzymatic steps of the glycolytic pathway are compartmentalised within glycosomes, in addition to other enzymes of other metabolic pathways including: gluconeogenesis, pentose phosphate pathway, purine salvage pathway, *de novo* pyrimidine biosynthesis, ether lipid biosynthesis, β-oxidation of fatty acids, mevalonate pathway, a peroxide detoxification system and sugar nucleotide biosynthesis (Figure 1.22) (Colasante et al., 2006; Michels et al., 2006; Güther et al., 2014; Allmann and Bringaud, 2017).

The compartmentalisation of these pathways within glycosomes requires an exchange of metabolites across the membrane. The glycosomal membrane contains pore-forming channels, with similar properties to peroxisomal pores, that connect the organelle with the cytosol. Indeed, three distinct channels with low substrate selectivity for non-bulky metabolites (< 500 Da) were detected, and their protein composition remains to be characterised (Gualdrón-López et al., 2012b). Transporters are required for bulky metabolites (> 500 Da, estimated on data from peroxisomes), such as the three half-size ABC transporters (GAT1, GAT2, GAT3) and two glycosome integral membrane proteins (GIM5A and GIM5B) (Maier et al., 2001; Igoillo-Esteve et al., 2011).

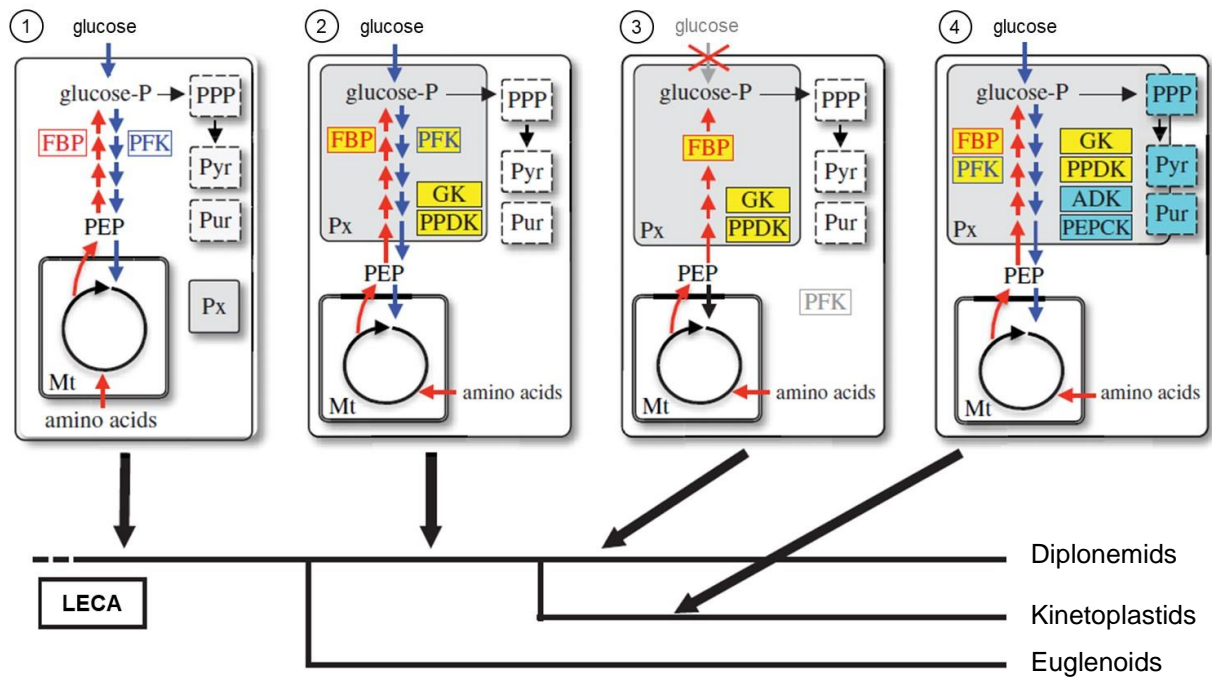


**Figure 1.24. A proposed metabolic model and peroxisome remodeling during evolution in Euglenozoa.**

**(1)** Peroxisomes (Px) and mitochondria (Mt) were present in the last eukaryotic common ancestor (LECA). Glycolysis (blue arrows), gluconeogenesis (red arrows), pentose phosphate pathway (PPP), pyrimidine biosynthesis (Pyr) and purine salvage (Pur) are cytosolic. PFK and FBPase (FBP) are critical allosteric enzymes in glycolysis and gluconeogenesis, respectively. **(2)** After divergence, a subset of glycolytic enzymes, FBPase, GK and PPDK (boxed in yellow) were sequestered in peroxisomes of the common ancestor of diplonemids and kinetoplastids. Both glycolysis and gluconeogenesis were functional within the organelle. **(3)** The ancestral diplonemid lost glycolysis. **(4)** The ancestral kinetoplastid further sequestered into peroxisomes a part of enzymes for PPP, Pyr, Pur and others such as PEPCK (From Morales et al., 2016).

### 1.6.1. Origin and evolution

The recent finding of glycolytic/gluconeogenic enzymes (glucokinase - GLK, PGI, FBPase, TIM, PGK) in addition to GK and PPDK in the peroxisomes of a free-living diplomonid suggests that the remodeling of peroxisomes towards functional glycosomes already occurred in the common ancestor of diplomonids and kinetoplastids. The model proposes that both glycolysis and gluconeogenesis were functional in the peroxisomes of this ancestor. After divergence, the ancestral diplomonid would have lost glycolysis to rely on amino acid metabolism and gluconeogenesis, while the ancestral kinetoplastid maintained the glycosomal glycolysis/gluconeogenesis and further sequestered other enzymes into the organelle, like PEPCK (Figure 1.24) (Morales et al., 2016).

Peroxisomes of different organisms can be replaced with new organelles adapted to face changing environmental conditions by pexophagy. This capacity of peroxisomal turnover is assumed to have represented an advantage in environmental adaptability during the course of evolution. Therefore, compartmentalisation of metabolic pathways into glycosomes can be considered as a selective advantage present in the ancestor of diplomonids and kinetoplastids that facilitated this metabolic reprogramming by pexophagy required to cope with different environments, and to some extent, opened the door to the development of parasitism (Herman et al., 2008; Gualdrón-López et al., 2012a; Cull et al., 2014).

### 1.6.2. Biogenesis and dynamics

Biogenesis of glycosomes occurs *via* similar and homologous mechanisms to those of peroxisomes in yeast, mammalian and plant cells. Several proteins called peroxins (PEX) are involved in the import of matrix proteins, the insertion of membrane proteins and the proliferation of the organelles by growth and division or *de novo* formation (see Table 1.3). To date, 15 peroxin homologues have been identified and characterised in trypanosomatids showing well conserved activities despite their relatively low sequence identity (15-35%) with peroxins in other organisms. Interestingly, silencing any peroxin genes by RNAi is lethal for *T. brucei* cells grown under standard conditions, which confirms the essentiality of glycosomes (Moyersoen et al., 2004; Galland and Michels, 2010; Gualdrón-López et al., 2013a; Haanstra et al., 2016).

Peroxin	Function	Mammal	Yeast	<i>T. brucei</i>
PEX1	AAA-ATPase complex	✓	✓	✓
PEX2	Ubiquitin ligase (E3), RING-subcomplex	✓	✓	✓
PEX3	Membrane anchor of PEX19	✓	✓	✓
PEX4	Ubiquitin conjugating enzyme (E2)		✓	✓
PEX5	PTS1-receptor, PTS2-co-receptor	✓	✓	✓
PEX6	AAA-ATPase complex	✓	✓	✓
PEX7	PTS2-receptor	✓	✓	✓
PEX8	Cargo release		✓	
PEX9	PTS1-receptor under defined growth condition		✓	
PEX10	Ubiquitin ligase (E3), RING-subcomplex	✓	✓	✓
PEX11	Membrane elongation, recruits the fission machinery	✓	✓	✓
PEX12	Ubiquitin ligase (E3), RING-subcomplex	✓	✓	✓
PEX13	PTS-receptor docking complex at the membrane	✓	✓	✓ <sup>a</sup>
PEX14	PTS-receptor docking complex at the membrane	✓	✓	✓
PEX15	Membrane anchor of AAA-ATPase complex		✓	
PEX16	Insertion of proteins into the membrane	✓	✓	✓
PEX17	PTS-receptor docking complex at the membrane		✓	
PEX18	PTS2-co-receptor		✓	
PEX19	Chaperon and receptor of PMPs	✓	✓	✓
PEX20	PTS2-co-receptor		✓	
PEX21	PTS2-co-receptor		✓	
PEX22	Subcomplex of ubiquitin conjugating enzyme (E2)		✓	✓
PEX23	Dysferlin domain-containing peroxins	✓	✓	
PEX24	Peroxisome assembly		✓	
PEX25	Membrane elongation, recruits the fission machinery		✓	
PEX26	Membrane anchor of AAA-ATPase complex	✓	✓	
PEX27	Negatively affects fission		✓	
PEX28	Controls peroxisome size and proliferation		✓	
PEX29	Forms ER subdomain for PPV exit site		✓	
PEX30	Forms ER subdomain for PPV exit site		✓	
PEX31	Forms ER subdomain for PPV exit site		✓	
PEX32	Controls peroxisome size and number		✓	
PEX33	PTS-receptor docking complex (in Fungi)			
PEX34	Functional orthologue of mammalian Pex16p		✓	
PEX35	Regulates peroxisome size and abundance		✓	
PEX36	Functional orthologue of mammalian Pex16p		✓	

**Table 1.3. Function of peroxins identified in mammals, yeast and *T. brucei*.**

<sup>a</sup>Two isoforms of PEX13: PEX13.1 and PEX13.2 are expressed in *T. brucei*. PMP: Peroxisomal Membrane Protein. PPV: pre-peroxisomal vesicle. Adapted from (Imanaka and Shimozawa, 2019)

The import of glycosomal matrix proteins, similarly to peroxisomal proteins, relies on the presence of peroxisomal targeting signals (PTS). The first type of signal, PTS1, is defined by the last three amino acid residues located at the C-terminal extremity of peroxisomal/glycosomal proteins (Figure 1.25A) and is recognised by the C-terminal tetratricopeptide repeat (TPR) domain of the cytosolic receptor PEX5. In addition, several studies showed that the nine residues upstream of PTS1 are important for interaction with the TPR domain of PEX5 and that the charge of these residues influences the efficiency of import (Brocard and Hartig, 2006; Hagen et al., 2015; DeLoache et al., 2016). The second type of signal, PTS2, is a longer sequence located at the N-terminal domain of peroxisomal/glycosomal proteins (Figure 1.25A) and is recognised by the cytosolic receptor PEX7, which then interacts with its co-receptor PEX5 and forms a ternary complex, therefore the import of PTS1 and PTS2 proteins into glycosomes depends on PEX5 (Galland and Michels, 2010).

Notably, a high-confidence proteome analysis of glycosomes revealed that only 60 out of the 158 proteins identified possess PTS-signals (Güther et al., 2014), while 74 proteins were found to contain a PTS signal *in silico*, mostly PTS1 (77% of them) (Opperdoes and Szikora, 2006). This clearly raises questions about the import of PTS-lacking proteins into glycosomes. In contrast to import machineries of other organelles, peroxisomes can import folded and even oligomeric proteins through a dynamic and transient translocation pore (Meinecke et al., 2010). One possibility for proteins lacking PTS is to be imported by piggybacking through interaction with a PTS-containing protein. This alternative will be described later.

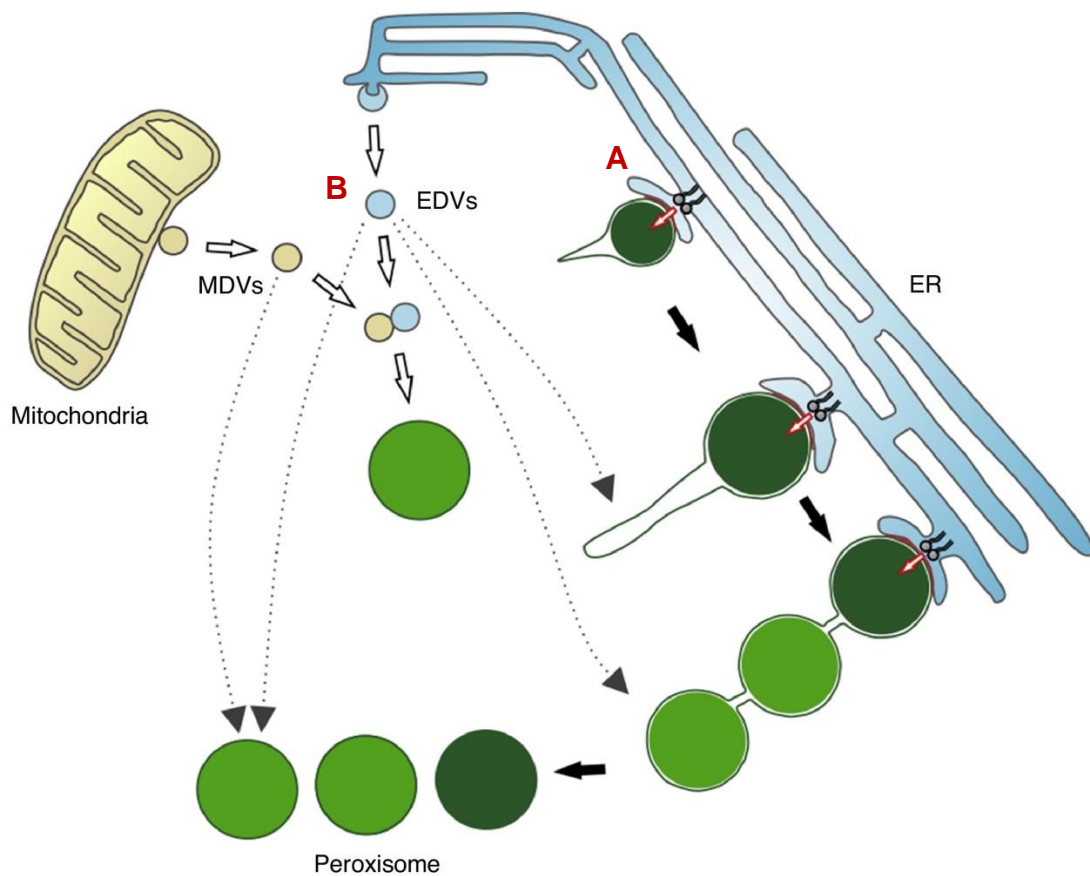
The model for import of glycosomal proteins is shown in Figure 1.25B. The complex formed by receptor (PEX5 or PEX5-PEX7) and cargo PTS-protein is directed to the peroxisomal membrane where PEX5 associates with a docking complex containing the membrane proteins PEX14 and PEX13. The intrinsically disordered N-terminal part of PEX5 interacts with the N-terminal domain of PEX14 and this association of cargo-receptor with the docking complex derives in formation of the pore, with PEX5 becoming inserted as an integral membrane protein (Schliebs et al., 1999; Erdmann and Schliebs, 2005; Meinecke et al., 2010; Dias et al., 2017).





Importantly, disrupting the PEX5-PEX14 interaction is lethal for *T. brucei* parasites, which validates glycosomal protein import as a drug target (Dawidowski et al., 2017). How is the cargo protein released from interaction with its receptor into the peroxisomal lumen remains unclear, as well as details for the PEX7-dependent import mechanism. After the translocation and releasing of cargo proteins, PEX 5 and PEX7 receptors need to be extracted from the membrane complex for either a new protein transport cycle or proteasomal degradation. To be released in the cytosol, PEX5 needs to be monoubiquitinated at a conserved cysteine residue in yeast and humans, while probably at a lysine residue in *T. brucei* (Gualdrón-López et al., 2013b). This process depends on the ubiquitin-conjugating PEX4, which is anchored to the membrane by PEX22 (Williams et al., 2012), and on the RING (Really Interesting New Gene)-complex comprising ubiquitin ligases PEX2, PEX10 and PEX12 (Figure 1.25B) (El Magraoui et al., 2012). Finally, monoubiquitinated PEX5 is released from the membrane thanks to the AAA ATPases PEX1 and PEX6 in an ATP-dependent manner (Platta et al., 2005; Pedrosa et al., 2018) and is deubiquitinated in the cytosol to start a new cycle. The process for recycling PEX7 receptor is still not well understood, and it seems to require the PEX5 export to take place (Rodrigues et al., 2014).

The import of peroxisomal membrane proteins (PMP) involves a different set of peroxins: PEX19, PEX3 and PEX16. The PEX19 receptor recognises membrane peroxisomal targeting signals (mPTSs) on PMPs in the cytosol (Figure 1.25B) (Saveria et al., 2007). The cargo-receptor complex is then transported to the membrane where PEX19 docks with PEX3 for subsequent insertion of the PMP into the membrane. PEX16 functions as the PEX3 receptor on peroxisomal membranes (Matsuzaki and Fujiki, 2008). Similarly to yeast and mammalian cells, where deletion or mutation of PEX3, PEX16 and PEX19 results in cells without peroxisomes, RNAi knock-down of any of these peroxins in *T. brucei* reduces glycosome abundance and mislocalises glycosomal proteins to the cytosol, which leads to growth defects and death (Banerjee et al., 2005, 2019; Kaelin et al., 2015, 2019).



Current Opinion in Cell Biology

**Figure 1.26. Mechanisms for peroxisome formation in mammalian cells.**

**A) Growth and division:** the peroxisomal membrane requires ER contact (red line) and lipid transfer (red arrow) to elongate, then it gets constricted and finally divided.

**B) De novo peroxisome formation:** pre-peroxisomal vesicles generated at the ER (EDV) and mitochondria (MDV) may fuse and mature into new import-competent peroxisomes. Light green: newly formed peroxisomes (From Costello and Schrader, 2018).

Analysis of PEX14 RNAi mutants revealed that the correct and complete sequestering of enzymes inside glycosomes is indispensable for parasites cultured in glucose- or glycerol-rich conditions, since glucose and glycerol became toxic to induced parasites. PCF trypanosomes were able to cope with mislocalisation of glycolytic enzymes when cultured in the absence of glucose (Furuya et al., 2002; Moyersoet et al., 2003; Haanstra et al., 2008). The metabolic mechanisms involved in this toxicity include extreme accumulation of intermediates like Gly3P in the presence of glycerol (Haanstra et al., 2008, 2014).

Peroxisomes can proliferate through fission by growth and division of pre-existing peroxisomes or can be generated *de novo* (Figure 1.26) (Smith and Aitchison, 2013). Since peroxin homologues to those from mammals and yeast involved in both processes have been characterised in *T. brucei*, it is likely that glycosomes are generated and proliferate in similar manners to peroxisomes. In mammalian cells, PEX11p $\beta$  mediates a polarised growth and formation of a tubular extension of the peroxisomal membrane which elongates and recruits PMPs and matrix proteins. This membrane extension then shrinks and is eventually split into individual spherical peroxisomes by factors involved in mitochondrial fission, like the dynamin-like protein DLP1 and DRP-interacting protein FIS1 (Delille et al., 2010; Smith and Aitchison, 2013; Costello and Schrader, 2018). *T. brucei* encodes orthologues of these two proteins, DLP1 and FIS1 (Chanez et al., 2006). Comparable to mammalian cells, where overexpression of PEX11p $\beta$  results in accumulation of pre-peroxisomal membrane structures composed of mature globular peroxisomes and tubular membrane extensions (Delille et al., 2010), overexpressing PEX11 in *T. brucei* leads to proliferation of glycosomal tubular structures (Lorenz et al., 1998).

Importantly, the ER contributes significantly to peroxisome biogenesis *via* growth and division by transferring lipids and some proteins through peroxisome-ER contacts present in 70-80% of peroxisomes in mammalian cells (Costello et al., 2017; Hua et al., 2017) (Figure 1.26).

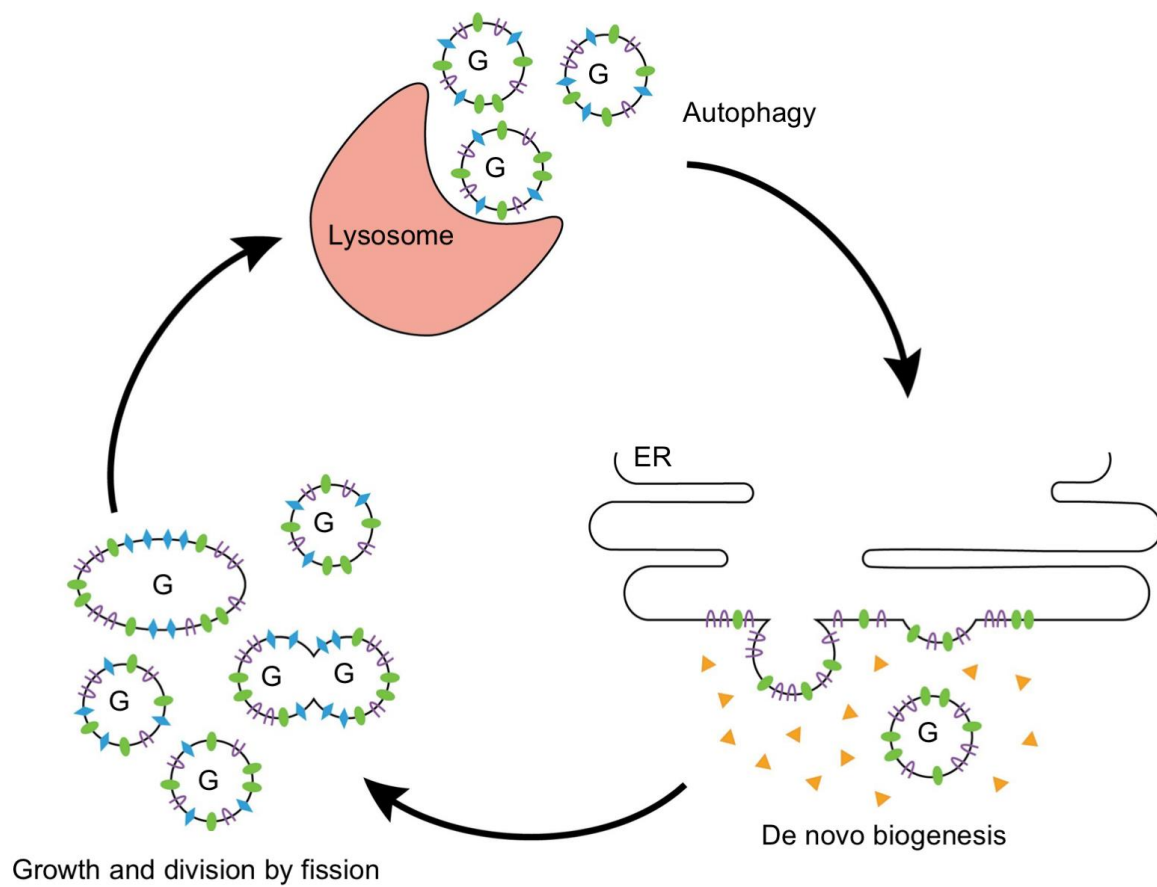


**Figure 1.27. Proliferation of glycosomes.**

Glycosomes can proliferate by fission of existing organelles or by *de novo* biogenesis. Autophagy, in this case called pexophagy, enables turnover of existing glycosomes (From Bauer and Morris, 2017).

Formation of peroxisomes *de novo* from ER requires PEX3, PEX16 and PEX19 participation. These PMPs are targeted to the ER where pre-peroxisomal vesicles are formed and released. According to the heterotypic fusion model in yeast, different pre-peroxisomal vesicles with different PMP content bud and fuse prior to maturation (Smith and Aitchison, 2013) while in the vesicle maturation model one type of vesicle progressively acquires the PMP repertoire prior to maturing into a newly formed peroxisome (Hoepfner et al., 2005). Moreover, a role for mitochondria in peroxisome biogenesis of mammals has been recently shown. In cells lacking peroxisomes, PEX3 targets mitochondria while PEX16 traffics to the ER. In this model, ER- and mitochondrial-derived pre-peroxisomal vesicles fuse to generate new import-competent peroxisomes (Figure 1.26) (Sugiura et al., 2017). How is the glycosomal population maintained in trypanosomes is not clearly understood, since *de novo* generation of glycosomes has not been described to date.

To maintain the number of peroxisomes in a cell, both proliferation by fission of pre-existing peroxisomes and *de novo* biogenesis from ER contribute to a variable extent depending on the organism and conditions. As mentioned in previous sections, the levels of glucose availability change during the life cycle of *T. brucei*, from high levels in the blood of mammalian hosts to almost undetectable levels in the fly. The parasites rapidly adapt to these environmental variations by changing the protein content of glycosomes (Bauer et al., 2013). A recent model proposes that glycosomes are degraded *via* autophagy (Herman et al., 2008) to be replaced by new organelles generated *de novo* from the ER containing different protein contents optimised to face the new conditions. These new organelles would then divide and proliferate through fission (Figure 1.27) (Bauer and Morris, 2017).

### 1.7. Piggybacking

Given the capacity of peroxisomes to import proteins in their native oligomeric state, a peroxisomal protein lacking a PTS that interacts with a PTS-containing protein can be imported into the organelle. This phenomenon is called piggyback import (Figure 1.28). Several examples of oligomeric protein import have been described so far (summarised in Table 1.4).

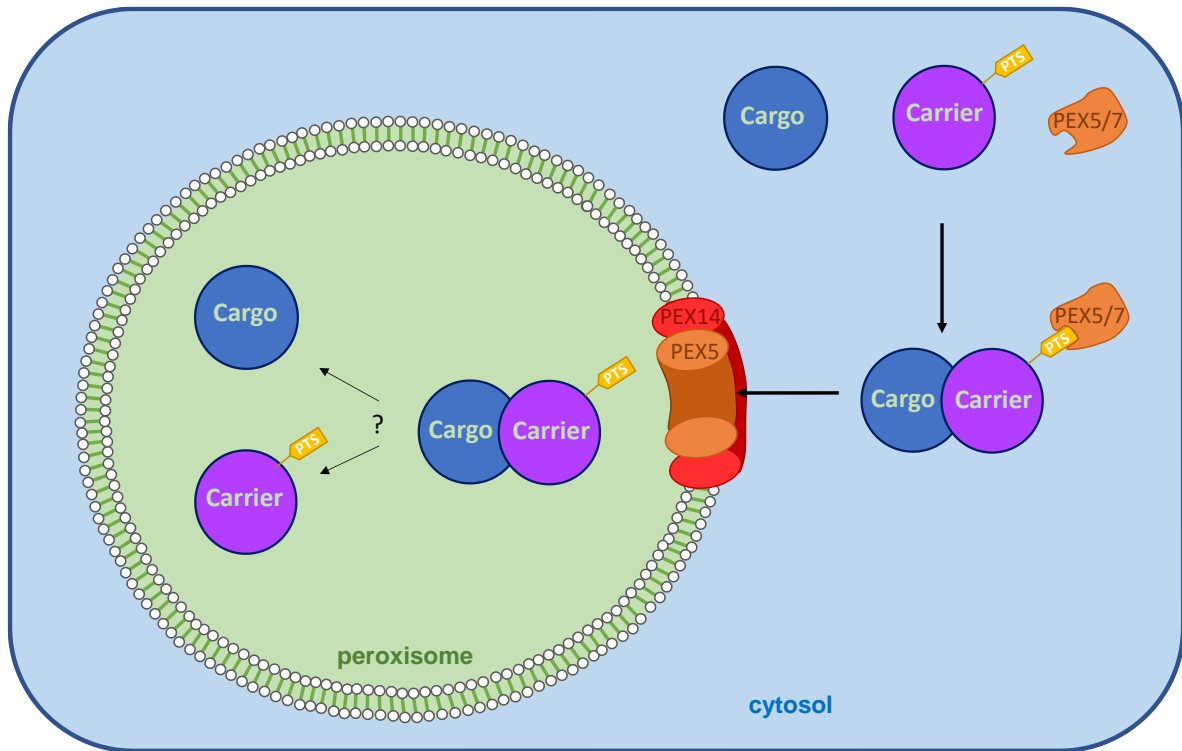


**Figure 1.28. Piggyback import model of peroxisomal matrix proteins.**

A peroxisomal protein lacking a PTS signal (cargo) interacts with a protein containing PTS1 or PTS2 signal (carrier). The complex is recognised by peroxisomal receptors PEX5 or PEX7 and imported into peroxisomes. Once in the matrix, interactions could be maintained or not, probably depending on its nature and the functional relation of the proteins involved.

In the case of homo-oligomer import, protein subunits lacking a PTS signal interact with PTS-containing subunits and then the complex is targeted to peroxisomes. The first reported examples, *i.e.* thiolase (Glover et al., 1994) and chloramphenicol acetyltransferase (McNew and Goodman, 1994) demonstrated that both PTS2 and PTS1-containing protein subunits can piggyback their PTS-lacking counterparts into peroxisomes. These reports of homo-oligomer import show the potentiality of the peroxisomal machinery to import oligomers. However, in a physiological context where all the subunits of the oligomer possess PTS signals, the use of one or more PTS to bind PEX5 is not clear. Importantly, the PEX5 receptor was shown to bind newly synthesized monomeric proteins which inhibits their oligomerization (Freitas et al., 2015). Indeed, catalase (Freitas et al., 2011), acyl-CoA oxidase and urate oxidase (Freitas et al., 2015) are more efficiently imported into peroxisomes as monomers than as oligomers. The preference of monomeric proteins as substrates over oligomers might depend on the proteins structure and the position of the PTSs signals in relation to the residues involved in oligomerization (Thoms, 2015).

In the case of hetero-oligomers, the import of a cargo protein depends on the PTS present in a carrier protein (Table 1.4). The first reported example was described in yeast for the  $\Delta^3$ ,  $\Delta^2$ -enoyl-CoA isomerase (ECI1P), which itself contains a weakly functioning PTS1. This protein is efficiently imported into peroxisomes thanks to its interaction with the related PTS1-containing DCI1P protein (Yang et al., 2001). These proteins are involved in  $\beta$ -oxidation of fatty acids and their expression is induced in oleic acid conditions (Gurvitz et al., 1999; Yang et al., 2001).

The first case of piggybacking described in mammals involves the superoxide dismutase (SOD1), which is imported into peroxisomes by interaction with the PTS1-containing CCS. The carrier CCS is the copper chaperone of SOD1, which contains a SOD-binding domain required for the interaction and the exchange of copper ions between the two proteins (Islinger et al., 2009). Another example in mammals corresponds to the lactate dehydrogenase (LDH) complex. In this particular case, a certain proportion of lactate dehydrogenase is found in peroxisomes thanks to a translational readthrough process of the gene coding for the LDHB subunit.

Homo-oligomer import				
Protein		PTS	Organism	Techniques used
3-Ketoacyl-CoA thiolase		PTS2	<i>Saccharomyces cerevisiae</i>	Density gradient centrifugation, IP <sup>1</sup>
Chloramphenicol acetyltransferase		PTS1	<i>Saccharomyces cerevisiae</i>	Density gradient centrifugation, IF <sup>2</sup>
Alanine-glyoxylate aminotransferase		PTS1	<i>Homo sapiens</i>	Immunoprecipitation, IF <sup>3</sup>
Malate dehydrogenase		PTS1	<i>Saccharomyces cerevisiae</i>	Subcellular fractionation, IP <sup>4</sup>
Isocitrate lyase		PTS1	<i>Gossypium hirsutum</i> <i>Ricinus communis</i> <i>Brassica napus</i>	IF <sup>5</sup>
Catalase		PTS1	<i>Candida boidinii</i> <i>Homo sapiens</i>	Density gradient centrifugation, fluorescence microscopy <sup>6</sup> IP, fluorescence microscopy and IF <sup>7</sup>
$\alpha/\beta$ -hydrolase Lpx1		PTS1	<i>Saccharomyces cerevisiae</i>	Y2H <sup>8</sup> , fluorescence microscopy and IF <sup>9</sup>
HEX		PTS1	<i>Neurospora crassa</i>	Differential centrifugation <sup>10</sup>
Acyl-CoA oxidase		PTS1	<i>Mus musculus</i>	IP, <i>in vitro</i> import assay, IF <sup>11</sup>
Hetero-oligomer import				
Cargo protein	Carrier protein	PTS	Organism	Techniques used
ECI1P	DCI1P	PTS1	<i>Saccharomyces cerevisiae</i>	Fluorescence microscopy <sup>12</sup>
SOD1	CCS	PTS1	<i>Rattus norvegicus</i>	Fluorescence microscopy and IF <sup>13</sup>
LDHA/B	LDHBx	hidden -PTS1	<i>Homo sapiens</i>	Fluorescence microscopy and IF <sup>14</sup>
PP2A-A2 PP2A-C2,C5	PP2A-B'0	PTS1	<i>Arabidopsis thaliana</i>	Bimolecular fluorecence complementation <sup>15</sup>
PNC1	GPD1	PTS2	<i>Saccharomyces cerevisiae</i>	Affinity and size-exclusion chromatography, density gradient centrifugation, fluorescence microscopy <sup>16</sup> Y2H, fluorescence microscopy <sup>17</sup> Y2H, IP, fluorescence microscopy <sup>18</sup>

**Table 1.4. Peroxisomal matrix proteins imported as oligomers.**

PTS1-less subunits can be piggybacked into peroxisomes when co-expressed with interacting subunits carrying a PTS (homo-oligomer import). Hetero-oligomer import depends on one PTS present in the carrier protein.

**References:** <sup>1</sup>(Glover et al., 1994), <sup>2</sup>(McNew and Goodman, 1994), <sup>3</sup>(Leiper et al., 1996), <sup>4</sup>(Elgersma et al., 1996), <sup>5</sup>(Lee et al., 1997), <sup>6</sup>(Horiguchi et al., 2001), <sup>7</sup>(Otera and Fujiki, 2012), <sup>8</sup>(Thoms et al., 2008), <sup>9</sup>(Thoms et al., 2011), <sup>10</sup>(Liu et al., 2011), <sup>11</sup>(Freitas et al., 2015), <sup>12</sup>(Yang et al., 2001), <sup>13</sup>(Islinger et al., 2009), <sup>14</sup>(Schueren et al., 2014), <sup>15</sup>(Kataya et al., 2015), <sup>16</sup>(Effelsberg et al., 2015), <sup>17</sup>(Kumar et al., 2016), <sup>18</sup>(Al-Saryi et al., 2017b).



LDHA and LDHB are imported as parts of heterotetramers containing at least one read-through (LDHBx) subunit with a seven amino acids extension (PTS1) that does not interrupt oligomerization and is recognised by PEX5 (Schueren et al., 2014).

The only example in plants consists of the regulatory subunit B'0 of the protein phosphatase 2A (PP2A) that has a PTS1 signal and facilitates the import of PTS-lacking scaffolding (A2) and catalytic (C2, C5) subunits. This PP2A heterotrimer has a role in  $\beta$ -oxidation of fatty acids in peroxisomes (Kataya et al., 2015).

The most recent report of piggybacking was described in yeast by three different groups and is the only one to illustrate hetero-oligomeric import *via* the PTS2-PEX7 and the coreceptor PEX21. This case includes the PTS2-carrying protein glycerol 3-phosphate dehydrogenase (GPD1), which can be imported into peroxisomes as a monomer or dimer, and the PTS-lacking cargo protein nicotinamidase (PNC1) (Effelsberg et al., 2015; Kumar et al., 2016; Al-Saryi et al., 2017b). Importantly, PNC1 co-import requires GPD1 to be imported as a dimer, since blocking dimerization of GPD1 disrupts the import of PNC1 into peroxisomes (Al-Saryi et al., 2017b). Recently, GPD1 was found to be implicated in the reoxidation of intraperoxisomal NADH, while the role of PNC1 inside peroxisomes remains unclear (Al-Saryi et al., 2017a).

The flexibility and ability of the peroxisomal importomer to allow translocation of different molecules with variable sizes has been shown by microinjecting gold particles (diameter between 4-9 nm) coated with PTS1-BSA (Walton et al., 1995), and more recently by probing import of large (up to 12.5 nm) oligomers of biotinylated mCherry repeat proteins coupled to streptavidin-PTS1, in addition to DNA and polysaccharides (Yang et al., 2018). This highlights the amazing capabilities of the peroxisomal import machinery.

There are no cases of piggybacking described so far in trypanosomatids, although it has been proposed as an explanation to the presence of PTS-lacking proteins within glycosomes on several occasions. In this thesis, I describe the first case of piggybacking in *T. brucei*, involving an enzyme of the sugar nucleotide biosynthetic pathway (UGP) and its PTS1-carrier, PEPCK.

Gene	Activity	Essential in vitro	Essential in vivo	Reference
<i>DPMS</i>	Dol-P-Man synthase	ND	ND	(Mazhari-Tabrizi et al., 1996)
<i>GPI10</i>	Dol-P-Man:Man <sub>2</sub> GlcNPI α1-2-mannosyltransferase	Yes	No	(Nagamune et al., 2000)
<i>ALG3</i>	Dol-P-Man:Man <sub>5</sub> GlcNAc <sub>2</sub> α1-3-mannosyltransferase	No	No	(Manthri et al., 2008)
<i>GT8</i>	UDP-GlcNAc:β-D-Gal-GPI β1-3-GlcNAc transferase	No	No	(Izquierdo et al., 2009b)
<i>UGGT</i>	UDP-Glc:glycoprotein α1-3-glycosyltransferase	No	No	(Izquierdo et al., 2009a)
<i>ALG12</i>	Dol-PMan:Man <sub>7</sub> GlcNAc <sub>2</sub> α1-6-mannosyltransferase	ND	ND	(Izquierdo et al., 2012)
<i>GT11</i>	UDP-GlcNAc:α3-Dmannoside β1-2-GlcNAc transferase I	No	No	(Damerow et al., 2014)
<i>GT3</i>	UDP-Gal : βGlcNAc β1-3 Galactosyltransferase	No	No	(Izquierdo et al., 2015)
<i>GT15</i>	UDP-GlcNAc:α1-6-Dmannoside β1-2-GlcNAc transferase II	No	No	(Damerow et al., 2016)

**Table 1.5. Characterised glycosyltransferases from *T. brucei***

Glycosyltransferases catalyse the transfer of sugar from an activated sugar donor to an acceptor (another sugar, protein, lipid, small molecule). The activity of the products of the genes presented here has been experimentally validated. The nomenclature includes donor, acceptor, linkage, activity and isomer number.

## 1.8. Glycobiology

Glycosylation is the most common and diverse post-translational modification. In parasites, glycosylation is crucial for the composition of the cell surface (see 1.4.5. Cell surface). *T. brucei* expresses complex glycoconjugates involving 38 different types of glycosidic linkages, suggesting that parasites have at least 38 unique glycosyltransferases (Izquierdo et al., 2009b). So far, nine glycosyltransferases have been identified and experimentally characterised, most of them involved in GPI side-chain modifications and complex N-glycan synthesis (Table 1.5). Only one gene encoding a fucosyltransferase has been recently identified in *T. brucei* and, more importantly, its activity is localised in the mitochondria and is essential for BSF (preprint Bandini et al., 2019).

Glycosyltransferases use activated forms of sugars called sugar nucleotides as substrates for glycosylation reactions in the endoplasmic reticulum (ER) and Golgi apparatus. Accordingly, these activated sugars are translocated by nucleotide sugar transporters (NSTs) into the lumen of the Golgi apparatus. In *T. brucei*, eight putative NSTs (1–8) have been identified and the substrate specificities of NST1–4 were experimentally determined. These four NSTs are expressed in both PCF and BSF trypanosomes. NST1 and 2 transport UDP-Gal/UDP-GlcNAc, NST3 transports GDP-Man and NST4 transports UDP-GlcNAc and GDP-Man. Silencing NST4 expression by RNAi leads to defects in glycosylation of surface proteins in both PCF and BSF cells (Liu et al., 2013).

### 1.8.1. Sugar nucleotide biosynthesis

Five sugar nucleotides are synthesized in *T. brucei*, i.e. UDP-glucose (UDP-Glc), UDP-galactose (UDP-Gal), UDP-*N*-acetylglucosamine (UDP-GlcNAc), GDP-mannose (GDP-Man) and GDP-fucose (GDP-Fuc) (Turnock and Ferguson, 2007). The biosynthetic pathways leading to production of sugar nucleotides are schematised in (Figure 1.29). All these sugar nucleotides can be produced from glucose or fructose, and UDP-GlcNAc, GDP-Man and GDP-Fuc can be formed from glucosamine and mannose.

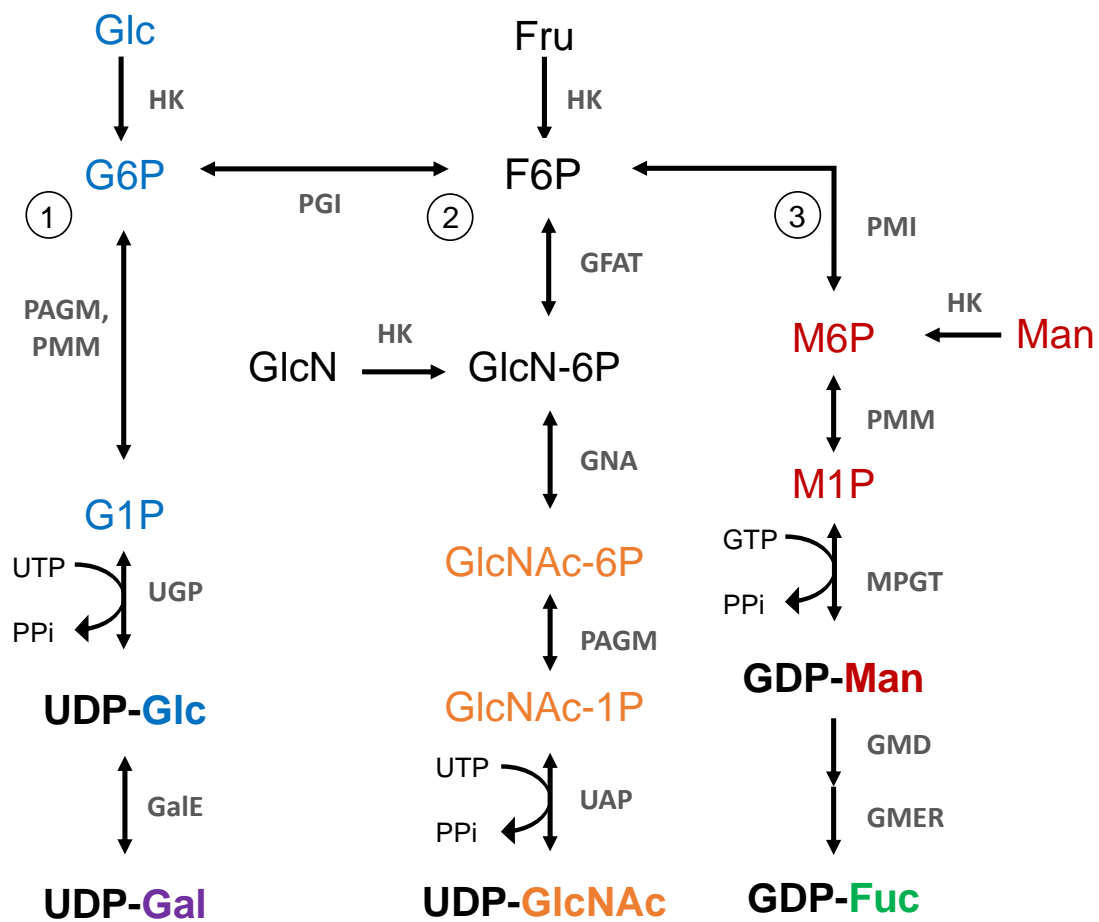


**Figure 1.29. Biosynthesis of UDP-Glc, UDP-Gal, UDP-GlcNAc, GDP-Man and GDP-Fuc in *T. brucei*.**

Glucose is taken up and phosphorylated to G6P, which is the starting point for the synthesis of sugar nucleotides (From Bandini et al., 2012). The 3 branches described in the text are highlighted by a circled number.

The pathways start with phosphorylation of glucose to glucose 6-phosphate (G6P) by hexokinase. As mentioned before, G6P feeds glycolysis and the pentose phosphate pathway (PPP) in addition to sugar nucleotide biosynthesis. In the *in vivo* context of the fly, where glucose is unavailable, G6P is provided via gluconeogenesis from proline (Figure 1.16). This G6P feeds three branches for biosynthesis of sugar nucleotides, *i.e.* UDP-Glc/UDP-Gal (first branch), UDP-GlcNAc (second branch) and GDP-Man/GDP-Fuc (third branch) (Figure 1.29).

In the first branch of *T. brucei*, phosphomannomutase (PMM) and phospho-*N*-acetylglucosamine mutase (PAGM) transfer the phosphate of G6P from position C6 to position C1 to produce glucose 1-phosphate (G1P), since phosphoglucomutase is absent. Each one of these enzymes (PMM and PAGM) has an additional role in producing mannose 1-phosphate (M1P) and *N*-acetylglucosamine 1-phosphate (GlcNAc-1-P), respectively. PMM is localised in the glycosomes, while PAGM has a dual glycosomal and cytosolic localisation (Table 1.6). In BSF, down-regulation of their expression by RNAi resulted in reduced levels of the respective sugar nucleotides, GDP-Man and UDP-GlcNAc. Importantly, no variations in UDP-Glc levels were detected in either of the RNAi cell lines, suggesting that PMM and PAGM activities are redundant for production of G1P (Bandini et al., 2012). The next steps in this branch lead to production of UDP-Glc catalysed by UDP-glucose pyrophosphorylase (UGP) and consecutive epimerisation of UDP-Glc to UDP-Gal by UDP-galactose 4-epimerase (GalE). UGP has been located in the glycosomes of BSF and GalE in glycosomes of PCF (Table 1.6). These enzymes will be described in detail in the next section (1.8.2). Alternatively, G6P is isomerised in fructose 6-phosphate (F6P) by phosphoglucose isomerase (PGI) that is used for the second and third branches (Figure 1.29).

In the second branch, UDP-GlcNAc is synthesized from F6P by the action of four enzymes. A putative gene (Tb927.7.5560) codes for a glucosamine-fructose-6-phosphate aminotransferase (GFAT), this protein has not been characterised so far. The following steps catalysed by glucosamine-phosphate *N*-acetyltransferase (GNA), PAGM and UDP-*N*-acetylglucosamine diphosphorylase (UAP) have been characterised and GNA and UAP were shown to be essential glycosomal enzymes for BSF parasites (Stokes et al., 2008; Mariño et al., 2011).

Enzyme	EC		Localisation	Targeting signals (PTS1 or PTS2)		
			in <i>T. brucei</i>	<i>T. brucei</i>	<i>T. cruzi</i>	<i>L. major</i>
UDP-Glucose/UDP-Galactose						
Hexokinase 1 and 2	HK	2.7.1.1	G <sup>1,2,3</sup>	PTS2	PTS2	PTS2
Phospho- <i>N</i> -acetylglucosamine mutase	PAGM	5.4.2.3	G/C <sup>4</sup>	-	-	-
Phosphomannomutase	PMM	5.4.2.8	G <sup>4</sup>	-	PTS1 (SKL)	PTS1 (SNL)
UDP-glucose pyrophosphorylase	UGP	2.7.7.9	G <sup>5</sup>	-	-	PTS1 (TNK)
UDP-galactose 4-epimerase	GalE	5.1.3.2	G <sup>6</sup>	PTS1 (TKL)	-	PTS2
UDP-N-acetylglucosamine						
Phosphoglucose isomerase	PGI	5.3.1.9	G <sup>1,2</sup>	PTS1 (SHL)	PTS1 (SHL)	PTS1 (AHL)
Glucosamine-fructose-6-phosphate aminotransferase	GFAT	2.6.1.16	C <sup>12</sup>	-	-	-
Glucosamine-phosphate <i>N</i> -acetyltransferase	GNA	2.3.1.4	G <sup>7</sup>	-	-	-
UDP- <i>N</i> -acetylglucosamine diphosphorylase	UAP	2.7.7.23	G <sup>8</sup>	PTS1* (SNM)	PTS1* (GNM)	PTS1* (ANM)
GDP-Mannose						
Phosphomannose isomerase	PMI	5.3.1.8	G <sup>2, 9</sup>	PTS1 (SHM)	PTS1 (AH-MI)	-
GDP-mannose pyrophosphorylase	MPGT	2.7.7.13	C <sup>10</sup>	-	-	-
GPD-Fucose						
GDP-mannose dehydratase	GMD	4.2.1.47	G <sup>11</sup>	-	-	AP
GDP-fucose synthetase	GMER	1.1.1.271	G <sup>11</sup>	PTS1* (ARK)	PTS1* (ARK)	AP

**Table 1.6. Enzymes of sugar nucleotide biosynthetic pathways.**

The localisation of the enzymes in *T. brucei* is reported here according to experimental data. Presence or absence of PTS corresponds to in silico prediction using protein sequences (Opperdoes and Szikora, 2006) or to analysis in the reference (\*).

G: Glycosomes, C: Cytosol, (-): No PTS detected, AP: absent pathway in this organism.

**References:** <sup>1</sup>(Opperdoes and Borst, 1977a), <sup>2</sup>(Güther et al., 2014), <sup>3</sup>(Morris et al., 2006), <sup>4</sup>(Bandini et al., 2012), <sup>5</sup>(Mariño et al., 2010), <sup>6</sup>(Roper et al., 2005), <sup>7</sup>(Mariño et al., 2011), <sup>8</sup>(Stokes et al., 2008), <sup>9</sup>(Kuettel et al., 2012), <sup>10</sup>(Denton et al., 2010), <sup>11</sup>(Turnock et al., 2007), <sup>12</sup>(<https://www.tryptag.org>).

In the third branch, GDP-Man is synthesized from F6P by the action of three enzymes already identified and characterised in *T. brucei* (Figure 1.29).

First, phosphomannoisomerase (PMI) catalyses the isomerisation of F6P to mannose 6-phosphate (M6P). Then, PMM transfers the phosphate group to produce M1P which, together with GDP, are coupled by GDP-mannose pyrophosphorylase (MPGT) to finally yield GDP-Man. The first two steps (PMI and PMM) are localised in glycosomes of BSF, while the last enzyme, MPGT, is localised in the cytosol. Therefore, GDP-Man is produced in the cytosol (Denton et al., 2010) and the three enzymes involved in its production are essential for BSF (Denton et al., 2010; Bandini et al., 2012; Kuettel et al., 2012).

The last sugar nucleotide, GDP-Fuc, is synthesized from GDP-mannose by consecutive action of two enzymes (Figure 1.29). Genes coding for GDP-mannose dehydratase (GMD) and GDP-fucose synthetase (GMER) have been identified in *T. brucei*. GMD was shown to be essential for both BSF and PCF, and localised in glycosomes (Turnock et al., 2007). Intriguingly, the substrate GDP-Man is produced in the cytosol, meaning that GDP-Man must re-enter the glycosomes to be used by GMD for production of GDP-Fuc.

In eukaryotic cells, the production of sugar nucleotides takes place in the cytosol, from where they are translocated to ER and the Golgi apparatus. Interestingly, 11 out of the 13 enzymes involved in sugar nucleotide biosynthetic pathways have been localised in *T. brucei*'s glycosomes, implicating that these sugar nucleotides are exchanged with the cytosol through the membrane. However, no sugar nucleotide transporters in the glycosomal membrane have been identified so far. From these 11 enzymes, only six possess a PTS in *T. brucei* (Table 1.6). How the rest of these enzymes reach the glycosomes is an open question. Piggybacking has been proposed to explain glycosomal localisation of the other five enzymes: PAGM, PMM, UGP, GNA and GMD. However, there is no evidence so far supporting this hypothesis.

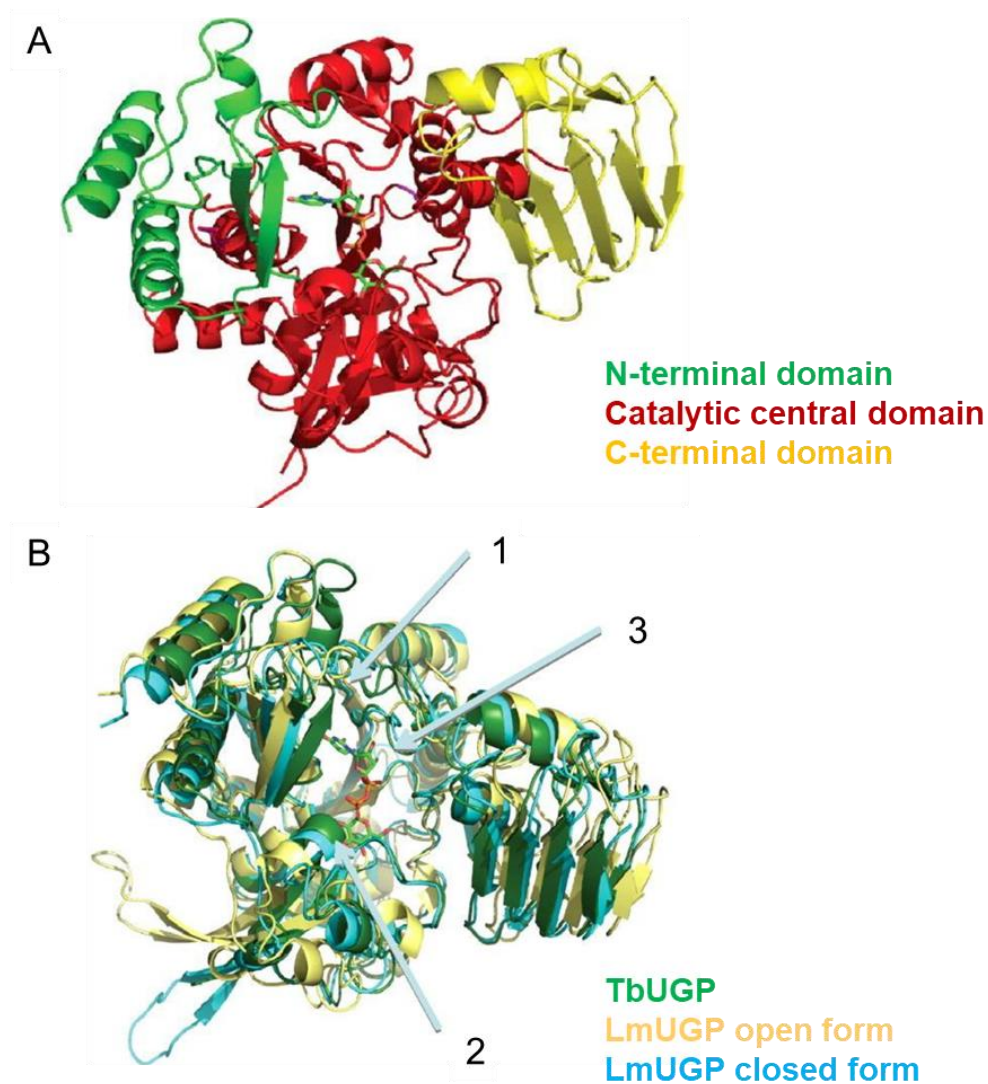


**Figure 1.30. 3D structure of TbUGP in complex with UDP-Glc.**

The three classical UGP domains present in TbUGP are illustrated in A. The overall 3D structure is compared with the *Leishmania major* LmUGP in panel B. Arrow 1 shows the additional 12 degree closure of TbUGP onto substrate compared to both open and closed conformations of LmUGP. Arrow 2 shows the sugar-binding loop (SB loop) aligning well with the closed conformation. Arrow 3 shows the nucleotide-binding loop (NB loop), similar to the one in LmUGP (From Mariño et al., 2010).



### 1.8.2. UDP-glucose pyrophosphorylases

UDP-glucose pyrophosphorylase (UGP, EC 2.7.7.9) catalyses the reversible coupling of G1P and UTP to produce UDP-Glc and inorganic pyrophosphate (PPi) in the presence of  $Mg^{2+}$  ions (Decker and Kleczkowski, 2019). Several UGPs from different organisms, including human, plants and protists have been characterised. This protein is formed by a N-terminal domain, a catalytic central domain and a C-terminal domain (Figure 1.30) and follows an ordered bi-bi mechanism for production of UDP-Glc. First, UTP binds to the enzyme in a closed conformation, this activates a conformational transition and shift of the nucleotide-binding (NB) loop. The binding pocket for the glucose ring is then formed, allowing G1P to bind. The structure changes, with the sugar-binding (SB) loop moving, stabilizing G1P and closing the structure, afterwards the reaction occurs. Finally, the product PPi is released followed by UDP-Glc (Fühning et al., 2013, 2015; Kleczkowski and Decker, 2015). Sequences of both NB-loop and SB-loop are well conserved among orthologues from different organisms including kinetoplastids, euglenids, yeast, plants and human (Figure 1.31).

UGPs from *T. brucei* and *L. major* have been cloned, expressed and characterised (Lamerz et al., 2006; Mariño et al., 2010; Fühning et al., 2013). Their overall structure is similar (Figure 1.30). Both enzymes are highly specific for G1P or UDP-Glc, unlike enzymes from other organisms, which may also use galactose (Decker et al., 2012; Ebrecht et al., 2015). The trypanosomatid and plant UGPs are active as monomers, while animal and fungal UGPs are active as octamers (Decker and Kleczkowski, 2019). It has been shown that the UGP activity can be regulated by different mechanisms, including reversible redox mechanisms. Three examples have been characterised in different protists. For instance, the monomeric UGP of *Entamoeba histolytica* and *Giardia lamblia* gets inactivated by  $H_2O_2$  due to a disulphide bond formed between two cysteine residues close to each other in the 3D structure, which impairs the nucleotide binding (Martínez et al., 2011; Ebrecht et al., 2015). In *Euglena gracilis*, the mechanism involves alkylation or oxidation of five cysteine residues inactivating the enzyme activity (Muchut et al., 2018). In these three cases, the catalytic activity can be recovered by adding reducing compounds like DTT. Another regulatory mechanism reported in yeast is phosphorylation (Smith and Rutter, 2007).

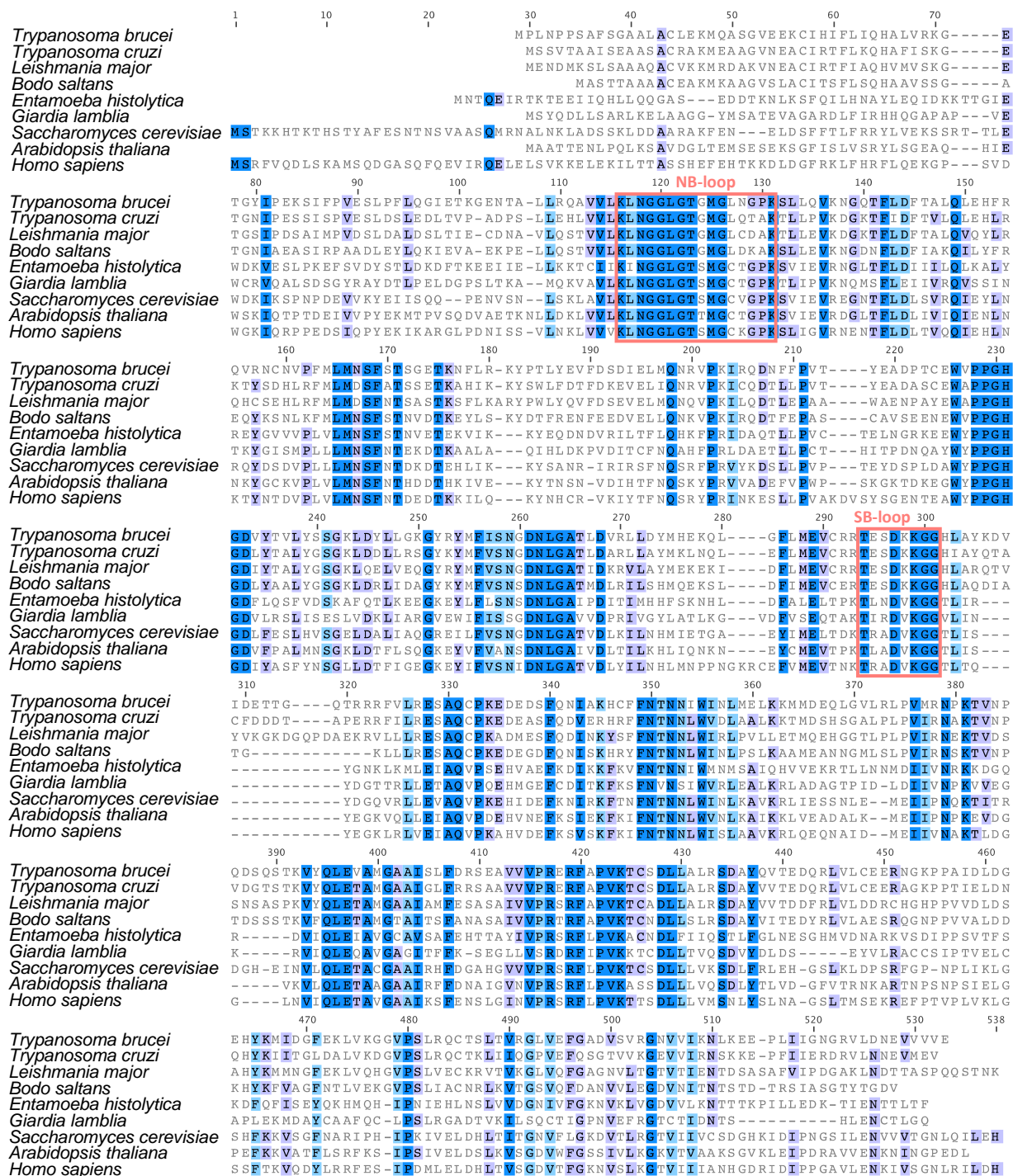


**Figure 1.31. Sequence alignments of UGP orthologues.**

Accession numbers: *T. brucei* (CBJ20765.1), *T. cruzi* (XP\_808700.1), *L. major* (XP\_001682505.1), *B. saltans* (CUG88789.1), *E. histolytica* (XP\_652750.2), *G. lamblia* (XP\_001706597.1), *S. cerevisiae* (NP\_012889.3), *A. thaliana* (NP\_186975.1), *H. sapiens* (NP\_006750.3). Identical or similar residues are shaded in colours depending on the number of sequences showing similarity, dark blue: 100%, light blue: 80-100%, purple: 60-80%. NB-loop and SB-loop are indicated in a red square (see text for details).

In this case, UDP-Glc produced by the isoform UGP1 is preferentially used for glycogen synthesis in the cytosol while UDP-Glc produced by the phosphorylated isoform UGP2 serves for glucan synthesis in the plasma membrane. In the case of some plants, oligomerization of UGPs can hinder the active site and inactivate the enzyme (Decker and Kleczkowski, 2019).

UGP activity is found in the cytosol of animal cells (Turnquist and Hansen, 1973), protists (Muchut et al., 2018) and plant cells (Kleczkowski et al., 2010). Additionally, it has been found in the Golgi apparatus, chloroplasts, membrane fractions and cell walls of plant cells (Kleczkowski et al., 2010). In trypanosomatids, UGP is found in the cytosol of *L. major* (Damerow, PhD thesis) and glycosomes of *T. brucei* (Mariño et al., 2010). The raison d'être of UGP localisation in different subcellular compartments has only been addressed in yeast cells, where the phosphorylation and concomitant targeting of UGP to the plasma membrane influence the fate of UDP-Glc production (Smith and Rutter, 2007).

As mentioned above, the main role of UDP-Glc is to act as a glucose donor for glycosylation reactions in the lumen of the endoplasmic reticulum (ER) and Golgi apparatus, however, UDP-Glc can be used for other cellular functions. First, it is used for glycogen biosynthesis in yeast (Decker and Kleczkowski, 2019). Second, is involved in glycoprotein quality control in the ER through glycosylation by the UDP-Glucose: Glycoprotein Glucosyltransferase (UGGT), which distinguishes between folded and unfolded glycoproteins hence only properly folded glycoproteins can exit the ER (Sousa and Parodi, 1995). Third, UDP-Glc is also an extracellular signalling molecule sensed by G protein-linked receptors in animals (Lazarowski and Harden, 2015) and likely in plants (Janse van Rensburg and Van den Ende, 2018). Fourth, in kinetoplastids, UDP-Glc is used for production of the modified thymine DNA base called base J involved in RNA Polymerase II transcription termination (Kieft et al., 2019). Finally, UDP-Glc is a precursor of UDP-Gal production by UDP-Glc-4'-epimerase (GalE).

*T. cruzi* and *L. major* can additionally synthesize UDP-Gal from galactose since galactokinases and UDP-sugar pyrophosphorylases (USP) have been identified (Damerow et al., 2010, 2015a; Yang and Bar-Peled, 2010; Lobo-Rojas et al., 2016). However, no *USP* nor *GALK* gene is present in the *T. brucei* genome, therefore UDP-Gal is only produced by epimerisation of UDP-Glc. Production of UDP-Gal is also essential for both BSF and PCF trypanosomes (Roper et al., 2002, 2005).

## 1.9. Aims

The compartmentalisation of metabolic pathways within organelles is one of the most interesting characteristics of trypanosomatid parasites. Several hypotheses have been proposed to understand the role of having glycolytic enzymes within glycosomes, however, other pathways that also occur in this organelle warrant further work.

In *T. brucei*, five sugar nucleotides are produced: UDP-Glucose, UDP-Galactose, GDP-Mannose, GDP-Fucose and UDP-N-acetylglucosamine. These activated forms of sugars are used for glycosylation reactions in the ER and Golgi apparatus. Interestingly, 11 out of the 13 enzymes involved in the pathways leading to production of nucleotide sugar are localised in the glycosomes.

The first part of this thesis is mainly focused on UGP (Tb927.10.13130), a key enzyme involved in the production of UDP-Glc, the precursor of UDP-Gal and a substrate for glycosylation reactions. I address several aspects including the subcellular localisation of UGP in PCF cells of *T. brucei*, its essentiality and the role of subcellular localisation in the production of UDP-Glc. Moreover, I characterised the PTS-independent mechanism of glycosomal import of UGP.

The second part of this thesis is focused on mitochondrial metabolism. I investigated the potential of excreted end products from glucose metabolism and TCA cycle intermediates to be used as carbon sources for energy metabolism of PCF cells and their effect of cell growth, under conditions similar to those encountered in the midgut of the insect vector.

## **2. RESULTS PART I: Glycosomal import of UDP-glucose pyrophosphorylase and its functionality in glycosomal and cytosolic UDP-glucose producing pathways**

This section addresses the biosynthesis of sugar nucleotides in *T. brucei* and an unconventional way of importing glycosomal matrix proteins into the organelle. I studied the subcellular localisation of UDP-glucose pyrophosphorylase (UGP), the enzyme responsible for UDP-glucose production. Sugar nucleotides are synthesized in the cytosol of eukaryotic cells, which seems not to be the case for *T. brucei*. In this parasite, UGP was reported to be localised in the glycosomes of bloodstream forms (BSF) (Mariño et al., 2010), in addition to other enzymes involved in biosynthesis of sugar nucleotides (Table 1.6). However, I show here that UGP is also localised in the cytosol of both PCF and BSF.

The first question addressed in this section of my thesis is related to the absence of a peroxisomal targeting signal (PTS) in *T. brucei* UGP. Since glycosomes are peroxisome-related organelles and the import machinery is conserved (Galland and Michels, 2010; Haanstra et al., 2016), most glycosomal proteins are expected to have a canonical PTS. However, proteomic analyses of purified glycosomes showed that a significant part of glycosomal proteins lacked PTS1 or PTS2 (Colasante et al., 2006; Güther et al., 2014). How are PTS-lacking proteins, including UGP, imported into glycosomes? In theory, the poorly described phenomenon of piggybacking could at some extent facilitate their import (Thoms, 2015). Unexpectedly, a proteomic analysis carried out in our laboratory on glycosomal-enriched fractions of procyclic trypanosomes showed that UGP was absent in the glycosomes of the PEPCK null mutant ( $\Delta pepck$ ). Therefore, the hypothesis was that the UGP is imported into glycosomes by piggybacking on the PTS1-containing glycosomal enzyme PEPCK, which acts as a carrier. Here I show evidence supporting this hypothesis and I studied the interactions between UGP and PEPCK.

The second question is related to the role of the enzyme, with regard to the dual cytosolic and glycosomal subcellular localisation. Considering that GalE, the following step of the pathway producing UDP-Gal from UDP-Glc, is essential for both BSF and PCF trypanosomes (Roper et al., 2005, 2005; Urbaniak et al., 2006), and that UDP-Glc is the only source of UDP-Gal, UGP is expected to be an essential enzyme.

In which of the two compartments, cytosol and/or glycosomes, is UGP functional? Does the subcellular localisation of UGP influence production of UDP-Glc? These questions were addressed by producing mutants expressing UGP in the cytosolic or glycosomal compartments, and comparing production of UDP-Glc by a metabolomics approach with cells expressing UGP in both compartments or not at all.

**The trypanosome UDP-glucose pyrophosphorylase is imported by piggybacking into glycosomes and is involved in the active ubiquitous cytosolic and unconventional glycosomal sugar nucleotide biosynthetic pathways.**

**Oriana Villafraz<sup>1</sup>, H     Baudouin<sup>1,2</sup>, Muriel Mazet<sup>1,2</sup>, Hanna Kulyk<sup>3</sup>, Jean-William Dupuy<sup>4</sup>, Erika Pineda<sup>1</sup>, Cyrille Bott  <sup>5</sup>, Daniel Inaoka<sup>6,7</sup>, Jean-Charles Portais<sup>3</sup>, Fr    ric Bringaud<sup>1,2,#</sup>**

<sup>1</sup> Univ. Bordeaux, CNRS, Microbiologie Fondamentale et Pathog  nicit   (MFP), UMR 5234, F-33000 Bordeaux, France

<sup>2</sup> Univ. Bordeaux, CNRS, Centre de R  sonance Magn  tique des Syst  mes Biologiques (CRMSB), UMR 5536, F-33000 Bordeaux, France

<sup>3</sup> LISBP, Universit   de Toulouse, CNRS, INRA, INSA, 135 Avenue de Rangueil, F-31077 Toulouse

<sup>4</sup> Univ. Bordeaux, Plateforme Prot  ome, F-33000, Bordeaux, France

<sup>5</sup> IAB, Universit   Grenoble Alpes, UMR-5309 CNRS Inserm, Institut Jean Roget, Universit   Grenoble Alpes, Domaine de la Merci, 38700 La Tronche, France

<sup>6</sup> Department of Biomedical Chemistry, Graduate School of Medicine, The University of Tokyo, Tokyo, Japan

<sup>7</sup> School of Tropical Medicine and Global Health, Department of Molecular Infection Dynamics, Shionogi Global Infectious Disease Division, Institute of Tropical Medicine (NEKKEN), Nagasaki University, Nagasaki, Japan

### **Contributions**

OV and FB designed the experiments. OV performed all the experiments in PCF and prepared samples for proteomics and IC-HRMS. HB and MM did preliminary work with *RNAi* UGP and UGP activity assays. EP performed experiments in BSF. HK and J-CP performed IC-HRMS analyses at the MetaToul platform (Toulouse). J-WD performed proteomic analysis at the Proteome platform (Bordeaux). DI started heterologous expression systems for PEPCK and UGP. CB was co-tutor of this work (ParaFrap program). OV and FB wrote the manuscript.

## 2.1. Abstract

*Trypanosoma brucei*, the etiological agent of sleeping sickness, has peroxisome-related organelles, called glycosomes, which contain metabolic pathways usually present in the cytosol of other eukaryotes, such as glycolysis and biosynthesis of sugar nucleotides. UDP-glucose pyrophosphorylase (UGP), an enzyme involved in the synthesis of a sugar nucleotide, UDP-glucose, is localised in the cytosol and glycosomes of the bloodstream and procyclic trypanosomes, despite the absence of any known peroxisomal targeting signal (PTS1 and PTS2). We showed that UGP is imported into glycosomes by piggybacking on the glycosomal PTS1-containing phosphoenolpyruvate carboxykinase (PEPCK) and identified the domains involved in the UGP/PEPCK interaction. Only 3-10% of the glycosomes show UGP/PEPCK proximity using the proximal ligation assay. These glycosomes probably correspond to organelles competent for protein import, in agreement with the model of peroxisome multiplication by growth of membrane extensions, protein import and fission. In addition, we showed that UGP is essential for growth of trypanosomes and that both the glycosomal and cytosolic metabolic pathways involving UGP are functional, since the lethality of the knock-down UGP mutant cell line (*RNAi*UGP) was rescued by expressing a recoded UGP in the organelle (*RNAi*UGP/*EXP*rUGP-GPDH). Our conclusion was supported by targeted metabolomic analyses (IC-HRMS) showing that the product of the UGP reaction (UDP-Glc) is no longer detectable in the *RNAi*UGP mutant, while it is still produced in cells expressing UGP exclusively in the cytosol (PEPCK null mutant) or the glycosomes (*RNAi*UGP/*EXP*rUGP-GPDH). Trypanosomatids are the only known organisms to have selected peroxisomal (glycosomal) sugar nucleotide biosynthetic pathways in addition to the canonical cytosolic ones.



## 2.2. Introduction

*Trypanosoma brucei* is a parasite responsible for human African trypanosomiasis, also known as sleeping sickness, a disease affecting sub-Saharan Africa that can be fatal if left untreated (Büscher et al., 2017). This parasite is transmitted through the bite of a tsetse fly and has a complex developmental cycle including bloodstream (BSF) and procyclic (PCF) forms found in the blood of mammalian hosts and the digestive tract of the insect, respectively. A major difference between these two forms is their mode of energy conservation, with the former depending on glucose *via* glycolysis and the latter being able to use glucose, proline and other amino acids as carbon sources (Bringaud et al., 2006). The complexity of *T. brucei*'s life cycle leads to a fast and high adaptation capacity mostly through metabolic changes related to energy metabolism. One of the factors playing a role in these efficient changes is the presence of peroxisome-related organelles called glycosomes. The glycosomes contain the six or seven first glycolytic steps, which are commonly present in the cytosol of other eukaryotic cells (Oppenheimer and Borst, 1977a). In addition, the glycosomes contain up to a dozen of other metabolic pathways, including the sugar nucleotide biosynthetic pathways, which are also exclusively cytosolic in other organisms (Allmann and Bringaud, 2017).

All eukaryotes, excepted trypanosomatids, synthesize sugar nucleotides in the cytosol and then transport them into the lumen of the endoplasmic reticulum or Golgi apparatus to feed glycosyltransferase-dependent glycosylation reactions (Bard and Chia, 2016). In the particular case of trypanosomatids, most of the enzymes involved in biosynthesis of sugar nucleotides are present in the glycosomes (Roper et al., 2005; Turnock et al., 2007; Stokes et al., 2008; Mariño et al., 2010, 2011; Bandini et al., 2012). Some of them are known to be essential for the parasite survival, probably because the cell surface and endosomal/lysosomal systems are rich in essential glycoconjugates (Ferguson, 1997).

Within the steps involved in production of sugar nucleotides, UDP-glucose pyrophosphorylase (UGP) catalyses the coupling of glucose 1-phosphate (G1P) and UTP to produce UDP-glucose (UDP-Glc) (Decker, 2018). UDP-Glc is a central metabolite that acts as a glucose donor in several pathways, as exemplified by UDP-Glc: glycoprotein glucosyltransferase (UGGT), which uses this sugar nucleotide as a glucosyl donor for protein glycosylation.

UDP-Glc has also an important role in glycoprotein quality control in the ER, because UGGT specifically glycosylates unfolded glycoproteins to prevent their exit into the cytosol (Sousa and Parodi, 1995).

UDP-Glc is also the obligate precursor of UDP-galactose (UDP-Gal) via a reaction catalysed by UDP-Glc 4'-epimerase (GalE), given that the parasite hexose transporters are unable to transport galactose (Tetaud et al., 1997). The lethality of the *T. brucei* GalE null mutant makes UDP-Glc production essential for the parasite (Roper et al., 2002). In the case of the closely related parasite *Leishmania major*, UDP-sugar pyrophosphorylase (USP) can also activate G1P, in addition to galactose 1-phosphate, while the *T. brucei* genome does not contain the *USP* orthologous gene. Consequently, the simultaneous deletion of the *USP* and *UGP* genes is required to deplete the *Leishmania* cells of UDP-Glc and UDP-Gal, leading to growth arrest and cell death (Damerow et al., 2015b). In contrast to the animal and fungal UGP, which are octameric (Fühling et al., 2015) and can be regulated by redox mechanisms (Martínez et al., 2011; Ebrecht et al., 2015; Muchut et al., 2018) or phosphorylation (Smith and Rutter, 2007), the characterised *T. brucei* and *Leishmania major* UGP are active as monomers and are regulated by allosteric mechanisms (Lamerz et al., 2006; Mariño et al., 2010; Fühling et al., 2013).

The *T. brucei* UGP is reported to be localised in glycosomes of BSF (Mariño et al., 2010). However, it does not contain any of the canonical peroxisomal targeting signals (PTS) required for import of proteins into the organelle, i.e. the PTS1 tripeptide ([STAGCN]-[RKH]-[LIVMAFY]) or PTS2 ([M]-X<sub>0/20</sub>-[RK]-[LVI]-X<sub>5</sub>-[HQ]-[ILAF], x refer to any amino acid with their number in subscript) located at the C- and N-terminal extremities of the peroxisomal/glycosomal proteins, respectively (Rucktäschel et al., 2011). Alternatively, proteins lacking a PTS can be imported into the organelle by piggybacking through interaction with a PTS-containing protein. The very few examples of piggybacking described so far in peroxisomes of mammals (Islinger et al., 2009; Schueren et al., 2014), plants (Kataya et al., 2015) and yeast (Titorenko et al., 2002; Al-Saryi et al., 2017b) involve homo-oligomeric proteins or functionally related proteins. Here we show that the *T. brucei* UGP (*i*) is an essential enzyme with a dual cytosolic and glycosomal localisation, (*ii*) is imported into the glycosomes by piggybacking on a PTS1-containing glycosomal enzyme, phosphoenolpyruvate carboxykinase (PEPCK) and (*iii*) belongs to functional cytosolic and glycosomal pathways leading to the production of UDP-Glc. The positive selection of functional

sugar nucleotide biosynthesis within glycosomes of trypanosomatids, while this pathway is exclusively cytosolic in the other eukaryotes, raises questions about its role in these parasites.

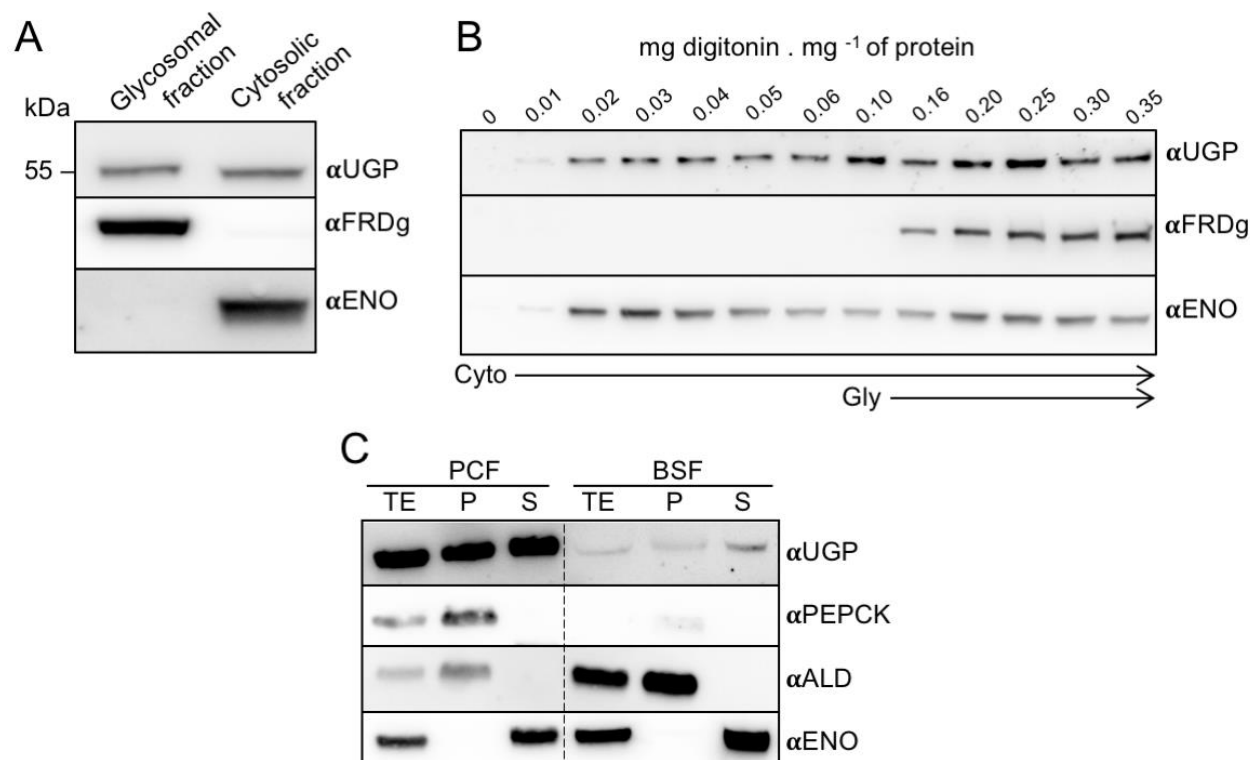


**Figure 2.32. UGP has a dual localisation in PCF and BSF.**

(A) UGP subcellular localisation in the PCF by differential centrifugation. Glycosome and cytosol-enriched fractions were analysed by western blot using the anti-UGP ( $\alpha$ UGP), as well as immune sera against the glycosomal NADH-dependent fumarate reductase ( $\alpha$ FRDg) and cytosolic enolase ( $\alpha$ ENO) markers.

(B) UGP localisation by digitonin titration. The supernatants collected from the parental cells incubated with 0-0.35 mg of digitonin per mg of protein were analysed by western blot using the immune sera indicated in the left margin.

(C) Comparison of the subcellular localisation and protein expression levels of UGP and PEPCK, as well as glycosomal (aldolase) and cytosolic (enolase) markers in PCF and BSF trypanosomes. Total extracts (TE), pellets (P) and supernatants (S) obtained after hypotonic lysis were analysed by western blot using the immune sera indicated.

## 2.3. Results

### **a) UDP-glucose pyrophosphorylase (UGP) has a dual glycosomal and cytosolic localisation**

Previous studies on the UGP subcellular localisation using immunofluorescence techniques revealed that the protein is associated with glycosomes of the BSF (Mariño et al., 2010), despite the absence of any known peroxisomal targeting signal (PTS1/PTS2). We raised an anti-UGP immune serum to confirm this unexpected glycosomal localisation of UGP in PCF. Three different methods were used to determine the subcellular localisation of UGP, based on western blotting analyses.

Firstly, glycosomal and cytosolic fractions were prepared by differential centrifugation and analysed by western blotting, using control antibodies against glycosomal (NADH-dependent fumarate reductase, FRDg) and cytosolic (enolase, ENO) proteins. The anti-UGP immune serum detected a 55 kDa protein corresponding to the expected size of UGP (theoretical MW: 54.5 kDa), which is approximately at the same concentration in both compartments considering that the same amount of protein is loaded in each lane (Figure 2.32A).

Secondly, the dual localisation of UGP was confirmed by digitonin titration. Figure 2.32B shows the western blotting analysis of supernatants obtained after treatment with different concentrations of digitonin. UGP started to be released together with the cytosolic marker enolase at low concentrations of detergent. Then, the UGP signal increased with the digitonin concentration required to release the glycosomal marker FRDg (0.16 mg of digitonin per mg of protein), confirming that UGP is present in both cytosol and glycosomes.

Lastly, the UGP subcellular localisation was addressed by performing hypotonic lysis, with both PCF and BSF trypanosomes. With this approach, cytosolic proteins are released in the supernatant while glycosomal proteins remain in the cellular pellet, as evidenced by the glycosomal aldolase and cytosolic enolase markers (Figure 2.32C). We observed that UGP is equally distributed over the two compartments in both PCF and BSF. Remarkably, UGP is ~50 times less abundant in BSF than in PCF, similarly to PEPCK as previously reported (Creek et al., 2015).

Protein	Accession	Peptide count	Unique peptides	Confidence score	Peptide counts.10 <sup>5</sup>		Ratio
					WT	$\Delta pepck$	WT/ $\Delta$
PEPCK	Tb927.2.4210	166	165	7594	19196.0	294.8	65.1
<b>UGP</b>	<b>Tb927.10.13130</b>	<b>11</b>	<b>11</b>	<b>522</b>	<b>276.8</b>	<b>14.0</b>	<b>19.8</b>
GAPDH	Tb927.6.4280	198	185	8136	378813.9	292511.8	1.3
PGI	Tb927.1.3830	69	67	2908	5973.4	6208.5	1.0
TIM	Tb927.11.5520	45	45	2104	46542.4	59134.8	0.8
ALDO	Tb927.10.5620	131	130	5202	75896.5	98160.4	0.8
HK	Tb927.10.2020	87	6	4344	1186.5	1802.6	0.7

**Table 2.7. Protein expression levels by label-free mass spectrometry proteomic analysis of glycosomal enriched fractions.**

Glycosome-enriched fraction obtained by differential centrifugation from parental (WT) and  $\Delta pepck$  cells were analysed by proteomics at the CGFB Proteome platform. The peptide counts for PEPCK, UGP and glycolytic control enzymes are shown. The ratio WT/ $\Delta$  was calculated by dividing the peptide counts of WT by those of  $\Delta pepck$ .

## **b) PEPCK-dependent import of UGP into glycosomes**

The previously obtained PEPCK null mutant ( $\Delta pepck$ ) (Ebikeme et al., 2010) has been extensively analysed, since this enzyme plays key roles in maintaining the glycosomal energy and redox balance. Moreover, in PCF cells lacking PEPCK the glucose metabolism is down-regulated while proline consumption and metabolism is activated. In the search for adaptations present in this mutant at the protein level, proteomic analyses by label-free mass spectrometry were conducted with samples of glycosome-enriched fractions obtained by differential centrifugation from parental and  $\Delta pepck$  trypanosomes. This analysis allowed the identification and quantification of 122 glycosomal proteins, as well as additional proteins since the samples are not purified glycosomes but enriched glycosomal fractions.

Selected results are shown in Table 2.7, the complete data are available at the ProteomeXchange Consortium (<http://proteomecentral.proteomexchange.org>) (see materials and methods, label-free quantitative proteomics).

As expected, the PEPCK peptide counts were reduced by 65-fold in glycosome-enriched fractions of the  $\Delta pepck$  mutant compared to the parental cell line. This strong reduction validated the effectiveness of the approach. Surprisingly, the UGP peptide counts were also considerably reduced (20-fold) in these glycosomal fractions of the  $\Delta pepck$  mutant, indicating that UGP is absent or considerably reduced in the glycosomes of the mutant. It is noteworthy that PEPCK (or UGP) peptide counts in the  $\Delta pepck$  mutant, are certainly due to peptides wrongly attributed to PEPCK (or UGP) by the algorithm.

The expression of UGP was then evaluated by western blotting analyses in total cell extracts and glycosome-enriched fractions of WT and  $\Delta pepck$  cells. Indeed, UGP is no more detected in the  $\Delta pepck$  glycosomes, while the protein was still present in the total cell extracts (Figure 2.33A). We produced a rescue cell line in the  $\Delta pepck$  expressing a tetracycline inducible copy of *PEPCK* ( $\Delta pepck/^{EXP}PEPCK$ ). This cell line expresses PEPCK in glycosomes at similar levels as parental cells after induction with tetracycline (Figure 2.33A).

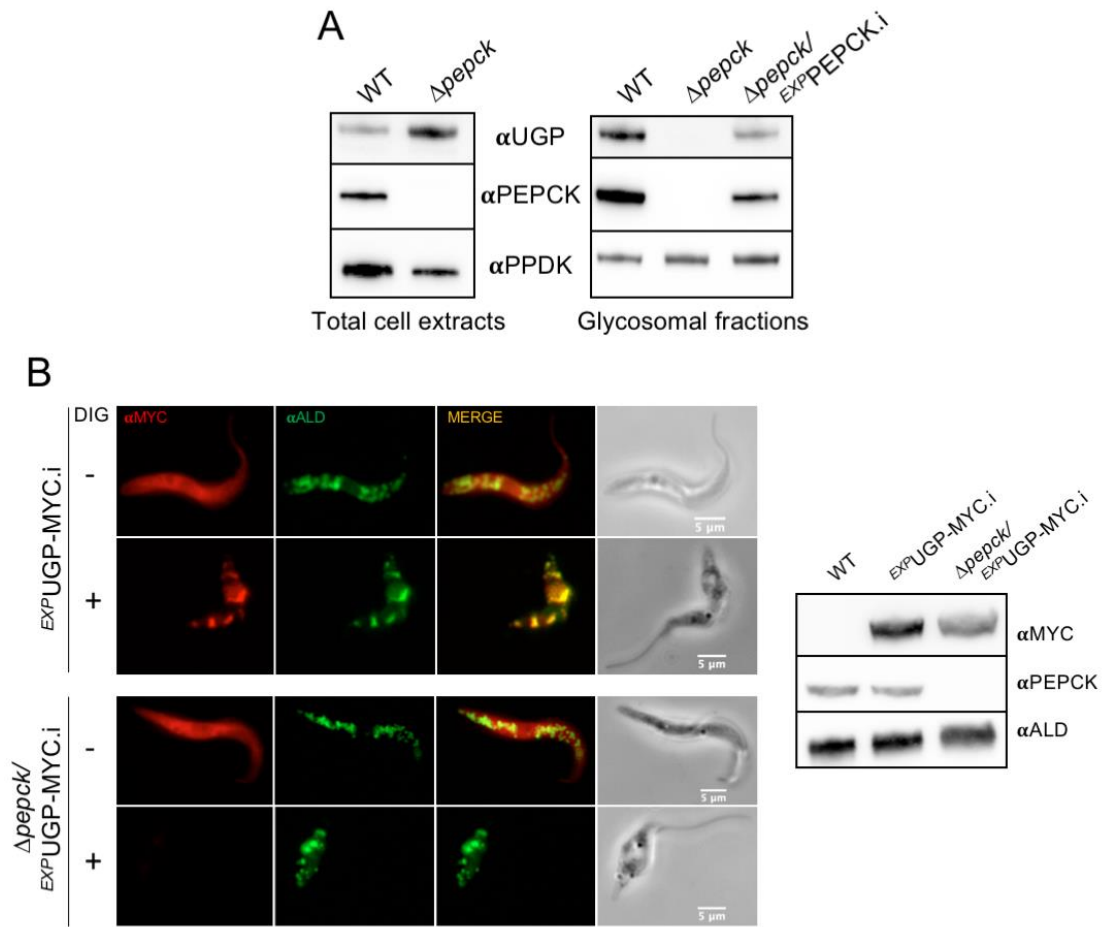


**Figure 2.33. UGP import into glycosomes depends on the PTS1-containing protein PEPCK.**

Panel A shows the western blot analysis of total cellular extracts and glycosomal fractions of WT,  $\Delta pepck$  null mutant and the tetracycline-induced  $\Delta pepck/EXPPEPCK$  rescue cell line ( $\Delta pepck/EXPPEPCK.i$ ) using the anti-UGP ( $\alpha UGP$ ), anti-PEPCK ( $\alpha PEPCK$ ) and anti-PPDK ( $\alpha PPDk$ , pyruvate phosphate dikinase) immune sera. In the left part panel B, the UGP subcellular localisation was analysed by immunofluorescence of cell lines expressing a recombinant MYC-tagged UGP in the WT ( $EXPUGP-MYC$  cell line) and  $\Delta pepck$  background ( $\Delta pepck/EXPUGP-MYC$ ), using anti-MYC ( $\alpha MYC$ , red) and the glycosomal ALD ( $\alpha ALD$ , green) control. The cells were treated (+ DIG) or not (- DIG) with 0.04 mg digitonin/mg of protein to remove or not the cytosolic UGP-MYC signal, respectively. The expression of UGP-MYC was controlled by western blots on total cell extracts (right panel) using the anti-MYC, anti-PEPCK and anti-ALD as loading control.



More importantly, the re-expression of the *PEPCK* gene in the PEPCK null background rescued the glycosomal localisation of UGP (Figure 2.33A). These data suggest that import of UGP into the glycosomes depends on the PTS1-containing PEPCK, probably by the so-called piggybacking mechanism not reported so far in trypanosomatids (Thoms, 2015; Walter and Erdmann, 2019).

Further immunofluorescence analyses were performed to show the subcellular localisation of UGP. Since the antibodies raised against native UGP detected an unspecific extra band of 70kDa (Supplementary Figure 2.48) and cannot be used for immunofluorescence analyses, we produced cell lines expressing a MYC-tagged UGP under the control of tetracycline in both the parental and the  $\Delta pepck$  backgrounds (Figure 2.33B).

The expression of the recombinant UGP-MYC in both  $EXP$ UGP-MYC and  $\Delta pepck/EXP$ UGP-MYC cell lines was confirmed by western blotting analysis. The  $\alpha$ MYC antibody recognises a single band of ~60 kDa (predicted MW: 59.7 kDa) (Figure 2.33B, right panel).

Immunofluorescence analyses showed a clear cytosolic pattern in the tetracycline induced  $EXP$ UGP-MYC.i and  $\Delta pepck/EXP$ UGP-MYC.i cell lines (Figure 2.33B, left panel). In addition, a signal that co-localises with the glycosomal marker aldolase was detected only after digitonin treatment of the  $EXP$ UGP-MYC.i cells (0.04 mg of digitonin per mg of protein) in order to permeabilize the plasma membrane and remove cytosolic signal. This confirms that the recombinant UGP-MYC exhibits a dual localisation like the native protein. Interestingly, the glycosomal signal was not detected in the  $\Delta pepck$ /UGP-MYC.i cell line after digitonin treatment, indicating that all UGP localises exclusively in the cytosol of this mutant. Altogether, these data support the role of PEPCK in the import of UGP into glycosomes.

### **c) Production and analysis of UGP-MYC and TY-PEPCK tagged cell lines**

To evidence the interaction between UGP and PEPCK, co-immunoprecipitation and native gel approaches were tested with no conclusive results and no evidence of protein interaction. This is not surprising if we consider that the association between UGP and PEPCK is probably a low affinity transient interaction, as reported for other piggybacking examples (Islinger et al., 2009).

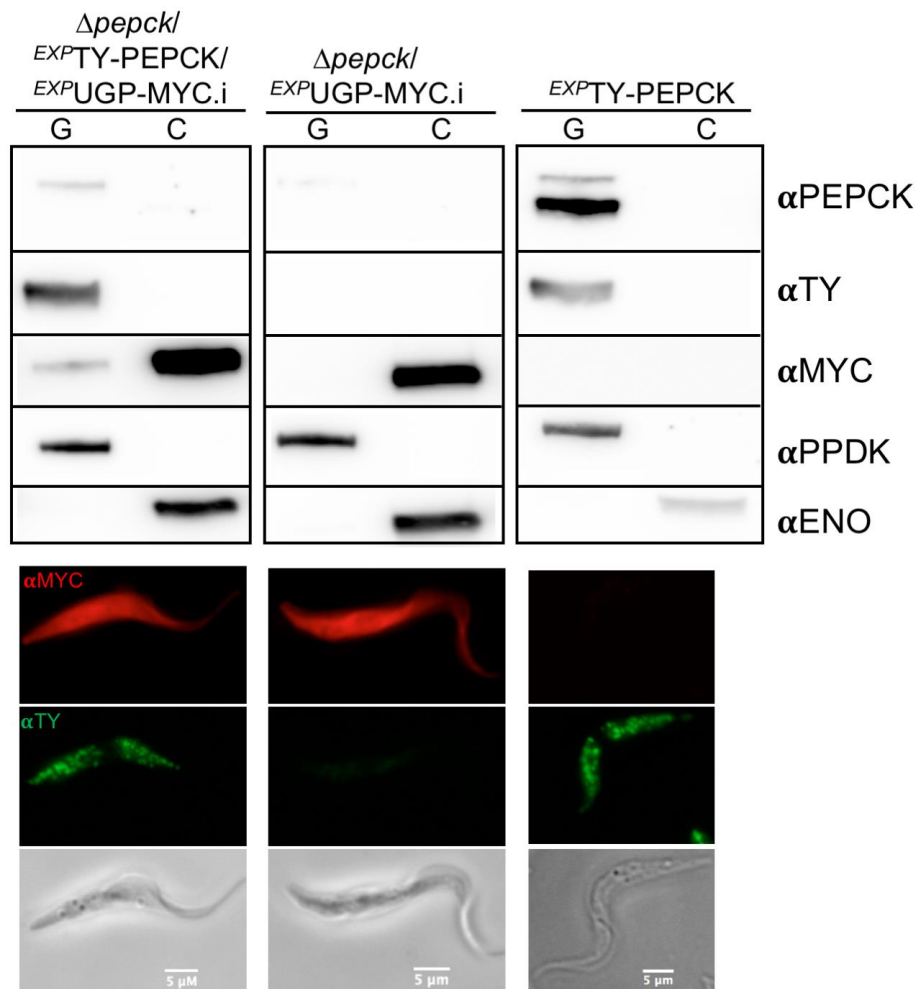


**Figure 2.34. Production of UGP-MYC and TY-PEPCK tagged cell lines.**

The top panel shows western blot analysis of glycosomal (G) and cytosolic (C) enriched fractions obtained by differential centrifugation of the  $\Delta pepck/EXPTY-PEPCK/EXPUGP-MYC$  and control  $EXPTY-PEPCK$  and  $\Delta pepck/EXPUGP-MYC$  cell lines. The anti-PEPCK recognises the tagged TY-PEPCK and the native PEPCK. The samples were also analysed with the anti-TY and anti-MYC, as well as with glycosomal (anti-PPDK) and cytosolic (anti-ENO) markers.

The low panel shows the validation of rabbit anti-MYC ( $\alpha MYC$ ) and mouse anti-TY ( $\alpha TY$ ) antibodies by immunofluorescence microscopy analyses.

As an alternative approach we used Proximity Ligation Assays (Duolink® PLA assay), which enables detecting protein interactions including transient/weak interactions *in situ* with high specificity and sensitivity (Söderberg et al., 2006). Briefly, fixed cells on a slide are incubated with two primary antibodies raised in two different species against proteins of interest before adding secondary antibodies coupled with oligonucleotides (PLA probes). When these probes are in proximity (<40 nm), connector oligos are ligated to form a circular DNA template that is subsequently amplified. Detection is performed using complementary oligonucleotide probes with a fluorescent label (Söderberg et al., 2006; Gullberg and Andersson, 2010).

Highly specific antibodies were required for the PLA assays. Since both anti-UGP and anti-PEPCK antibodies recognise unspecific extra bands on western blot analysis of total cell extracts, we produced a cell line expressing TY-tagged PEPCK (TY-PEPCK) and MYC-tagged UGP (UGP-MYC) recombinant proteins in the  $\Delta pepck$  null background ( $\Delta pepck/^{EXP}TY\text{-PEPCK}/^{EXP}UGP\text{-MYC}$ ) (Figure 2.34).

To produce this cell line, the second *PEPCK* allele of the  $\Delta pepck/PEPCK$  single allele knock-out cell line was replaced by a TY-PEPCK copy encoding TY-tagged PEPCK at its N-terminal extremity to preserve the PTS1 motif required for glycosomal import. This  $\Delta pepck/^{EXP}TY\text{-PEPCK}$  cell line was then transfected with the pLew100- $^{EXP}UGP\text{-MYC}$  plasmid to express UGP-MYC under the control of tetracycline ( $\Delta pepck/^{EXP}TY\text{-PEPCK}/^{EXP}UGP\text{-MYC}$ ). As controls, the UGP-MYC and TY-PEPCK recombinant proteins have been independently expressed in the  $\Delta pepck$  ( $\Delta pepck/^{EXP}UGP\text{-MYC}$ ) and parental ( $^{EXP}TY\text{-PEPCK}$ ) backgrounds, respectively.

The expression of both recombinant proteins, the glycosomal import of TY-PEPCK and UGP-MYC and the specificity of the primary antibodies were confirmed by western blot analyses of enriched glycosomal and cytosolic fractions (Figure 2.34, top panel) and immunofluorescence analyses (Figure 2.34, low panel).

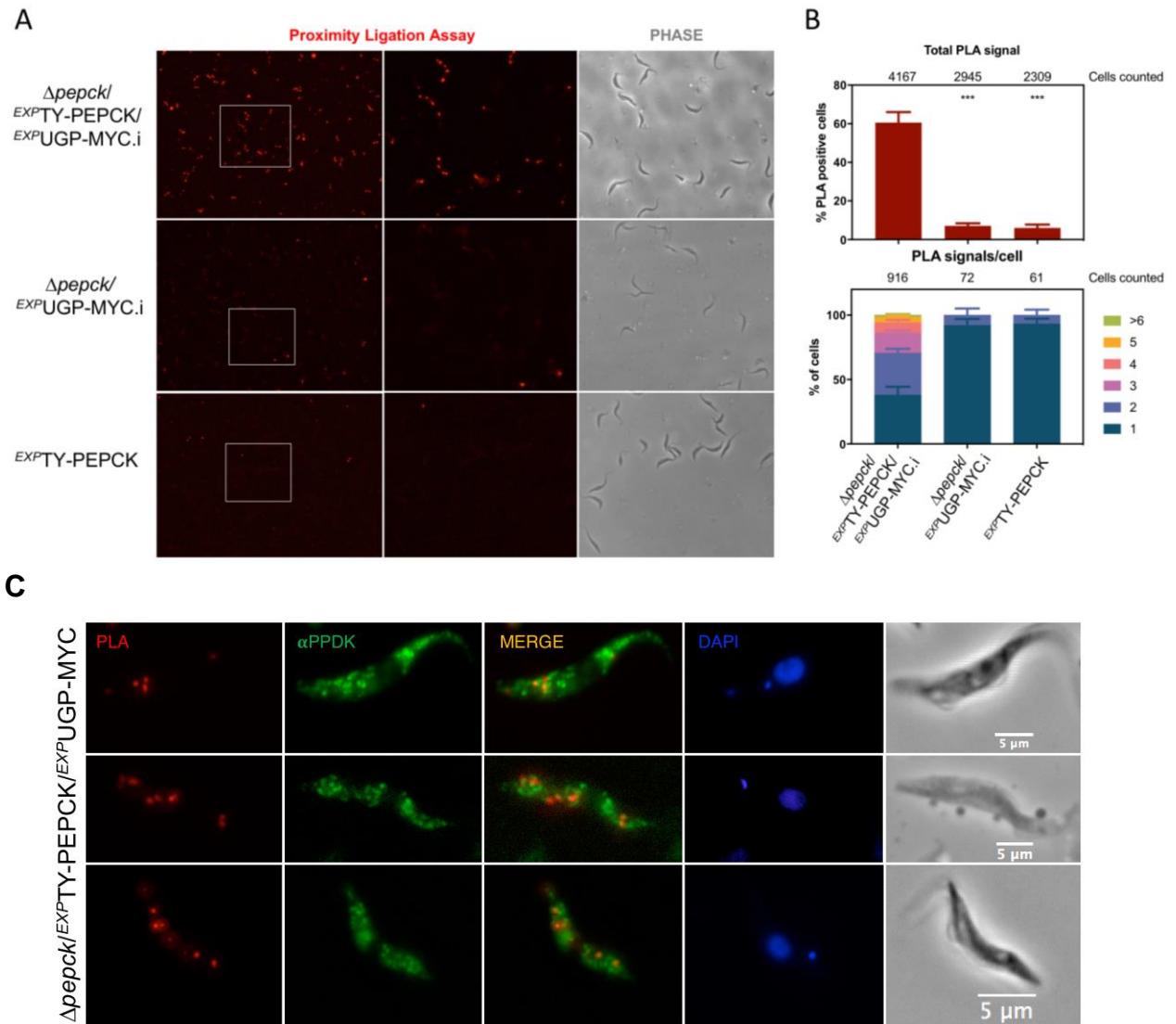


**Figure 2.35. UGP interacts transiently with PEPCK.**

Panel A shows *in situ* proximity ligation assay (PLA) analysis of the interaction between MYC-tagged UGP and TY-tagged PEPCK in the  $\Delta pepck$ / $EXP^{TY-PEPCK}$ / $EXP^{UGP-MYC.i}$  cell line. The  $EXP^{PEPCK-TY}$  and  $\Delta pepck$ / $EXP^{UGP-MYC.i}$  cell lines expressing only one recombinant protein were used as negative controls. The central (PLA) and right (phase contrast) panels are enlargements of the white rectangles shown in the left panel. In panel B, the % of PLA positive cells is shown for each cell line and the total cell number counted is indicated on the top of the graph. The percentage values correspond to the average of 18 pictures randomly taken from 3 independent experiments. Significant differences between samples are indicated: \*\*\* $p < 0.001$ . The number of PLA signals per cell was analysed by counting manually the number of dots using ImageJ for positive cells (low panel). In panel C, the localisation of PLA signal was analysed in detail and compared with the PDK glycosomal marker ( $\alpha PDK$ ) by counterstaining after the Duolink *In Situ* Protocol.

As expected, TY-PEPCK showed a glycosomal localisation, however its level of expression was ~8 times lower than that of the native protein (Figure 2.34, top panel, compare the upper and lower band of  $\alpha$ PEPCK signal in the  $^{EXP}$ PEPCK-TY cell line, respectively). Despite this difference in expression levels, the recombinant UGP-MYC is imported into the glycosomes of the tetracycline induced  $\Delta pepck/^{EXP}$ TY-PEPCK/ $^{EXP}$ UGP-MYC.i cell line, while remaining exclusively in the cytosol of the  $\Delta pepck/^{EXP}$ UGP-MYC.i cell line. Both  $\alpha$ MYC (rabbit) and  $\alpha$ TY (mouse) were validated to be specific and sensitive enough to perform the PLA analysis.

#### **d) UGP interacts with PEPCK in some glycosomes**

By using the PLA assay with a fluorescent detection system, we expect to observe discrete spots derived from single-molecule protein interaction events (Gullberg and Andersson, 2010). Figure 2.35 shows that PLA positive puncta (red signal) corresponding to TY-PEPCK/UGP-MYC hetero-oligomers were observed in 61% of the  $\Delta pepck/^{EXP}$ TY-PEPCK/ $^{EXP}$ UGP-MYC.i cells, while only 7% and 6% of the control  $\Delta pepck/^{EXP}$ UGP-MYC.i and  $^{EXP}$ PEPCK-TY cells were positive, respectively.

In addition, 92% of the positive  $\Delta pepck/^{EXP}$ UGP-MYC.i and  $^{EXP}$ PEPCK-TY control cells contained a single dot, while the number of dots per cell in the  $\Delta pepck/^{EXP}$ TY-PEPCK/ $^{EXP}$ UGP-MYC.i population was higher, with 62% of the cells showing 2 to 10 dots (Figure 2.35B). It is important to note that the number of positive cells used to count the number of dots per cell is 10 times higher for the  $\Delta pepck/^{EXP}$ TY-PEPCK/ $^{EXP}$ UGP-MYC.i (916 cells) than for  $\Delta pepck/^{EXP}$ UGP-MYC.i (72 cells) and  $^{EXP}$ PEPCK-TY (61 cells) since few positive cells are detected in these control cell lines. These data are in agreement with interactions between UGP-MYC and TY-PEPCK in  $\Delta pepck/^{EXP}$ TY-PEPCK/ $^{EXP}$ UGP-MYC.i cells, while the very few red dots observed within the control  $\Delta pepck/^{EXP}$ UGP-MYC.i and  $^{EXP}$ PEPCK-TY cells represent background signals.

Staining with an immune serum against the glycosomal PPDK showed that the PLA signals are found in very close proximity to the PPDK-containing organelles without showing clear co-localisation with them (Figure 2.35C). This suggests the existence of different pools of glycosomes with different import capacities as observed for peroxisomes in mammalian cells (Huybrechts et al., 2009; Delille et al., 2010; Costello and Schrader, 2018, Gualdrón-Lopez et al., 2013b) (see the discussion section).

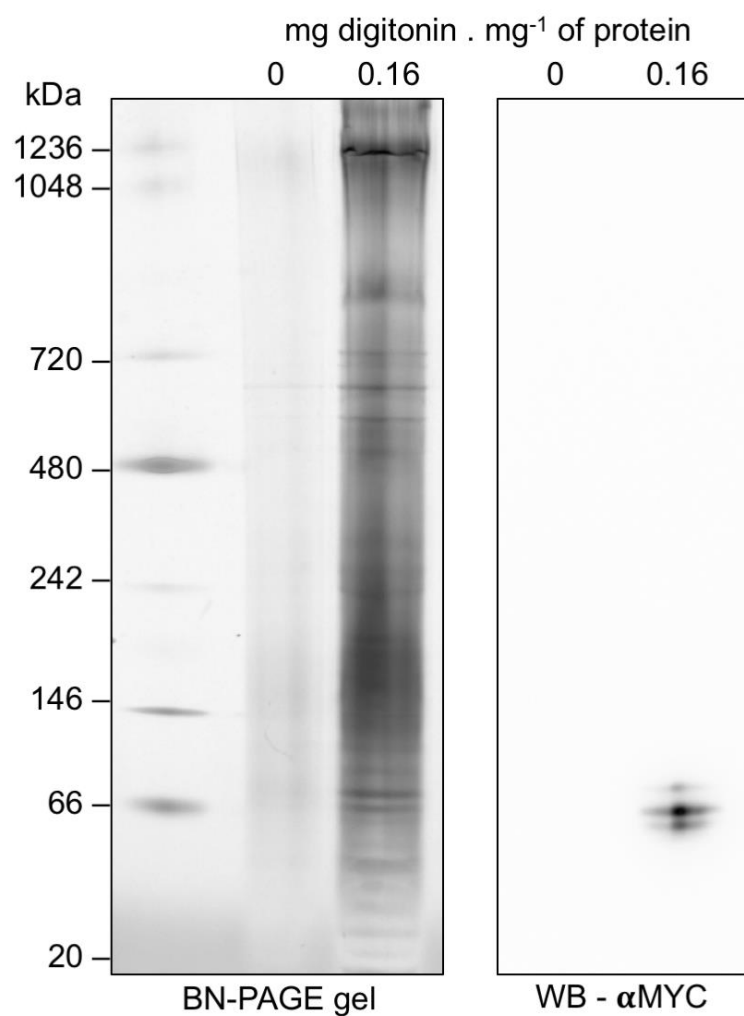


**Figure 2.36. Analysis of UGP oligomerization in native gel.**

The oligomeric state of tagged UGP-MYC was evaluated in the *EXP*UGP-MYC.i cell line. Supernatants obtained after digitonin treatment (0.16 mg of digitonin per mg of protein) or not (0) were analysed by BN-PAGE (left panel) and western blot (right panel) using the anti-MYC (αMYC) antibody.

### e) Determination of critical parts for PEPCK-UGP interaction

To investigate which part of UGP and PEPCK interacts with its piggybacking partner, truncated versions of each protein were expressed in the parental or  $\Delta pepck$  cell lines, respectively. Since *T. cruzi* PEPCK forms homodimers (Trapani et al., 2001) and the residues involved in dimerization are conserved in *T. brucei* (Supplementary Figure 2.49), the truncated PEPCK proteins were expressed in the  $\Delta pepck$  cell line to prevent heterodimer formation. In contrast, UGP is reported to be monomeric (Lamerz et al., 2006; Mariño et al., 2010) and was only detected as monomer in native gel analyses (Figure 2.36). Accordingly, native and recombinant UGP proteins are not expected to directly interact, thus UGP truncations were expressed in parental cells.

We used the endogenous tagging approach to express 10xTY tagged-UGP proteins and truncations. Briefly, a DNA sequence encoding a 10xTY tag and the blasticidin resistance cassette was amplified from pPOTv7 plasmid using long primers that incorporate a 5' overhang of 80 nucleotides homologous to *UGP* and its UTR. Cells were transfected with the PCR amplicon that fuses the tag to *UGP* by homologous recombination (Dean et al., 2015). Alternatively, one of the alleles was entirely replaced with a recoded *rUGP* fused to the 10xTY tag and blasticidin resistance cassette. This recoded version was used to evaluate the correct replacement of *UGP* by PCR.

The UGP was 10xTY tagged at either N-terminal or C-terminal ends ( $^{EXP}TY$ -UGP<sub>1-485</sub> and  $^{EXP}UGP_{1-485}$ -TY cell lines, respectively). Both UGP versions were expressed and the subcellular distribution was evaluated by western blot analysis of enriched glycosomal and cytosolic fractions (Figure 2.37A). Surprisingly, the N-terminal tag affected glycosomal import of UGP, since the glycosomal localisation of TY-UGP<sub>1-485</sub> was decreased by ~9-fold compared to the native UGP in parental cells (Figure 2.37A, left panel). However, no changes were observed in the glycosome:cytosol ratio for the C-terminal tagged UGP<sub>1-485</sub>-TY (Figure 2.37A, right panel). Consequently, the truncated UGP versions tagged at the C-terminal end were used for subsequent analyses.

The panel B of Figure 2.37 shows the expression of recoded *rUGP* versions truncated from their N-terminal extremity (UGP<sub>XXX-485</sub>-TY). The correct insertion of the recombinant fragments in the *UGP* locus was confirmed by PCR (Figure 2.38).

It is to note that the UGP coding sequence used for the UGP<sub>XXX-485</sub>-TY constructs was recoded from position 165 to 337 amino acids to become resistant to the RNAi construct (see below).

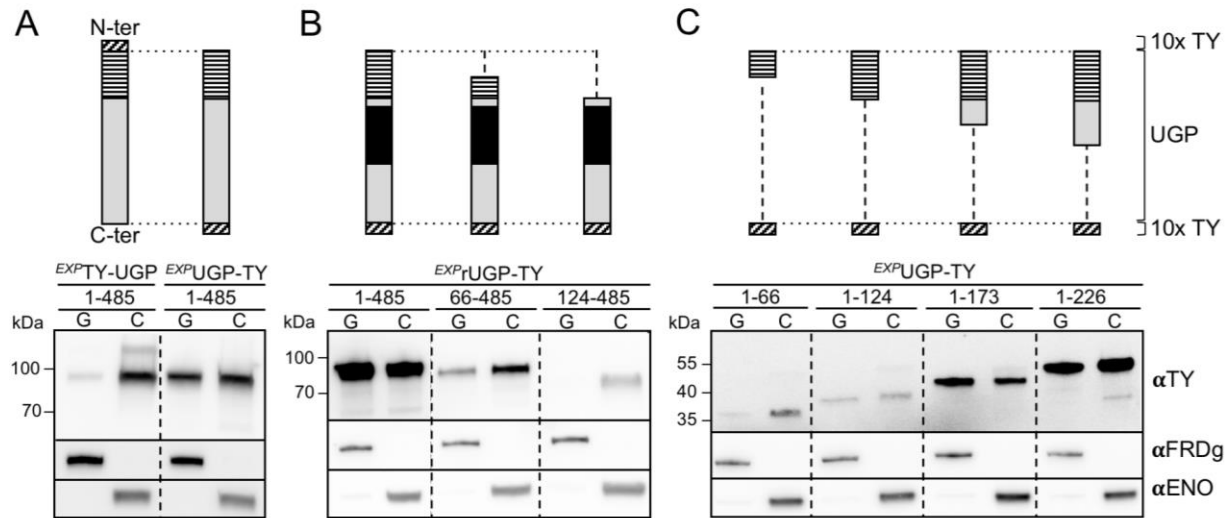


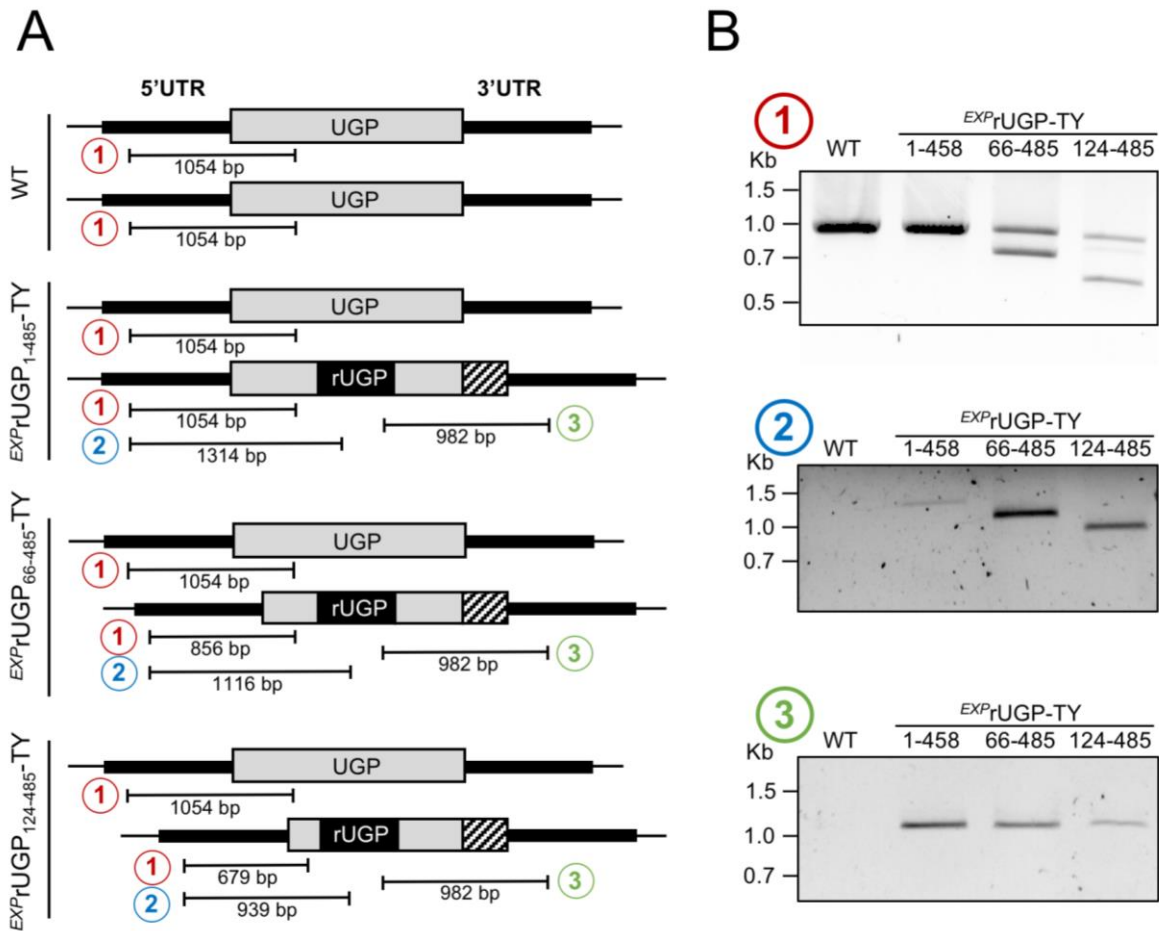
**Figure 2.37. The N-terminal 123 residues of UGP are required for import into the glycosomes.**

The top of the figure shows schematic representations of the 10xTY-tagged native or recoded UGP and the corresponding truncations. The 123-residues peptide required for UGP import, the recoded part of UGP and the 10xTY tags are highlighted by horizontally hatched boxes, black boxes and obliquely hatched boxes, respectively. The lower part of the figure shows western blot analyses of glycosomal (G) and cytosolic (C) fractions produced from cell lines expressing 10xTY-tagged recombinant UGP, using the anti-TY antibody ( $\alpha$ TY) as well as immune sera from glycosomal ( $\alpha$ FRDg) and cytosolic ( $\alpha$ ENO) markers.

Panel A shows UGP recombinant proteins tagged at the N-terminal ( $EXP^{TY}$ -UGP<sub>1-485</sub>) or C-terminal ( $EXP$ UGP<sub>1-485</sub>-TY) extremities, while panels B and C show truncated UGP tagged at the C-terminal extremity.

The truncations designed from the N-terminal end lack the first 65 (66-485) or 123 (124-485) residues (panel B), while truncations designed from the C-terminal end contain the N-terminal first 66 (1-66), 124 (1-124), 173 (1-173) or 226 (1-226) residues (panel C).





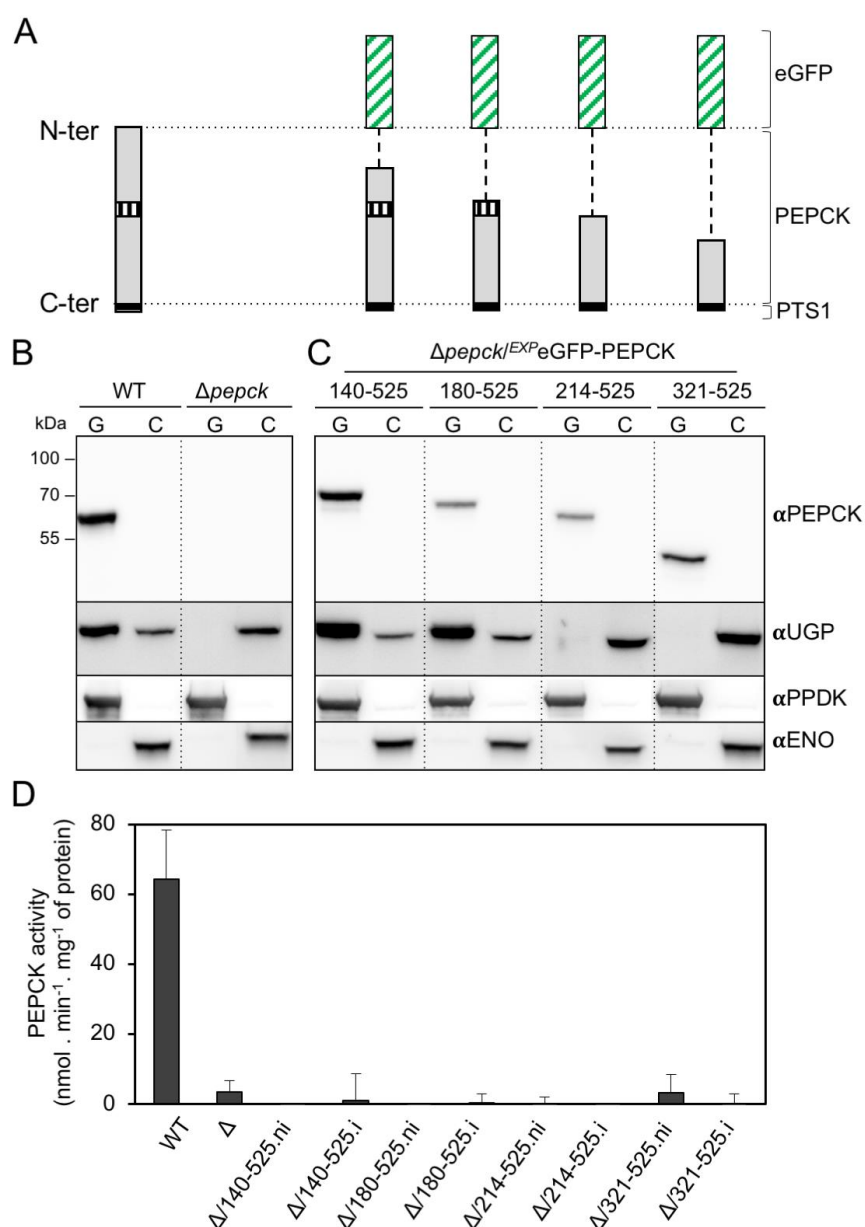


**Figure 2.39. A 34-residue peptide of PEPCK is required for glycosomal import of UGP.**

Panel A shows schematic representations of the endogenous PEPCK and eGFP-PEPCK recombinant proteins expressed in the  $\Delta pepck$  background, in which the 34-residue peptide required for UGP import (vertically hatched boxes) is highlighted. Panels B and C show western blot analyses of glycosomal (G) and cytosolic (C) fractions obtained from the parental and  $\Delta pepck$  cell lines (panel B), as well as from cell lines expressing truncated eGFP-PEPCK recombinant proteins ( $\Delta pepck/EXP$  eGFP-PEPCK<sub>XXX-525</sub>), with anti-PEPCK ( $\alpha$ PEPCK) and anti-UGP ( $\alpha$ UGP) immune sera. Glycosomal ( $\alpha$ PPDK) and cytosolic ( $\alpha$ ENO) markers were used to check the quality of glycosomal and cytosolic fractions.

Panel D shows PEPCK activity determined in total extracts of WT,  $\Delta pepck$  ( $\Delta$ ) and the non-induced (.ni) and induced (.i)  $\Delta pepck/EXP$  eGFP-PEPCK<sub>XXX-525</sub> cell lines.

The panel C of Figure 2.37 shows the expression of UGP versions truncated from their C-terminal extremity (UGP<sub>1-XXX</sub>-TY). The UGP<sub>124-485</sub>-TY truncated protein was no more imported inside the glycosomes (Figure 2.37B), while glycosomal import of the UGP<sub>1-124</sub>-TY, UGP<sub>1-173</sub>-TY and UGP<sub>1-226</sub>-TY proteins was not affected (Figure 2.37C), suggesting that the N-terminal domain up to position 123 contains residues interacting with PEPCK.

The truncated recombinant UGP missing (UGP<sub>66-485</sub>-TY) or containing only (UGP<sub>1-66</sub>-TY) the N-terminal 66 residues were imported into glycosomes, although with a lower efficiency compared to the parental cell line, suggesting that key residues of the PEPCK-binding site are located on either side of position 66 (Figure 2.37B-C). Additionally, the presence of the PEPCK binding site in the N-terminal extremity of UGP may explain the low glycosomal import of the N-terminal tagged TY-UGP<sub>1-485</sub> recombinant protein (Figure 2.37A).

We performed a similar analysis to determine the PEPCK region involved in UGP glycosomal import, by expressing truncated versions of recombinant PEPCK in the *Δpepck* background using the pLew100 vector. The PEPCK was truncated from its N-terminal extremity in order to maintain the C-terminal PTS1 required for glycosomal import of both PEPCK and UGP. Unfortunately, none of the truncated PEPCK peptides were detectable by western blotting in total cell extracts, probably due to protein instability. To resolve this stability issue, the truncated PEPCK peptides were fused to the C-terminal extremity of the green fluorescent protein (eGFP) and used to produce four different cell lines (Figure 2.39). We determined the glycosomal import of UGP in these *Δpepck*<sup>EXP</sup>eGFP-PEPCK<sub>XXX-525</sub> cell lines by western blot analyses of glycosomal and cytosolic fractions.

As mentioned above, UGP is no more detected in the glycosomes isolated from the parental *Δpepck* mutants (Figure 2.39B). The glycosomal import of UGP was not affected in the absence of the N-terminal first 140 and 180 residues of PEPCK (*Δpepck*<sup>EXP</sup>eGFP-PEPCK<sub>140-525</sub> and *Δpepck*<sup>EXP</sup>eGFP-PEPCK<sub>180-525</sub> cell lines), while deletion of the N-terminal first 214 and 321 residues abolished glycosomal import of UGP, which remained exclusively in the cytosolic fractions (Figure 2.39C). This suggests that the 34-residues peptide between amino acids positions 180 and 214 of PEPCK is required for UGP import into the glycosomes. Importantly, none of the eGFP-PEPCK truncations have PEPCK activity, indicating that the import of UGP is not related to PEPCK activity inside the glycosomes (Figure 2.39D).

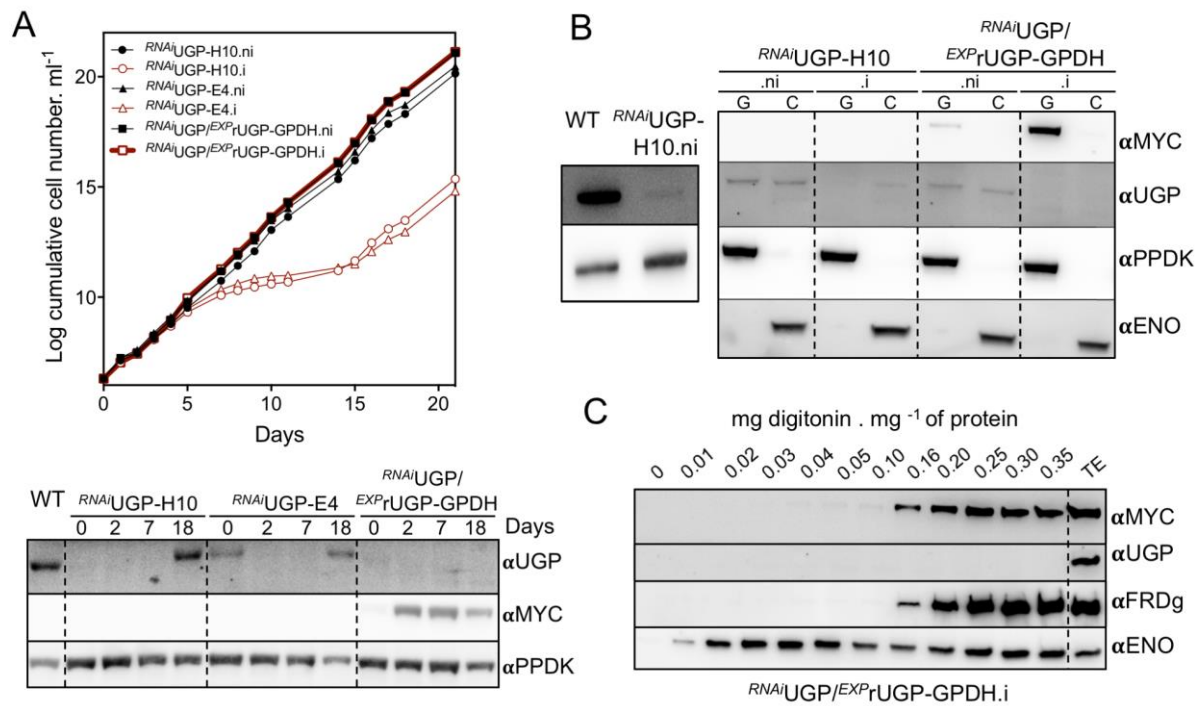


**Figure 2.40. Production and functional analyses of *RNAiUGP* cell lines.**

Panel A shows growth curves of the tetracycline-induced (.i) and non-induced (.ni) *RNAiUGP-H10*, *RNAiUGP-E4* and *RNAiUGP/EXPrUGP-GPDH* cell lines. The expression of the native UGP and recombinant rUGP-GPDH upon induction was monitored by western blot analysis using anti-UGP (αUGP) and anti-MYC (αMYC) immune sera, respectively, and anti-PPDK (αPPDK) as loading control (low panel).

Panel B shows western blot analyses of glycosomal (G) and cytosolic (C) fractions produced from the parental cells (WT), as well as tetracycline-induced (.i) and non-induced (.ni) *RNAiUGP-H10* and *RNAiUGP/EXPrUGP-GPDH* cell lines using immune sera described in precedent figures. The left panel was used to quantify relative expression of UGP in glycosomes of non-induced *RNAiUGP-H10* mutant.

The glycosomal localisation of recombinant rUGP-GPDH (αMYC) was confirmed by western blot analyses of supernatants obtained after digitonin titration of *RNAiUGP/EXPrUGP-GPDH.i* cell line, using immune sera described in precedent figures (panel C). The control lane TE corresponds to total extract from *EXPrUGP-GPDH.i* cell line.

#### **f) The UGP protein is essential for *T. brucei***

The stem-loop RNAi strategy was used with the conditional pLew100 vector to address the role of UGP in the procyclic trypanosomes. The plasmid pLew-UGP-SAS contained a sense and antisense version of an UGP fragment separated by 42-bp (see material and methods). This plasmid permits tetracycline-inducible expression of the stem-loop that triggers the RNA interference machinery of the parasite (Ngô et al., 1998; Wirtz et al., 1999).

Two <sup>RNAi</sup>UGP cell lines obtained from individual transfections (H10 and E4) showed a strong reduction of growth 7 days after tetracycline induction, indicating that UGP is essential for PCF viability (Figure 2.40A, top panel). The efficiency of the RNAi targeting UGP was confirmed by western blot analysis after induction with tetracycline (Figure 2.40A, low panel) and activity determinations in the glycosomal and cytosolic extracts of the <sup>RNAi</sup>UGP-H10.i cell line (see Figure 2.45). Indeed, the UGP was not detected either by western blot analysis or activity measurements.

For both RNAi cell lines, the growth rate was restored 18 days post-induction, concomitantly with the re-expression of the native UGP (Figure 2.40A, low panel). This re-expression of RNAi targeted genes is often observed for trypanosome essential genes (Ebikeme et al., 2010). It is noteworthy that the UGP expression was barely detectable in the non-induced <sup>RNAi</sup>UGP-H10 total cell extracts.

Western blotting analyses of enriched glycosomal and cytosolic fractions, which proved to be more sensitive than on total cell extracts, showed that UGP expression was reduced by ~30-fold compared to the parental cells without any significant effect on growth (Figure 2.40B, left panel). This suggests that UGP activity is present in large excess in parental PCF. It is also noteworthy that a ~30-fold reduction of UGP expression in the <sup>RNAi</sup>UGP-H10.ni cell line did not affect distribution of UGP between glycosomal and cytosolic compartments (Figure 2.40B, right panel). After five days of induction, UGP was no more detectable in the glycosomal fractions and was reduced by ~2-fold in the cytosol (Figure 2.40B, right panel). These small amounts of UGP were not sufficient to sustain growth of PCF.

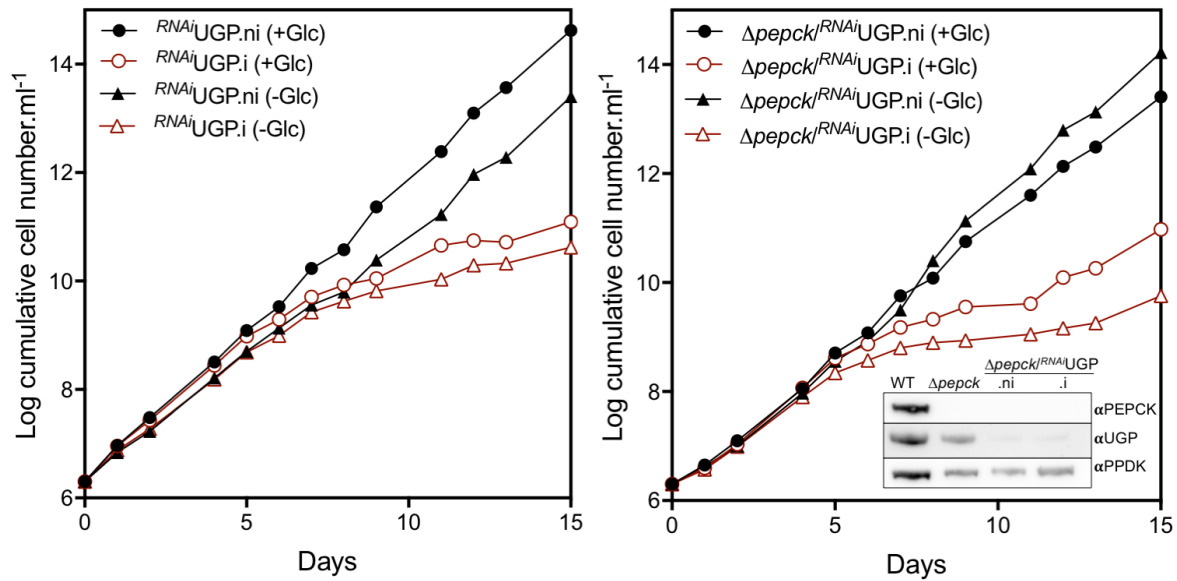


**Figure 2.41. Functional analysis of *RNAi*UGP cell lines in the presence or the absence of glucose.**

Growth curves of the tetracycline-induced (.i) and non-induced (.ni) *RNAi*UGP and  $\Delta pepck/RNAi$ UGP cell lines. The cells were grown in SDM79-GlcFree medium in the presence of 10 mM glucose (+Glc) or in the absence of glucose with 50 mM N-acetylglucosamine to inhibit the uptake of residual glucose (-Glc). The expression of PEPCK and UGP was monitored by western blot analysis (inset right panel) with the immune sera indicated in the right margin.

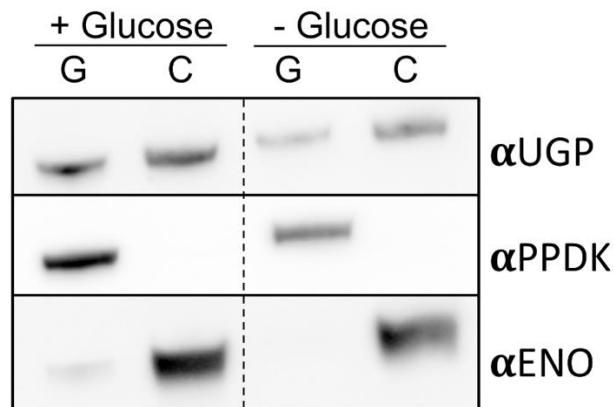


**Figure 2.42. Subcellular localisation of UGP in the presence or the absence of glucose.**

The ratio glycosomal/cytosolic UGP was compared between the procyclic trypanosomes grown in the presence (+) or the absence (-) of glucose. The figure shows a western blot analysis of glycosomal (G) and cytosolic (C) fractions obtained after subcellular fractionation. Glycosomal ( $\alpha$ PPDK) and cytosolic ( $\alpha$ ENO) markers are also shown.

To determine whether UGP is also required for growth of the procyclic trypanosomes in the insect-like glucose-free conditions, the parasites were cultivated in the absence of glucose, as described before (Wagnies et al., 2018).

The growth of the *<sup>RNAi</sup>UGP.i* is similar in the presence or the absence of glucose (Figure 2.41, left panel), indicating that UGP is probably also essential in the insect vector, which is considered to be free of glucose (Bursell, 1981).

We also produced an *<sup>RNAi</sup>UGP* in the  $\Delta pepck$  background ( $\Delta pepck/<sup>RNAi</sup>UGP.i$ ) and evaluated the essentiality of UGP in the presence or the absence of glucose. The growth of this cell line was similar to the single mutant *<sup>RNAi</sup>UGP.i* regardless of the amounts of glucose in the medium (Figure 2.41, right panel).

Finally, to investigate if the glucose availability has an effect on the subcellular distribution of UGP within the glycosomal and cytosolic subcellular compartment, we cultivated the *<sup>RNAi</sup>UGP* cells during three weeks in SDM79-GlcFree medium in the presence or the absence of glucose and prepared glycosomal and cytosolic fractions by differential centrifugation. The western blotting analysis showed that the UGP subcellular localisation is not affected by the absence of glucose (Figure 2.42).

Altogether, these data confirm that UGP is an essential enzyme with a dual glycosomal and cytosolic localisation in glucose-rich and glucose-depleted conditions.

#### **g) Targeting a recombinant UGP exclusively to the glycosomes**

To elucidate in which subcellular compartment the UDP-Glc/UDP-Gal biosynthetic pathway is active (glycosomes and/or cytosol), it was necessary to express UGP exclusively in the cytosol or in the glycosomes of the parasite.

The exclusive cytosolic localisation of UGP in the viable  $\Delta pepck$  mutant demonstrated that UGP is functionally active in the cytosol (Figure 2.41, right panel). However, the UGP glycosomal import needed optimisation to study the role of the glycosomal pathway. To do so, a recombinant *UGP* gene recoded to become resistant to the RNAi construct (*rUGP*, Figure 5.66) was fused at its 3'-extremity with a 3xMYC tag followed by different glycosomal targeting peptides (PTS1), namely the last C-terminal 12 residues of glycosomal FRDg (*rUGP-FRDgPTS1*), the full-length PTS1-containing glycosomal glycerol-3-phosphate dehydrogenase (*GPDH*) gene (*rUGP-GPDH*), and the full-length PTS1-containing glycosomal phosphoglycerate (*PGKc*) gene (*rUGP-PGKc\**).

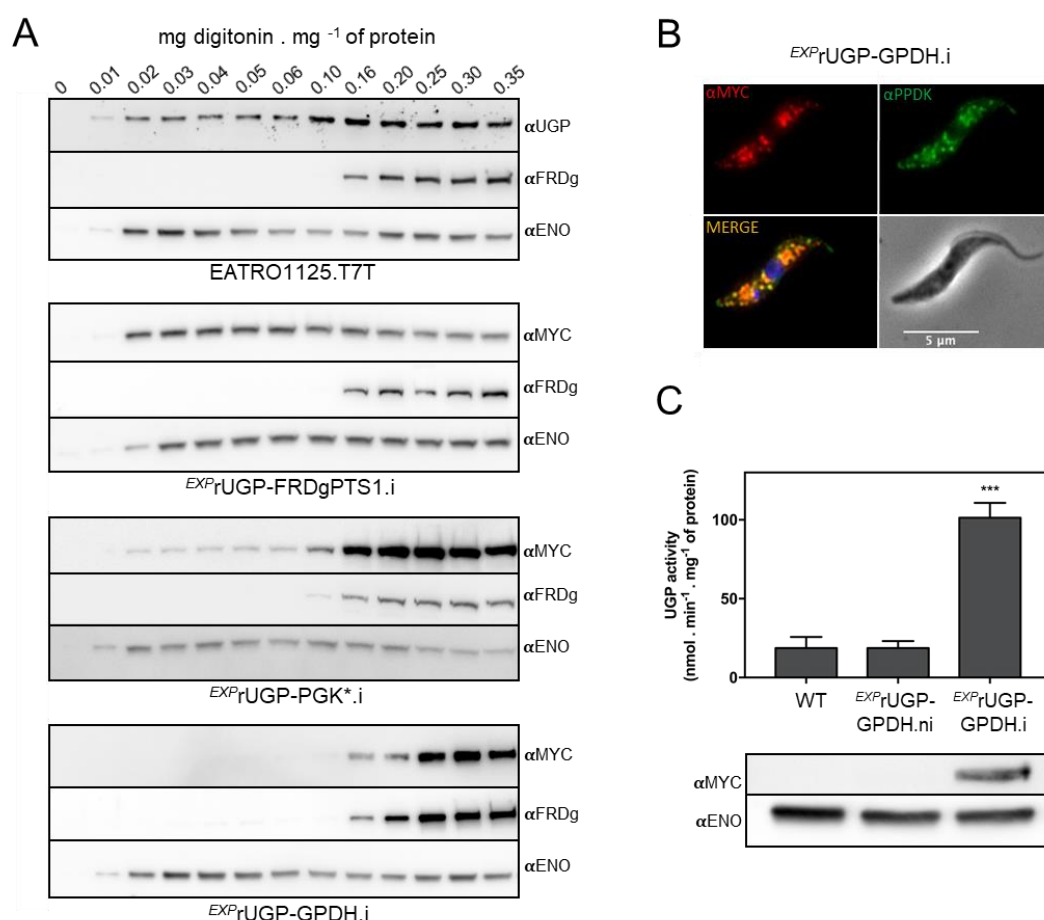


**Figure 2.43. Expression of a glycosomal recombinant UGP.**

In panel A, the subcellular localisation of the recombinant UGP was monitored by western blot analysis of supernatants obtained after digitonin titration of the tetracycline induced (.i) *EXPUGP-FRDgPTS1*, *EXPUGP-PGKc\** and *EXPUGP-GPDH* cell lines using anti-MYC (αMYC) antibody. The anti-UGP immune serum (αUGP) was used to detect UGP in parental cells fractions (top panel). Anti-FRDg (αFRDg) and anti-ENO (αENO) immune sera were used as glycosomal and cytosolic markers, respectively.

Panel B shows an immunofluorescence analysis of *EXPUGP-GPDH.i* cell line using the immune sera indicated.

Panel C shows the UGP activity measured in total cell extracts of parental (WT) and tetracycline-induced (.i) and non-induced (.ni) *EXPUGP-GPDH* cell lines (n=3, SEM). Significant differences between samples are indicated: \*\*\*p < 0.001. Western blot analysis of *EXPUGP-GPDH* expression with anti-MYC (αMYC) and anti-ENO (αENO, loading control) immune sera is shown below the graph.



Since glycosomal expression of PGK is lethal for the PCF trypanosomes (Deramchia et al., 2014), the codon of the lysine residue (K215) essential for the PGK enzymatic activity (Bernstein et al., 1998) was replaced by the alanine codon. These recombinant proteins were conditionally expressed in the parental cell line and their distribution between the glycosomal and cytosolic compartments was determined by digitonin titration and western blotting analysis using the anti-MYC antibody (Figure 2.43A).

The rUGP-FRDgPTS1 and cytosolic enolase showed the same cytosolic profile, which implies that the extended FRDg PST1 motif is not sufficient for glycosomal import of UGP. In contrast, the rUGP-PGKc\* recombinant protein is mostly associated to the glycosomes, but a minor part remained in the cytosol. Therefore, none of these fusion proteins was considered efficiently imported into glycosomes to be used for further experiments.

Finally, the rUGP-GPDH (~100 kDa) and the glycosomal FRDg proteins were both released with a minimum of 0.16 mg digitonin per mg protein, which is consistent with the exclusively glycosomal localisation of this recombinant protein (Figure 2.43A, low panel). The glycosomal localisation of this rUGP-GPDH was also confirmed by immunofluorescence analysis, since the rUGP-GPDH signal recognised with the anti-MYC co-localised with the glycosomal PPDK signal (Figure 2.43B).

We then confirmed that rUGP-GPDH had UGP activity in total cell extracts (Figure 2.43C). The activity values increased by 5-fold in the *EXPrUGP-GPDH.i* cell line compared to the non-induced (.ni) and parental cell lines, which validated the functionality of the rUGP-GPDH protein. Importantly, expression of the rUGP-GPDH had no effect on morphology, growth and survival of the *EXPrUGP-GPDH* cell line.

#### **h) Expression of the glycosomal rUGP-GPDH rescues the lethality of the *RNAiUGP* mutant**

The *EXPrUGP-GPDH* construct (pHD1336-rUGP-GPDH), which produces an exclusively glycosomal rUGP, was introduced into the *RNAiUGP-H10* cell line. Western blot analyses showed that native UGP was no more detectable in glycosomal and cytosolic fractions of the *RNAiUGP/EXPrUGP-GPDH.i* cell line, while the dying *RNAiUGP.i* cells still expressed residual amounts of UGP in the cytosol (Figure 2.40B, right panel).

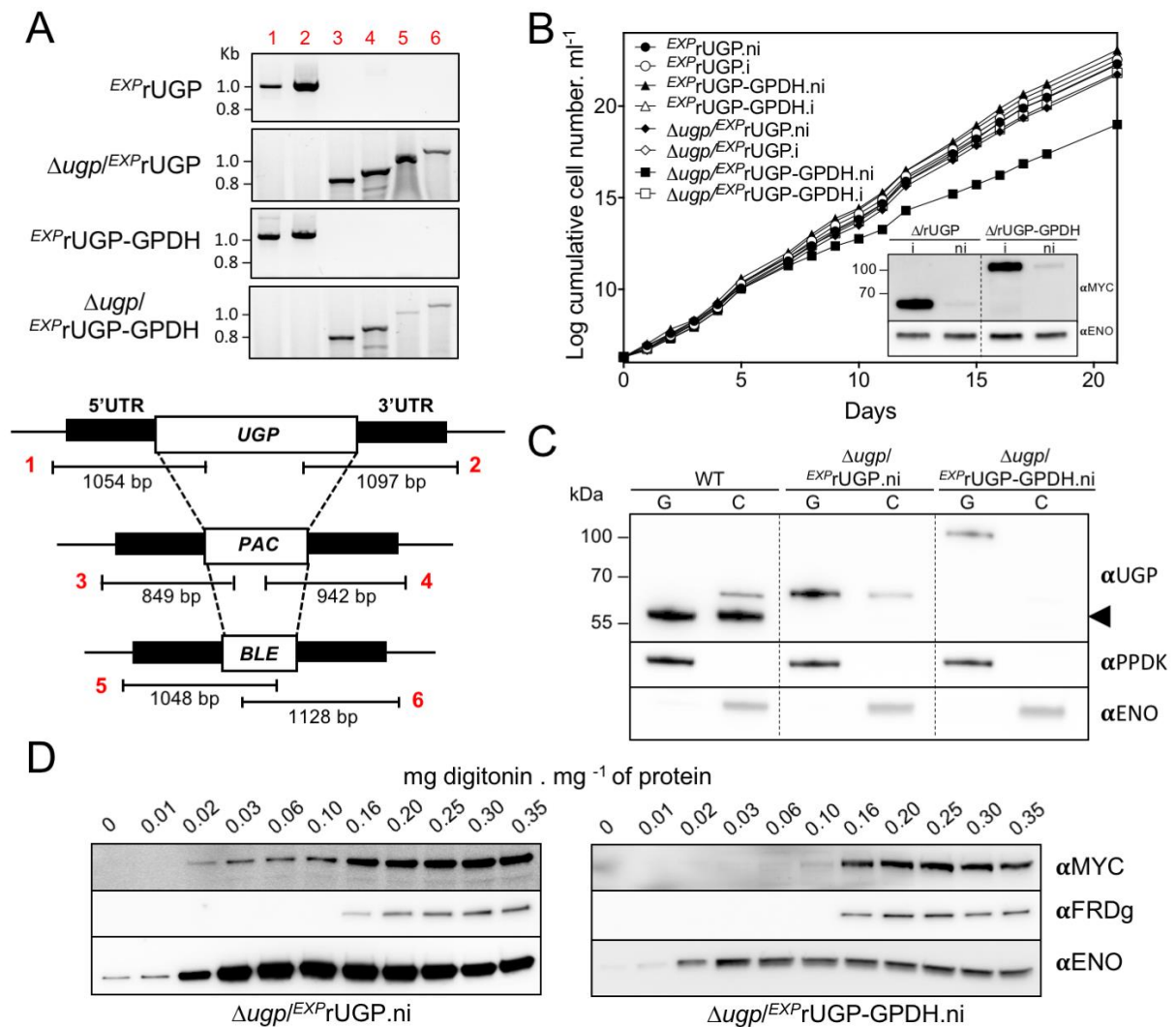


**Figure 2.44. Production and functional analyses of  $\Delta$ *ugp* cell lines.**

Panel A shows a PCR analysis of genomic DNA isolated from the parental (*EXP*rUGP and *EXP*rUGP-GPDH) and null mutant ( $\Delta$ *ugp*/*EXP*rUGP and  $\Delta$ *ugp*/*EXP*rUGP-GPDH) cell lines. Both knock-outs were obtained in the presence of tetracycline. Primers are designed on sequences flanking the 5'UTR and 3'UTR fragments used to target *UGP* gene depletion (black boxes) and on the ORF of the *UGP* gene, as well as the puromycin (*PAC*) and phleomycin (*BLE*) resistance genes (white boxes). In panel B, the growth of the cell lines was followed for 21 days, in the presence (.) or the absence (.ni) of tetracycline. Western blot analyses with anti-MYC ( $\alpha$ MYC) and anti-ENO ( $\alpha$ ENO, loading control) of the tetracycline-induced (.) and non-induced (.ni, 18 days after tetracycline removal)  $\Delta$ *ugp*/*EXP*rUGP and  $\Delta$ *ugp*/*EXP*rUGP-GPDH mutants are shown in the inset. Panel C shows glycosomal (G) and cytosolic (C) fractions obtained after subcellular fractionation of the UGP null cell lines in the absence of tetracycline (5 days). The arrowhead highlights the native UGP only in parental (WT) cells. In panel D, the UGP null cell lines were analysed by digitonin titration 5 days after removal of tetracycline. Western blot of supernatants confirmed the dual localisation of rUGP in  $\Delta$ *ugp*/*EXP*rUGP cell line and the exclusive glycosomal localisation of recombinant rUGP-GPDH in  $\Delta$ *ugp*/*EXP*rUGP-GPDH cell line with anti-MYC ( $\alpha$ MYC).

The exclusive glycosomal subcellular localisation of the recombinant rUGP-GPDH protein in the *<sup>RNAi</sup>UGP/EXP*rUGP-GPDH.i cell line observed by cellular fractionation (Figure 2.40B) was confirmed by digitonin titration (Figure 2.40C). In this context of absence of cytosolic UGP, the viability of the *<sup>RNAi</sup>UGP/EXP*rUGP-GPDH.i cell line (Figure 2.40A) strongly supports the hypothesis that the glycosomal pathway is functional.

#### **i) The $\Delta ugp^{EXP}$ rUGP-GPDH cell line is viable**

Considering that UGP is an essential protein, knock-out mutants were produced in two cell lines expressing tetracycline-inducible recombinant UGP, *i.e.* glycosomal/cytosolic rUGP (recoded UGP followed by a MYC tag) and glycosomal rUGP-GPDH.

After transfection with the recombinant plasmids expressing rUGP or rUGP-GPDH, the *UGP* alleles were replaced by the *PAC* and *BLE* markers in the presence of tetracycline to obtain the  $\Delta ugp^{EXP}$ rUGP or  $\Delta ugp^{EXP}$ rUGP-GPDH cell lines expressing the recombinant rUGP or rUGP-GPDH, respectively.

Deletion of both *UGP* alleles was confirmed by PCR (Figure 2.44A) and western blot (Figure 2.44C) analyses. Surprisingly, tetracycline removal did not induce death of the parasites as expected (Figure 2.44B), since the recombinant rUGP and rUGP-GPDH proteins were still expressed after 18 days in the absence of tetracycline (Figure 2.44B inset). However, the growth of the  $\Delta ugp^{EXP}$ rUGP-GPDH cell line is slightly affected after tetracycline removal, which is consistent with the essential role of UGP.

More importantly, the viability of the double mutant  $\Delta ugp^{EXP}$ rUGP-GPDH supports our hypothesis that the glycosomal pathway is functional. These data supporting the functional role of the glycosomal UGP were confirmed by determining the subcellular localisation of rUGP-GPDH in the  $\Delta ugp^{EXP}$ rUGP-GPDH cell line. To do so, we used the differential centrifugation and digitonin titration approaches. Five days after removal of tetracycline, the viable  $\Delta ugp^{EXP}$ rUGP-GPDH cell line expresses the recombinant rUGP-GPDH exclusively in the glycosomal compartment (Figure 2.44C-D). These data confirmed that the UDP-Glc/UDP-Gal biosynthetic pathway, which includes UGP, is active in the glycosomes. As expected, the MYC-tagged rUGP showed a dual glycosomal and cytosolic localisation in the  $\Delta ugp^{EXP}$ rUGP control cell line (Figure 2.44C-D).

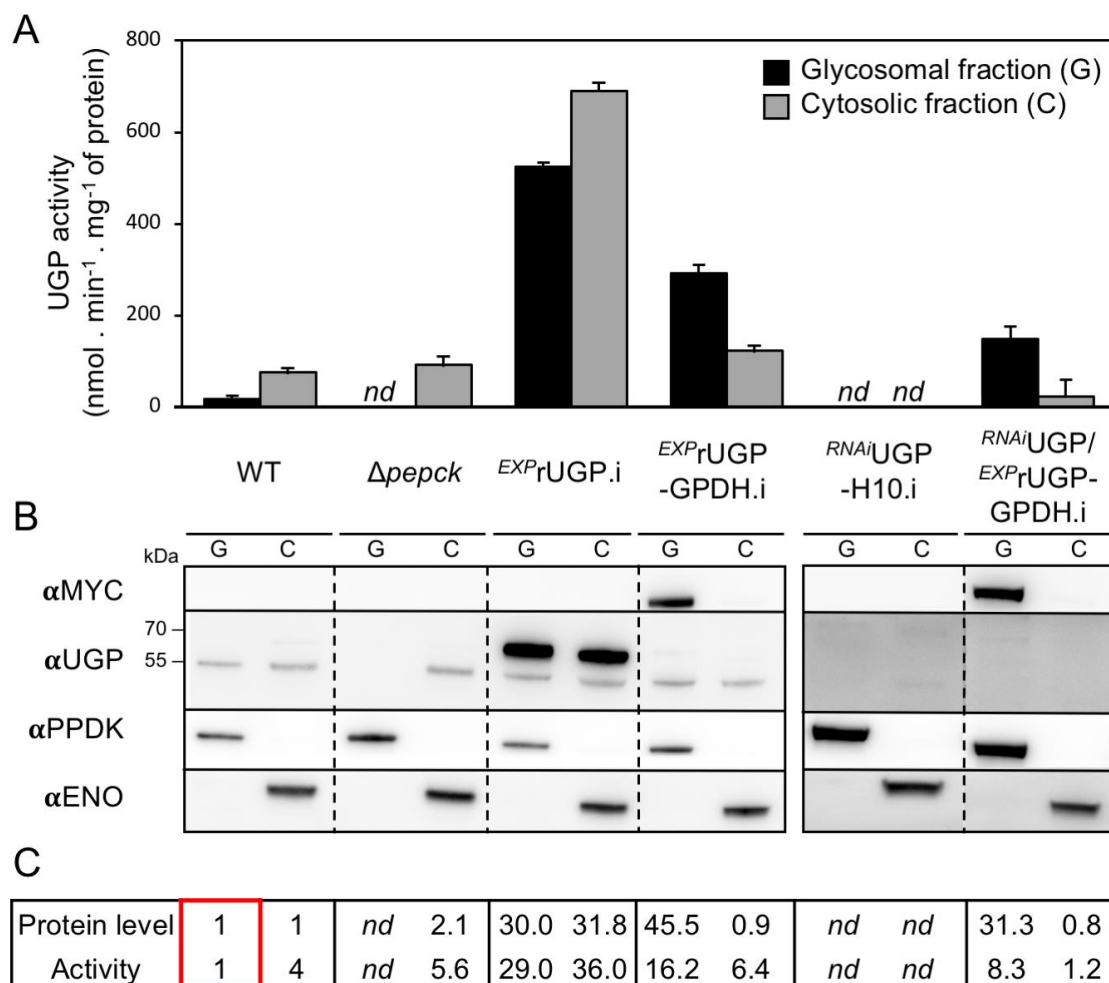


**Figure 2.45. Analysis of cell lines expressing UGP in different compartments.**

UGP activity was determined in enriched glycosomal and cytosolic fractions of the WT,  $\Delta pepck$ , *EXP*rUGP.i, *EXP*rUGP-GPDH.i, *RNAi*UGP-H10.i and *RNAi*UGP/*EXP*rUGP-GPDH.i cell lines (Panel A, n=3, SEM). The cytosolic and glycosomal UGP activities were normalised to the cytosolic malic enzyme and the glycosomal glycerol kinase activities, respectively. Significant differences between WT and mutants are indicated for each compartment: \*\*\*p < 0.001, \*\*p < 0.01, \*p < 0.05.

Panel B shows a representative western blot analysis of the corresponding cell lines. The recombinant rUGP-GPDH was detected with anti-MYC antibody ( $\alpha$ MYC). Glycosomal ( $\alpha$ PPDK) and cytosolic ( $\alpha$ ENO) markers are also shown.

Panel C shows relative amounts of UGP determined by western blot and specific activity (average of n=3). For these comparative analyses, the protein and activity levels detected in the glycosomal fraction of the WT cells were used as references with the arbitrary value of 1 (boxed values).

nd, non-detectable; .i, tetracycline induced; .ni, non-induced.

#### **j) The glycosomal and cytosol UGP-containing pathways are functional**

To confirm the functionality of the glycosomal and cytosolic pathways involving UGP, cell lines expressing the native and/or recombinant UGP in both subcellular compartments (WT, *EXP*rUGP.i and *EXP*rUGP-GPDH.i), only in the cytosol ( $\Delta$ *pepck*), only in the glycosomes (*RNAi*UGP/*EXP*rUGP-GPDH.i) or not at all (*RNAi*UGP-E10.i) were further analysed (Figure 2.45). This included determining the expression levels of UGP in the glycosomal and cytosolic fractions by western blotting and enzymatic activities, as well as quantifying intracellular metabolites, including the substrate (G1P) and the product (UDP-Glc) of the UGP enzymatic reaction by mass-spectrometry based metabolomics profiling approach (IC-HRMS).

The native UGP showed a specific activity in the glycosomal fraction 4-times lower than in the cytosolic fraction of the parental cells, which suggests that the glycosomal sequestration of UGP affects its activity by a yet unknown mechanism. The ratio between enzymatic activity and relative amount of proteins detected by western blotting in the cytosolic fractions of *EXP*rUGP.i is ~3.5-times lower than in the parental WT cells, suggesting that the C-terminal MYC tag affects UGP activity. Similarly, the ratio between glycosomal enzymatic activity and protein level is 2.8-times lower for the recombinant rUGP-GPDH than in WT or rUGP cells, suggesting that UGP fusion with GPDH also affects UGP activity (Figure 2.45C).

We also confirmed that the coupling enzyme (UDP-Glc dehydrogenase) used in the UGP activity assays was not affected by the presence of the same amounts of glycosomal or cytosolic samples (273 *versus* 245 mU.mg<sup>-1</sup> of protein, respectively). Anyway, the activity of the recombinant rUGPs, which is ~30 times more expressed in the *EXP*rUGP.i than the native UGP, was not affected in glycosomes, as the enzyme specific activity is similar in the glycosomal and the cytosolic fractions (Figure 2.45C). It is also noteworthy that the UGP activity was detected in the cytosol of the *RNAi*UGP/*EXP*rUGP-GPDH.i, while the native UGP is not detectable by western blot (Figure 2.45B) and the recombinant rUGP-GPDH is exclusively glycosomal (Figure 2.43). This is certainly due to the rupture of a few glycosomes during the grinding step designed to primarily disrupt the plasma membrane.

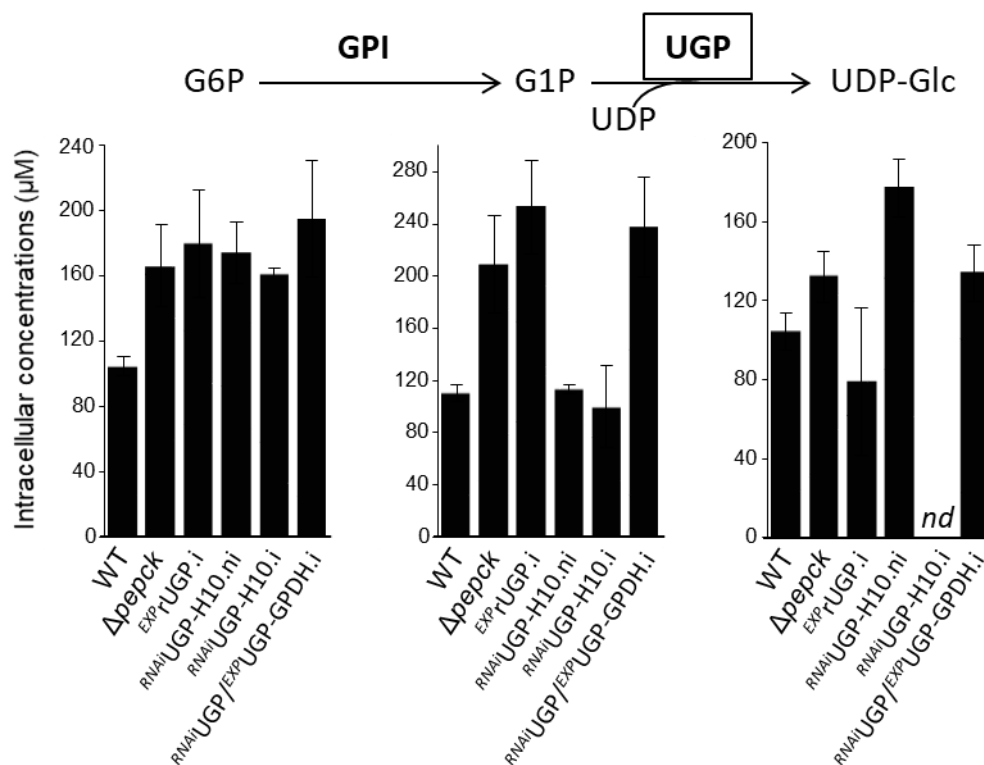


**Figure 2.46. PCF produces UDP-Glc in glycosomes and cytosol.**

IC-HRMS analyses of intracellular metabolites collected from WT,  $\Delta pepck$ ,  $EXP rUGP.i$ ,  $RNAiUGP-H10.ni$ ,  $RNAiUGP-H10.i$  and  $RNAiUGP/EXP rUGP-GPDH.i$  cell lines incubated in glucose-rich SDM79 medium (.i, tetracycline induced; .ni, non-induced.). Only G6P, G1P and UDP-Glc are shown in this figure, for other hexose phosphates and triose phosphates see Figure 2.47.

To confirm the role of UGP subcellular localisation in UDP-Glc production, we used mass-spectrometry based metabolomics to determine the intracellular amounts of G6P, G1P and UDP-Glc (Figure 2.46), as well as other metabolites (Figure 2.47) in the cell lines mentioned above cultivated in SDM79 medium.

This metabolomics approach was validated with the analysis of the  $\Delta pepck$  cell line. The metabolic flux through the Gly3P/DHAP shuttle, used to maintain the glycosomal redox balance, has been reported to be increased in the absence of PEPCCK (Ebikeme et al., 2010). Indeed, the level of Gly3P is increased by ~3-times in the  $\Delta pepck$  mutant compared to all the other cell lines analysed (Figure 2.47).

Regarding the sugar nucleotide biosynthetic pathways, only UDP-Glc and UDP-GlcNAc were identified and quantified with this methodology (Figure 2.47). The levels of UDP-Glc detected (80-170  $\mu$ M) are comparable to those previously reported for procyclic trypanosomes (110 to 540  $\mu$ M) (Turnock and Ferguson, 2007) (Figure 2.46). UDP-Glc is no longer detectable in  $RNAi$ UGP.i cell line, which shows that UGP is the only enzyme producing UDP-Glc in PCF trypanosomes (Figure 2.46). It is also of note that UDP-Glc is detected in non-induced  $RNAi$ UGP cells at levels similar to parental cells, despite the ~30-fold reduction of UGP protein levels (Figure 2.40B), which shows that PCF trypanosomes express a large excess of UGP.

More importantly, UDP-Glc is produced in cells expressing UGP exclusively in the cytosol ( $\Delta pepck$ ) or in glycosomes ( $RNAi$ UGP/ $EXP$ rUGP-GPDH.i) at levels similar to those of WT cells, which confirms the functionality of the pathway in both subcellular compartments (Figure 2.46).

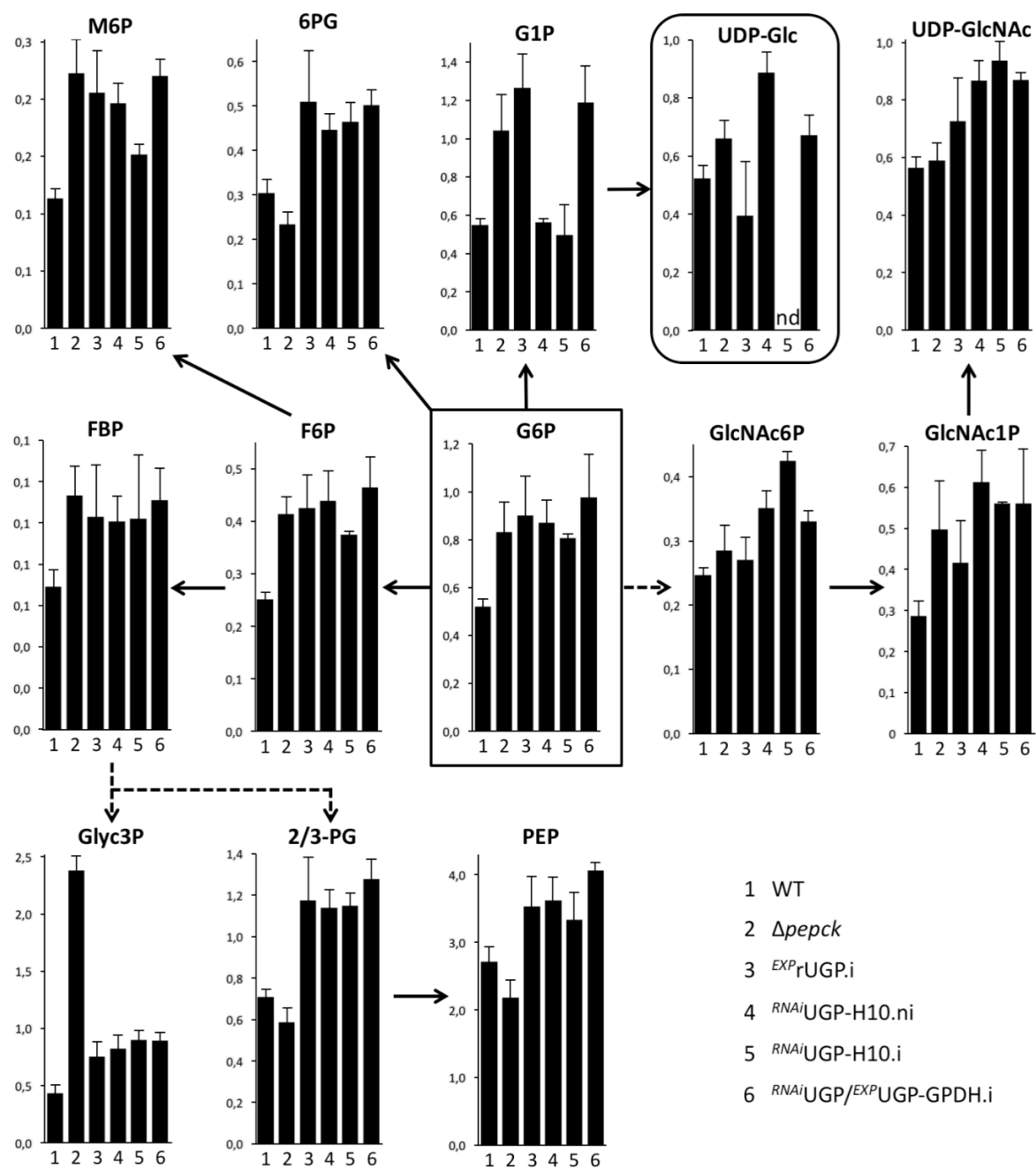
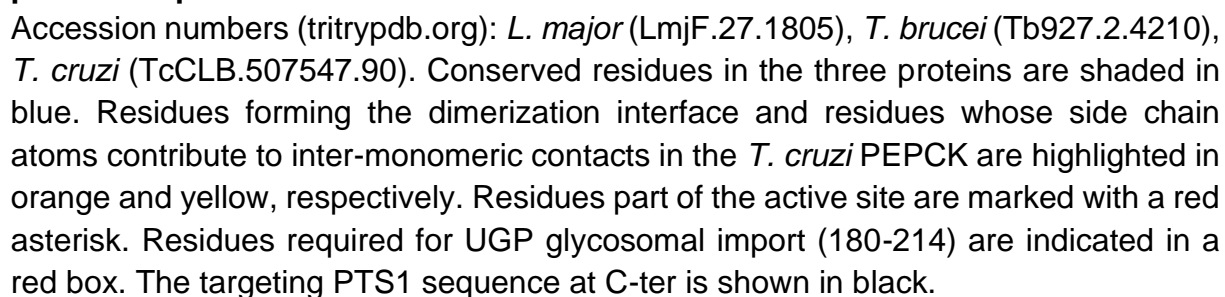
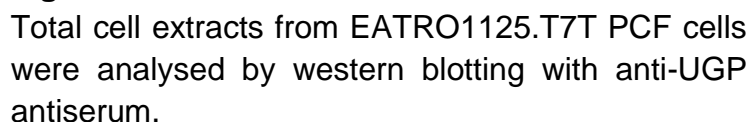




**Figure 2.47. IC-HRMS analyses of intracellular metabolites**

IC-HRMS analyses of intracellular metabolites collected from WT (1),  $\Delta pepck$  (2), *EXP*rUGP.i (3), *RNAi*UGP-H10.ni (4), *RNAi*UGP-H10.i (5) and *RNAi*UGP/*EXP*rUGP-GPDH.i (6) cell lines incubated in glucose-rich SDM79 medium (.i, tetracycline induced; .ni, non-induced). Hexose phosphates, triose phosphates and sugar nucleotides are shown. The amounts of metabolites are expressed as  $\mu\text{mol/l}$ .



## 2.4. Supplementary results

This section contains additional information that will not be part of the manuscript in preparation.

Figure 2.48 shows the test of anti-UGP antiserum produced by COVALAB with the peptide antigens GYIPEKSIFPVES and RNGKPPAIDLGEH. In total extracts of PCF trypanosomes, this antibody recognises an unspecific extra band of 70 kDa as already mentioned. Therefore, we produced cell lines expressing MYC and TY-tagged UGP to avoid unspecific signal in western blotting analysis of UGP truncations, immunofluorescence and Proximity Ligation assays.

A comparison of *L. major*, *T. brucei* and *T. cruzi* PEPCK sequences is shown in Figure 2.49. Residues involved in dimerization and forming part of the active site are indicated, using the *T. cruzi* enzyme as reference (Trapani et al., 2001). A high degree of conservation between *T. brucei* and *T. cruzi* PEPCK proteins is evidenced, suggesting that *T. brucei* PEPCK can form dimers. If PEPCK oligomerization influences interaction and glycosomal import of UGP has yet to be determined. Importantly, the residues identified as required for UGP import are conserved as well within the three species (Figure 2.49, red boxed).

In contrast, the N-terminal residues of UGP possibly containing the PEPCK binding site are not conserved between trypanosomatids (Figure 2.50). This might explain the absence of detectable UGP in the glycosomes of *L. major*, which is only 55% identical to the *T. brucei* UGP.

Moreover, residues involved in octamerization of human and yeast UGPs are absent in the *T. brucei* sequence (Figure 2.50, in yellow), supporting the presence of monomeric active forms in the parasites.

As previously mentioned, UGP can be regulated by a redox mechanism in some protists. This mechanism regulating *E. histolytica* and *G. lamblia* UGP activity requires the presence of two cysteine residues (Cys<sup>108</sup>, Cys<sup>378</sup>) that form a disulphide bond (Martínez et al., 2011; Ebrecht et al., 2015). In *T. brucei* UGP one of these residues is not conserved suggesting that UGP activity is not regulated by this mechanism (Figure 2.50, red squares).



## 2.5. Discussion

Trypanosomatids are known to sequester a cascade of consecutive glycolytic enzymes into glycosomes, originated as modified peroxisomes, in addition to enzymes of other pathways including gluconeogenesis, the pentose phosphate pathway and sugar nucleotide biosynthesis (Gualdrón-López et al., 2012a; Allmann and Bringaud, 2017). Here we have addressed three questions related to the glycosome biology by analysing UGP, a key enzyme of the sugar nucleotide biosynthesis involved in UDP-Glc synthesis:

(i) The physiological role of this glycosomal pathway remains unknown since it is also present in the cytosol, the subcellular compartment where biosynthesis of sugar nucleotides takes place in the other eukaryotes.

(ii) Most of the glycosomal enzymes are imported into the organelle by peroxisomal targeting signals (PTS1 or PTS2), however a number of them lack PTS, including half of those involved in sugar nucleotide biosynthesis (Opperdoes and Szikora, 2006) and the mechanism leading to the import of the latter has not been investigated so far in trypanosomatids.

(iii) Mammalian peroxisomes can multiply by growth and division followed by protein import into newly produced organelles, and can be formed by the *de novo* route, but what about glycosomes?

Here we showed that (i) the glycosomal pathway leading to production of UDP-Glc and UDP-Gal is functional and is essential in the PCF trypanosomes, in the absence of the cytosolic pathway, (ii) UGP is imported in the glycosomes by piggybacking on the PTS1-containing PEPCK and (iii) PEPCK and UGP interact into only a few glycosomes, which may represent newly produced glycosomes competent for protein import.

All trypanosomatids use G1P as a precursor to synthesize UDP-Glc, which is the substrate of UDP-Glc 4'-epimerase (GalE) to produce UDP-Gal, these two sugar nucleotides being involved in glycosylation reactions. This pathway is essential for BSF and PCF *T. brucei* since the  $\Delta galE$  null mutant is lethal (Roper et al., 2002, 2005; Urbaniak et al., 2006), however the essentiality of the enzyme(s) producing UDP-Glc was not addressed before in *T. brucei* (Mariño et al., 2010).

*Leishmania* spp. use, besides UGP, UDP-sugar pyrophosphorylase (USP) to produce UDP-Glc. Consequently, both USP and UGP enzymes must be blocked to deplete the cells in UDP-Glc and UDP-Gal and to induce cell death in *L. major* (Damerow et al.,

2010, 2015b). In *T. brucei*, not only the deletion of the unique *UGP* gene is lethal, but also there are no detectable amounts of UDP-Glc in the *RNAi*UGP.i cell lines. These data are consistent with the absence of the *USP* - or alternative enzyme - gene in the *T. brucei* genome.

We also observed that the specific activity of UGP in PCF trypanosomes (20 mU.mg<sup>-1</sup> of protein) is rather low in comparison to those determined in *L. major* (370 mU.mg<sup>-1</sup> of protein) (Lamerz et al., 2006). However, UGP is expressed in large excess with regard to the requirements in PCF since the ~30 fold reduction of UGP expression in the *RNAi*UGP.ni cell line is not deleterious for the cells and does not affect UDP-Glc production levels. Similarly, strong (~30 fold) overexpression of rUGP in the *EXPr*UGP.i cell line had effects on neither growth nor UDP-Glc levels. Therefore, UGP does not represent a control point in this pathway. This is consistent with the analysis of the conditional  $\Delta$ *galE* mutant, in which the amounts of UDP-Gal dropped by 80% within 24 h after removal of tetracycline, while the amounts of UDP-Glc were unaffected (Urbaniak et al., 2006).

In contrast, *GalE* seems to control the metabolic flux, since (i) the ratio of UDP-Gal/UDP-Glc is about 1:2.2, 1:2.2 and 1:4.3 in *T. brucei*, *L. major* and *T. cruzi*, suggesting that conversion of UDP-Glc to UDP-Gal is the rate limiting step of the pathway (Turnock and Ferguson, 2007) and (ii) a single allele knock-out of *GalE* in *T. cruzi* epimastigotes showed deficiency with respect to galactose metabolism (MacRae et al., 2006). Overall, these data show that the cellular amounts of UDP-Glc are not regulated by the activity of the UDP-Glc forming enzymes in trypanosomatids, but by an independent mechanism probably involving the cellular glycosyltransferase activities consuming UDP-Glc.

UGP is known to be primarily localised in the cytosol of eukaryotic cells. In contrast, this enzyme has shown a dual glycosomal and cytosolic localisation in *T. brucei*, with similar concentrations in the two subcellular compartments. These results go beyond previous reports where only a glycosomal localisation was detected in BSF trypanosomes, since as stated by the authors, "the results obtained using immunofluorescence do not allow to discern if some UGP may be present in the cytosol" (Mariño et al., 2010).

Here we took advantage of digitonin titration approaches, to demonstrate the cytosolic localisation of UGP, since the classical grinding-based cellular fractionation used to enrich glycosomes may release organellar proteins in the cytosolic fractions, leading



to an overestimation of the cytosolic localisation of proteins. Interestingly, the same approach was also used to show that the *Leishmania major* UGP is exclusively expressed in the cytosol (Damerow 2010, PhD thesis).

The absence of detectable amounts of UGP in the glycosomes of *L. major* is probably due to the absence of the PEPCK binding site in the *Leishmania* UGP orthologue, which is only 55% identical to the *T. brucei* UGP (43.3% of the N-terminal 66 residues possibly containing the PEPCK binding site are not conserved), while the *T. brucei* and *L. major* PEPCK show 81.3% of identity (32 out of the 34 residues possibly involved in the PEPCK/UGP interaction are conserved). Therefore, UGP in *Leishmania* probably cannot enter glycosomes by the same route as in *T. brucei*. As mentioned above, *L. major* also uses USP to produce UDP-Glc, which is exclusively cytosolic (Damerow et al., 2010, 2015; Damerow 2010, PhD thesis). These data suggest that, in contrast to *T. brucei*, UDP-Glc is not produced inside the glycosomes of *Leishmania* spp.

The functionality of the glycosomal and cytosolic UGP-containing pathways, was validated by the viability of mutants expressing UGP exclusively in glycosomes (*RNAi*UGP/*EXP*rUGP-GPDH.i) or the cytosol ( $\Delta$ *pepck*), respectively, and the detection of UDP-Glc in both cell lines. This first direct evidence of a functional production of sugar nucleotides inside glycosomes raises two questions.

First, how UDP-Glc and UDP-Gal leave the glycosomes to reach the endoplasmic reticulum and the Golgi apparatus where they are required as substrates of glycosyltransferases for protein glycosylation? The glycosomal membrane is considered to be impermeable to bulky metabolites such as nucleotides, since the size limitation of the general diffusion pore is in the order of 400 Da (as inferred by comparing with peroxisomal pores) (Gualdron-López et al., 2012a). Consequently, exchange of sugar nucleotides between the glycosomal and cytosolic compartments requires transporters. However, the only transporters known to be associated with the glycosomal membrane are the ABC transporters GAT1, GAT2 and GAT3, with GAT1 likely transporting acyl-CoAs (Igoillo-Esteve et al., 2011; Yernaux et al., 2006) and proteomics analyses of glycosomal membrane fractions did not reveal additional candidates (Colasante et al., 2013). Further work is certainly required to confirm the presence of such sugar nucleotide transporters in the glycosomal membrane.

Second, what is the role of sugar nucleotide biosynthesis inside the glycosomes, since the cytosolic pathway is functional in the procyclic trypanosomes, as observed in all eukaryotes? In others eukaryotes, UGP has already been described in Golgi

apparatus, chloroplasts, membrane fractions and cell walls, where it also provides UDP-Glc to produce glycoconjugates, such as glycoproteins, glycopeptides, glycosides and glycolipids (Kleczkowski et al., 2010). Interestingly, the yeast UGP also shows a dual subcellular localisation depending on phosphorylation at the N-terminus S11 residue, with the non-phosphorylated cytosolic and phosphorylated cell wall enzymes being involved in glycogenesis and cell wall glucan synthesis, respectively (Smith and Rutter, 2007).

All these biosynthetic pathways require glycosyltransferases, which have not been detected in the glycosomal proteomes (Colasante et al., 2006; Güther et al., 2014). In addition, none of trypanosome proteins involved in the glycosylation processes contain a PTS (Opperdoes and Szikora, 2006), which strongly support the view that UDP-Glc and UDP-Gal are not produced in the glycosomes to feed glycosylation reactions inside the organelle. Alternatively, glycosomal UDP-Glc could have a signalling role, as previously observed in animals and plants (Chambers et al., 2000; Janse van Rensburg and Van den Ende, 2018).

Here we show that UGP from *T. brucei* is imported into glycosomes by piggybacking on the PTS1-containing protein PEPCK, since all UGP remains in the cytosol of  $\Delta pepck$  mutant and re-expression of PEPCK rescues UGP import (Figure 2.33). Remarkably, this is the first evidence of piggybacking so far in trypanosomatids, although it has been proposed as an explanation to the presence of PTS-lacking proteins within glycosomes, including four other enzymes involved in the sugar nucleotide biosynthetic pathways, i.e. phosphoacetylglucosamine mutase, phosphomannomutase, glucosamine-phosphate N-acetyltransferase and GDP-mannose 4,6 dehydratase (Turnock et al., 2007; Mariño et al., 2011; Bandini et al., 2012).

To demonstrate that other glycosomal proteins are also imported by piggybacking, their carrier needs to be depleted, which implies to systematically analyse the glycosomal protein content of knock-out or knock-down mutants of glycosomal proteins, as we performed here to identify the PEPCK/UGP association.

As mentioned above, the UGP concentrations are similar in the cytosolic and glycosomal compartments. Since glycosomes represent 4% of the total parasite volume (Opperdoes et al., 1984), only a small fraction of the cytosolic UGP pool is imported into the glycosomes (~4%), suggesting that the efficiency of UGP import by piggybacking on PEPCK is relatively low. This relatively low efficiency has also been



described for three other examples of physiological hetero-oligomeric import by piggybacking into peroxisomes reported so far, *i.e.* the mammalian superoxide dismutase (SOD1) (Islinger et al., 2009), the mammalian lactate dehydrogenase (LDH) (Schueren et al., 2014) and the yeast pyrazinamidase/nicotinamidase (PNC1) (Effelsberg et al., 2015; Kumar et al., 2016; Al-Saryi et al., 2017b), which are co-imported with the PTS-containing copper chaperone SOD1 (CCS), read-through-extended LDH (LDHBx) and glycerol-3-phosphate dehydrogenase (GPD1), respectively. These three co-imported proteins display dual peroxisomal and cytosolic localisation with the majority remaining within the cytosol (in the range of 98%) (Thoms, 2015), as observed for the UGP/PEPCK co-import (~96%).

The reason of this relatively low import efficiency has been elucidated by the demonstration that the PST1 receptor (PEX5), required for peroxisomal import of PTS1-containing proteins, binds preferentially to monomers compared to oligomers (Freitas et al., 2015). Consequently, the PST1-containing proteins are efficiently imported mainly in the form of monomers, while the import efficiency of proteins lacking PTS is considerably reduced because of the hetero-oligomeric interactions with the PST1-containing carrier required for their peroxisomal import.

Interestingly, although low is the efficiency of hetero-oligomer import, weak protein-protein interactions are sufficient to support piggyback import. Indeed, blue native gels failed to show interaction between the mammalian SOD and CCS partners (Islinger et al., 2009) and synthetic substrates designed to evaluate the import of proteins showed dissociation constants ( $K_d$ ) differing over three orders of magnitude, with even an apparent  $K_d$  of  $\sim 6 \times 10^{-3}$  M allowing the detection of piggyback import (Yang et al., 2018). Similarly, despite several attempts, we did not observe any interaction between UGP and PEPCK using co-immunoprecipitation or native gels, suggesting that these interactions are weak and transient.

In agreement with this weak interaction, PEPCK is in large excess compared to UGP, as illustrated by the ~30-fold higher enzymatic activity of PEPCK compared to UGP (670 *versus* 20 mU.mg<sup>-1</sup> of protein) (Hunt and Köhler, 1995) and the ~100-fold higher peptide counts for PEPCK than UGP in proteomics analyses of glycosomal fractions from PCF (Table 2.7). The same PEPCK/UGP ratio was also estimated in BSF, since both proteins are ~50-times less expressed than in PCF (Figure 2.32C) (Creek et al., 2015).

In conclusion, our results support the role of hetero-oligomeric import by piggybacking as an alternative route for import of glycosomal proteins, as described for peroxisomes of mammals and yeast. More importantly, the UGP/PEPCK association provides the first example of hetero-oligomeric import by piggybacking involving two proteins not functionally related, since PEPCK is involved in the maintenance of the glycosomal redox and ATP/ADP balances, as well as gluconeogenesis (Ebikeme et al., 2010; Deramchia et al., 2014). Among the other known examples of piggybacking, CCS is the chaperone of SOD1 (Islinger et al., 2009), the PST1-containing phosphatase B subunit and phosphatases A/C subunits form an heterotrimeric enzymatic complex (Kataya et al., 2015), LDH and LDHBx are encoded by the same gene (Schueren et al., 2014), however, the peroxisomal functions of PNC1, which is imported by GPD1 are unknown (Al-Saryi et al., 2017a).

The regions of interaction between piggybacking partners in hetero-oligomeric complexes have been studied in two of the examples reported so far. N-terminal residues (positions 5–17) as well as C-terminal residues (positions 293, 299 and 300–305) of LDH are involved in the contact between subunits of the tetramer (Jafary et al., 2019). To be imported into peroxisomes, the LDH tetramer must contain at least one read-through LDHBx subunit with a seven amino acids extension (PTS1) that does not interrupt oligomerization and is recognised by PEX5 (Schueren et al., 2014). Differently, the SOD-binding domain of CCS is required for heterodimerization and consequent import, in addition to the exchange of copper ions between the two proteins. This SOD-binding domain is localised between residues 86–234 of CCS (CCS contains 274 aa, including a PTS1 signal) and is 47% identical to SOD1 (Casareno et al., 1998).

In the case reported here, we show that the N-terminal region of UGP up to position 123 is required for the import into glycosomes by interacting with a region close to the active site of PEPCK between positions 180 and 214. This PEPCK region is far away from the monomer-monomer interface in the dimeric *Trypanosoma cruzi* PEPCK structure (residues 10-13, 15, 16, 19, 25-31, 279 and 290-293) (Trapani et al., 2001), suggesting that PEPCK could interact with UGP as a dimer. Importantly, the region of interaction with UGP is also distant from the PTS1 signal of PEPCK. All together these observations suggest that the main requirement for two proteins to be imported together into peroxisomes/glycosomes is the interaction region to be located far from the PTS.

Since the formation of the UGP/PEPCK heterodimer may occur mainly during UGP import into the organelle, the analysis of the UGP/PEPCK interactions using the PLA approach provides new insights regarding glycosomal import of proteins and multiplication of the organelles. In mammalian cells, peroxisomes multiply by growth and division using an asymmetric process generating new peroxisomes via formation of a membrane compartment and subsequent import of newly synthesised matrix proteins (Huybrechts et al., 2009; Delille et al., 2010; Costello and Schrader, 2018). In mammalian cells, overexpression of the membrane peroxin Pex11p $\beta$  resulted in the formation of pre-peroxisomal membrane structures composed of mature globular domains and tubular extensions, the latter being matured by import of matrix proteins (Delille et al., 2010). Equivalent clusters of tubular glycosomal membranes were also observed by overexpressing Pex11 in *T. brucei* (Lorenz et al., 1998) and clusters of elongated glycosomes have more recently been observed in BSF trypanosomes by whole cell reconstruction using 3D electron microscopy (Hughes et al., 2017). In addition, *T. brucei* expresses Fis1 and Dpl1, two key proteins involved in the fission of newly produced peroxisomes in other eukaryotes (Morgan et al., 2004; Chanez et al., 2006).

Overall, these observations confirm the hypothesis that the peroxisome-related glycosomal organelles can multiply by growth and division as observed for the mammalian peroxisomes. This also implies that the new peroxisomes/glycosomes produced by growth and division are the most competent organelles for protein import and that they represent only a limited fraction of the organelle population.

We thus propose that the structures showing UGP/PEPCK close proximity by PLA correspond to newly produced import-competent glycosomes.

Considering (i) that PEPCK and UGP mainly physically interact during import at the glycosomal membrane, because of the weak and transient interactions between these non-functionally related proteins, (ii) that only up to 10 dot per cell correspond to physical proximity between PEPCK and UGP, with most cells containing 2-5 dots (Figure 2.35), while PEPCK and UGP appear localised in almost all, if not all, glycosomes (Figure 2.33 and Figure 2.34) and (iii) that the number of glycosomes was estimated to 60-65 per G1 trypanosome cell (Tetley and Vickerman, 1991; Hughes et al., 2017), one may consider that the 3-10% of the organelles showing UGP/PEPCK interaction by PLA are newly produced glycosomes importing the matrix proteins, including PEPCK and UGP.

### 3. RESULTS PART II. Analysis of TCA intermediates and metabolites excreted from glucose metabolism as alternative carbon sources

This aspect explored in my thesis relates to mitochondrial metabolism of the insect (tsetse fly) midgut PCF trypanosomes. I present a comprehensive analysis of the carbon sources capable of feeding the central metabolism. As discussed in the introduction, the PCF prefers to use glucose to support their central carbon metabolism *in vitro* (Bringaud et al., 2006). However, in the fly midgut, trypanosomes rely on proline metabolism (Mantilla et al., 2017), due to the presumed low abundance, or absence, of free glucose in the haemolymph and tissues of the insect vector, which relies on amino acids for energy production. In this particular *in vivo* context, PCF has developed an energy metabolism based on proline (See Figure 1.17).

In this part of the results section, I evaluated the utilisation of other carbon sources possibly available in the digestive tract and other organs of the insect, as well as pathways of the central carbon metabolism used by the trypanosomes *in vivo*.

Can trypanosomes use excreted end products from glucose metabolism and TCA cycle intermediates as carbon sources? If so, how are they metabolised? Are there any effects on the growth of the parasites?

To answer these questions, I used EATRO1125.T7T parental cells and a dozen of mutants impaired for enzymes of the TCA cycle, proline degradation and acetate production pathways to perform isotopic profiling of the exometabolome by proton ( $^1\text{H}$ )-NMR analysis, in addition to Alamar Blue assays and growth curves to evaluate effects on the growth of parasites.

The following manuscript soon to be submitted for publication shows that (i) procyclic form of *T. brucei* efficiently metabolises succinate, alanine, pyruvate, malate and  $\alpha$ -ketoglutarate, (ii) after all extracellular glucose has been consumed, succinate and alanine excreted from its metabolism are further metabolised into acetate, the ultimate excreted end product, (iii) the TCA cycle intermediates succinate, malate and  $\alpha$ -ketoglutarate stimulate growth of the parasites in *in vivo*-like conditions (2 mM proline, without glucose) and (iv) the metabolic capacity of the parasite is higher than previously reported, with a complete TCA cycle working in PCF trypanosomes under some conditions.

## **Procyclic trypanosomes recycle glucose catabolites and TCA cycle intermediates to stimulate growth in *in vivo*-like conditions**

**Oriana Villafraz<sup>1</sup>, Marc Biran<sup>2</sup>, Nicolas Plazolles<sup>1</sup>, Edern Cahoreau<sup>3</sup>, Rodolpho Ornit Oliveira Souza<sup>4</sup>, Stefan Allmann<sup>5</sup>, Emmanuel Tetaud<sup>1</sup>, Loïc Rivière<sup>1</sup>, Ariel M. Silber<sup>4</sup>, Michael P. Barrett<sup>6,7</sup>, Alena Zíková<sup>8</sup>, Michael Boshart<sup>5</sup>, Jean-Charles Portais<sup>3</sup>, Frédéric Bringaud<sup>1,2#</sup>**

<sup>1</sup> Univ. Bordeaux, CNRS, Microbiologie Fondamentale et Pathogénicité (MFP), UMR 5234, F-33000 Bordeaux, France

<sup>2</sup> Univ. Bordeaux, CNRS, Centre de Résonance Magnétique des Systèmes Biologiques (CRMSB), UMR 5536, F-33000 Bordeaux, France

<sup>3</sup> LISBP, Université de Toulouse, CNRS, INRA, INSA, 135 Avenue de Rangueil, F-31077 Toulouse

<sup>4</sup> Laboratory of Biochemistry of Tryps - LaBTryps, Department of Parasitology, Institute of Biomedical Sciences, University of São Paulo, São Paulo, Brazil

<sup>5</sup> Fakultät für Biologie, Genetik, Ludwig-Maximilians-Universität München, Grosshadernerstrasse 2-4, D-82152 Martinsried, Germany

<sup>6</sup> Wellcome Centre for Integrative Parasitology, Institute of Infection, Immunity and Inflammation, College of Medical, Veterinary and Life Sciences, University of Glasgow, Glasgow, United Kingdom

<sup>7</sup> Glasgow Polyomics, Wolfson Wohl Cancer Research Centre, Garscube Campus, College of Medical Veterinary and Life Sciences, University of Glasgow, Glasgow, United Kingdom

<sup>8</sup> Institute of Parasitology, Biology Center, Czech Academy of Sciences and Faculty of Science, University of South Bohemia, České Budějovice 370 05, Czech Republic

### **Contributions**

OV, NP and FB designed the experiments. OV performed 90% of the experiments. MBI performed all <sup>1</sup>H-NMR analyses and quantifications at the CRMSB. NP performed 10% of experiments (kinetic analysis and standardization of Alamar Blue assays). EC and JCP identified hydroxyglutarate by <sup>1</sup>H-NMR analysis at 800 MHz and prepared Figure 3.59. ROOS contributed with OV to 20% of the Alamar Blue assays and sample preparations for <sup>1</sup>H-NMR. SA produced the  $\Delta idhm$  cell line provided by MBo. OV, MBI, JCP and FB analysed the data. MPB provided the <sup>RNAi</sup>PROD<sup>H</sup> cell line. AZ provided the SCoAS material. MBo provided IDHm and ACO material. OV and FB wrote the manuscript. ET, LR, AMS, MPB, AZ, MBo, and JCP contributed to discussions of results and revision of the manuscript.

### 3.1. Abstract

*Trypanosoma brucei*, a protist responsible for human African trypanosomiasis (HAT) also known as sleeping sickness, is transmitted by the tsetse fly (*Glossina* sp.), where the procyclic forms of the parasite develop in the proline-rich (1-2 mM) and glucose-depleted digestive tract. Proline is essential for the midgut colonisation of the parasite in the insect vector, however other carbon sources could be available and used to feed its central metabolism. Here we show that procyclic trypanosomes can consume and metabolise metabolic intermediates, including those excreted from glucose catabolism (succinate, alanine and pyruvate), with the exception of acetate, which is the ultimate end product excreted by the parasite. Among the tested metabolites, the tricarboxylic acid (TCA) cycle intermediates (succinate, malate and  $\alpha$ -ketoglutarate) stimulated growth of the parasite in the presence of 2 mM proline. The pathways used for their metabolism were mapped by proton-NMR metabolic profiling and phenotypic analyses of a dozen RNAi and/or null mutants affecting central carbon metabolism. We showed that (i) malate is converted to succinate by both the reducing and oxidative branches of the TCA cycle, which demonstrates that procyclic trypanosomes can use the full TCA cycle, (ii) the enormous rate of  $\alpha$ -ketoglutarate consumption (15-times higher than glucose) is possible thanks to the balanced production and consumption of NADH at the substrate level and (iii)  $\alpha$ -ketoglutarate is toxic for trypanosomes if not appropriately metabolised as observed for an  $\alpha$ -ketoglutarate dehydrogenase null mutant. In conclusion, these data show that PCF trypanosomes can efficiently metabolise, in addition to proline, several metabolites that stimulate their growth and could help the parasite to face challenging environments in the fly.

### 3.2. Introduction

*Trypanosoma brucei* is a hemoparasitic unicellular eukaryote that causes Human African Trypanosomiasis (HAT), also known as sleeping sickness. The disease, fatal if untreated, is endemic in 36 countries in sub-Saharan Africa, with about 70 million people living at risk of infection (Büscher et al., 2017). The *T. brucei* life cycle is complex and the parasite must adapt to several dynamic environments encountered both in the insect vector, tsetse fly, and in the mammalian hosts. This is accomplished by cellular development, including adaptations of energy metabolism. Here, we focus on the insect midgut procyclic stage (PCF) of the parasite by providing a comprehensive analysis of the carbon sources capable of feeding its central metabolism.

In glucose-rich mammalian blood, the metabolism of *T. brucei* bloodstream forms (BSF) relies on glucose, with most of the glycolysis taking place in specialised peroxisomes called glycosomes (Oppenheimer and Borst, 1977a). BSF convert glucose as their primary carbon source to the excreted end product pyruvate, although low but significant amounts of acetate, succinate and alanine are also produced (Visser and Oppenheimer, 1980; Mazet et al., 2013). In contrast, the PCF mainly converts glucose to excreted acetate and succinate, in addition to smaller amounts of alanine, pyruvate and lactate (Bringaud et al., 2006). Although PCF trypanosomes prefer to use glucose to support their central carbon metabolism *in vitro* (Lamour et al., 2005; Coustou et al., 2008), they rely on proline metabolism in the fly midgut (Mantilla et al., 2017). This is due to the presumed low abundance, or absence, of free glucose in the haemolymph and tissues of the insect vector, which rely on amino acids for their energy (Bursell, 1981). In this particular *in vivo* context, PCF has developed an energy metabolism based on proline, which is converted to alanine, succinate and acetate (Obungu et al., 1999; Coustou et al., 2008).

As in other organisms, *T. brucei* PCF catabolism of proline is achieved by oxidation to glutamate, through proline dehydrogenase (PRODH, step 1 in Figure 3.51) (Lamour et al., 2005) and pyrroline-5 carboxylate dehydrogenase (P5CDH, step 3) (Mantilla et al., 2017). RNAi-mediated down-regulation of *P5CDH* expression (*RNAi*P5CDH) is lethal for the PCF grown in glucose-depleted medium containing 6 mM proline (glucose-depleted conditions) and abolishes fly infections. This demonstrated that proline is essential for growth and development of insect-stage trypanosomes *in vivo* (Mantilla et al., 2017). Then, glutamate is converted by alanine aminotransferase (AAT, step 4)

to the TCA cycle intermediate  $\alpha$ -ketoglutarate (Spitznagel et al., 2009), which is further metabolised to succinate (steps 5-6) and malate (steps 7 and 10) *via* the TCA cycle enzymes working in the oxidative direction (Coustou et al., 2008). Alternatively, glutamate dehydrogenase, which catalyses an oxidative deamination of glutamate, could also be involved in the production of  $\alpha$ -ketoglutarate, as proposed for *T. cruzi*, but this has never been demonstrated in *T. brucei* (Duschak and Cazzulo, 1991). Malate is then converted by the malic enzymes to pyruvate (step 15) (Allmann et al., 2013), which serves as a substrate, together with glutamate, for AAT to produce  $\alpha$ -ketoglutarate and secreted alanine (step 4). Alternatively, pyruvate is converted by the pyruvate dehydrogenase complex (PDH, step 16) to acetyl-CoA, which is further metabolised into the excreted end product acetate by two redundant enzymes, i.e. acetyl-CoA thioesterase (ACH, step 17) and acetate:succinate CoA-transferase (ASCT, step 18) (Millerioux et al., 2012). It is noteworthy that oxidation of acetyl-CoA through the TCA cycle (dashed lanes in Figure 3.51), initiated by production of citrate by citrate synthase (CS, step 12), has not been detected so far in *T. brucei* (Van Weelden et al., 2003).

The essential role of the trypanosome proline metabolism in the insect vector has been well established (Mantilla et al., 2017). However, the utilisation of other carbon sources possibly available in the digestive track and other organs of the insect, as well as pathways of the central carbon metabolism used by the trypanosomes *in vivo*, are currently unknown or poorly understood. For instance, the transient availability of glucose for trypanosomes directly following tsetse blood meals could contribute significantly to parasite development in the midgut of the fly. In addition, possible metabolic interactions between trypanosomes and intestinal symbiotic bacteria might also be taken into account, as illustrated by the positive correlation between the presence of the facultative symbiont *Sodalis glossinidius* and the ability of the tsetse fly to be infected by *T. brucei* (Welburn et al., 1993; Hall et al., 2019).

Here we showed that the procyclic form of *T. brucei* efficiently metabolises carbon sources other than glucose and proline, such as succinate, alanine, pyruvate, malate and  $\alpha$ -ketoglutarate.

Interestingly, the TCA cycle intermediates succinate, malate and  $\alpha$ -ketoglutarate stimulate growth of the parasites in *in vivo*-like conditions (2 mM proline (Balogun, 1974), without glucose). We also took advantage of the high metabolic rate of these



TCA cycle intermediates, to study the metabolic capacity of the parasite. This approach provided the first evidence for a possible complete TCA cycle in PCF trypanosomes.

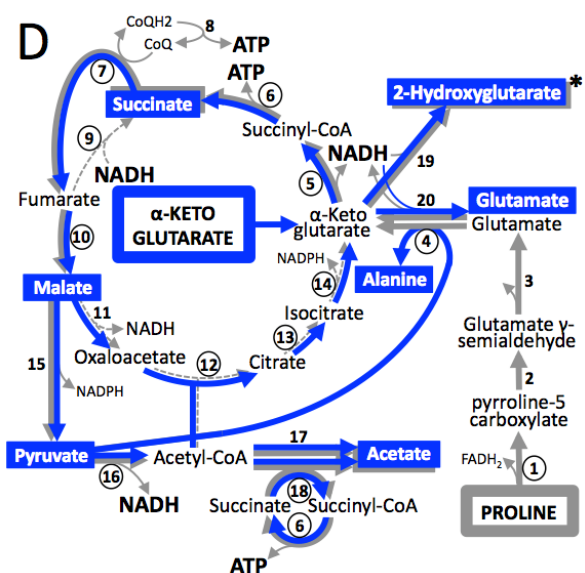
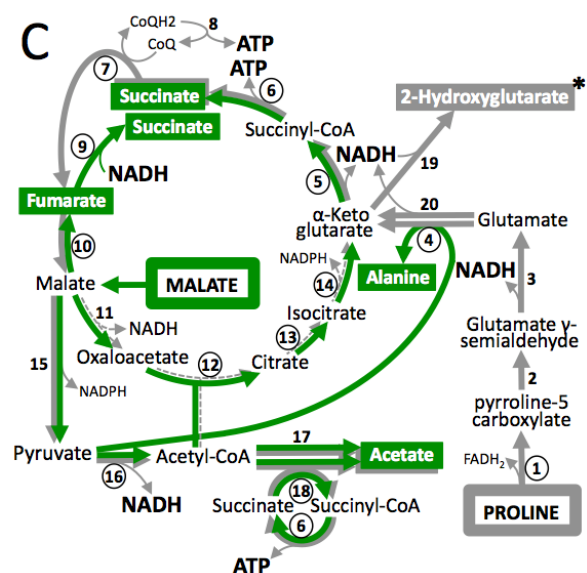
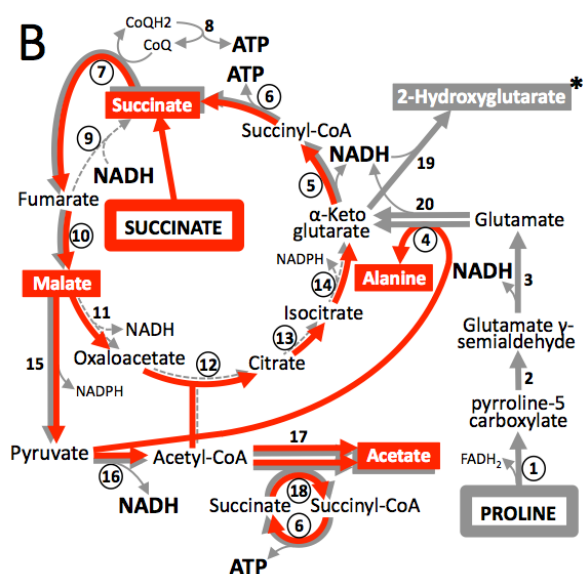
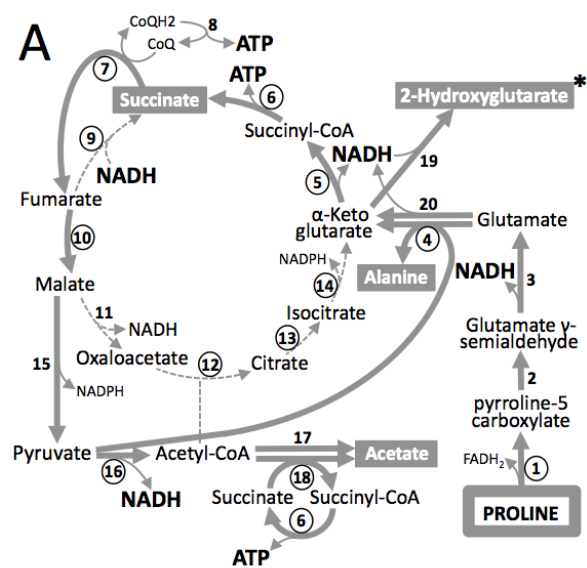


**Figure 3.51. Proline metabolism of the PCF trypanosomes in the presence of other carbon sources.**

Panels A, B, C and D correspond to schematic metabolic representations of PCF trypanosomes incubated in glucose-depleted medium, containing proline (grey arrows) without or with succinate (red arrows), malate (green arrows) and  $\alpha$ -ketoglutarate (blue arrows), respectively. End products excreted from catabolism of proline and the other carbon sources are shown in rectangles with the corresponding colour code, the enzyme numbers under investigation are circled and enzymatic reactions of proline metabolism that have not been shown to occur in parental PCF are represented by dashed lanes. The production and consumption of ATP and NAD<sup>+</sup> are indicated in bold and the asterisks mean that production of 2-hydroxyglutarate from proline has not been previously described for PCF.

**Enzymes** : 1, proline dehydrogenase (PRODH); 2, spontaneous reaction; 3, pyrroline-5 carboxylate dehydrogenase (P5CDH); 4, alanine aminotransferase (AAT); 5,  $\alpha$ -ketoglutarate dehydrogenase complex (KDH); 6, succinyl-CoA synthetase (SCoAS); 7, succinate dehydrogenase (SDH, complex II of the respiratory chain); 8, respiratory chain and mitochondrial ATP synthetase (oxidative phosphorylation); 9, mitochondrial NADH-dependent fumarate reductase (FRDm1); 10, mitochondrial fumarase (FHm); 11, mitochondrial malate dehydrogenase (MDHm); 12, citrate synthase (CS); 13, aconitase (ACO); 14, mitochondrial isocitrate dehydrogenase (IDHm); 15, mitochondrial malic enzyme (ME<sub>m</sub>); 16, pyruvate dehydrogenase complex (PDH); 17, acetyl-CoA thioesterase (ACH); 18, acetate:succinate CoA-transferase (ASCT); 19, unknown enzyme; 20, possibly NADH-dependent glutamate dehydrogenase.

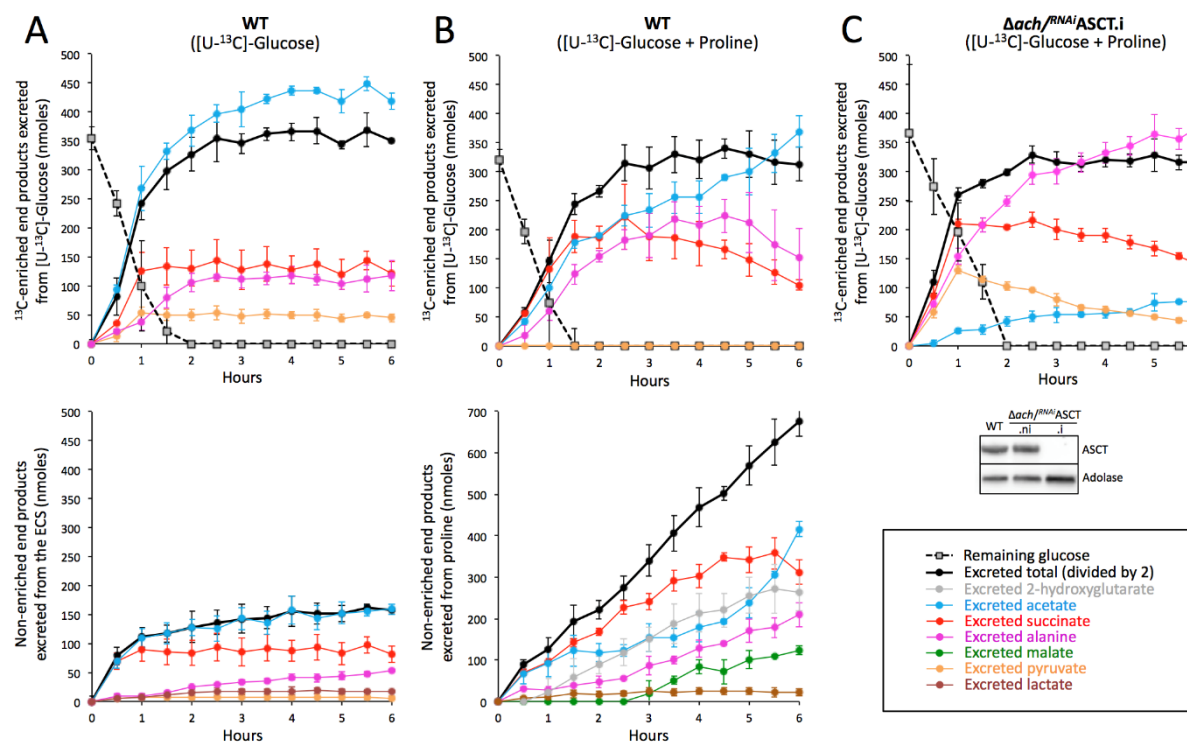


**Figure 3.52. Kinetic analyses of end products excretion from [U-<sup>13</sup>C]-glucose and proline metabolism.**

PCF cells were incubated for 6 h in PBS containing 0.5 mM [U-<sup>13</sup>C]-glucose in the presence (panel B) or not (panel A) of 4 mM non-enriched proline (Pro). Excreted end products were analysed in the spent medium every 0.5 h by <sup>1</sup>H-NMR spectrometry. The top panels A and B show the amounts of <sup>13</sup>C-enriched end products excreted from [U-<sup>13</sup>C]-glucose metabolism. The bottom panels show the amounts of non-enriched end products produced from the metabolism of the unknown internal carbon source (panel A) or from the metabolism of proline plus the unknown internal carbon source (panel B). In panel C, the kinetics of end products excreted from 0.5 mM [U-<sup>13</sup>C]-glucose in the presence of 4 mM proline was determined for the  $\Delta ach^{RNAi} ASCT.i$  mutant cell line as performed in panel B. Western blot controls with the anti-ASCT and anti-aldolase immune sera are shown below the graph.

### 3.3. Results

#### a) Procyclic trypanosomes can re-metabolise end products excreted from glucose degradation

To study the capacity of trypanosomes to metabolise unexpected carbon sources, such as those possibly excreted from the metabolism of the fly microbiota, we developed a model in which procyclic trypanosomes (PCF) have the possibility of re-consuming partially oxidised metabolites excreted from their own glucose catabolism. It is noteworthy that this model may also represent an *in vivo* situation, when established PCF faces a new blood meal of the insect.

In this experimental model, the parasites were incubated at high density in PBS containing low amounts of  $^{13}\text{C}$ -enriched glucose ([U- $^{13}\text{C}$ ]-glucose, 0.5 mM) in the presence or the absence of 4 mM proline. The production and possible re-consumption of excreted end products from the metabolism of [U- $^{13}\text{C}$ ]-glucose and/or non-enriched proline was monitored by analysing the medium over-time during a 6 h incubation using the  $^1\text{H}$ -NMR profiling approach. This quantitative  $^1\text{H}$ -NMR approach was previously developed to distinguish between [ $^{13}\text{C}$ ]-enriched and non-enriched excreted molecules produced from [ $^{13}\text{C}$ ]-enriched and non-enriched carbon sources, respectively (Mazet et al., 2013; Bringaud et al., 2015; Millerioux et al., 2018).

In these conditions, all glucose is consumed within the first 1.5-2 h (Figure 3.52A-B). When [U- $^{13}\text{C}$ ]-glucose is the only carbon source, PCF convert it to  $^{13}\text{C}$ -enriched acetate, succinate, alanine and pyruvate, in addition to lower amounts of non-enriched metabolites produced from an unknown internal carbon source (ICS) (Millerioux et al., 2013; Bringaud et al., 2015; Wagnies et al., 2018). After 1 h of incubation, net production of  $^{13}\text{C}$ -enriched succinate and pyruvate stopped while glucose remained in the medium. Interestingly,  $^{13}\text{C}$ -enriched acetate was still excreted even after glucose depletion, suggesting that acetate was produced from the metabolism of excreted end products, such as succinate and pyruvate (Figure 3.52A, top panel). The same pattern was observed from the non-enriched excreted metabolites produced from the ICS (Figure 3.52A, low panel). Addition of proline strongly stimulated this re-utilisation of glucose-derived succinate (Figure 3.52B, top panel).

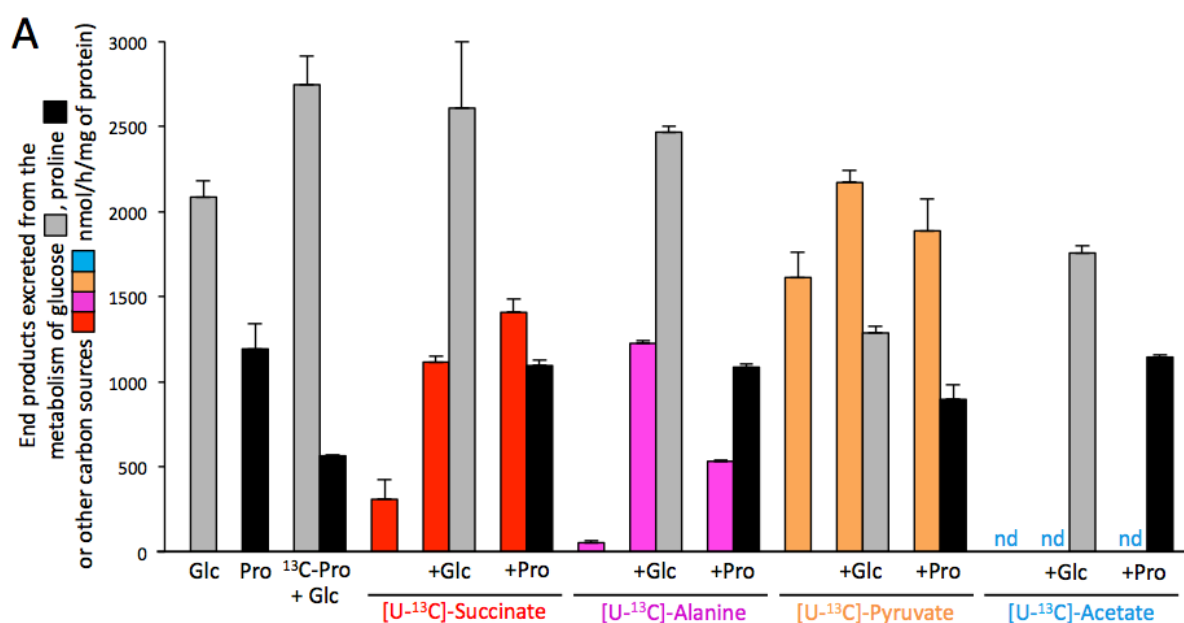


**Figure 3.53. Proton (<sup>1</sup>H) NMR analyses of end products excreted from the metabolism of <sup>13</sup>C-enriched succinate, alanine, pyruvate and acetate.**

PCF trypanosomes were incubated for 6 h in PBS containing 4 mM [U-<sup>13</sup>C]-succinate, [U-<sup>13</sup>C]-alanine, [U-<sup>13</sup>C]-pyruvate or [U-<sup>13</sup>C]-acetate alone or in combination with 4 mM glucose (+Glc) or proline (+Pro) before analysis of the spent medium by <sup>1</sup>H-NMR spectrometry. As reference, the same experiment was performed with 4 mM proline (Pro), 4 mM glucose (Glc) or 4 mM glucose with 4 mM [U-<sup>13</sup>C]-proline (<sup>13</sup>C-Pro). The amounts of each end product excreted are documented in Table 3.8.

In these incubation conditions, glucose-derived pyruvate was no longer excreted since it is used as a substrate by alanine aminotransferase (AAT, step 4 in Figure 3.51) to convert proline-derived glutamate to  $\alpha$ -ketoglutarate (Coustou et al., 2008). Alanine was also re-used, although with a 2.5 h delay compared to succinate. This re-utilisation was also seen for proline-derived succinate (Figure 3.52B, low panel) as proline-derived acetate increased at the expense of succinate after 4.5 h of incubation. Altogether these data suggested glucose-derived and/or proline-derived succinate, pyruvate and to a lower extent alanine can be re-utilised and converted to acetate. Since acetate is produced by both the acetate:succinate CoA-transferase (ASCT, step 18 in Figure 3.51A) and the acetyl-CoA thioesterase (ACH, step 17), the role of the acetate branch in the further metabolism of excreted end products was addressed. The same time-course was conducted on the  $\Delta ach/RNAi$ ASCT double mutant, in which ASCT expression was knocked-down by RNAi in the null ACH background. After 2 days of incubation, the tetracycline induced  $\Delta ach/RNAi$ ASCT ( $\Delta ach/RNAi$ ASCT.i) cell line showed 80% reduction of acetate production from glucose metabolism, compared to the parental cell line (Figure 3.52B-C), which is consistent with the 90% reduction of acetate excretion previously described for this cell line (Millerioux et al., 2013). The residual acetate production was attributed to incomplete down-regulation of ASCT expression, although ASCT could not be detected by Western blot (Millerioux et al., 2013) (Figure 3.52C). The excretion of glucose-derived pyruvate in the  $\Delta ach/RNAi$ ASCT.i mutant relates to the limited capacity of the acetate branch. Interestingly, succinate and pyruvate excreted during the first hour of incubation are re-consumed and converted to acetate and alanine, indicating that alanine is the ultimate excreted end product when the acetate branch is limiting (Figure 3.52C).

## **b) Succinate, pyruvate and alanine are metabolised in the presence of glucose or proline**

To determine how the main end products excreted from glucose catabolism (succinate, alanine, pyruvate or acetate) are metabolised in the presence or absence of glucose or proline, we analysed by quantitative  $^1\text{H}$ -NMR the exometabolome of PCF incubated with  $[\text{U-}^{13}\text{C}]$ -succinate,  $[\text{U-}^{13}\text{C}]$ -alanine,  $[\text{U-}^{13}\text{C}]$ -pyruvate or  $[\text{U-}^{13}\text{C}]$ -acetate in the presence or absence of equal amounts of non-enriched glucose or proline (Figure 3.53).

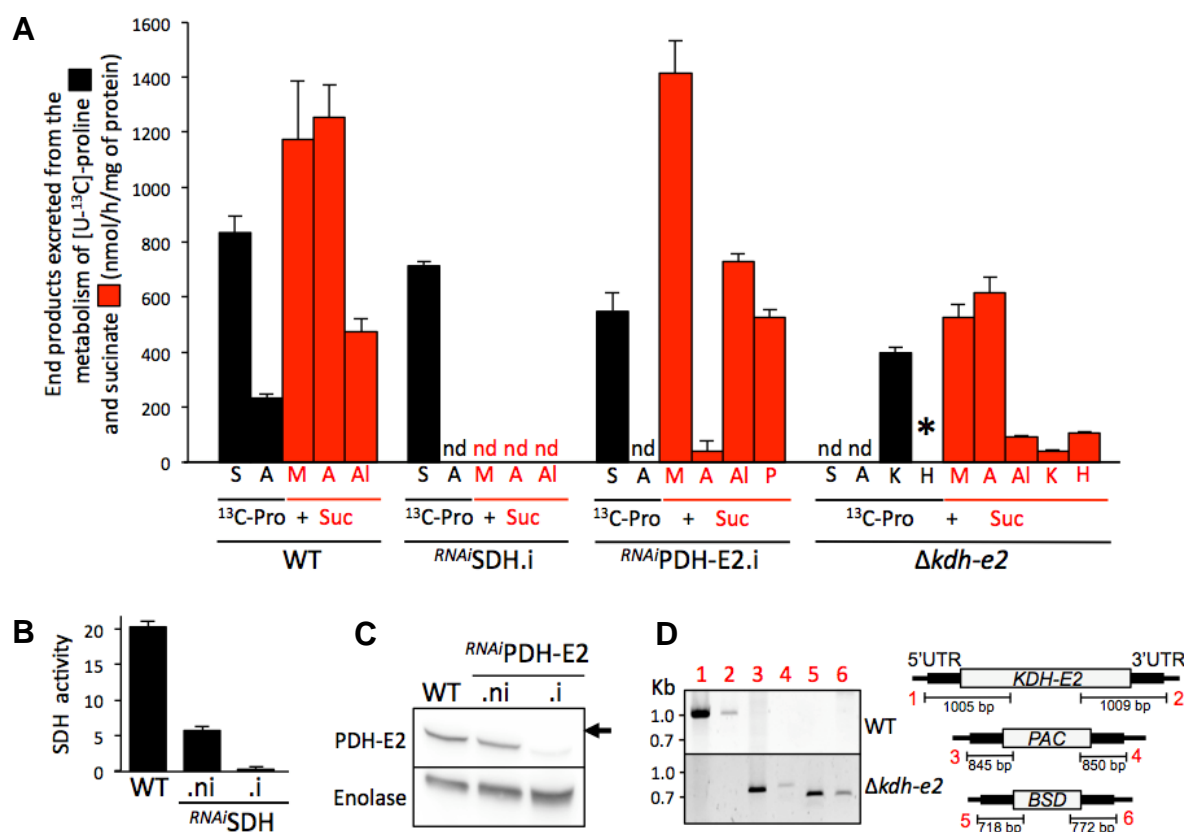


**Figure 3.54. <sup>1</sup>H-NMR analyses of end products excreted from the metabolism of <sup>13</sup>C-enriched succinate.**

Panel A shows <sup>1</sup>H-NMR spectrometry experiments performed on the parental (WT), *RNAiSDH.i*, *RNAiPDH-E2.i* and  $\Delta kdh-e2$  cell lines incubated with 4 mM [U-<sup>13</sup>C]-proline and 4 mM succinate. Because of high background, <sup>13</sup>C-enriched 2-hydroxyglutarate (H) produced from [U-<sup>13</sup>C]-proline cannot be quantified, however, it is detectable in the  $\Delta kdh-e2$  cell line as indicated by an asterisk (\*). Traces of fumarate produced from these carbon sources are not shown in the figure.

**Abbreviations:** A, acetate; Al, alanine; H, 2-hydroxyglutarate; K,  $\alpha$ -ketoglutarate; M, malate; P, pyruvate; S, succinate; nd, not detectable; \*, detectable but not quantifiable. The efficiency of RNAi-mediated down-regulation of SDH and PDH-E2 expression in the tetracycline-induced (.i) or non-induced (.ni) cell line was determined by SDH activity assays (panel B) and Western blotting with the anti-PDH-E2 and anti-enolase (control) immune sera (panel C).

Panel D shows a PCR analysis of genomic DNA isolated from the parental (WT) and  $\Delta kdh-e2$  cell line. Lanes 1 to 6 of the gel picture correspond to different PCR products described in the right panel. As expected, PCR amplification of the *KDH-E2* gene (lanes 1-2) was only observed in the parental cell line, while *PAC* and *BSD* PCR-products were observed only in the  $\Delta kdh-e2$  mutant (lanes 3-4 and 5-6, respectively).



Succinate was poorly consumed alone, however, the presence of glucose or proline stimulates its consumption by 3.6- and 4.6-fold, respectively (Figure 3.53). This is consistent with the increased conversion of glucose-derived succinate to acetate, in the presence of proline (Figure 3.52A-B). The amounts of excreted end products from proline catabolism were only 8% reduced in the presence of succinate, compared to a 53% reduction in the presence of glucose (Figure 3.53). This suggests that, in contrast to the previously reported glucose-induced down-regulation of proline metabolism (Lamour et al., 2005; Coustou et al., 2008), succinate addition does not limit the rate of proline metabolism. In the presence of [U-<sup>13</sup>C]-proline, succinate is converted to malate, acetate, alanine and traces of fumarate, which represent 40.5%, 43.2%, 16.4% and 1.5% of the excreted end products, respectively (Figure 3.54A).

According to the current metabolic model, succinate enters the tricarboxylic acid (TCA) cycle where it is converted to fumarate by succinate dehydrogenase (SDH, step 7 in Figure 3.51B) and to malate by the mitochondrial fumarase (FHM, step 10). The malic enzymes then produce pyruvate (MEM, step 15 and the cytosolic M<sub>EC</sub> not shown), which feeds the AAT (step 4) for production of alanine, or the pyruvate dehydrogenase (PDH) complex plus the ACH/ASCT steps (steps 17 and 18) for production of acetate. In agreement with this model, extracellular succinate and proline-derived succinate were no longer metabolised to acetate by the *<sup>RNAi</sup>SDH.i* cell line (Figure 3.54A). As expected, acetate production from succinate, as well as from proline, was abolished in the tetracycline-induced PDH subunit E2 RNAi mutant cell line (*<sup>RNAi</sup>PDH-E2.i*). The effective block of PDH activity is reflected by the increased excretion of succinate-derived pyruvate, the substrate of the PDH complex (Figure 3.54A).

[U-<sup>13</sup>C]-Alanine was poorly metabolised alone, but addition of glucose or proline considerably stimulated its consumption, with the production of <sup>13</sup>C-enriched end products being 23-fold and 10-fold increased, respectively (Figure 3.53). <sup>13</sup>C-enriched acetate represents 100% and 82% of the excreted end products from [U-<sup>13</sup>C]-Alanine in the presence of proline and glucose, respectively. [U-<sup>13</sup>C]-Pyruvate was converted to <sup>13</sup>C-enriched alanine and acetate in the presence or absence of glucose or proline. The rate of end product excretion was only increased by 35% and 17% in the presence of glucose and proline, respectively (Figure 3.53). In contrast, no <sup>13</sup>C-enriched molecules were detected by <sup>1</sup>H-NMR in the exometabolome of PCF incubated with [U-<sup>13</sup>C]-acetate, in the presence or absence of glucose or proline, suggesting that acetate is not further metabolised through the central metabolism.

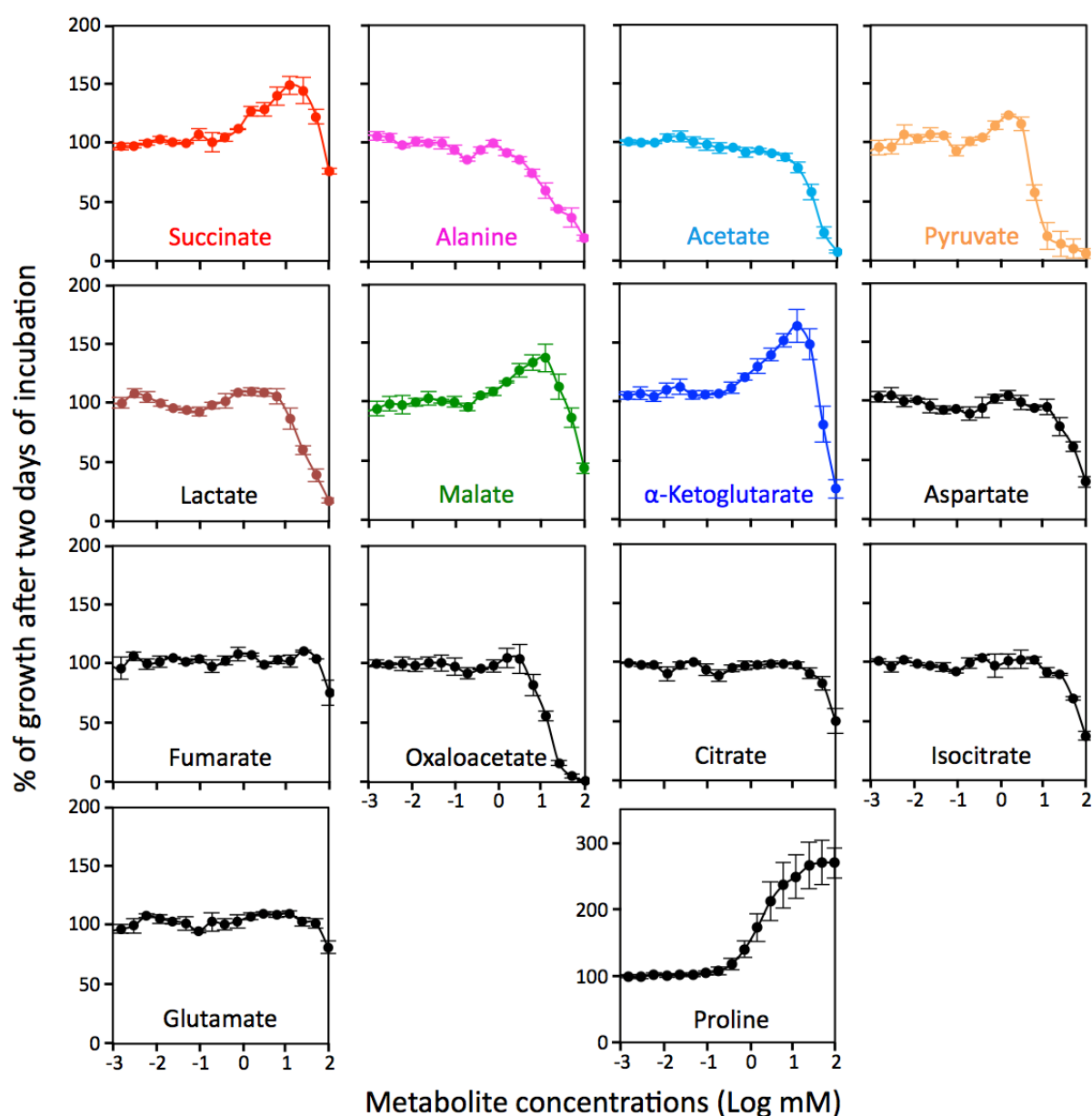


**Figure 3.55. Alamar Blue assays with a series of metabolites.**

Growth of the PCF trypanosomes in the glucose-free SDM79 medium containing 2 mM proline in the presence of added 10  $\mu$ M to 100 mM metabolite, using the Alamar Blue assay. Incubation was started at  $2 \times 10^6$  cell density and the Alamar Blue assay was performed after 48 h at 27°C as described before (Wargnies et al., 2018).

Together, these data show that acetate is the ultimate excreted end product of the metabolism of glucose and other carbon sources, while succinate, pyruvate and alanine, which are also excreted, can be re-utilised and converted to acetate.

**c) TCA cycle intermediates stimulate growth of the PCF in *in vivo*-like conditions**

The midgut of the tsetse fly, the natural environment of PCF, lacks glucose between blood meals and contains proline in the low mM range (1-2 mM) (Balogun, 1974), which is used by the parasite for its energy metabolism (Mantilla et al., 2017). To determine if succinate, alanine, acetate, pyruvate and lactate stimulate growth of the parasite in insect-like conditions, we estimated the growth of the PCF trypanosomes as a function of increasing concentrations of these metabolites in the glucose-free SDM79 medium containing 2 mM proline, using the Alamar Blue assay, as previously described (Wagnies et al., 2018). Among them, succinate (1 to 10 mM) was able to stimulate growth, with a maximum effect at 10 mM, while pyruvate showed a moderate effect (Figure 3.55).

This succinate-dependent growth stimulation is observed in the presence of up to 2 mM proline, but not in high-proline conditions (12 mM) (Figure 3.56A). As controls, 1 to 20 mM proline stimulated growth in the presence of 0.2 mM and 2 mM proline, but not in the presence of 12 mM proline. Among six other TCA cycle intermediates tested plus glutamate and aspartate, malate and  $\alpha$ -ketoglutarate also stimulated growth in the presence of 2 mM proline (and 0.2 mM), with a maximum effect on growth also at 10 mM (Figure 3.55 and Figure 3.56A).

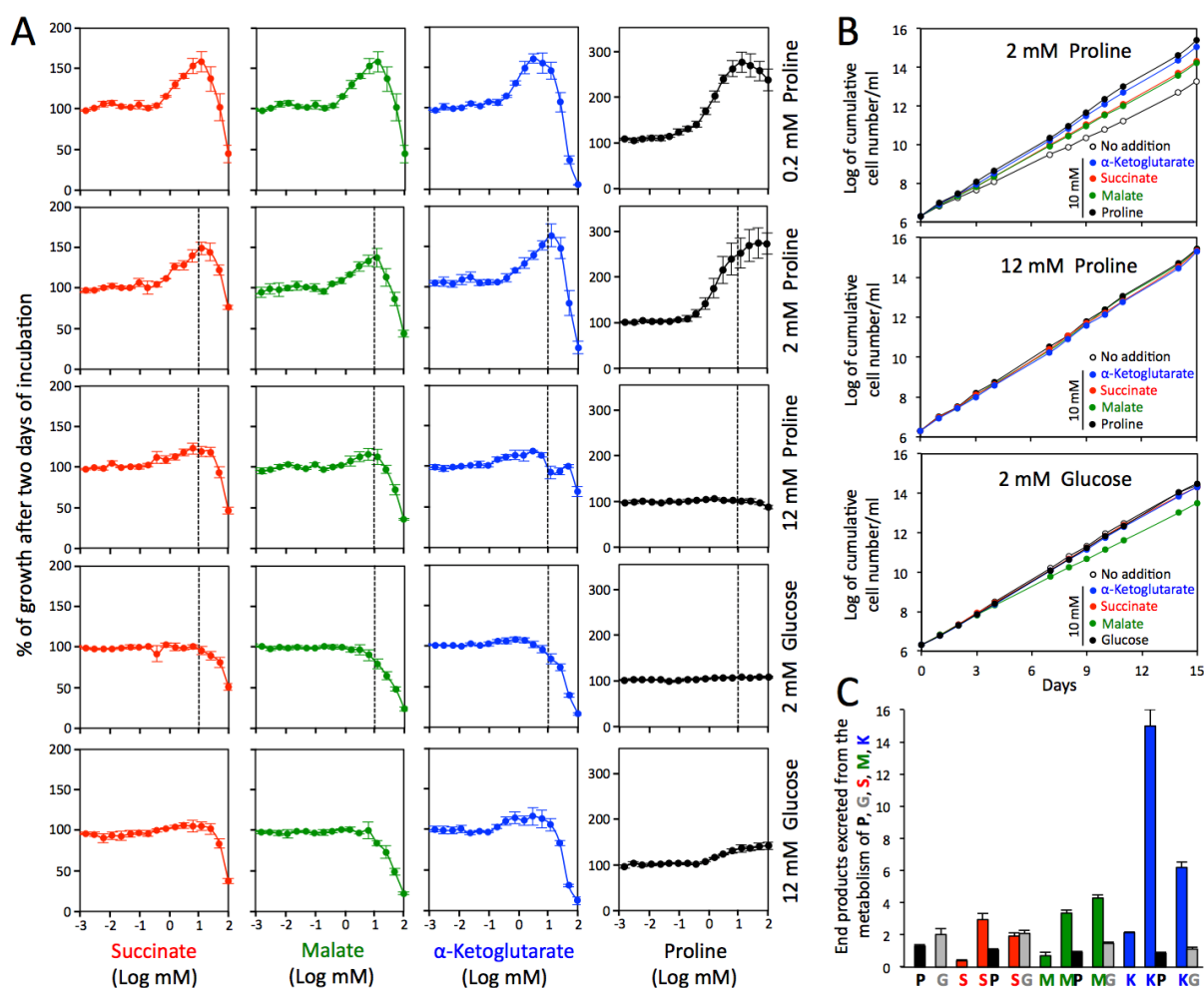


**Figure 3.56. Succinate, malate and  $\alpha$ -ketoglutarate stimulate growth of the PCF.**

Panel A shows growth of the PCF trypanosomes in the glucose-free SDM79 medium containing 0.2 mM, 2 mM (low-proline) or 12 mM (high-proline) proline, 2 mM glucose/2 mM proline (low-glucose) or 12 mM glucose/2 mM proline (high-glucose) in the presence of added 10  $\mu\text{M}$  to 100 mM succinate, malate,  $\alpha$ -ketoglutarate or proline, using the Alamar Blue assay. The dashed line indicates the concentrations of succinate, malate,  $\alpha$ -ketoglutarate or proline (10 mM) used in panel B, which shows growth curves of the PCF in low-proline, high-proline and low-glucose conditions in the presence or not of 10 mM of each metabolite. Cells were maintained in the exponential growth phase (between  $10^6$  and  $10^7$  cells/ml), and cumulative cell numbers reflect normalisation for dilution during cultivation.

In panel C, the PCF trypanosomes were incubated for 6 h in PBS containing 4 mM succinate (S), malate (M) or  $\alpha$ -ketoglutarate (K), in the presence or absence of 4 mM [ $U$ - $^{13}\text{C}$ ]-proline (P) or [ $U$ - $^{13}\text{C}$ ]-glucose (G), before analysis of the spent medium by  $^1\text{H}$ -NMR spectrometry. As control, the cells were also incubated with 4 mM [ $U$ - $^{13}\text{C}$ ]-proline (P) or [ $U$ - $^{13}\text{C}$ ]-glucose (G) alone. The amounts of end products excreted from the metabolism of proline (black), glucose (grey), succinate (red), malate (green) and  $\alpha$ -ketoglutarate (blue) are expressed as  $\mu\text{mol excreted/h/mg}$  of protein.

This growth stimulation was confirmed by performing growth curves of cells maintained in the exponential growth phase (between  $10^6$  and  $10^7$  cells/ml) over 15 days in the presence of 2 mM proline and 10 mM of succinate, malate or  $\alpha$ -ketoglutarate (Figure 3.56B).

The culture in the presence of these metabolites reduced the doubling time by approximately 1.2 fold, resulting in an increased growth rate compared to 2 mM proline alone. As observed for succinate, NMR analysis of excreted end products from the metabolism of malate and  $\alpha$ -ketoglutarate showed that the addition of equimolar amounts of [U- $^{13}\text{C}$ ]-proline induced an increase of the rate of malate and  $\alpha$ -ketoglutarate consumption by 5.7 and 6.6 fold, respectively (Figure 3.56C). 6.9 and 2.8 fold increases of malate and  $\alpha$ -ketoglutarate consumption were seen as well with [U- $^{13}\text{C}$ ]-glucose, respectively.

The effect of succinate, malate and  $\alpha$ -ketoglutarate was also determined on the PCF grown in glucose-rich conditions. At most, succinate,  $\alpha$ -ketoglutarate and the proline control have a minor stimulatory effect in the presence of 2 mM or 12 mM glucose (2 mM proline) (Figure 3.56A-B). However, addition of 10 mM malate to PCF grown in the presence 2 mM glucose slightly slowed growth of the parasite (Figure 3.56B). Malate was consumed 22% more in glucose-rich than in glucose-depleted conditions and its presence induced a 27% reduction of glucose consumption (Figure 3.56C), suggesting that switch to partial malate metabolism is less efficient than catabolism of glucose alone.



#### **d) The TCA cycle is used to metabolise malate in procyclic trypanosomes**

<sup>1</sup>H-NMR spectrometry analyses showed that, in the presence of proline, malate is converted in almost equal amounts to fumarate and succinate (35.9% and 38.6% of the excreted end products), in addition to alanine and acetate (14.9% and 10.6% of the excreted end products) (Figure 3.57). According to the current view, malate is converted by the malic enzymes to pyruvate (step 15 in Figure 3.51C), the precursor for the production of alanine and acetate, as described above (steps 4 and 16-18). As observed for the metabolism of succinate, production of acetate from malate is abolished in the *RNAi*PDH-E2.i cell line (Figure 3.57), with an accumulation of malate-derived pyruvate and alanine.

Malate can also be converted by FHm to fumarate (step 10), which is further reduced to succinate by the mitochondrial NADH-dependent fumarate reductase (FRDm1, step 9). It is to note that the cytosolic (FHc) and glycosomal (FRDg) isoforms of these two enzymes, respectively, could also be involved in succinate production (Coustou et al., 2005, 2006), justifying the use of the *RNAi*FRDg/m1.i and *RNAi*FHc/m.i double mutants to study the production of succinate from malate.

Succinate production from malate was reduced but not abolished in either of these two double mutants, suggesting that PCF uses an alternative pathway in addition to this reducing branch (Figure 3.57). Indeed, malate is also reduced to succinate by TCA cycle enzymes (steps 11-14 and 5-6), as inferred by diminished secretion of malate-derived succinate in the  $\Delta$ aco (aconitase, step 13) and  $\Delta$ kdh-e2 ( $\alpha$ -ketoglutarate dehydrogenase subunit E2, step 5) mutant cell lines (Figure 3.57).

Two other lines of evidence supported the utilisation of the oxidative branch of the TCA cycle to produce succinate. First, the  $\Delta$ kdh-e2 null mutant excreted  $\alpha$ -ketoglutarate from malate metabolism. Second, the expected abolition of fumarate production from malate in the *RNAi*FHc/m.i double mutant (Figure 3.57), implies that the malate-derived succinate cannot be produced by the fumarate reductase activity, but by the TCA cycle activity. The relatively high flux of malate consumption is probably the consequence of an efficient maintenance of the mitochondrial redox balance, with NADH molecules produced in the oxidative branches (succinate production through the TCA cycle and acetate production) being reoxidised, at least in part, by the reductive branch (succinate production by fumarate reductases).

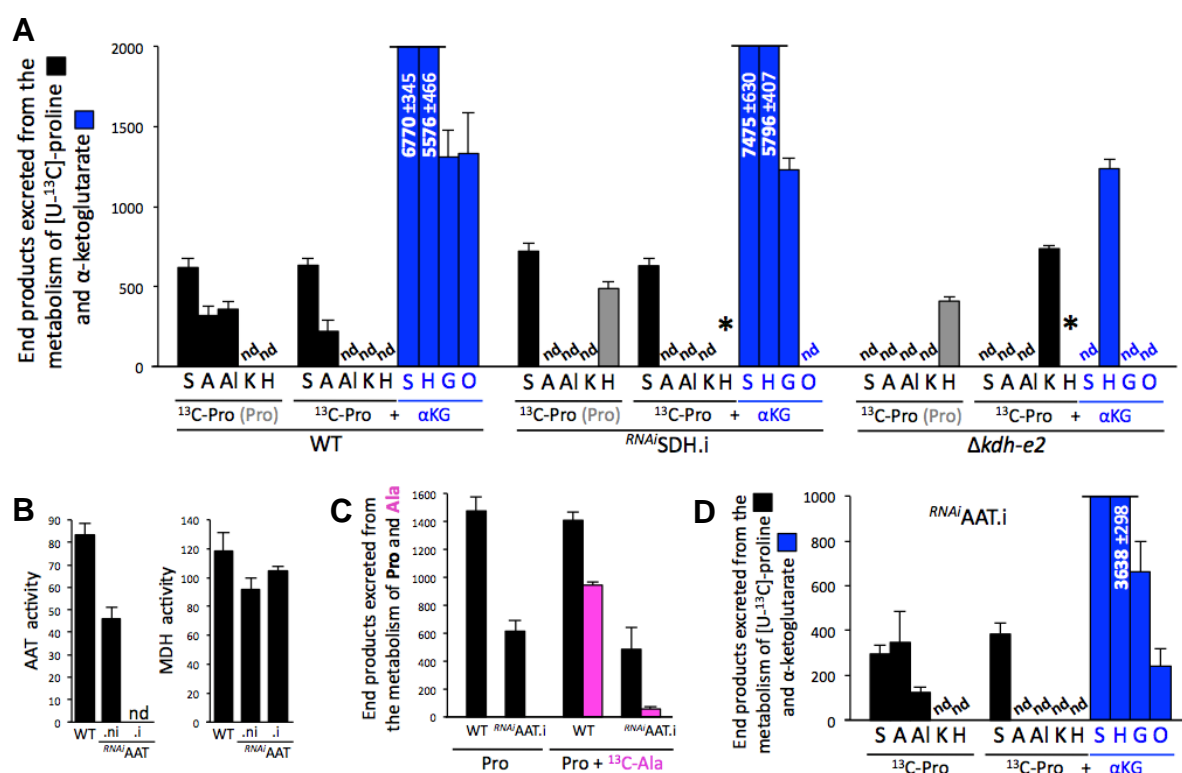


**Figure 3.58. <sup>1</sup>H-NMR analyses of end products excreted from the metabolism of α-ketoglutarate.**

The parental (WT), *RNAiSDH.i* and *Δkdh-e2* cell lines were incubated in the presence of [U-<sup>13</sup>C]-proline alone (<sup>13</sup>C-Pro) or with α-ketoglutarate (<sup>13</sup>C-Pro + αKG) (panel A). Because of high background, <sup>13</sup>C-enriched 2-hydroxyglutarate produced from [U-<sup>13</sup>C]-proline cannot be quantified, however, asterisks (\*) mean that it is detectable. Since the amounts of 2-hydroxyglutarate produced from non-enriched proline are quantifiable, the values are indicated with grey columns when applicable. The excreted amounts are indicated in the truncated columns (nmol/h/mg of protein).

The AAT and MDH (control) enzymatic activities of the parental (WT) and the tetracycline-induced (.i) and non-induced (.ni) *RNAiAAT* cell lines are shown in panel B. In panel C, the WT and *RNAiAAT.i* cells were incubated in 4 mM proline (Pro) with or without 4 mM [U-<sup>13</sup>C]-alanine (<sup>13</sup>C-Ala), before analysis of the spent medium by <sup>1</sup>H-NMR spectrometry. The amounts of end products excreted from the metabolism of proline (black) and alanine (pink) are expressed as nmol excreted/h/mg of protein. Panel D is equivalent to panel A, except that the *RNAiAAT.i* is analysed.

**Abbreviations:** A, acetate; Al, alanine; F, fumarate; G, glutamate; H, 2-hydroxyglutarate; K, α-ketoglutarate; nd, not detectable; M, Malate; O, malate + pyruvate + acetate + alanine; S, succinate; \*, detected but not quantifiable.



This resembles the malate dismutation phenomenon well described in anaerobic parasites (Bringaud et al., 2010; Müller et al., 2012). It is to note that, in the presence of proline, succinate was also converted to  $\alpha$ -ketoglutarate through the TCA cycle as inferred by the accumulation of excreted non-enriched  $\alpha$ -ketoglutarate of the  $\Delta kdh-e2$  null mutant incubated with succinate and [U- $^{13}\text{C}$ ]-proline (Figure 3.54A).

### **e) Metabolism of $\alpha$ -ketoglutarate in the presence of proline**

To our surprise,  $^1\text{H}$ -NMR spectrometry analysis of  $\alpha$ -ketoglutarate metabolism showed that its rate of consumption in the presence of equal amounts (4 mM) of proline ( $\sim 15$   $\mu\text{mole/h/mg}$  of protein) is  $\sim 15$ -times higher compared to that of glucose ( $\sim 1$   $\mu\text{mole/h/mg}$  of protein), the latter having previously been considered as the most rapidly degraded carbon source by the PCF trypanosomes (Lamour et al., 2005). As observed for the metabolism of succinate and malate, the rate of  $\alpha$ -ketoglutarate degradation is increased in the presence of proline or glucose (Figure 3.56C).

In the presence of proline,  $\alpha$ -ketoglutarate is mainly converted to equivalent amounts of succinate and 2-hydroxyglutarate (45.5% and 37.2% of the excreted end products, respectively), with significant amounts of glutamate (8.7%), acetate (3.6%), pyruvate (3.1%) and malate (1.6%), as well as less than 1% of alanine and lactate (Figure 3.58A). The production of 2-hydroxyglutarate and glutamate from  $\alpha$ -ketoglutarate was validated by comparing the exometabolome of the PCF incubated with [U- $^{13}\text{C}$ ]-proline or [U- $^{13}\text{C}$ ]-proline/ $\alpha$ -ketoglutarate with 2-hydroxyglutarate and glutamate standards (Figure 3.59).

According to the current model, succinate is produced from  $\alpha$ -ketoglutarate by the successive action of  $\alpha$ -ketoglutarate dehydrogenase (KDH, step 5 in Figure 3.51D) and succinyl-CoA synthetase (SCoAS, step 6). Succinate then feeds production of malate, pyruvate, alanine and acetate, as evidenced by their absence in the exometabolome of the *RNAi*SDH.i cell line incubated with [U- $^{13}\text{C}$ ]-proline and  $\alpha$ -ketoglutarate (Figure 3.58A).

The  $\Delta kdh-e2$  null mutant excretes only 2-hydroxyglutarate from metabolism of  $\alpha$ -ketoglutarate, suggesting that a single reduction step, catalysed by an as yet unknown enzyme, produces 2-hydroxyglutarate from  $\alpha$ -ketoglutarate (Engqvist et al., 2014; Intlekofer et al., 2017).

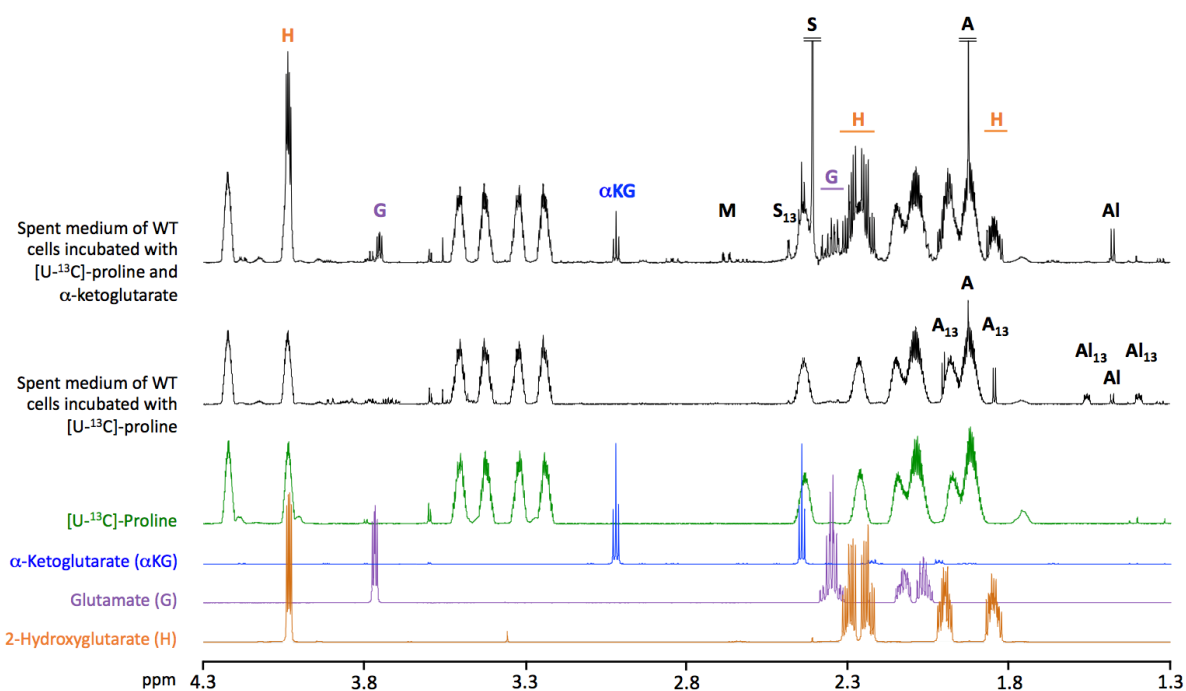


**Figure 3.59. Identification of 2-hydroxyglutarate by  $^1\text{H}$ -NMR analysis.**

The analysis of samples (black) and controls (coloured) was performed at 800 MHz on a Bruker Advance spectrometer. Acetate (A), alanine (Al), glutamate (G), 2-hydroxyglutarate (H),  $\alpha$ -ketoglutarate ( $\alpha\text{KG}$ ), malate (M), proline and succinate (S) were identified. The resonances corresponding to  $^{13}\text{C}$ -enriched molecules are indicated in index.

It has recently been proposed that 2-hydroxyglutarate detected in the *T. brucei* BSF metabolome results from the promiscuous action of the NADH-dependent malate dehydrogenase on  $\alpha$ -ketoglutarate (Johnston et al., 2019).

2-hydroxyglutarate is also produced from malate and succinate by the  $\Delta kdh-e2$  null mutant (Figure 3.54A and Figure 3.57). Revisiting NMR spectrometry data showed that 2-hydroxyglutarate is also excreted by the parental PCF from proline metabolism in the presence (Figure 3.52) and in the absence (Table 3.8) of glucose. It is noteworthy that  $^{13}\text{C}$ -enriched 2-hydroxyglutarate molecules produced from  $[\text{U-}^{13}\text{C}]$ -proline are barely detectable due to high background and observed but not quantifiable in the  $^{RNAi}SDH.i$  and  $\Delta kdh-e2$  cell lines (Figure 3.54A and Figure 3.57).

Since,  $\alpha$ -ketoglutarate is produced from glutamate by the AAT transamination reaction (step 4) (Spitznagel et al., 2009), the  $^{RNAi}AAT.i$  cell line was studied to determine if AAT is sufficient to catalyse the reverse reaction. The AAT activity was no longer detectable in the  $^{RNAi}AAT.i$  cell line (Figure 3.58B), however, the catabolism of proline was only 2.5-fold reduced in the  $^{RNAi}AAT.i$  cell line compared to the parental cell line (Figure 3.58C). In addition, the  $^{RNAi}AAT.i$  cell line still produced glutamate from  $\alpha$ -ketoglutarate (Figure 3.58D). This suggests that an alternative enzyme is involved in the reversible conversion of glutamate to  $\alpha$ -ketoglutarate. Interestingly, alanine conversion to acetate, which theoretically requires the AAT activity working in the direction of glutamate production (Figure 3.51), was 20-fold reduced in the  $^{RNAi}AAT.i$  cell line (Figure 3.58C), suggesting that the alternative enzyme is not another aminotransferase. Thus, the best candidate is the NADH-dependent glutamate dehydrogenase previously described in trypanosomatids (Duschak and Cazzulo, 1991; Bringaud et al., 1997).

It is noteworthy that the possible NADH consumption through reduction of  $\alpha$ -ketoglutarate to 2-hydroxyglutarate ( $5.6 \pm 0.47$   $\mu\text{mol produced/h/mg of protein}$ ) and glutamate ( $1.3 \pm 0.17$   $\mu\text{mol produced/h/mg of protein}$ ) may compensate NADH production by the KDH reaction ( $6.8 \pm 0.35$   $\mu\text{mol of succinate produced/h/mg of protein}$ ).

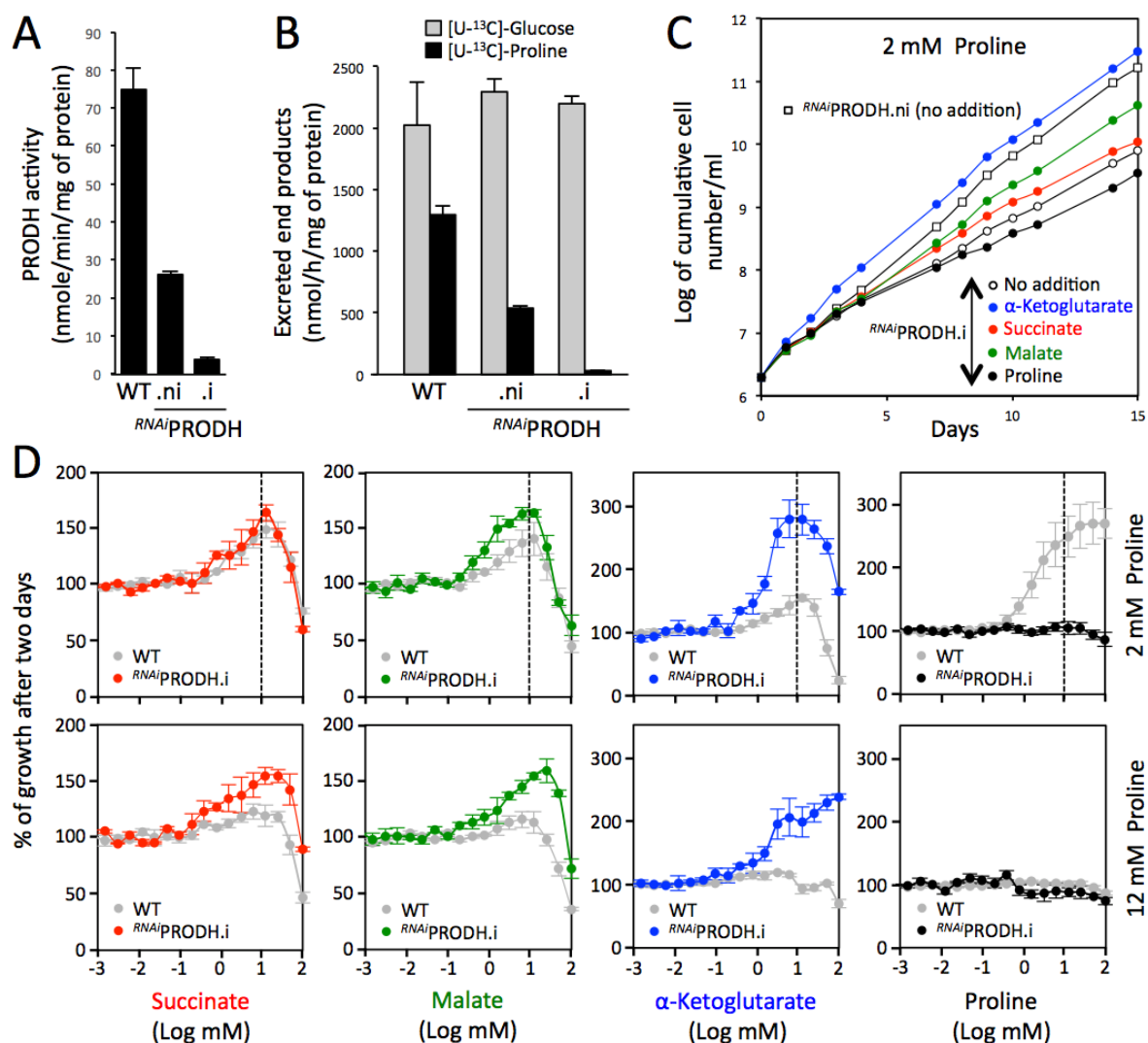


**Figure 3.60. Growth of the *RNAiPROD.H.i* mutant is rescued by  $\alpha$ -ketoglutarate.**

The efficiency of RNAi-mediated down-regulation of PROD.H expression in the tetracycline-induced (.i) or non-induced (.ni) *RNAiPROD.H* cell line, as well as in the parental cell line (WT) was determined by PROD.H activity assay (panel A) and <sup>1</sup>H-NMR quantification of end products excreted from metabolism of proline and glucose in two independent experiments (panel B).

Panel C shows growth curves of the *RNAiPROD.H.i* cell line in glucose-free medium containing 2 mM proline, in the presence (coloured circles) or absence (open circles) of 10 mM  $\alpha$ -ketoglutarate, malate, succinate or proline. Cells were maintained in the exponential growth phase and cumulative cell numbers reflect normalisation for dilution during cultivation.

The effect of 10 mM succinate, malate,  $\alpha$ -ketoglutarate or proline on growth of the parental and *RNAiPROD.H.i* cell lines in glucose-free medium containing 2 mM proline, using the Alamar Blue assay is shown in panel D.

#### **f) $\alpha$ -Ketoglutarate rescued the growth defect of the *RNAi*PROD*H*.i and *RNAi*AAT.i mutants**

We previously showed that proline dehydrogenase (PROD*H*), which catalyses the first step of the proline degradation pathway, is important for the growth of the PCF in glucose-depleted conditions (Lamour et al., 2005). Growth of the *RNAi*PROD*H*.i cell line was considerably reduced but not abolished in glucose-depleted conditions, probably because of the residual PROD*H* activity (Figure 3.60A) and residual conversion of proline to excreted end products (Figure 3.60B). As expected, proline did not rescue growth of the *RNAi*PROD*H*.i mutant in glucose-depleted conditions. However, succinate and malate improved growth of the mutant and more importantly  $\alpha$ -ketoglutarate completely rescued its growth (Figure 3.60C), even in the presence of 12 mM proline (Figure 3.60D).

Unfortunately, we failed to obtain the  $\Delta$ *prodH* null mutant in standard glucose-rich conditions, with or without 10 mM  $\alpha$ -ketoglutarate, probably because minimal proline degradation is required even in the presence of glucose. As mentioned above, proline metabolism was 2.5-fold reduced in the *RNAi*AAT.i mutant cell line (Figure 3.58C). This caused a slight growth defect in glucose-depleted conditions that was rescued by the addition of  $\alpha$ -ketoglutarate, as observed for the *RNAi*PROD*H*.i mutant (Figure 3.62B).

Collectively, these data suggest that metabolism of  $\alpha$ -ketoglutarate, and to a lesser extent in the case of the *RNAi*PROD*H*.i cell line, succinate and malate, compensate for the lack of proline metabolism.

To confirm these data, the ability of these carbon sources to replace proline was tested under long-term growth conditions. Because of the auxotrophy of *T. brucei* for proline, which is necessary for protein biosynthesis, the growth medium contained 0.2 mM proline. In these conditions, the growth defect observed in the absence of additional carbon source is partially rescued with the same efficiency by 10 mM  $\alpha$ -ketoglutarate, glucose, succinate and malate (Figure 3.61). Interestingly, the growth rate in low-proline conditions is the same whether in the presence of glucose or malate/succinate/ $\alpha$ -ketoglutarate, thus confirming that these TCA cycle intermediates are excellent carbon sources for PCF.

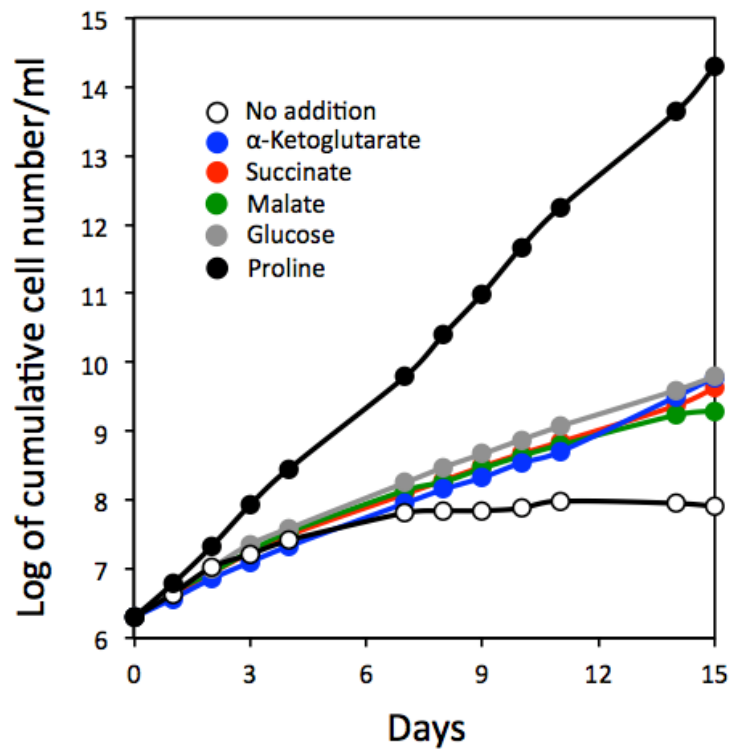


**Figure 3.61. Growth of PCF trypanosomes in low-proline conditions (0.2 mM).**

Cells were grown in glucose-depleted SDM79 medium in the presence or the absence of 10 mM proline, glucose,  $\alpha$ -ketoglutarate, succinate or malate. Cells were maintained in the exponential growth phase (between  $10^6$  and  $10^7$  cells/ml), and cumulative cell numbers reflect normalisation for dilution during cultivation.

### **g) $\alpha$ -Ketoglutarate is toxic if not metabolised at a high rate**

As mentioned above, proline metabolism was strongly affected in the  $\Delta kdh-e2$  mutant, with only production of  $\alpha$ -ketoglutarate and 2-hydroxyglutarate (Figure 3.57 and Figure 3.58A). As a consequence, growth of the  $\Delta kdh-e2$  mutant was compromised in glucose-depleted medium containing 2 mM or 10 mM proline, while the addition of 10 mM malate or succinate rescued this growth phenotype (Figure 3.62A-B). However, addition of  $\alpha$ -ketoglutarate at concentrations as low as 1 mM was detrimental for the survival of the  $\Delta kdh-e2$  mutant (Figure 3.62A-B). This toxic effect of  $\alpha$ -ketoglutarate was confirmed by the reduced growth of the  $RNAiSDH.i$  and  $RNAiSCoAS.i$  mutants, which are also affected in  $\alpha$ -ketoglutarate metabolism (Figure 3.62B). It is also of note that expression of SCoAS was not fully abolished in the  $RNAiSCoAS.i$ , which may explain the moderate reduction of its growth (Figure 3.62C). These data suggest that accumulation of  $\alpha$ -ketoglutarate or one of its metabolic derivatives is toxic to PCF trypanosomes.

We cannot exclude that reduction of  $\alpha$ -ketoglutarate to isocitrate, citrate or one of their metabolic products is responsible for this phenotype (Figure 3.51). To block the possible citrate/isocitrate production from  $\alpha$ -ketoglutarate in the  $\Delta kdh-e2$  and  $RNAiSCoAS$  backgrounds, the *IDHm* gene was knocked-down or knocked-out to produce the  $\Delta kdh-e2/RNAiIDHm$  and  $\Delta idhm/RNAiSCoAS$  cell lines, respectively. Growth of these tetracycline-induced double mutants was strongly impaired by addition of  $\alpha$ -ketoglutarate as observed for the  $\Delta kdh-e2$  and  $RNAiSCoAS.i$  single mutants, while  $\alpha$ -ketoglutarate stimulated growth of the  $\Delta idhm$  as observed for the parental cell line (Figure 3.62A). This confirmed that accumulation of  $\alpha$ -ketoglutarate itself is responsible for this phenomenon.

It is noteworthy that accumulation of succinate was not toxic for trypanosomes, as exemplified by the absence of effect of 10 mM succinate on growth of the  $RNAiSDH.i$  cell line (Figure 3.62B), which was no longer able to metabolise succinate (Figure 3.54). As expected, malate stimulated growth of this mutant (Figure 3.62B).

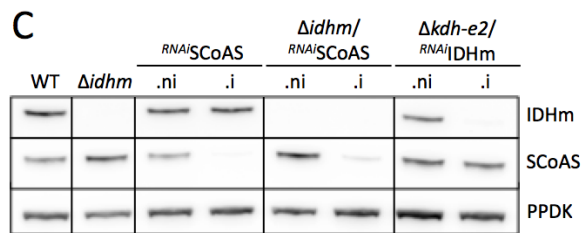
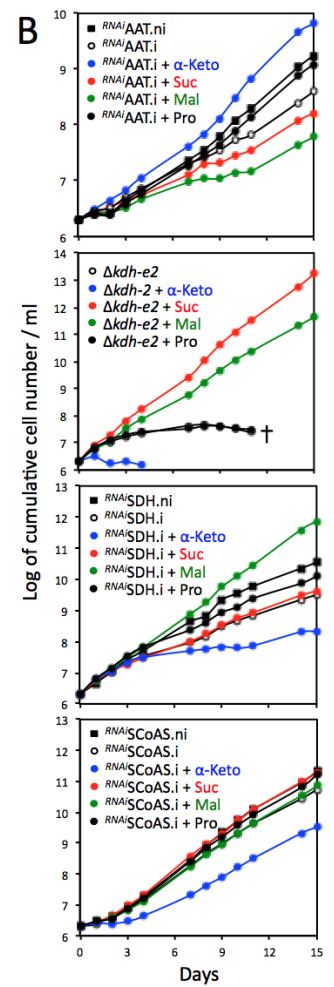
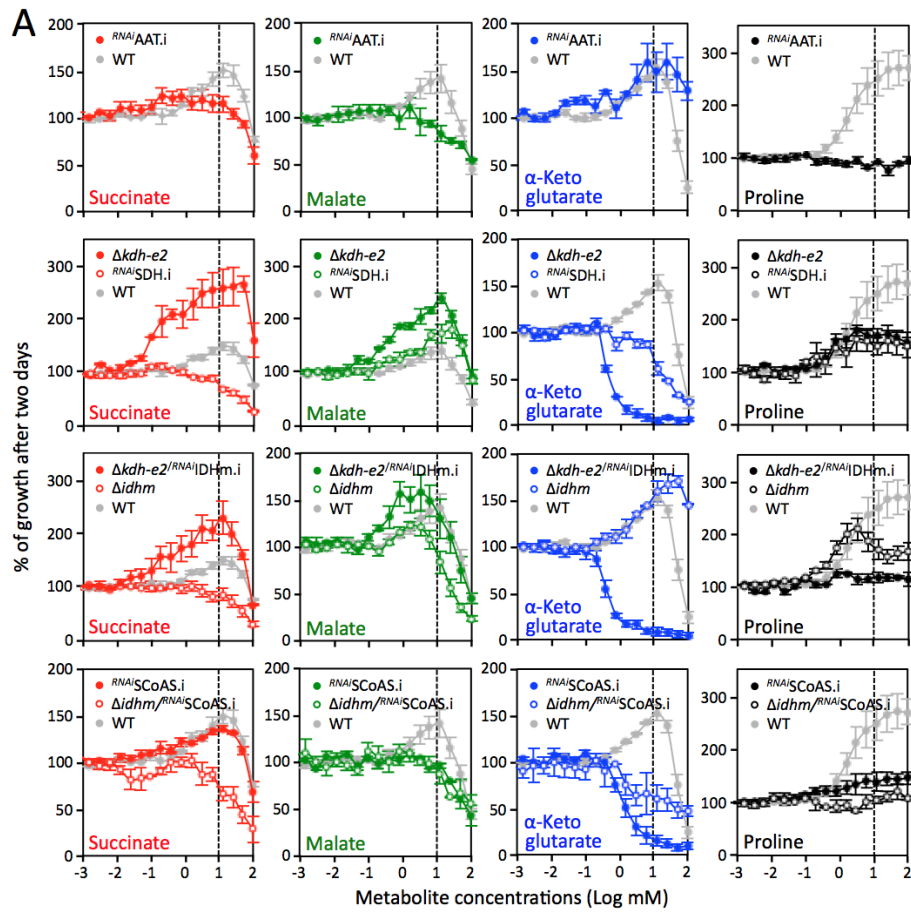




**Figure 3.62.  $\alpha$ -ketoglutarate is toxic for the  $\Delta kdh-e2$ ,  $RNAi$ SCoAS.i and  $RNAi$ SDH.i cell lines.**

Panel A compares the effect of succinate, malate,  $\alpha$ -ketoglutarate or proline (10 mM) on growth of the parental and mutant cell lines in glucose-free SDM79 medium containing 2 mM proline, using the Alamar Blue assay.

Panel B shows growth curves of the  $RNAi$ AAT,  $\Delta kdh-e2$ ,  $RNAi$ SDH and  $RNAi$ SCoAS cell lines incubated in glucose-free medium containing 2 mM proline, in the presence (coloured circles) or absence (open circles) of  $\alpha$ -ketoglutarate, malate, succinate or proline (10 mM) (.i, tetracycline-induced cells; .ni, non-induced cells). Cells were maintained in the exponential growth phase and cumulative cell numbers reflect normalisation for dilution during cultivation.

Panel C shows Western blot analyses with the immune sera indicated in the right margin of the parental (WT),  $\Delta idhm$  and tetracycline-induced (.i) and non-induced (.ni)  $RNAi$ SCoAS,  $\Delta idhm/RNAi$ SCoAS and  $\Delta kdh-e2/RNAi$ IDHm cell lines.

<sup>13</sup> C-enriched carbon source	/	/	/	Proline	Succinate	Succinate	Succinate	Alanine	Alanine	Alanine	Pyruvate	Pyruvate	Pyruvate	Acetate	Acetate	Acetate
Non-enriched carbon source	ICS <sup>a</sup>	Glucose + ICS	Proline + ICS	Glucose + ICS	ICS	Glucose + ICS	Proline + ICS	ICS	Glucose + ICS	Proline + ICS	ICS	Glucose + ICS	Proline + ICS	ICS	Glucose + ICS	Proline + ICS
Number of samples	6	3	6	3	6	6	6	3	3	3	3	3	3	3	3	3
End products excreted from the metabolism of [carbon sources] (nmoles/hour/10e8 cells)																
Malate [Suc, Ala, Pyr or Ace] <sup>b</sup> Malate [ICS]	nd <sup>c</sup>				96 ±115 nd	345 ±16	426 ±57	nd nd	nd	nd	nd nd	nd	nd	nd nd	nd	nd
Malate [Glucose and ICS] <sup>d</sup> Malate [Proline and ICS] <sup>e</sup>		nd	nd	nd nd		188 ±39	nd		98 ±6	nd		nd	nd		68 ±9	nd
Fumarate [Suc, Ala, Pyr or Ace] Fumarate [ICS]	3 ±2				nd 8 ±2	8 ±3	nd	nd nd	nd	nd	nd nd	nd	nd	nd nd	nd	nd
Fumarate [Glucose and ICS] Fumarate [Proline and ICS]		8 ±4	7 ±1	18 ±2 nd		22 ±2	11 ±2		10 ±2	nd		nd	4 ±2		nd	1 ±1
Hydroxyglutarate [Suc, Ala, Pyr or Ace] Hydroxyglutarate [ICS]	nd				nd nd	nd	nd	nd nd	nd	nd	nd nd	nd	nd	nd nd	nd	nd
Hydroxyglutarate [Glucose and ICS] Hydroxyglutarate [Proline and ICS]		nd	205 ±11	nd nd		nd	194 ±14		nd	326 ±11		nd	212 ±20		nd	196 ±4
Succinate [Suc, Ala, Pyr or Ace] Succinate [ICS]	23 ±12				nd 210 ±12	nd	nd	54 ±15 31 ±7	101 ±1		nd 27 ±1	170 ±12	nd	nd 30 ±3	nd	nd
Succinate [Glucose and ICS] Succinate [Proline and ICS]		288 ±15	186 ±36	390 ±9 185 ±4*		1009 ±188	820 ±34		191 ±3	269 ±6		113 ±4	130 ±6		237 ±8	166 ±1
Pyruvate [Suc, Ala, Pyr or Ace] Pyruvate [ICS]	nd				nd nd	nd	nd	nd nd	118 ±1		nd 113 ±6	nd	nd	nd nd	nd	nd
Pyruvate [Glucose and ICS] Pyruvate [Proline and ICS]		40 ±2	nd	nd nd		nd	nd		34 ±2	nd		584 ±19	nd		109 ±4	nd
Acetate [Suc, Ala, Pyr or Ace] Acetate [ICS]	88 ±16				158 ±5 102 ±4	762 ±35	726 ±78	nd 20 ±6	1006 ±23	532 ±4	182 ±7 90 ±4	760 ±17	240 ±31	nd 161 ±4	nd	nd
Acetate [Glucose and ICS] Acetate [Proline and ICS]		1728 ±81	580 ±82	2015 ±171 335 ±8*		1350 ±144	191 ±13		332 ±7	119 ±3		678 ±18	385 ±29		1411 ±33	479 ±5
Alanine [Suc, Ala, Pyr or Ace] Alanine [ICS]	65 ±9				55 ±5 31 ±5	nd	255 ±34	nd 205 ±53			1021 ±45 nd	1033 ±34	1227 ±60	nd 57 ±3	nd	nd
Alanine [Glucose and ICS] Alanine [Proline and ICS]		22 ±1	223 ±34	323 ±8 44 ±2*		23 ±5	46 ±9		2080 ±28	532 ±9		56 ±2	242 ±27		44 ±3	303 ±6
Lactate [Suc, Ala, Pyr or Ace] Lactate [ICS]	nd				nd 14 ±15	nd	nd	nd nd	nd	nd	230 ±104 nd	208 ±12	420 ±111	nd nd	nd	nd
Lactate [Glucose and ICS] Lactate [Proline and ICS]		nd	nd	nd nd		16 ±18	9 ±10		nd	nd		nd	nd		nd	nd
Total [Suc, Ala, Pyr or Ace] Total [ICS]	179 ±23				309 ±115 365 ±28	1115 ±38	1408 ±83	54 ±15 256 ±66	1226 ±25	532 ±4	1613 ±147 224 ±8	2171 ±71	1887 ±187	nd 248 ±7	nd	nd
Total [Glucose and ICS] Total [Proline and ICS]		2085 ±94	1193 ±148	2746 ±169 565 ±9*		2608 ±392	1261 ±34		2734 ±36	1245 ±19		1430 ±39	972 ±83		1800 ±47	1145 ±14

**Table 3.8. Excreted end products from the metabolism of carbon sources in the PCF trypanosomes.**

The parasites were incubated during 6 h in PBS with 4 mM [U-<sup>13</sup>C]-succinate, [U-<sup>13</sup>C]-alanine, [U-<sup>13</sup>C]-pyruvate or [U-<sup>13</sup>C]-acetate in the presence of the absence of 4 mM glucose or proline.

<sup>a</sup> ICS (internal carbon source): intracellular carbon source of unknown origin metabolised by the PCF trypanosomes.

<sup>b</sup> The amount of end products excreted (here malate) from the carbon source indicated in brackets, expressed as nmoles excreted per h and per 10<sup>8</sup> cells.

<sup>c</sup> *nd*: not detectable

<sup>d</sup> End products excreted (here malate) from glucose or the ICS, which are both non-enriched

<sup>e</sup> End products excreted (here malate) from proline or the ICS, which are both non-enriched. The asterisks mean that in this particular experiment the values correspond to proline only, since it is <sup>13</sup>C-enriched.

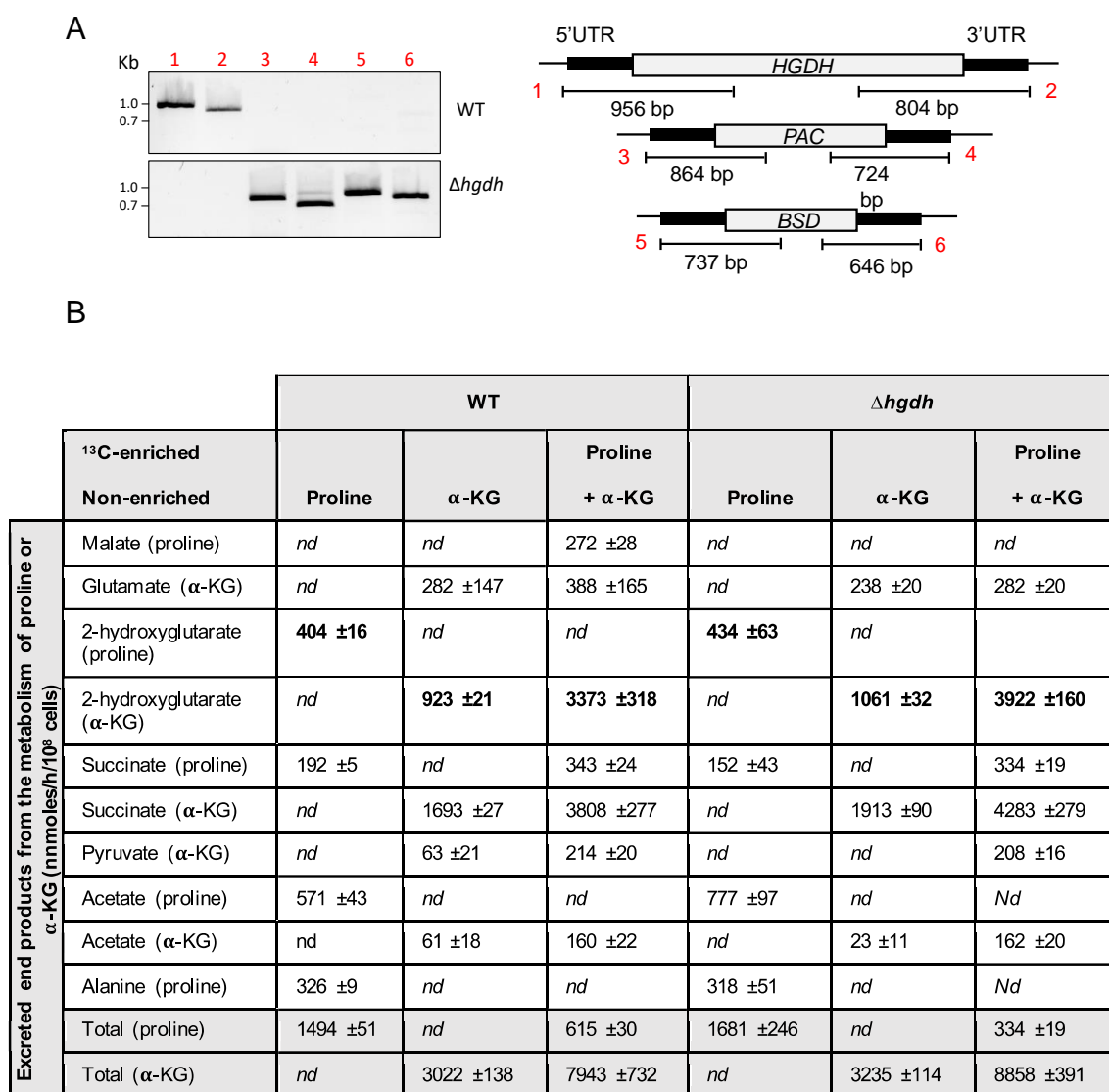


**Figure 3.63. Analysis of the  $\Delta hgdh$  mutant.**

Panel A shows a PCR analysis of genomic DNA isolated from the parental (WT) and  $\Delta hgdh$  cell lines. PCR amplification of the *HGDH* gene (lanes 1-2) is only observed in the parental cell line, while *PAC* and *BSD* PCR-products are only observed in the  $\Delta hgdh$  (lanes 3-4 and 5-6), respectively.

In panel B, the PCF trypanosomes were incubated for 6 h in PBS containing 4 mM proline, 4 mM  $\alpha$ -ketoglutarate in the presence or absence of 4 mM [U-<sup>13</sup>C]-proline before analysis of the exometabolome by <sup>1</sup>H-NMR spectrometry. The amounts of end products excreted from the metabolism of  $\alpha$ -ketoglutarate and proline are expressed as nmoles excreted/h/10<sup>8</sup> cells.

### 3.4. Supplementary results

This section contains additional information that will not be part of the manuscript in preparation.

We have shown that PCF trypanosomes excrete 2-hydroxyglutarate from proline metabolism, in addition to the high amounts excreted from  $\alpha$ -ketoglutarate metabolism (Figure 3.58 and Table 3.8). We wondered if a putative annotated *2HGDH* gene (Tb927.10.9360) coding for a 2-hydroxyglutarate dehydrogenase was responsible for the production of 2-hydroxyglutarate. To analyse the function of this HGDH, we replaced both HGDH alleles by blasticidin and puromycin resistant cassettes to produce the null mutant  $\Delta hgdh$  (Figure 3.63A).  $^1\text{H}$ -NMR spectrometry analyses were performed with parental and  $\Delta hgdh$  cells incubated with proline and  $\alpha$ -ketoglutarate. No difference was observed in the production of 2-hydroxyglutarate (Figure 3.63B), indicating that this HGDH is not responsible for production of the excreted 2-hydroxyglutarate, and that other enzymes might be involved (see discussion). Actually, HGDH has been described to perform the reverse reaction in other model organisms, i.e. production of  $\alpha$ -ketoglutarate from 2-hydroxyglutarate (Engqvist et al., 2014). Our data are consistent with the same role of HGDH in *T. brucei*.

Another remaining question is related to the production of glutamate from  $\alpha$ -ketoglutarate observed in the alanine aminotransferase mutant ( $RNAiAAT$ ). To test the hypothesis that NADH-dependent glutamate dehydrogenase (GluDH) could be the alternative enzyme involved in glutamate production, we generated  $RNAiGluDH$  cell lines. Since no antibodies were available to test down-regulation of GluDH expression, we measured GluDH enzymatic activity in total cell extracts from parental and three clones induced (.i) or not (.ni) with tetracycline (Figure 3.64). Unfortunately, significant GluDH activity was still detected after five days of induction, indicating that the RNAi was not efficient to continue the analysis by  $^1\text{H}$ -NMR spectrometry.

Finally, we showed that malate is toxic for the  $\Delta aco$  cell line. Growth of this cell line was stimulated by succinate,  $\alpha$ -ketoglutarate and proline in the absence of glucose. (Figure 3.65). However, addition of less than 1 mM malate had a strong negative effect on its growth, as confirmed by the death of the  $\Delta aco$  mutant 5 days after the addition of 10 mM malate (Figure 3.65B). These data strongly suggest that accumulation of citrate, the substrate of aconitase, is responsible for the death of the  $\Delta aco$  mutant when the flux in this branch of the TCA cycle is increased in the presence of malate.

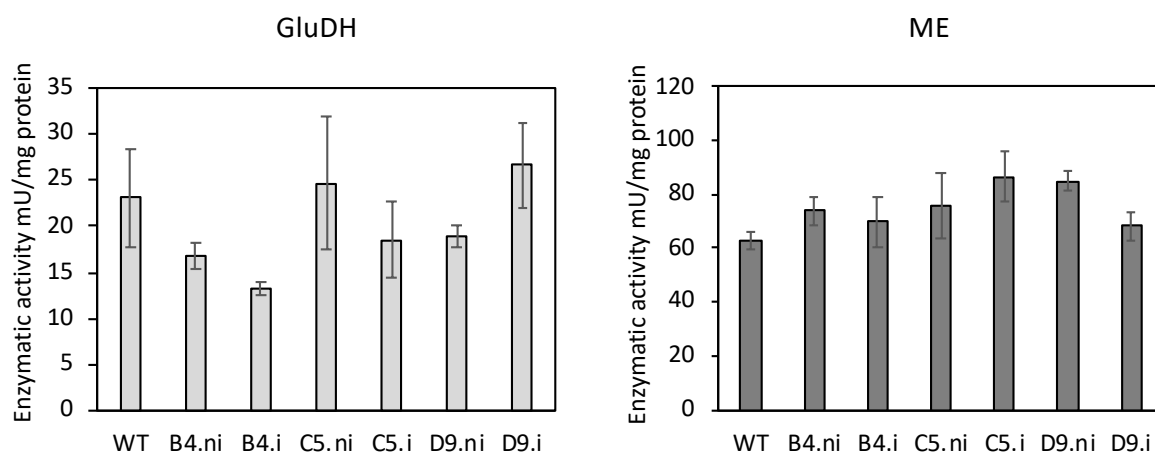


**Figure 3.64. Analysis of *RNAi* GluDH cell lines.**

Procyclic EATRO1125.T7T cells were transfected with the pLew-GluDH-SAS plasmid to generate the *RNAi* GluDH cell line. Down-regulation of glutamate dehydrogenase (GluDH) expression in three clones (B4, C5 and D9) was evaluated by enzymatic activity assays. Malic enzyme (ME) activity was determined as control.

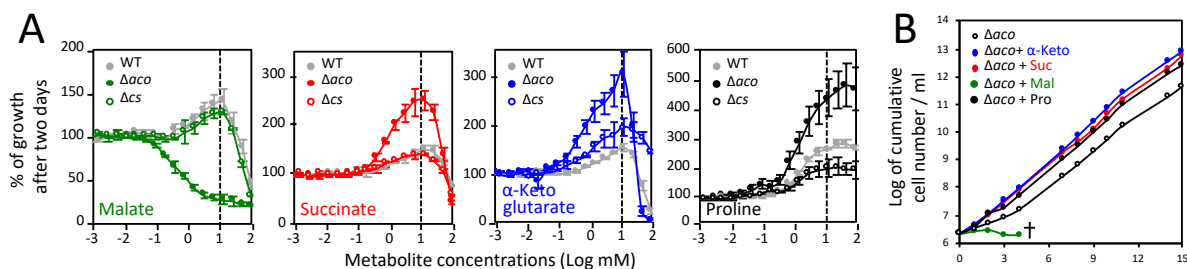


**Figure 3.65. Malate is toxic for the  $\Delta$ aco cell line.**

Panel A compares the effect of 10 mM succinate, malate,  $\alpha$ -ketoglutarate, or proline on growth of the parental,  $\Delta$ aco and  $\Delta$ cs cell lines incubated in glucose-depleted medium containing 2 mM proline, using the Alamar Blue assay. Growth curves of the  $\Delta$ aco cell line incubated in the same glucose-depleted medium, in the presence (coloured circles) or absence (open circles) of 10 mM malate (Mal), succinate (Suc),  $\alpha$ -ketoglutarate ( $\alpha$ -Keto) or proline (Pro) are shown in panel B.

To exclude toxicity of oxaloacetate, acetyl-CoA or one of their metabolic products, the same experiment was conducted on the citrate synthase null mutant ( $\Delta cs$ ), the enzyme that catalyses production of citrate from oxaloacetate and acetyl-CoA. The  $\Delta cs$  behaves like the parental cells, with no effect of malate on its growth, which confirms that accumulation of citrate or one of its metabolic products is toxic for the PCF trypanosomes. These data are in agreement with the relatively high metabolic flux in the TCA cycle in the presence of malate.

### 3.5. Discussion

Procyclic trypanosomes have developed a central metabolic network adapted to the metabolism of glucose and proline (Ryley, 1962; Obungu et al., 1999; Bringaud et al., 2006). Here we showed that the parasite efficiently metabolises a number of other carbon sources, including pyruvate, alanine and the TCA cycle intermediates succinate, malate and  $\alpha$ -ketoglutarate. Several reports previously described the ability of African trypanosomes to consume and metabolise TCA cycle intermediates. For instance,  $\alpha$ -ketoglutarate has been described to stimulate respiration and to sustain mobility of the stumpy forms of *T. brucei*, which are a growth-arrested transition form found in the bloodstream that are pre-adapted to differentiation into PCF (Vickerman, 1965; Flynn and Bowman, 1973; Bienen et al., 1993; Dewar et al., 2018).

In the sixties, Riley showed that TCA cycle intermediates, including  $\alpha$ -ketoglutarate, succinate, malate and fumarate, stimulate oxygen consumption of *T. brucei rhodesiense* culture forms (PCF) (Ryley, 1962). However, the metabolism of these TCA cycle intermediates by PCF trypanosomes has not been investigated so far in the context of the insect-like environment, that is to say in the absence of glucose but with proline present in the low millimolar range (1-2 mM), as described for the midgut of the tsetse fly (Balogun, 1974).

Here we showed that in the presence of 2 mM proline, consumption and metabolism of succinate, malate and  $\alpha$ -ketoglutarate take place. More importantly, addition of 1-10 mM of any one of these three TCA cycle intermediates stimulates growth of the parasite and rescues growth of the parasite in the presence of 2 mM and 0.2 mM proline, respectively.

We took advantage of the unexpectedly high mitochondrial metabolic capacity developed by the PCF trypanosomes in the presence of  $\alpha$ -ketoglutarate, succinate or malate to carry out a detailed analysis of the TCA cycle and its branched pathways. This allowed us to show (i) the high metabolic capacity of the malate/ $\alpha$ -ketoglutarate branch of the TCA cycle, (ii) the toxicity of  $\alpha$ -ketoglutarate intracellular accumulation and (iii) the production of hydroxyglutarate from metabolism of  $\alpha$ -ketoglutarate and proline.



(i) Van Weelden et al. previously demonstrated that the PCF trypanosomes cultured in rich medium do not need to oxidise glucose *via* a complete TCA cycle fed with glucose-derived acetyl-CoA (van Weelden et al., 2003). They showed that the growth rate of the  $\Delta$ aco and parental cell lines was identical in the standard glucose-rich medium and, more importantly, the malate/ $\alpha$ -ketoglutarate branch of the TCA cycle (steps 11-14 in (Figure 3.51A) showed no significant activity in PCF trypanosomes, as measured by [ $^{14}$ C]-CO<sub>2</sub> release from labelled glucose. However, these data do not exclude a functional malate/ $\alpha$ -ketoglutarate branch, which is used under specific nutritional conditions or in particular developmental stages, and the sensitivity of the used assay was limited.

Here we have demonstrated the functionality of this metabolic branch by forcing the parasite to use it in the presence of 10 mM malate and 2 mM proline. In these conditions, malate is converted to succinate *via* both the reducing (steps 9-10 in Figure 3.51C) and oxidative (steps 11-14 and 5-6) branches of the TCA cycle. Indeed, fumarate production from malate is abolished in the *RNAi*FHc/m.i mutant (step 10), while succinate production from malate is little affected, and succinate production is only reduced by 1.8-fold in the *RNAi*FRDg/m.i mutant (step 9).

These data can only be explained by a significant metabolic flux through the malate/ $\alpha$ -ketoglutarate branch of the TCA cycle fed with extracellular malate. Since this branch of the TCA cycle does not seem to be important in standard culture conditions in the wild type PCF trypanosomes (van Weelden et al., 2003), its main function in the procyclic trypanosomes could be the production of citrate and/or isocitrate to supply other metabolic pathways. This hypothesis is consistent with the glycosomal localisation of the IDHg isoform, which requires isocitrate for NADH and/or NADPH production within the organelle (Wang et al., 2017).

However, as opposed to most eukaryotes, trypanosomes do not use TCA-cycle derived citrate to produce the precursor of *de novo* fatty acid biosynthesis, acetyl-CoA, in the cytosol. The parasites lack the key enzyme of this pathway, i.e. cytosolic acetyl-CoA lyase, and instead use the cytosolic AMP-dependent acetyl-CoA synthetase to produce acetyl-CoA from acetate (Rivière et al., 2009).

Interestingly, Doleželová and colleagues recently took advantage of an *in vitro* differentiation assay based on the RNA-binding protein 6 (RBP6) over-expression to show that all the enzymes of the malate/ $\alpha$ -ketoglutarate branch of the TCA cycle are

strongly over-expressed upon differentiation into the epimastigote forms of *T. brucei* (Doleželová et al., 2020). This suggests that this branch of TCA cycle and/or the full TCA cycle is required for epimastigotes and/or during differentiation of procyclics into epimastigotes.

(ii) Accumulation of the TCA cycle intermediate  $\alpha$ -ketoglutarate is toxic for PCF, while accumulation of succinate in the *RNAi*SDH.i mutant cultivated in the presence of 10 mM succinate is not toxic.  $\alpha$ -Ketoglutarate toxicity was deduced from the death of the  $\Delta kdh-e2$  and  $\Delta kdh-e2/RNAi$ IDHm.i mutants in the presence of  $\alpha$ -ketoglutarate, which is not efficiently metabolised in these mutants compared to the parental cell line.

$\alpha$ -Ketoglutarate is a key metabolite at the interface between metabolism of carbon and nitrogen (Forchhammer and Selim, 2020), which has recently emerged as a master regulator metabolite in several organisms including bacteria, yeast, plant and animal species (Huergo and Dixon, 2015). Consequently, intracellular accumulation of large amounts of  $\alpha$ -ketoglutarate could affect several essential pathways, by mechanisms that are currently unknown.

(iii) 2-Hydroxyglutarate is a five-carbon dicarboxylic acid occurring naturally in animals, plants, yeasts and bacteria. It has recently been described as an epigenetic modifier that governs T cell differentiation and plays a role in cancer initiation and progression (Engqvist et al., 2014; Ryan et al., 2019). This metabolite was also detected in the metabolome of BSF trypanosomes, being derived from the metabolism of glutamate (Johnston et al., 2019).

Here we showed that 2-hydroxyglutarate represents 37% of the total end products excreted by PCF from catabolism of  $\alpha$ -ketoglutarate. The excretion rate of 2-hydroxyglutarate is 3.4 times higher than that corresponding to all end products from glucose metabolism (6.77 *versus* 2.02  $\mu$ mole/h/mg of protein). This highlights the high capacity of the enzyme responsible for reduction of  $\alpha$ -ketoglutarate to 2-hydroxyglutarate. This reaction probably results from the promiscuous action of malate dehydrogenase on  $\alpha$ -ketoglutarate, as previously described in mammalian cells (Rzem et al., 2007; Intlekofer et al., 2017).

Importantly, the NADH-consuming reaction leading to production of 2-hydroxyglutarate compensates for the NADH-producing reactions involved in the production of other end products excreted from  $\alpha$ -ketoglutarate metabolism and may explain the very high  $\alpha$ -ketoglutarate metabolic flux.

Therefore, maintenance of the mitochondrial redox balance required for  $\alpha$ -ketoglutarate metabolism is performed by fast-acting substrate level reactions, with little or no involvement of the respiratory chain activity, which operates at a lower speed compared to substrate level reactions.

Most cells express 2-hydroxyglutarate dehydrogenase enzymes (2HGDH), which irreversibly catalyse the reverse oxidative reaction in order to prevent the loss of carbon moieties from the TCA cycle and would protect from the accumulation of 2-hydroxyglutarate (Engqvist et al., 2014). The *T. brucei* genome contains a putatively annotated *2HGDH* gene (Tb927.10.9360), however since 2-hydroxyglutarate is produced in high quantities in PCF organisms it is uncertain if it has this activity in these cells.

Trypanosomatids convert carbon sources to partially oxidised end products that are excreted into the environment (Bringaud et al., 2006). Some of these metabolites constitute good alternative carbon sources for the parasite, as exemplified by efficient metabolism of alanine by *T. cruzi*, while this amino acid is also excreted from glucose breakdown (Girard et al., 2018).

We show that end products excreted from the metabolism of glucose by PCF trypanosomes, such as succinate, alanine and pyruvate, are re-consumed after glucose has been used up.  $^{13}\text{C}$ -enriched succinate and alanine excreted from catabolism of  $[\text{U-}^{13}\text{C}]$ -glucose are re-consumed and converted to  $^{13}\text{C}$ -enriched acetate after glucose depletion. This phenomenon resembles the “acetate switch” described in prokaryotes, in which abundant or preferred nutrients, such as glucose, are first fermented to acetate, followed by the import and utilisation of that excreted acetate to enhance survival of the cells (Wolfe, 2005). This “acetate switch” occurs when cells deplete their environment of acetate-producing carbon sources.

We previously described that PCF trypanosomes cultivated in rich conditions use ~5 times more glucose than proline to feed their central carbon metabolism, and switch to proline metabolism in the absence of glucose by increasing its rate of consumption up to 5 fold (Lamour et al., 2005; Coustou et al., 2008).

Glucose is first fermented to excreted acetate, succinate, alanine and pyruvate before switching to proline that is primarily metabolised in the mitochondrion with an increased contribution of the respiratory chain activity. Here we showed that this “proline switch” is accompanied by the re-utilisation and conversion of glucose-derived

end products (succinate, pyruvate and alanine) to acetate.

As opposed to bacteria or yeasts, however, acetate does not feed carbon metabolism of PCF and is the ultimate excreted end product from the breakdown of the different carbon sources, including succinate and alanine. The ratio between the two main excreted end products from glucose metabolism (acetate/succinate) has been reported to be between 0.3 and 4 in different studies (van Weelden et al., 2003; Coustou et al., 2006), which has been interpreted to reflect a high flexibility of flux distribution between the acetate and succinate branches of the metabolic network (Ghozlane et al., 2012; Bringaud et al., 2015). In light of our observations, however, it appears that the conversion of excreted glucose-derived succinate to excreted acetate, following uptake and further metabolism of succinate, provides an alternative explanation for these heterogeneous data.

In conclusion, metabolism of  $\alpha$ -ketoglutarate, succinate or malate stimulates growth of the procyclic trypanosomes by supplementing proline, the main carbon source used by the parasite in the tsetse. The parasite may take advantage of this peculiarity to complete its parasitic cycle *in vivo*. Incidentally, it has recently been shown *in vitro* that differentiation of procyclics to epimastigotes and/or the growth of the latter require an increased consumption of carbon sources, probably to meet an increased energy demand (Doleželová et al., 2020). This higher energy demand may also be required in inhospitable organs of the fly or structures difficult to cross, such as the proventriculus. Indeed, the proventriculus is an active immune tissue of the insect that represents a hurdle to the spread of trypanosomes from the midgut to the salivary glands, since only a few trypanosomes can pass through it. Unfortunately, with the exception of amino acids (Balogun, 1974), the content of metabolites in the tsetse midgut, including the proventriculus, has not been studied so far. TCA cycle intermediates could be abundant where, for example, tsetse resident symbionts such as *Sodalis glossinidius* metabolise N-acetylglucosamine and glutamine to produce partially oxidised end products, which are released to the midgut lumen of the fly (Hall et al., 2019). These may then promote trypanosome development.

## 4. GENERAL DISCUSSION AND PERSPECTIVES

### 4.1. Overview Part I: UDP-glucose pyrophosphorylase (UGP)

Glycosomes contain metabolic pathways usually present in the cytosol of eukaryotes, such as glycolysis and biosynthesis of sugar nucleotides. Here we have shown that UGP, the enzyme responsible for synthesis of UDP-glucose, is localised in the cytosol and glycosomes of the bloodstream and procyclic trypanosomes, despite the absence of any consensus motif of a peroxisomal targeting signal (PTS1 and PTS2).

We described the first example of piggybacking in trypanosomatids, where UGP is imported into glycosomes by interacting with the glycosomal PTS1-containing phosphoenolpyruvate carboxykinase (PEPCK). In addition, we showed that UGP is essential for growth of trypanosomes and that both the glycosomal and cytosolic metabolic pathways involving UGP are functional.

### 4.2. *T. brucei* UGP features

We showed that UGP is responsible for UDP-glucose production since deletion of the unique *UGP* gene is lethal and this sugar nucleotide was not detected in the knock-down UGP mutant cell line (*<sup>RNAi</sup>UGP*) by targeted metabolomic analyses. Accordingly, no *USP* gene is present in the *T. brucei* genome, while it has been identified in *L. major* and *T. cruzi* where it uses a wide range of sugar-1-phosphates to produce UDP-sugars. Moreover, UDP-Gal is only produced by epimerisation of UDP-Glc in *T. brucei*, as mentioned before. Unfortunately, we were not able to detect UDP-Gal in any of the cell lines, due to methodological limitations in our metabolomics experiments. We assume that the *<sup>RNAi</sup>UGP.i* cell line must be depleted of UDP-galactose.

It is to note that, despite the ~30-fold reduction of UGP protein levels observed in non-induced *<sup>RNAi</sup>UGP* cells, UDP-Glc was detected at levels similar to parental cells. Additionally, no significant variation in UDP-Glc levels was evidenced in the *<sup>EXP</sup>rUGP.i* cell line, which strongly overexpressed rUGP (~30 fold). We concluded that an excess of UGP exists in PCF trypanosomes and that this enzyme does not represent a control point in the pathway.

Intriguingly, we detected lower levels of UGP specific activity in the glycosomal fractions than in the cytosolic fractions of the parental cells (4-fold difference) which suggests that the glycosomal sequestration of UGP affects its activity by a yet unknown mechanism.

How is the UGP activity generally regulated? UGPs from different organisms have been studied in detail, especially in plants where UDP-Glc is relevant for the formation of important cell wall polymers, such as cellulose, callose, and hemicellulose, in addition to the role in production of glycoconjugates (Decker and Kleczkowski, 2019). Several regulatory mechanisms of UGP activity have been described, including oligomerization, reversible redox mechanisms and post-translational modifications such as phosphorylation.

While human and yeast UGPs are active as octamers and the C-terminal residues involved in oligomerization are conserved, the enzyme is only active as monomer in plants and trypanosomatids. Interestingly, plant UGPs can also be found as dimers, however the two monomers interact in such a way that the active site is hindered and the activity is lost (McCoy et al., 2007). The activity of trypanosomatids UGPs is probably not regulated by oligomerization since *T. brucei* and *L. major* UGPs are monomeric and lack the C-terminal residues involved in oligomerization (Lamerz et al., 2006; Mariño et al., 2010).

Two types of UGP activity regulation by redox mechanisms have been reported in protists, which handle monomeric UGPs as well. The first one, described for *E. histolytica* and *G. lamblia*, depends on the reversible formation of an intrasubunit disulphide bond that (i) is formed in the presence of oxidants such as H<sub>2</sub>O<sub>2</sub>, (ii) inactivates the enzyme and (iii) can subsequently be reduced (e.g. by adding DTT) to recover the activity (Martínez et al., 2011; Ebrecht et al., 2015). The residues required for this redox inactivation are not conserved in *T. brucei* suggesting that the UGP activity is not regulated by this mechanism.

The second mechanism was described in *Euglena gracilis*. Although the enzymatic activity is also disrupted by oxidants and recovered by reducing agents, the cysteine residues present in this UGP are not close enough to form intra disulphide bonds as in the previous examples. Instead, the mechanism of redox inactivation involves alkylation or oxidation (to sulfenic acid derivatives) of five out of the seven cysteine residues present in the protein, which modulates enzyme activity and protein structure (Muchut et al., 2018). We cannot discard that some of the 10 cysteine residues present in *T. brucei* UGP could be involved in redox regulatory mechanisms similar to those observed in *E. gracilis*. This could be tested *in vitro* by enzymatic activity assays of recombinant purified enzyme in the presence of oxidant and reductive reagents.

Finally, phosphorylation plays a key role in regulation of UGP in yeast. In this case, the activity of the enzyme is not altered but the subcellular localisation determines whether UDP-Glc is used to make storage (cytosolic) or structural (plasma membrane) carbohydrates (Smith and Rutter, 2007). Although several candidate residues from *T. brucei* UGP are predicted *in silico* to be phosphorylated, the protein was not identified in a phosphoproteomic analysis performed in BSF and PCF trypanosomes (Urbaniak et al., 2013). Moreover, a recent proteomic analysis of several post-translational modifications (PTM) including acylations, phosphorylation, trimethylation, ubiquitination and glycosylation revealed that *T. brucei* UGP is not modified by any means (Wan et al., 2019). This same study also addressed proteins from the closely related African trypanosome *T. evansi*. It is noteworthy that *T. evansi* UGP is crotonylated in a lysine residue conserved in *T. brucei*. Confirmation of these results is needed as *T. brucei* UGP could also be modified (Zhang et al., 2020). Crotonylation is a PTM recently identified that has been mostly described as an histone mark, although it has been found in non-histone proteins. The role of crotonylation in modulating protein functions remains to be elucidated (Wan et al., 2019).

### **4.3. Functions of UDP-glucose**

As already mentioned, our data strongly supports the functionality of UGP in producing UDP-Glc inside *T. brucei* glycosomes. Since GalE is also a glycosomal protein, UDP-Gal would also be produced inside the organelle. UDP-Glc and UDP-Gal must certainly leave the glycosomes to reach the endoplasmic reticulum and the Golgi apparatus, where they are required for glycosylation reactions. This exchange of sugar nucleotides between glycosomes and cytosol implies the existence of transporters in the glycosomal membrane, which remain to be identified and characterised. Could the UDP-Glc produced inside glycosomes be directly channelled to the ER thanks to contacts between the two organelles, which may be an alternative to the transporter hypothesis?

As previously discussed, the ER is important for peroxisome biogenesis and physical contact sites between peroxisomes and the ER have been recently identified in yeast and human cells (Schuldiner and Zalckvar, 2017). In yeast, this contact depends on the PEX3 protein present in both compartments being held together by another protein, the peroxisome inheritance factor Inp1p (Knoblauch et al., 2013).

In human cells, it was recently shown that the peroxisomal ACBD5 protein and the VAPA/B ER proteins form a tether complex that maintain the peroxisome-ER contacts (Costello et al., 2017; Hua et al., 2017). In this last case, the FFAT motif of the ACBD5 protein interacts with the MSP domain of the VAP proteins. For instance, PEX3 was recently identified (Banerjee et al., 2019; Kalel et al., 2019) and orthologues of VAPB can be found in the *T. brucei* genome, which is not the case for Inp1p and ACBD5 proteins. If contacts between ER and glycosomes are maintained by similar protein interactions in *T. brucei* cells must still be determined.

Two examples of UDP-Glc channelling have been previously described. A membrane-bound UGP was proven to couple UDP-Glc synthesis and transport into Golgi vesicles prepared from mammalian cells (Persat et al., 1984). In yeast, the already mentioned phosphorylated UGP that is targeted to the cell periphery produces UDP-Glc that might be directly channelled to enzymes involved in cell wall synthesis (Smith and Rutter, 2007).

Alternatively, glycosomal UDP-Glc could have a signalling role, as previously observed in animals and more recently proposed in plants. UDP-Glc receptors of the G protein-coupled group have been identified in mammalian cells, where they can activate several downstream signalling cascades in response to stress conditions (Chambers et al., 2000; Harden et al., 2010). In plants, no receptor has been associated with UDP-Glc although G-protein-receptor candidates have been identified and several data support the role of this sugar nucleotide as a signalling molecule (Janse van Rensburg and Van den Ende, 2018). In this sense, it would be interesting to assess the potential of UDP-Glc as a signalling molecule in trypanosomatids as well.

One might ask if the entire pool of these sugar nucleotides is exchanged between the glycosomal and cytosolic compartments, or if they might have also functions inside the organelle. Glycosyltransferases would be required for glycosylation reactions to occur inside glycosomes. However, proteomic and *in silico* analyses have not identified any glycosomal glycosyltransferase candidate, suggesting that glycosylation reactions do not occur inside the organelle.



#### **4.4. The UGP-PEPCK interaction, a new way to study import of glycosomal proteins**

Here we showed that UGP is imported into glycosomes by piggybacking on the glycosomal PTS1-containing phosphoenolpyruvate carboxykinase (PEPCK). Here, the failure of co-immunoprecipitation and native gels techniques even in the presence of crosslinkers are suggestive of weak and transient interactions between these two proteins. This conclusion is consistent with the observation that only ~10% of UGP is imported into the organelle, while PEPCK is in large excess compared to UGP. This indeed supports the idea that the interaction is transient and that efficiency of UGP import through piggybacking is not optimal in this context. Interestingly, diminution of 30-fold the amount of UGP in the non-induced RNAi cell line resulted in the same distribution between glycosomes and cytosol. Accordingly, BSF express 50-times less amounts of PEPCK and UGP and the distribution of UGP is similar in both compartments. It could be interesting to determine the minimal amounts of PEPCK required for import of UGP.

The proximal ligation assays (PLA) showed UGP/PEPCK interaction *in situ* for only 3-10% of the glycosomes. Considering the model of peroxisome multiplication by growth of membrane extensions, protein import and fission (Costello and Schrader, 2018), we hypothesised that these PLA-positive glycosomes are newly produced organelles importing matrix proteins. PLA signals were observed in very close proximity to PEPCK-containing glycosomes without showing clear co-localisation with them, suggesting that different pools of glycosomes with different import capacities exist within the cells, in agreement with the current knowledge of the peroxisome biology and the heterogeneity of the glycosome population (Gualdrón-Lopez et al., 2013b). To confirm our hypothesis, it is important to show co-localisation of the PLA signal with new-born glycosomes, which are considered to be competent for protein import. This could be done by using antibodies against PEX11, which is present in all glycosomes, including those newly produced by growth and division. Since, PLA is compatible with sample preparations for better resolution with confocal or super-resolution microscopy (Bedzhov and Stemmler, 2015; Chen et al., 2018), it would be interesting to determine in detail in which glycosomes the UGP/PEPCK interaction occurs, using the available glycosomal markers such as PEX11.

Could the disruption of glycosomal fission affect PLA signals? This can be tested by disrupting expression of key proteins involved in the fission of newly produced peroxisomes, like Fis1 and Dpl1 (Morgan et al., 2004; Chanez et al., 2006), which are expressed in trypanosomes (Niemann et al., 2013), in parallel with expression of tagged UGP/PEPCK to perform PLA assays. Since no additional antibiotic markers are available in our double tagged cell line (contains *HYG*, *NEO*, *BSD*, *PAC* and *BLE* resistance genes), the CRISPR-Cas9 technology already implemented in the Laboratory would solve this issue.

To go further in the UGP/PEPCK interaction studies, we started in collaboration with Dr. D. Inaoka to express and purify PEPCK and UGP from *E. coli*. Heterologous expression of soluble PEPCK has been successful and it is still ongoing for UGP. Future perspectives on this aspect would include *in vitro* analyses of interactions between recombinant PEPCK and UGP, determination of key residues involved in the interaction and ideally co-crystallization of both proteins.

#### **4.5. Is piggybacking a rule or an exception?**

There was no case of piggybacking described so far in trypanosomatids, although it has been proposed as an explanation to the presence of PTS-lacking proteins within glycosomes. The fact that PEPCK and UGP have no apparent functional relation broadens the possible combinations of carrier-cargo proteins being imported as hetero-oligomers which, was assumed to involve related proteins in the few cases described so far in yeast, mammals and plants (Islinger et al., 2009; Schueren et al., 2014; Effelsberg et al., 2015; Kataya et al., 2015).

In accordance with the methodology we used to identify the PEPCK/UGP association, a systematic analysis of knock-out or knock-down mutants lacking glycosomal proteins could demonstrate that other glycosomal proteins are also imported by piggybacking, since they are expected to disappear from glycosomes where their carrier is depleted. We performed proteomic analyses of enriched glycosomal fractions obtained from mutants in which expression of a glycosomal protein is affected, *i.e.*  $\Delta fbpase$  grown with glucose,  $\Delta fbpase$  grown with glycerol,  $\Delta idhg$ ,  $\Delta ppdk$ ,  $RNAiG6PDH$ ,  $RNAiGK$ ,  $RNAiPFK$  and  $RNAiGPDH$ . In these analyses, we did not observe any significant reduction of peptide counts for proteins other than those targeted by knock-down or knock-out. This very preliminary analysis leaves the question open.

#### 4.6. Overview Part II: Alternative carbon sources for PCF

Proline is essential for the midgut colonisation of *T. brucei* parasites in the insect vector (Mantilla et al., 2017), however other carbon sources could be available and used to feed its central metabolism. We demonstrate that procyclic trypanosomes can consume and metabolise metabolites excreted from glucose degradation (succinate, alanine and pyruvate) and TCA cycle intermediates (malate and  $\alpha$ -ketoglutarate in addition to succinate). These three last intermediates stimulate growth of the parasite in *in-vivo* like conditions (2 mM proline and absence of glucose) (Balogun, 1974). We also showed that the reducing and oxidative branches of the TCA cycle can be used to convert malate into succinate, and that  $\alpha$ -ketoglutarate is consumed at an incredibly high rate (15-times higher than glucose) thanks to the balanced production and consumption of NADH at the substrate level.

#### 4.7. PCF trypanosomes metabolise carbon sources other than glucose and proline

We show that *T. brucei* PCF trypanosomes metabolise succinate, malate and  $\alpha$ -ketoglutarate by using proton  $^1\text{H}$ -NMR analyses of the exometabolome. Curiously, these metabolites are better consumed in the presence of proline or glucose, with rates of consumption increased between 3 to 7 fold. This suggests that proline or glucose might provide the cells with additional metabolic intermediates and cofactors that would facilitate metabolism of succinate, malate and  $\alpha$ -ketoglutarate.

We also observed that  $\alpha$ -ketoglutarate is toxic when not metabolised, as observed in the null  $\Delta kdh$  mutant, probably because of its accumulation within the cells. Mass spectrometry analyses would be helpful to confirm  $\alpha$ -ketoglutarate accumulation and discern if other metabolites are also increased. As already mentioned, this accumulation of large amounts of  $\alpha$ -ketoglutarate could regulate several essential pathways and it would be interesting to study this hypothetical mechanisms of regulation (Huergo and Dixon, 2015).

Regarding citrate toxicity, the lethality of the  $\Delta aco$  mutant in the presence of 10 mM malate, while growth of the  $\Delta cs$  mutant is not affected by the addition of malate, is certainly the consequence of accumulation of malate-derived citrate. The observed reduction of growth of the parental PCF cells in glucose-rich medium containing 10 mM malate, can also be interpreted as the consequence of citrate accumulation from

the metabolism of malate. Indeed, in these growth conditions, PCF switched to a slight preference for malate metabolism with a 20% reduction of glucose metabolism, while consuming three-times more malate than glucose. The high metabolic flux within the malate/ $\alpha$ -ketoglutarate branch of the TCA cycle, in the presence of extracellular malate, certainly induced an accumulation of citrate that is sufficient to affect the parasite growth. The reason of citrate toxicity is, however, currently unknown.

It is also crucial to analyse in detail the metabolite content of different organs of naive and infected tsetse flies to finally define if these TCA cycle intermediates could play a role in the development of trypanosomes within the insect. NMR or mass spectrometry approaches could be used for metabolic profiling of tsetse fly organs.

#### **4.8. Unravelling new mitochondrial capabilities**

We have explored most of the metabolic reactions/pathways used for metabolism of succinate, malate and  $\alpha$ -ketoglutarate by combining  $^1\text{H}$ -NMR metabolic profiling and phenotypic analyses of mutants under mostly artificial conditions. This implies that we have used relatively high concentration of metabolites (4 mM for NMR analysis and 10 mM for growth curves) to demonstrate the functionality of different mitochondrial metabolic branches by forcing the system, which does not necessarily reflect the *in vivo* conditions. Thus, it is important to consider that our observations supporting a complete functional TCA cycle in trypanosomes might be debated, since real conditions where this might happen *in vivo* remain to be clarified. To further address this question, some of the null mutants produced, such as  $\Delta kdh-e2$ , should be used to challenge flies in order to investigate the role of the target gene *in vivo*.

#### **4.9. Role of metabolites in trypanosomes differentiation**

*T. brucei* differentiation from procyclics to epimastigotes and metacyclic trypomastigotes can be induced *in vitro* by overexpressing the RNA-binding protein RBP6, simulating the process occurring in the tsetse fly (Kolev et al., 2012).

A recent analysis describing the metabolic adaptations occurring during differentiation showed, among other changes, an increase in expression of genes involved in proline metabolism, such as proline transporters, enzymes involved in proline catabolism and some TCA cycle enzymes (Doleželová et al., 2020).

In light of these new data and considering that the proline concentration in the fly is in the range 1-2 mM (Balogun, 1974), we hypothesize that proline might be limiting for epimastigotes differentiation and development, which is compensated with the upregulation of proline metabolism. In this context, other carbon sources such as succinate, malate and  $\alpha$ -ketoglutarate could have an important role in supplementing proline to support energy metabolism of differentiating forms. We are currently testing this hypothesis by using the RBP6 system (Wagnies et al., 2018; Doleželová et al., 2020). If these metabolites are efficiently consumed by epimastigotes or if they could have a role in differentiation has yet to be determined. We will take advantage of the  $^1\text{H}$ -NMR profiling approach already developed for procyclic trypanosomes, in addition to immunofluorescence analysis using a surface marker (BARP) to study metabolism of epimastigotes. Our preliminary results suggest that  $\alpha$ -ketoglutarate stimulates growth of RBP6-induced differentiating forms incubated in the presence of 2 mM proline, suggesting that this metabolite is also consumed by epimastigotes.

## 5. MATERIALS AND METHODS

### 5.1. Materials

#### 5.1.1. Trypanosomes

The *T. brucei brucei* cell lines used in this work express constitutively the bacteriophage T7 RNA polymerase (T7RNAPol) and the tetracycline repressor (TetR). These TetR-HYG T7RNAPOL-NEO cells are maintained in the presence of both antibiotics hygromycin (HYG) and neomycin (NEO). Adding tetracycline allows the inducible expression of genes under the control of the T7 promoter.

The procyclic form of *T. brucei* EATRO1125.T7T strain was cultured at 27°C in SDM79 medium containing 10% (v/v) heat inactivated fetal calf serum (FCS) and 5 µg/ml hemin (Brun and Schönenberger, 1979) and in the presence of hygromycin (25 µg/ml) and neomycin (10 µg/ml). All mutant cell lines have initially been produced and cultivated in this standard SDM79 medium which contains 10 mM glucose and 5 mM proline.

Alternatively, the cells were cultivated in a glucose-depleted medium (SDM80) where glucose is not added and there is only glucose coming from serum, or a glucose-free medium (SDM79-GlcFree) where the glucose from the serum is consumed by cultivating the parasites during three days and then filtering the media. Both are derived from SDM79 and were additionally supplemented with 50 mM N-acetylglucosamine, a specific inhibitor of glucose transport that prevents consumption of residual glucose (Allmann et al., 2013; Wagnies et al., 2018).

The bloodstream form of *T. brucei* 427 90–13 strain was cultured at 37°C in IMDM supplemented with 10% (v/v) heat-inactivated fetal calf serum (FCS), 0.25 mM β-mercaptoethanol, 36 mM NaHCO<sub>3</sub>, 1 mM hypoxanthine, 0.16 mM thymidine, 1 mM sodium pyruvate, 0.05 mM bathocuprone and 2 mM L-cysteine (Hirumi and Hirumi, 1989).

#### 5.1.2. Plasmids and bacteria

pGEM®-T Vector Systems was used to clone PCR products for different purposes, like generating cassettes for production of *T. brucei* UGP null mutants.

The pLew100 plasmid (Wirtz et al., 1999) integrates into the spacer rRNA region of *T. brucei* genome and contains the bleomycin resistance gene (*ble*) for phleomycin selection of resistant parasites.

```

rUGP 1 10 20 30 40 50 60 70 80 90 100
UGP ATGCCGCTAA ACCCTCCTTC AGCCTTTTCA GGGGCAGCTT TGGCCTGCTT GGAAAAAATG CAGGCATCAG GTGTTGAGGA GAAGTGATTT CATATTTTCC
rUGP 110 120 130 140 150 160 170 180 190 200
UGP TCATCCAACA CGCTCTTGTG CGGAAAGGAG AAACCGGCTA TATACCCGAG AAGTCAATAT TTCCGGTGGA ATCTCTTCCC TTCCTTCAGG GTATCGAAAC
rUGP 210 220 230 240 250 260 270 280 290 300
UGP GAAGGGAGAA AACACTGCGT TACTGCGACA AGCGGTCGTT CTTAAACTCA ACGGCGGTCT TGGTACCGGG ATGGGGTTGA ACGGCCCCAA GAGCCTGCTA
rUGP 310 320 330 340 350 360 370 380 390 400
UGP CAGGTGAAGA ATGGCCAGAC GTTTCCTTGAC TTCACAGCCC TGCAGTTGGA GCATTTTCGT CAAGTGCGTA ACTGTAACTG GCCGTTTATG CTGATGAACT
rUGP 410 420 430 440 450 460 470 480 490 500
UGP CGTTTTCCAC ATCGGGAGAA ACTAAGAATT TTCTTCGGAA GTATCCTACC TTGTACGAGG TGTTCGACTC AGACATCGAA CTCATGCAAA ACAGAGTGCC
rUGP 510 520 530 540 550 560 570 580 590 600
UGP GAAATATAGC CAGGATAACT TTTTCCCGGT GACCTATGAA GCGATCCCAA CCTGTGAATG GGTCATGGCG ATCTTTAAAC CGTCTTATAA
rUGP 610 620 630 640 650 660 670 680 690 700
UGP AAGCATAGC CAGGATAACT TTTTCCCGGT GACCTATGAA GCGATCCCAA CCTGTGAATG GGTCATGGCG ATCTTTAAAC CGTCTTATAA
rUGP 710 720 730 740 750 760 770 780 790 800
UGP AATTAATGCA TGAGAAACAA CTGGGCTTCC TGATGGAAGT CTGTCGCGCA ACCGAATCAG ATAAGAAAGG TGGCCATTTA GCCTATAAAG ACGTATAGA
rUGP 810 820 830 840 850 860 870 880 890 900
UGP TGAATCAACA GGTGAGACCC GTCGTCGATT CGTACTACGG GATCTGCAAC AATGCCCTAA GAGGAGAGAA GACAGTTTCC AGAATATAGC CAATCAATGC
rUGP 910 920 930 940 950 960 970 980 990 1,000
UGP TTTTTCACAA CCAATTAATAT ATGGATCAAC CTGATGGAAT TAAATTAATAT GATGGATGAA CAATTTAGGTG TCTCTCGGCT ACCCTGCTATG CGTAAATCCGA
rUGP 1,010 1,020 1,030 1,040 1,050 1,060 1,070 1,080 1,090 1,100
UGP AATACGTTCAA CCCGAGGAC AGTCAATCAA CGAAGGTGTA CCAGCTGAGG GTGGCGATGG GTGCCGCAAT TTCTCTATTT GATAGATCGG AAGCAGTAGT
rUGP 1,110 1,120 1,130 1,140 1,150 1,160 1,170 1,180 1,190 1,200
UGP GGTTCACAGG GAGCGTTTG CACCTGTGAA GACTTGCACT GATCTACTTG CGTTAAGGTC TGATGCGTAT CAGGTGACGG AGGATCAGCG TCTTGTTCTG
rUGP 1,210 1,220 1,230 1,240 1,250 1,260 1,270 1,280 1,290 1,300
UGP TGTGAGGAGC GAAATGGAAA GCCACCAGCT ATTGATCTTG ACGGTGAGCA TTACAAGATG ATTGACGGAT TCGAAAAGCT AGTGAAGGGA GGAGTGCCAT
rUGP 1,310 1,320 1,330 1,340 1,350 1,360 1,370 1,380 1,390 1,400
UGP CCTTGCGACA ATGCACATCA CTTACCGTCC GTGGATTGGT GGAATTTGGT CCGGACGTTT CCGTTAGAGG GAAATGTGGT ATTAATAAAT TGAAGGAAGA
rUGP 1,410 1,420 1,430 1,440 1,450 1,458
UGP GCCTCTGATC ATTTGGGAAC GACGCGTTCT TGACAAATGAG GTTGTTGGTAG TCGAGTAG
UGP GCCTCTGATC ATTTGGGAAC GACGCGTTCT TGACAAATGAG GTTGTTGGTAG TCGAGTAG

```

**Figure 5.66.** Sequence alignment of the recoded *rUGP* sequence (*rUGP*) and native *UGP*.

The residues modified to change the coding sequence without affecting the coded amino acid residue are shaded. For cloning purposes, the last nucleotide of a HindIII restriction site at position 1276 was modified (shaded T in *UGP* and A in *rUGP*).

The DNA fragment of interest is inserted downstream the T7 promoter followed by the tetracycline operator (TetO) allowing transcription in the presence of tetracycline. The plasmid is linearised with the NotI restriction enzyme, which cuts in the middle of the rDNA spacer region, therefore it integrates by homologous recombination downstream the ribosomal gene locus. This plasmid was extensively used for production of knock-down (RNAi) mutants and for overexpression of recombinant or tagged proteins. Two previously modified versions, pLew100-X-MYC and pLew100-eGFPX, were used to produce MYC and GFP tagged proteins.

The pHD1336 plasmid (Yernaux et al., 2006) also integrates into the spacer rRNA region and contains the blasticidin-S-deaminase resistance gene (*bsd*) for blasticidin selection of resistant parasites. This plasmid was used for expression of recombinant UGP. A synthetic plasmid containing a recoded version was used for targeting UGP to glycosomes. The sequence of the recoded *UGP* is shown in Figure 5.66.

The pPOTv7-BLAST-10xTY1 plasmid was used as backbone for PCR amplification using long primers designed according to Dean et al. (2015), in order to produce endogenously 10xTy1 tagged proteins. The bacteria *E. coli* XL1-blue and Stellar™ were used for cloning, amplification and long-term storage of plasmids.

## **5.2. Methods**

### **5.2.1. Molecular biology**

#### **a) Cloning and sequencing**

For restriction enzyme dependent cloning, PCR product and plasmid were digested with the same restriction enzymes before incubation with the bacteriophage T4 Ligase overnight at 4°C. The mix was then used to transform XL1-blue bacteria.

For In-Fusion® HD Cloning (Clontech), the DNA sequence of interest was amplified by PCR using primers with 15 bp overhangs complementary to the vector ends once linearised with restriction enzymes. The insert and plasmid were purified and mixed in 3:1 ratio with the 1x In-Fusion® Enzyme Premix containing recombinase. After incubation for 15 min at 50°C and cooled down on ice, the mix was used to transform Stellar bacteria.

The AQUA Cloning method is similar to In-Fusion, except that insert and vector are incubated in pure water for 5 min at room temperature (RT) before being used for transformation of bacteria. In this case, the recombination occurs inside the bacteria,



	Position	Primer name	Sequence 5'-3'	RE	Plasmid/ PCR product	Comments
PEPCK Tb927.2.4210		Fw pPEPCKex1-5	GCCCAAT <b>GATATC</b> ACAATGGCTCCTATAATTCACAA	EcoRV	pLew100	Rescue $\Delta pepck$
		Rv pPEPCKex1-3	CACGCC <b>GGATCCC</b> CTAACATATTAAAGACGCGAAGC	BamHI		
	418	Fw pgfpPEPCKtc1-5	GCTGTACAAG <b>GCTCGAG</b> ACAATGGACTATGTCATCTACAA CG	XhoI	pLew100	Expression GFP- PEPCK 140-525
	538	Fw GFP-PEPCK 180	GCTGTACAAG <b>GCTCGAG</b> GTCATT <b>ACGCGT</b> ACAATGTACGC TGGTGAAATGAAG	XhoI MluI	pLew100	Expression GFP- PEPCK 180-525
	640	Fw GFP-PEPCK 214	GCTGTACAAG <b>GCTCGAG</b> GCTAAC <b>ACGCGT</b> ACAATGGGTG ACGTGACGGTCTTC	XhoI MluI	pLew100	Expression GFP- PEPCK 214-525
	955	Fw pgfpPEPCKtc3-5	GCTGTACAAG <b>GCTCGAG</b> ACAATGCTTTCGAAGGCTGTTGC	XhoI	pLew100	Expression GFP- PEPCK 321-525
		Rv pgfpPEPCKex1-3	ATTACCCGGT <b>TCTAGAC</b> CTAACATATTAAAGACGCGAAG C	XbaI	pLew100	Expression GFP- PEPCK
		Fw FWPEPCK- TagNter	CTCTACAGCCGTCTTCAACAATTAACATTTTACGTTCTTAT ACTTATATATTTGTTGTATTGCCCAATCATAACACAgta taatgcagacctgctgc		PCR product	N-terminal tag
		Rv RvPEPCK- TagNter	GTCAGTTGGGAGTCCTTTTCAAGCTTAAGAGCCCACTCC ACCAACTCGGGGCGGTGAGATTCTTGTGAATTATAGGA GCactaccgatcctgatcc			

**Table 5.9. PCR primers sequences and features concerning PEPCK mutant cell lines.**

Restriction enzyme recognition sites are highlighted.

thanks to its own machinery (Beyer et al., 2015). Both methods were used as alternatives for restriction enzyme dependent cloning.

The plasmids were finally sequenced to ensure the cloning was accurate. 1.5 µl of plasmid (100 ng/ml) were mixed with 2 µl of one primer (2 µM) for the sequencing reaction using ABI BigDye Terminator Kit v3.1 for Ready to Load service (Eurofins, genomics). Alternatively, 15 µl of plasmid were mixed with 2 µl of one primer (10 µM) and sent with SmartSeq Kit (Eurofins, genomics). All the primer sequences and plasmids are summarised in Table 5.9 and Table 5.10.

## **b) DNA purification**

### **- Plasmid DNA**

The rapid boiling method was used for small scale preparations of plasmids (2 ml of bacterial culture) for analysis by restriction enzyme digestion, sequencing or subsequent cloning. For transfection of trypanosomes, plasmid DNA was purified using the NucleoSpin Plasmid Mini kit (Macherey-Nagel) from 10 ml of bacterial culture.

### **- Genomic DNA**

For analysis of *T. brucei* mutants,  $2 \times 10^7$  cells were resuspended in 150 µl of TELT buffer (50 mM Tris-HCl pH: 8, 62.5 mM EDTA, 2.5M LiCl, 4% Triton X-100) and incubated 5 min at RT. Then, 150 µl of Phenol: Chloroform 1:1 were added to the suspension, mixed by inversion and incubated 5min. After centrifugation for 5 min at 13,000 g, the upper aqueous phase (DNA) was recovered in a new tube. gDNA was precipitated by adding 300 µl of 100% ethanol and inverting the tube for 15 sec. After 10 min centrifugation at 13,000 g, the pellet was washed with 1 ml of ethanol. Finally, precipitated DNA was dried, resuspended in deionised water (dH<sub>2</sub>O), quantified and used for PCR analysis.

## **5.2.2. Cell biology**

### **a) Growth of *T. brucei*: curves and Alamar blue assays**

The growth was followed by counting the cells daily with a Guava EasyCyte™ cytometer. The cells were then diluted and maintained at a density of  $2 \times 10^6$  cells/ml. The log of cumulative cells number by ml was plotted against time (in days). When differences in the slope were observed, the doubling time in hours was calculated.

P	Primer name	Sequence 5'-3'	RE	Plasmid/ PCR product	Comments
UGP Tb927.10.13130	Fw FwUGP3xMYC	TAAATTTCACAAAGCTTACAATGCCGCTAAACCCCTCTTC	HindIII	pLew100	Expression [ <sup>EXP</sup> UGP-MYC, $\Delta pepck$ / <sup>EXP</sup> UGP-MYC, <sup>EXP</sup> TY-PEPCK/ <sup>EXP</sup> UGP-MYC, $\Delta pepck$ / <sup>EXP</sup> TY-PEPCK/ <sup>EXP</sup> UGP-MYC]
	Rv RvUGP3xMYC	CGATCGGCCGCCATATGCTCGACTACCACAACCTCATT	NdeI		
	Fw TagNUGPFw	CAGAACGAACAGAAAAATACGCAAGCTCATAAGATCAGATACCTCGGAACGGTGTCAGTGTGTGCTGTGTGTGCACAGAgataatgcagactgtctgc		PCR Product	N-terminal tag [ <sup>EXP</sup> TY-UGP <sub>1-485</sub> ]
	Rv TagNUGPRv	TCCTCAACACCTGATGCCCTGCATTTTTTCCAAGCAGGCCAAAGCTGCCCTGAAAAGGCTGAAGGAGGGTTTACGGGCATactaccgatcctgatcc			
	Fw TagCUGPFw	TGGTTATTAATAATTTGAAGGAAGAGCCTCTGATCATTGGGAACGGACGCGTTCTTGACAATGAGGTTGTGGTAGTCGAGgggtctgtagtggttc		PCR Product	C-terminal tag [ <sup>EXP</sup> UGP <sub>1-485</sub> -TY]
	198 Fw UGP E66	TCCGGAAGGAGAAACCGGCTATATACCCGAGAAGTCAATATTTCCGGTGGAATCTCTTCCCTTCCCTCAGGGTATCGAAGgttctgtagtggttc		PCR Product	C-terminal tag – truncation 1-66 [ <sup>EXP</sup> UGP <sub>1-66</sub> -TY]
	372 Fw N124	GCCTGCTACAGGTGAAGAATGCCAGACGTTTCTTGACTTCACAGCCC TGACGTTGGAGCATTTTCGTCAAGTGCCTAACgggttctgtagtggttc		PCR Product	C-terminal tag – truncation 1-124 [ <sup>EXP</sup> UGP <sub>1-124</sub> -TY]
	519 Fw N173	AGTATCTACCTTGACGAGGTGTTTGACTCAGACATCGAACTCATGC AAAACAGAGTGCCCAAGATAAGGCAAGACAATgggttctgtagtggttc		PCR Product	C-terminal tag – truncation 1-173 [ <sup>EXP</sup> UGP <sub>1-173</sub> -TY]
	678 Fw A226	ACAGTAGTGGTAAGTTGGATTACCTGTTGGGCAAGGCTACCGCTACA TGTTTATATCAACCGAGACAACCTTTGGCGCGgggttctgtagtggttc		PCR Product	C-terminal tag – truncation 1-226 [ <sup>EXP</sup> UGP <sub>1-226</sub> -TY]
	Rv TagCUGPRv	TGCAAGTACTTGTGTGTACCACTTTCTAACCTCCCCCTTTTCTC TTTAGATGTGACAGGTAAAGCTGTTTATCAcctaattgagagacctgtgc		PCR product	C-terminal tag [ <sup>EXP</sup> UGP <sub>1-XXX</sub> -TY]
	Fw FwUGP-66-OL	CAGAACGAACAGAAAAATACGCAAGCTCATAAGATCAGATACCTCGGAACGGTGTCAGTGTGTGCTGTTGTGTGCACAGCAATGACGAAGGGAGAA AACACTGCG			Construction of plasmid pGEM®-T Easy-UGP-66-TY by Overlapping PCR
	Rv RvUGP-66-OL	ACCGGAACCACTACCAGAACCCTCGACTACCACAACCTCATTGTC			
	Fw FwUGPcTag-OL	GACAATGAGGTTGTGGTAGTCGAGGGTCTCGTAGTGTGTTCCGGT			
	Rv TagCUGPRv	TTCAGTACTTGTGTGTACCACTTTCTAACCTCCCCCTTTTCTC TTTAGATGTGACAGGTAAAGCTGTTTATCAcctaattgagagacctgtgc			
	Fw FwUGPprecComp OL	CCATGGCGCGCCGCGCAGAACGAACAGAAAAATACGCAAGCTCATAA GATCAGATACCTCGGAACGGTGTGCTGTTGTGTGCACACGA ATGCCGCTAAACCCCTCCTTCAGCC	SacII	pGEM®-T Easy	C-terminal tag 1-485 (Cloning rUGP in pGEM®-T Easy-UGP-66-TY) [ <sup>EXP</sup> UGP <sub>1-485</sub> -TY]
	198 Fw FwUGPprec66OL	CCATGGCGCGCCGCGCAGAACGAACAGAAAAATACGCAAGCTCATAA GATCAGATACCTCGGAACGGTGTGCTGTTGTGTGCACACGA ATGACGAAGGGAGAAACACTGCG	SacII	pGEM®-T Easy	C-terminal tag 66-485 (Cloning rUGP-66 in pGEM®-T Easy-UGP-66-TY) [ <sup>EXP</sup> rUGP <sub>66-485</sub> -TY]
	372 Fw FwUGP124OL	CCATGGCGCGCCGCGCAGAACGAACAGAAAAATACGCAAGCTCATAA GATCAGATACCTCGGAACGGTGTGCTGTTGTGTGCACACGA ATGTGTAACGTGCCGTTTATGCTG	SacII	pGEM®-T Easy	C-terminal tag 124-458 (Cloning rUGP-124 in pGEM®-T Easy-UGP-66-TY) [ <sup>EXP</sup> rUGP <sub>124-485</sub> -TY]
	Rv RvUGPprec66OL	TTGTGTGTACCTCAAGCTTAGAACCGGAACCGGAACCACTACCAGAAC CCTCGACTACCACAACCTCATTGTG	HindIII	pGEM®-T Easy	C-terminal tag rUGP [ <sup>EXP</sup> rUGP <sub>XXX-485</sub> -TY]
	Fw UGPo5'5'	ACATGAAGAATGGGAAGATATTGATG*			Confirm <i>in situ</i> tagging and $\Delta ugp$ 5'UTR (*)
	Rv UGPo5'3'	CGAGTTTCATCAGCATAAACGG*			
	Rv rUGPo5'3'	CCATTAGAAATGAACATATACC			
	Fw rUGPTYoFw	GTCATGCGTAATCCGAAAACC			Confirm <i>in situ</i> tagging
	Rv rUGPTYoRv	CGTACACAGCGGCATAGATTG			
	Fw pUGP-S5	GCAAAAAAGCTTGCCCAAGATAAGGCAAGACAATT	HindIII	pLew100	Cassette sense RNAi [ <sup>RNAi</sup> UGP-H10, <sup>RNAi</sup> UGP-E4, <sup>RNAi</sup> UGP/ <sup>EXP</sup> rUGP-GPDH]
	Rv pUGP-S3	CTGTCCCTCGAGTTCACCGTCTTGGGGTTTCGCAT	XhoI		
	Fw pUGP-AS3	TGCGGCAAGCTTCGCCACCTCGAGCTGGTACACCTTCGTTGATTGAC	HindIII	pLew100	Cassette antisense RNAi [ <sup>RNAi</sup> UGP-H10, <sup>RNAi</sup> UGP-E4, <sup>RNAi</sup> UGP/ <sup>EXP</sup> rUGP-GPDH]
	Rv pUGP-AS5	AACAGAGGATCCAGATAAGGCAAGACAATTC	XhoI BamHI		
	Fw PUGP5UTR-5	GTGTGTCCATGGGTGAGTGTTAACGAACACACACTCACACACATA	NcoI HpaI	pGEM®-T	Cassette 5'UTR $\Delta ugp$ [ $\Delta ugp$ / <sup>EXP</sup> rUGP, $\Delta ugp$ / <sup>EXP</sup> rUGP-GPDH]
	Rv PUGP5UTR-3	AGGAGGCTCGAGCGGCATCTAGAACACACACAGCACACTGACA	XhoI XbaI		
	Fw PUGP3UTR-5	AATGAGTCTAGAGTAGTCAAGCTTGATAAAAACAGCTTACCTGTCAC	XbaI HindIII	pGEM®-T	Cassette 3'UTR $\Delta ugp$ [ $\Delta ugp$ / <sup>EXP</sup> rUGP, $\Delta ugp$ / <sup>EXP</sup> rUGP-GPDH]
	Rv PUGP3UTR-3	TGTTTTCTCGAGAAAGGTGTTAACAAACACACTGTTCCCAATT	XhoI HpaI		
	Fw UGPo3'5'	GGAAGCAGTAGTGGTTCCAAG			Confirm $\Delta ugp$ 3'UTR
	Rv UGPo3'3"	GCTGACTAACACAAACCATGTATC			

**Table 5.10. PCR primers sequences and features concerning UGP mutant cell lines.**

The Alamar Blue assay was used to study the effect of different metabolites on parasites growth. Resazurin, the compound used in this assay, is a redox indicator dye (blue) that is reduced to resorufin (pink) by metabolically active cells and is commonly used to determine cytotoxicity since there is a direct correlation between its reduction and the quantity of living cells (O'Brien et al., 2000).

To perform this experiment, PCF trypanosomes at a final density of  $2 \times 10^6$  cells/ml were diluted in 200  $\mu$ l of glucose-free medium supplemented with 5 mM proline/10 mM glucose, 2 mM proline or 12 mM proline containing 1  $\mu$ M to 100 mM of the analysed metabolite and incubated for 48 h at 27°C in microplates, before adding 20  $\mu$ l of 0.49 mM Alamar Blue reagent. After 2 h of incubation with resazurin, the fluorescence was measured with the microplate reader Fluostar Optima (BMG Labtech) at 550 nm excitation wavelength and 600 nm emission wavelength as previously described (Wargnies et al., 2018). The growth is represented as percentage of fluorescence (considering the value for intact cells as 100%) vs log of metabolite concentration.

Both techniques were used to assess the growth of mutant cell lines disrupted in expression of enzymes from proline degradation, TCA cycle and acetate production pathways (Table 5.11)

## **b) Transfection**

$10^7$  PCF trypanosomes from parental or mutant cell lines were centrifuged and washed twice in 5 ml of ZPFM solution (152 mM NaCl, 8 mM KCl, 8 mM  $\text{Na}_2\text{HPO}_4$ , 1.5 mM  $\text{KH}_2\text{PO}_4$ , 0.5 mM  $\text{Mg}_4\text{-Ac-H}_2\text{O}$  and 90  $\mu$ M  $\text{CaAc-H}_2\text{O}$ ). The cells were then resuspended in 500  $\mu$ l and incubated with 5 to 10  $\mu$ g of linearised DNA during 5min in ice. Electroporation was performed at 1500 V, 25  $\mu$ F and  $\infty$  resistance using the Gene Pulser XCell Electroporation System (Bio-Rad). Trypanosomes were immediately transferred to 4 ml of conditioned SDM79 medium (filtered medium obtained after culture of trypanosomes in exponential phase) supplemented with 20% of FCS. 24h later, the transformants were cloned in the presence of the antibiotic for selection. Cells resistant to the antibiotic were observed after approximately 10 days.

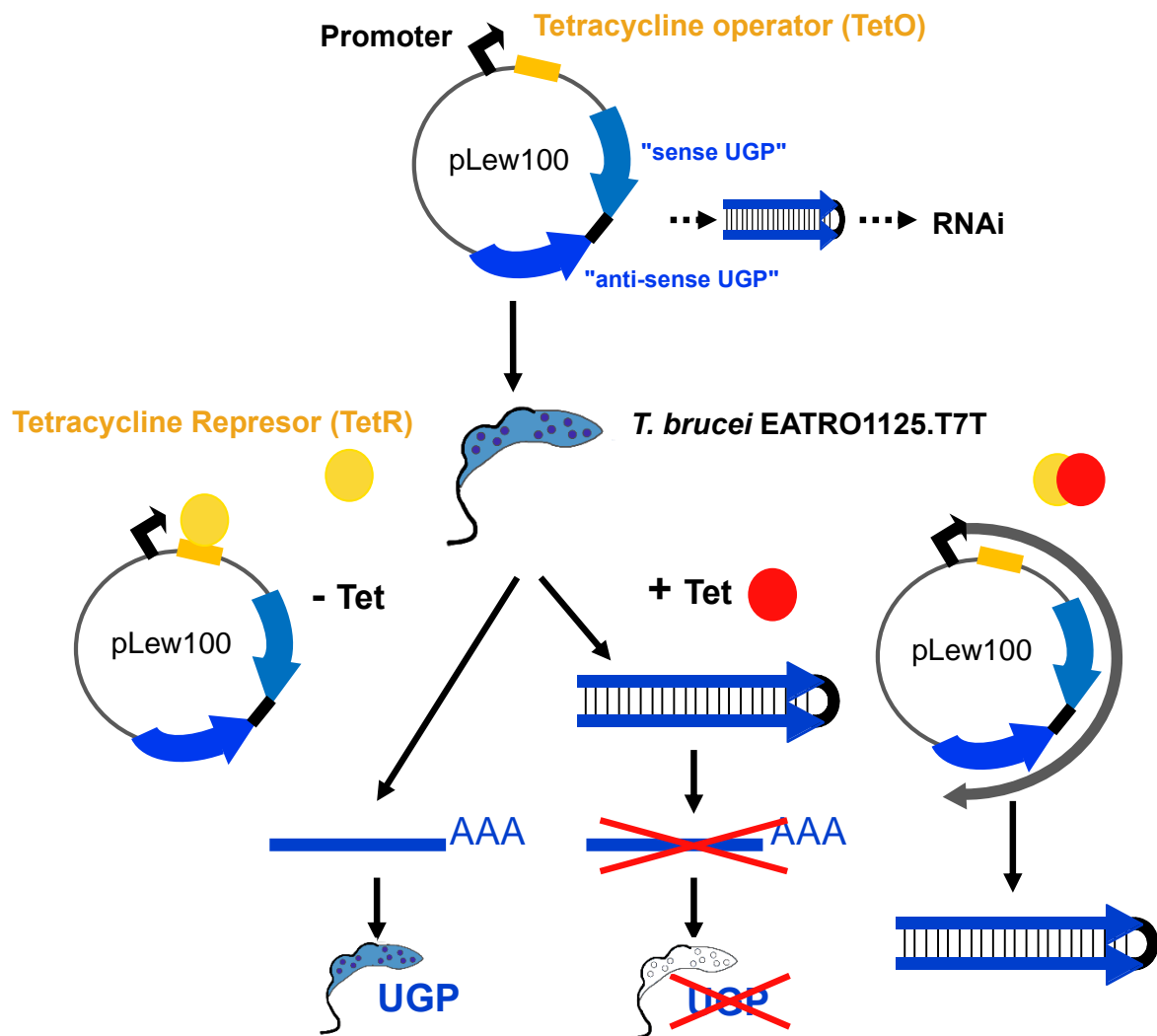


**Figure 5.67. UGP knock-down by RNAi in *T. brucei*.**

The pLew100 plasmid permits tetracycline-inducible expression of a stem loop composed by sense and anti-sense strands that trigger the RNA interference machinery.

### c) Inhibition of gene expression by RNA interference (RNAi)

The inhibition by RNAi of gene expression in the PCF trypanosomes was performed by expression of stem-loop “sense/antisense” (SAS) RNA molecules of the targeted sequences introduced into the pLew100 or a single fragment in the p2T7<sup>Ti</sup>-177 vector (Wirtz et al., 1999; Wickstead et al., 2002).

For targeting UGP, a PCR-amplified 579-bp fragment, containing the antisense UGP sequence was inserted between HindIII and BamHI restriction sites of pLew100 plasmid. Then, the separate 537-bp PCR-amplified fragment containing the sense *UGP* sequence was inserted upstream the antisense sequence, using HindIII and XhoI restriction sites. The resulting plasmid pLew-UGP-SAS contains a sense and antisense version of the UGP fragment separated by a 42-bp fragment. Procyclic EATRO1125.T7T cells were transfected with the pLew-UGP-SAS plasmid to generate the *RNAi*UGP cell line (Figure 5.67). This *RNAi*UGP cell line was later transfected with a plasmid coding for a recoded UGP (Figure 5.66) targeted to glycosomes (pHD1336-rUGP-GPDH) to generate the *RNAi*UGP/*EXP*rUGP-GPDH mutant (see production of glycosomal recombinant UGP proteins).

For targeting SCoAS, a 591 bp fragment of the beta subunit of SCoAS (Tb927.10.7410) was PCR amplified and cloned into the p2T7-177 plasmid using the BamHI and HindIII restriction sites (p2t7-177-SCoAS). p2t7-177-SCoAS plasmid to generate the *RNAi*SCoAS cell line. This plasmid was provided by A. Zikova.

For targeting IDHm, a 1127 bp fragment of IDHm (Tb927.8.3690) was amplified from genomic AnTat1.1 DNA and cloned into the p2t7-177 plasmid using the BamHI and HindIII restriction sites. Procyclic EATRO1125.T7T cells were transfected with p2t7-177\_IDHm<sup>RNAi</sup> to generate the *RNAi*IDHm cell line. This plasmid was provided by M. Borshart.

All transfected cells were selected in SDM79 medium containing hygromycin (25 µg/ml), neomycin (10 µg/ml) and phleomycin (5 µg/ml), with addition of blasticidin (20 µg/ml) for the *RNAi*UGP/*EXP*rUGP-GPDH cell line.

Enzymatic step	Cell line	Produced in this work	Reference
PRODHD	<i>RNAi</i> PRODHD		(Lamour et al., 2005)
AAT	<i>RNAi</i> AAT		(Spitznagel et al., 2009)
KDH-E2	$\Delta kdh-e2$	✓	
KDH-E2/IDHm	$\Delta kdh-e2/^{RNAi}$ IDHm <sup>1</sup>	✓	
SCoAS	<i>RNAi</i> SCoAS <sup>2</sup>	✓	
SDH	<i>RNAi</i> SDH		(Coustou et al., 2008)
FRDg/m	<i>RNAi</i> FRDg/m		(Coustou et al., 2005)
FHc/m	<i>RNAi</i> FHc/m		(Coustou et al., 2006)
ACO	$\Delta aco^1$		
IDHm	$\Delta idhm^1$		
IDHm/SCoAS	$\Delta idhm/^{RNAi}$ SCoAS <sup>2</sup>	✓	
PDH	<i>RNAi</i> PDH-E2		(Coustou et al., 2008)
ASCT/ACH	$\Delta ach/^{RNAi}$ ASCT		(Millerioux et al., 2012)
HGDH	$\Delta hgdh^3$	✓	

**Table 5.11. Mutant cell lines disrupted in expression of enzymes of proline degradation, TCA cycle and acetate production pathways used in this work.**

The majority of the cell lines are part of the mutant collection from the intermediary and energy metabolism of trypanosomes (iMET) team, either produced in the laboratory or provided by collaborators. New cell lines produced in this work are indicated.

<sup>1</sup>The plasmid p2t7-177\_IDHm<sup>RNAi</sup> and the cell lines  $\Delta aco$  and  $\Delta idhm$  were provided by M. Boshart.

<sup>2</sup>The plasmid p2t7-177\_SCoAS<sup>RNAi</sup> was provided by A. Zíková.

<sup>3</sup>HGDH : candidate gene for L-2-hydroxyglutarate dehydrogenase, mitochondrial, putative. Accession number Tb927.10.9360.

#### d) Production of null mutants

Replacement of the *UGP* gene by the phleomycin and puromycin resistance markers *via* homologous recombination was performed with DNA fragments containing the resistance marker gene flanked by the UTR sequences. Briefly, an *HpaI* DNA fragment containing the *PAC* and *BLE* resistance marker genes preceded by the *UGP* 5'UTR fragment (522 bp) and followed by the *UGP* 3'UTR fragment (526 bp) were cloned in the pGEM-T plasmid. The *UGP* knock-out mutants were generated in cell lines expressing tagged recoded versions of *UGP*, named *EXP*r*UGP* and *EXP*r*UGP*-GPDH, and in the presence of tetracycline. The selected cell lines *rUGP<sup>Ti</sup>-BLA TetR-HYG T7RNAPOL-NEO Δugp::PAC/Δugp::BLE* and *rUGP::GPDH<sup>Ti</sup>-BLA TetR-HYG T7RNAPOL-NEO Δugp::PAC/Δugp::BLE* are called *Δugp<sup>EXP</sup>rUGP* and *Δugp<sup>EXP</sup>rUGP-GPDH*, respectively.

To delete the genes encoding the E2 subunit of KDH (KDH-E2), the resistance markers blasticidin (BLA) and puromycin (PAC) were PCR amplified using long primers with 80 bp corresponding to the 5'UTR and 3'UTR region of the *KDH-E2* gene (Tb927.11.9980). To replace the two *KDH-E2* alleles, the EATRO1125.T7T PCF was transfected with 10 µg of purified PCR products encoding the resistance markers flanked by UTR regions. The selected *Δkdh-e2::PAC/Δkdh-e2::BLA* cell line was named *Δkdh-e2*. The cell line *Δkdh-e2/RNAiIDHm* was generated by transfecting the *Δkdh-e2* cell line with p2t7-177\_IDHm<sup>RNAi</sup> followed by selection with phleomycin.

#### e) Expression of tagged proteins

##### - Endogenous tagging

The *UGP* gene was *in situ* tagged either at the N-terminal or C-terminal extremities (Dean et al., 2015). Briefly, the DNA sequence encoding 10xTY1 tag and BLA resistance cassette was amplified from the pPOTv7-10xTY1 vector using long primers that incorporate 5' overhanging 80 nt homologous to the *UGP* gene and its UTR (Table 5.10). For production of *UGP* truncated versions 10xTY1 tagged at their C-terminal extremity, the forward primers were designed within the *UGP* gene extension to produce proteins containing the N-terminal first 66 (1-66), 124 (1-124), 173 (1-173) and 226 (1-226) residues. The PCR products were precipitated with ethanol before use for transfection and cells were selected in SDM79 containing blasticidin (20 µg/ml).



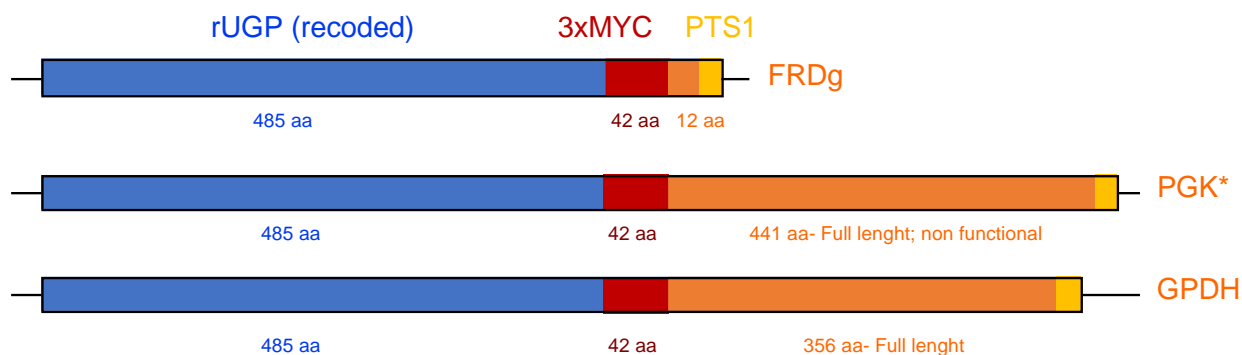


**Figure 5.68. Production of glycosomal recombinant rUGP proteins.**

Recoded rUGP fused to a 3xMYC tagged and different glycosomal targeting signals were produced in order to target UGP to the glycosomes.

PGK\* was mutated in two residues essential for catalytic activity. PGK and GPDH correspond to full-length genes, while only 12 C-terminal residues of FRDg were used.

We also expressed truncated versions of the recoded UGP lacking either the first 66 or 124 residues fused to a 10xTY1 tag at their C-terminal extremity. The PCR fragments corresponding to the complete or truncated *rUGP* gene fused to TY tag and blasticidin cassette from pPOTv7 were obtained by overlapping PCR and cloned into pGEM-T. Cells were transfected with 10 ug of plasmid digested with NotI. The *PEPCK* gene was also *in situ* tagged at the N-terminal extremity as described above (Table 5.9).

#### - Over-expression

Inducible systems based on the pLew100 and pHD1336 vectors were used to express different tagged and fused versions of UGP and PEPCK. Induction of expression of the recombinant proteins was performed in all cases by addition of 1 µg/ml tetracycline. The *UGP* gene was cloned in the HindIII-NdeI restriction sites of pLew100-X-MYC, which was designed for expression of recombinant proteins tagged at the C-terminal extremity with 3xMYC epitopes. The EATRO1125.T7T parental cell line,  $\Delta pepck$  (Ebikeme et al., 2010) and  $\Delta pepck$ /TY-PEPCK cell lines were transfected with the pLew100-UGP-MYC tetracycline inducible plasmid and cells were selected in SDM79 containing 5 µg/ml of phleomycin.

The *EXP*rUGP cell line was obtained by transfecting the EATRO1125.T7T parental cell line with the pHD1336 vector containing the recoded *rUGP* followed by a 3xMYC tag sequence. This cell line was used to produce the null *UGP* mutant in the presence of tetracycline.

For rescue of the  $\Delta pepck$  cell line, the *PEPCK* gene was cloned in the HindIII-BamHI restriction sites of pLew100. For expression of eGFP-PEPCK truncated versions, the  $\Delta pepck$  cell line was transfected with the pLew100 tetracycline inducible plasmid containing truncated versions of PEPCK fused at the N-terminal extremity with eGFP, which was used to increase the stability of the recombinant truncated proteins. PCR fragments corresponding to the truncations of PEPCK at residues 140, 180, 214 and 321 were inserted between the XhoI and XbaI restriction sites of the pLew100-eGFPX plasmid. The transfected cells were selected in SDM79 containing 5 µg/ml of phleomycin.

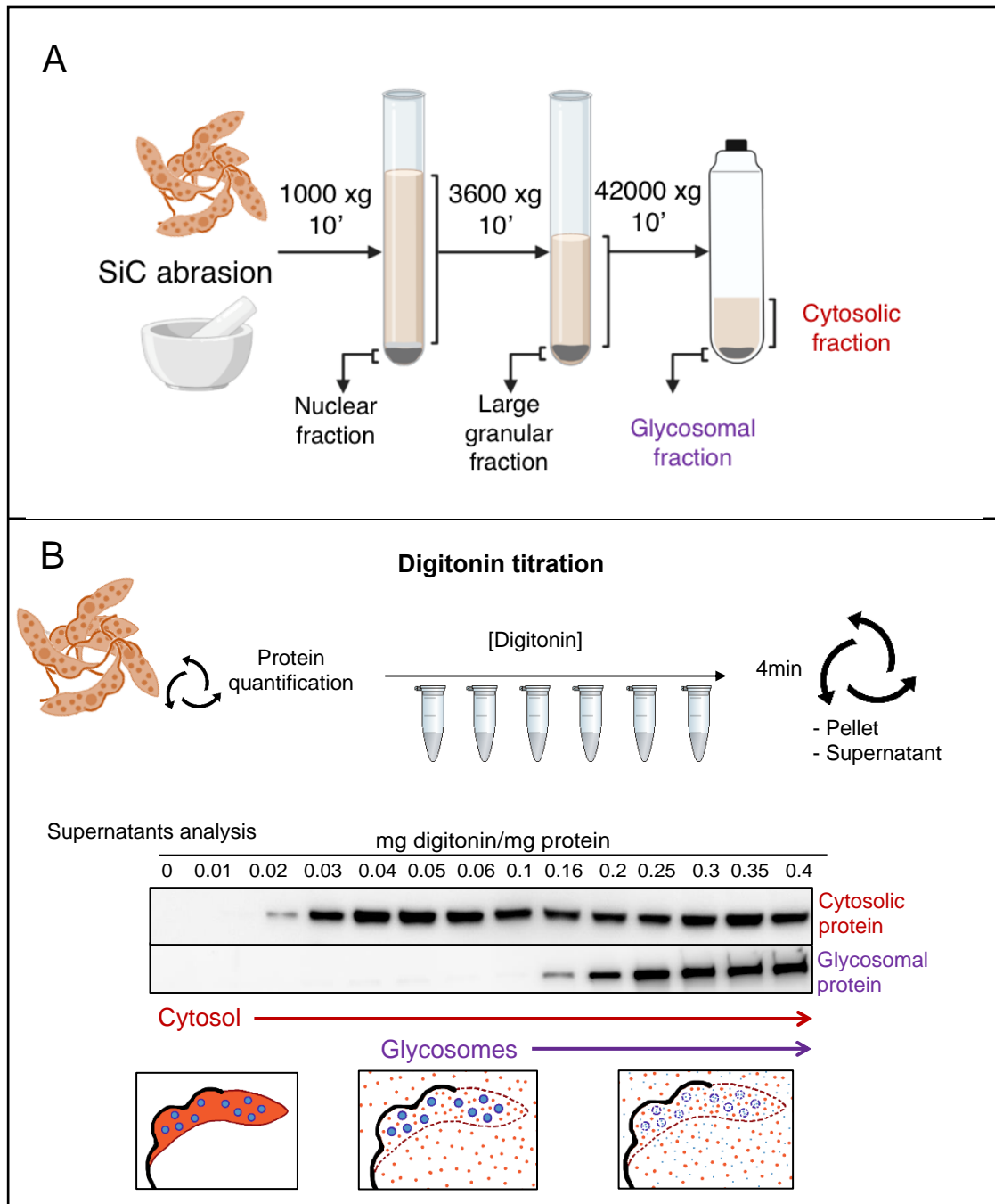


**Figure 5.69. Principal techniques used for subcellular localisation of proteins.**

(A) Mechanical rupture of parasites by abrasion with silicon carbide precedes the differential centrifugation protocol to obtain an enriched cytosolic fraction and an enriched glycosomal fraction. (B) In a permeabilization by digitonin titration, equal amounts of cells in terms of protein content are incubated with increasing concentrations of detergent before being centrifuged. Cytosolic proteins are released with low digitonin concentrations while glycosomal proteins require higher digitonin levels to be released.

### - **Glycosomal recombinant UGP proteins**

To target UGP exclusively to the glycosomes, the rUGP was fused at its C-terminal extremity to a 3xMYC tag followed by (i) the sequence encoding the last C-terminal 12 residues of the glycosomal fumarate reductase (*FRDg*) gene, which contains a PTS1 (rUGP-FRDgPST1), (ii) the full-length PTS1-containing phosphoglycerate (*PGKc*) gene (rUGP-PGKc\*) and (iii) the full-length PTS1-containing glycerol-3-phosphate dehydrogenase (*GPDH*) gene (rUGP-GPDH) (Figure 5.68). The lysine residue, K215, essential for the PGK enzymatic activity (Bernstein et al., 1998) was replaced by the alanine codon. In order to increase the net charge of residues at the C-terminus, which is a major determinant of peroxisomal import efficiency (DeLoache et al., 2016), we modified one residue in the C-terminal extremity of PGK (TLRNRW-SSL instead of TLSNRW-SSL) and of GPDH (PARPRT-SKM instead of PALPRT-SKM). The pHD1336-rUGP-FRDgPST1 plasmid, provided by the GeneCust Company, was used for cloning the synthesized genes (GeneCust) *PGKc*\* and *GPDH* in its MluI-BamHI restriction sites. The EATRO1125.T7T parental cell line was transfected and blasticidin resistant cell lines were selected in SDM79 containing 20 µg/ml of the antibiotic.

### **5.2.3. Biochemistry**

#### **a) Differential centrifugation**

This technique allows separation of various subcellular particles depending on their differences in the sedimentation coefficients. In this work, it was used to obtain enriched glycosomal and cytosolic fractions to assess the subcellular localisation of UGP and its recombinant versions (Figure 5.69). To do so, PCF cell homogenates were obtained by grinding pre-washed cells with silicon carbide (200 mesh) in STE buffer (25 mM Tris, 1 mM EDTA, 250 mM sucrose, pH: 7.8) (Opperdoes and Borst, 1977a) supplemented with 'Complete EDTA-Free' protease inhibitor cocktail (Roche). The cells were microscopically checked for at least 90% disruption. The lysates were diluted in 7 ml of STE, centrifuged at 1,000 g and then at 5,000 g for 10 min each at 4 °C. The supernatants were centrifuged at 42,000 g for 10 min at 4°C to yield the glycosome-enriched pellets and the cytosolic fractions (supernatants). The glycosomal pellets were washed once with 1 ml of STE before centrifugation at 42,000 g for 10 min at 4°C and resuspension in 0.2 ml of STE.

Primary antibodies			
Name	Species	Dilution	Source/Ref
Anti-TY	Mouse	WB 1:5,000 IF 1:5,000	BB2-Gift from K. Gull, Oxford, UK
Anti-MYC	Mouse	WB 1:1,000 IF 1:100	9E10-Gift from K. Ersfeld, Hull, UK
Anti-MYC	Rabbit	IF 1:1,000	Sigma, C3956
Anti-UGP	Rabbit	WB 1:100	COVALAB GYIPEKSIFPVES and RNGKPPAIDLDEH peptides
Anti-PEPCK	Rabbit	WB 1:1,000	Proteogenix HDGTLDQADYEVYPG and TDLKQFNETHKELVT peptides
Anti-PPDK	Mouse	IF 1:2	(Bringaud et al., 1998)
	Rabbit	WB 1:1,000	
Anti-ENO	Rabbit	WB 1:100,000	Gift from P. Michels, Edinburgh, UK
Anti-ALD	Rabbit	WB 1:5,000 IF 1:1,000	Gift from P. Michels, Edinburgh, UK
Anti-FRDg	Rabbit	WB 1:1,000	(Besteiro et al., 2002)
Anti-FRD	Rabbit	WB 1:100	(Coustou et al., 2005)
Anti-FH	Rabbit	WB 1:100	(Coustou et al., 2006)
Anti-IDHm	Rabbit	WB 1:500	Gift from M. Boshart, Germany
Anti-PDH	Rabbit	WB 1:500	(Ebikeme et al., 2010)
Anti-ASCT	Rabbit	WB 1:500	(Rivière et al., 2004)
Anti-SCoAS	Rabbit	WB 1:500	Gift from A. Zikova, Czech Republic
Secondary antibodies			
Anti-mouse HRP	Goat	WB 1:5,000	Bio-Rad
Anti-rabbit HRP	Goat	WB 1:10,000	Bio-Rad
Anti-mouse Alexa Fluor 594	Donkey	IF 1:100	ThermoFisher
Anti-mouse Alexa Fluor 488	Donkey	IF 1:100	ThermoFisher
Anti-rabbit Alexa Fluor 594	Donkey	IF 1:100	ThermoFisher
Anti-rabbit Alexa Fluor 488	Donkey	IF 1:100	ThermoFisher

**Table 5.12. Primary and secondary antibodies used for western blot and immunofluorescence analysis.**

Protein content was quantified with Pierce (Thermo Scientific™) at 660 nm. Equivalent amounts of protein from glycosomal (G) and cytosolic (C) fractions were analysed by western blotting.

#### **b) Digitonin permeabilization**

Digitonin is a non-ionic detergent that can interact with neutral lipids (cholesterol or ergosterol) present in the parasite membranes. Incubating cells with digitonin produces a selective permeabilization depending on the concentration of detergent used, so the protein content from different subcellular compartments is released. An accurate subcellular localisation can be determined by enzymatic activity assays or western blotting (Heise and Oppendoes, 1999) (Figure 5.69). To evaluate the subcellular localisation of UGP and its recombinant versions, PCF trypanosomes were washed two times in cold PBS and resuspended at 10 mg of protein per ml in STE buffer supplemented with 150 mM NaCl and the Complete™ Mini EDTA-free protease inhibitor cocktail (Roche). Cell aliquots (100 µl) were incubated with increasing quantities of digitonin (Sigma) for 4 min at 25°C, before centrifugation at 14,000 g for 2 min. The supernatants were analysed by western blotting.

#### **c) Cell fractionation by hypotonic lysis**

To compare levels of expression and localisation of both UGP and PEPCK in BSF and PCF parasites,  $2 \times 10^8$  cells of each form were washed in PBS and hypotonically lysed in the presence of protease inhibitors by incubating in 5 mM Na<sub>2</sub>HPO<sub>4</sub>, 0.3 mM KH<sub>2</sub>PO<sub>4</sub> for 30 min at 4°C before centrifugation at 14,000 g for 15 min. The pellet was solubilised in SDS 2% and both supernatant and pellet were analysed by western blotting.

#### **e) Blue-native PAGE (BN-PAGE)**

To determine the oligomerization state of UGP, polyacrylamide gel electrophoresis was performed under native conditions.  $10^8$  cells were washed in PBS and resuspended in SoTE (0.6 M sorbitol, 2 mM EDTA, 20 mM Tris-HCl, pH: 7.5) (Panicucci et al., 2017). Cells were incubated with 0 or 0.16 mg of digitonin per mg of protein for 4 min at 25°C, before centrifugation at 14,000 g for 2 min. The supernatants were analysed by BN-PAGE on a precast (3–12%) Bis-Tris polyacrylamide gel (Invitrogen) according to standard methods.

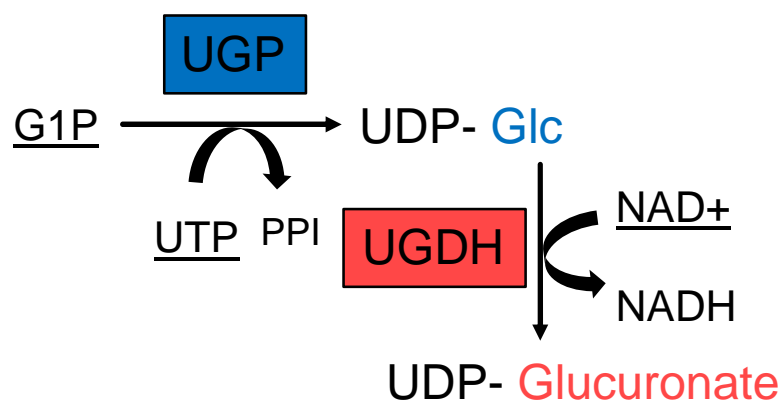


**Figure 5.70. UGP activity assay.**

The activity is detected by following the reduction of  $\text{NAD}^+$  at 340 nm in a coupled assay with UDP-glucose dehydrogenase (UGDH). The substrates added in the reaction mix are underlined

#### **f) SDS-PAGE and Western Blots**

Total protein extracts ( $5 \times 10^6$  cells), glycosomal and cytosolic fractions, or supernatants obtained after digitonin treatment were separated by SDS-PAGE (10%) and immunoblotted onto TransBlot Turbo Midi-size PVDF Membranes (Bio-Rad). Immunodetection was performed as described (Sambrook, 1989) using the primary antibodies and conditions summarised in Table 5.12. Revelation was performed using the Clarity western ECL Substrate as described by the manufacturer (Bio-Rad). Images were acquired and analysed with the ImageQuant LAS 4,000 luminescent image analyser.

#### **g) Enzymatic activity assays**

The UGP activity in total lysates and aliquots of glycosomal and cytosolic fractions was measured as described (Lamerz et al., 2006) following the reduction of  $\text{NAD}^+$  at 340 nm in the presence of 50 mM Tris-HCl (pH: 7.8), 10 mM  $\text{MgCl}_2$ , 1 mM 2-mercaptoethanol, 1 mM UTP, 1 mM G1P, 1 mM  $\text{NAD}^+$  and 0.05 units of UDP-Glc dehydrogenase (Figure 5.70). For normalisation of the UGP activities, the malic enzyme activity was determined in the total cell extracts and the cytosolic fractions, as described before (Allmann et al., 2013). For normalisation of the UGP activities in glycosomal extracts, the glycerol kinase activity was determined as described before (Králová et al., 2000).

The PEPCK activity was measured by following the oxidation of NADH at 340 nm in the presence of 100 mM MOPS (pH: 7.5), 20 mM  $\text{NaHCO}_3$ , 1 mM DTT, 3 mM  $\text{MnCl}_2$ , 1 mM ADP, 0.2 mM NADH and 6 units of malate dehydrogenase. The reaction was started by the addition of 5 mM PEP (Hunt and Köhler, 1995).

The proline dehydrogenase (PRODH) and succinate dehydrogenase activities (SDH) were measured following the reduction of the electron-accepting dye dichlorophenolindophenol (DCPIP) at 600 nm (Brown and Wood, 1993). The assays contained 11 mM MOPS pH: 7.5, 11 mM  $\text{MgCl}_2$ , 11% glycerol, 56  $\mu\text{M}$  DCPIP, 0.9 mM PMS, 10 mM of proline for PRODH activity or 20 mM of succinate for SDH activity. To prepare the samples, PCF cells were harvested, washed twice with STE buffer (25 mM Tris-HCl pH: 7.4, 1 mM EDTA, 0.25 M sucrose, Protease inhibitors) and treated with 0.35 mg digitonin per mg of protein during 4 min at room temperature. After centrifugation 2 min at  $12,000 \times g$ , the enzymatic activities were determined in the pellets resuspended in STE.



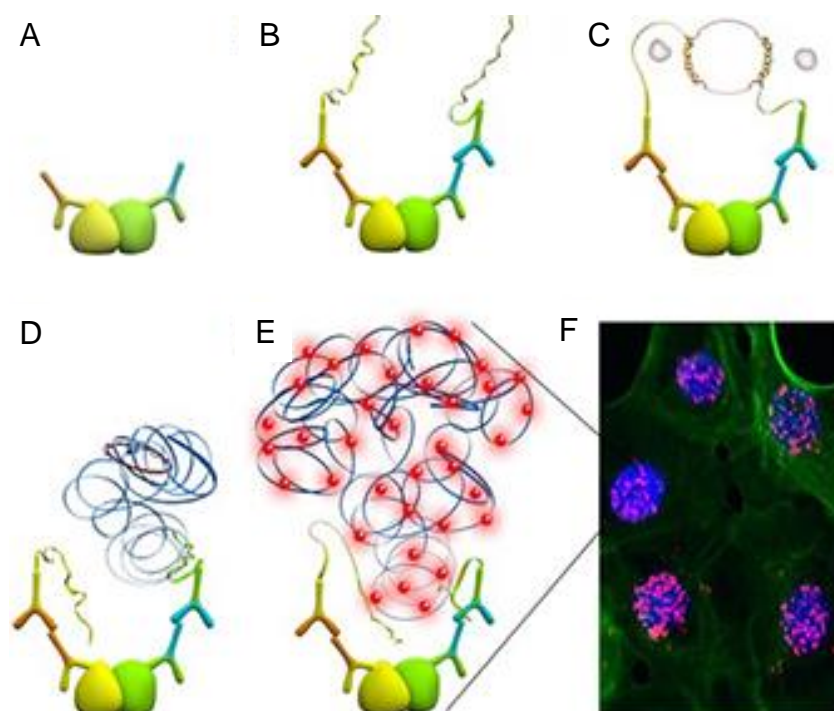


**Figure 5.71. Duolink® Proximity Ligation Assay reaction.**

(A) Fixed and solubilised cells spread on slides are incubated with two primary antibodies produced in different organisms (ex. rabbit and mouse). The yellow and green globules represent epitopes or tags on two different proteins that are interacting.

(B) Secondary antibodies coupled to oligonucleotides (PLA probes) bind to the primary antibodies.

(C) Connector oligos join the PLA probes through a ligation step.

(D) The resulting closed, circular DNA template is amplified by DNA polymerase.

(E) For detection, oligos coupled to fluorochromes hybridize to repeated sequences in the amplicons.

(F) PLA signals are detected as discrete red spots and provide the intracellular localisation of the proteins interaction.

(From <https://www.sigmaaldrich.com/technical-documents/protocols/biology/how-pla-works.html>)

The alanine aminotransferase (ALAT) activity was measured following the oxidation of NADH at 340 nm (Bergmeyer, 1983). The malate dehydrogenase (MDH) activity was determined as a control (Aranda et al., 2006).

#### **5.2.4. Imaging**

##### **a) Immunofluorescence Microscopy**

In order to visualize subcellular localisation of MYC tagged UGP versions, cells were washed twice with PBS and then treated (+) or not (-) with 0.04 mg of digitonin per mg of protein to release the cytosolic content during 4 min at 25°C.

After centrifugation at 14,000 g for 2 min and washing, the cellular pellets were resuspended in PBS and fixed with 4% paraformaldehyde (PFA) for 10 min at RT, before neutralization with 1 M glycine. The cells were spread on poly-L-lysine-coated slides and permeabilised with 0.05% Triton X-100. After incubation in PBS containing 4% BSA overnight, cells were incubated for 45 min with diluted primary antibodies (Table 5.12). After washing with PBS, samples were incubated for 45 min with secondary antibodies depending on the primary antibodies used. Slides were washed and mounted with SlowFade Gold (Molecular Probes). Images were acquired with Metamorph software on a Zeiss Imager Z1 or Axioplan 2 microscope as previously described (Albisetti et al., 2017).

##### **b) Proximity Ligation Assay (PLA)**

For protein interaction studies, the *In situ* proximity ligation assay (PLA) was performed using the Duolink™ *In Situ* Red Starter Kit Mouse/Rabbit (Sigma-Aldrich) following the manufacturer's recommendations (Figure 5.71). To perform the assay, PFA-fixed and Triton X-100 permeabilised cells were spread on slides as described above. The cells were blocked with Duolink Blocking Solution for 60 min at 37°C. Primary antibodies rabbit anti-MYC (1/1,000) and mouse anti-TY1 (1/5,000) were diluted in Duolink Antibody Diluent and incubated 60 min at room temperature. The slides were washed for 10 min in wash buffer A and incubated with PLUS and MINUS PLA probes diluted in Duolink Antibody Diluent for 60 min at 37°C. Ligation and amplification steps were performed according to the manufacturer's instructions.

After washing, cells were blocked with PBS-BSA 4% overnight. The cells were counterstained with mouse anti-PPDK ( $\alpha$ PPDK). Slides were mounted in Duolink *In Situ* Mounting Medium with DAPI. Images were acquired as described for

immunofluorescence and analysed using ImageJ. Cells were counted manually using cell counter ImageJ plugin.

### **5.2.5. Proteomics and metabolomics**

#### **a) Label-free quantitative proteomics**

Enriched glycosomal fractions were loaded on a 10% acrylamide SDS-PAGE gel and proteins were visualised by Colloidal Blue staining. The steps of sample preparation, protein digestion and LC-MS parameters used for nanoLC-MS/MS analysis on a Q-Exactive were previously described (Pineda et al., 2018). Sequest HT and Mascot 2.4 algorithms through Proteome Discoverer 1.4 Software (Thermo Fisher Scientific Inc.) were used for protein identification in batch mode by searching against a *Trypanosoma brucei* protein database (11,119 entries, release 46). This database was down-loaded from <http://tritrypdb.org> website. Two missed enzyme cleavages were allowed. Mass tolerances in MS and MS/MS were set to 10 ppm and 0.02 Da. Oxidation of methionine, acetylation of lysine and deamidation of asparagine and glutamine were searched as dynamic modifications. Carbamidomethylation on cysteine was searched as static modification. Peptide validation was performed using Percolator algorithm (Käll et al., 2007) and only “high confidence” peptides were retained corresponding to a 1% False Discovery Rate (FDR) at peptide level. Raw LC-MS/MS data were imported in Progenesis QI (version 2.0; Nonlinear Dynamics, a Waters Company) for feature detection, alignment, and quantification. All sample features were aligned according to retention times by manually inserting up to fifty landmarks followed by automatic alignment to maximally overlay all the two-dimensional (m/z and retention time) feature maps. Singly charged ions and ions with higher charge states than six were excluded from analysis. All remaining features were used to calculate a normalisation factor for each sample that corrects for experimental variation. Peptide identifications (with FDR<1%) were imported into Progenesis. Only non-conflicting features and unique peptides were considered for calculation of quantification at protein level. A minimum of two peptides matched to a protein was used as the criterion for identification as a differentially expressed protein.

The mass spectrometry proteomics data were deposited to the ProteomeXchange Consortium (<http://proteomecentral.proteomexchange.org>) via the PRIDE partner repository (Deutsch et al., 2020) with the dataset identifier PXD020190. Cell lines

analysed in this study included EATRO1125.T7T parental WT,  $\Delta pepck$ ,  $\Delta fbpase$  grown with glucose,  $\Delta fbpase$  grown with glycerol,  $\Delta idh$ ,  $RNAiG6PDH$ ,  $RNAiGK$ ,  $RNAiGPDH$ .

### **b) Mass spectrometry analyses of intracellular metabolites by IC-HRMS**

Parental and mutant cell lines grown in SDM79 medium were collected on filters by fast filtration preparation ( $2 \times 10^7$  cells per filter) as described before (Ebikeme et al., 2010). Metabolites were analysed by a liquid anion exchange chromatography Dionex™ ICS-5000+ Reagent-Free™ HPIC™ (Thermo Fisher Scientific™, Sunnyvale, CA, USA) system coupled to a Thermo Scientific™ LTQ Orbitrap Velos™ hybrid FT mass spectrometer (Thermo Fisher Scientific, San Jose, CA, USA). The metabolites were separated within 48 min, using linear gradient elution of KOH applied to an IonPac AS11 column (250 x 2 mm, Dionex™) equipped with an AG11 guard column (50 x 2 mm, Dionex™) at a flow rate of 0.35 ml/min. The column and autosampler temperature were 30°C and 4°C, respectively. Injected sample volume was 15  $\mu$ l. Mass detection was carried out in a negative electrospray ionization (ESI) mode. The settings of the mass spectrometer were as follows: spray voltage 2.7 kV, capillary and desolvation temperature 350°C, maximum injection time 50 ms. Nitrogen was used as sheath gas (pressure 50 units) and auxiliary gas (pressure 5 units). The automatic gain control (AGC) was set at  $1e6$  for full scan mode with a mass resolution of 60,000 (at 400  $m/z$ ). Data acquisition was performed using Thermo Scientific Xcalibur software. The identification of metabolites relied upon matching accurate masses from FTMS scan (mass tolerance of 5 ppm) and retention time using TraceFinder 3.2 software. The absolute levels of intracellular metabolites were quantified based on isotope-dilution mass spectrometry (IDMS) approach. The cell lines analysed in this study were EATRO1125.T7T parental WT,  $\Delta pepck$ ,  $EXP$ rUGP,  $RNAi$ UGP-H10,  $RNAi$ UGP/ $EXP$ UGP-GPDH.

### **c) Analysis of excreted end products by proton NMR**

$2 \times 10^7$  *T. brucei* PCF cells were collected by centrifugation at 1,400 g for 10 min, washed once with phosphate-buffered saline (PBS) and incubated in 1 ml (single point analysis) of PBS supplemented with 2 g/l  $NaHCO_3$  (pH: 7.4). For kinetic analysis,  $10^9$  cells were incubated in 15 ml under the same conditions. Cells were maintained for 6 h at 27°C in incubation buffer containing one or two  $^{13}C$ -enriched or non-enriched carbon sources. The integrity of the cells during the incubation was checked by

microscopic observation. The supernatant (1 ml) was collected and 50 µl of maleate solution in D<sub>2</sub>O (10 mM) was added as internal reference. H-NMR spectra were performed at 500.19 MHz on a Bruker Avance III 500 HD spectrometer equipped with a 5 mm cryoprobe Prodigy. Measurements were recorded at 25°. Acquisition conditions were as follows: 90° flip angle, 5,000 Hz spectral width, 32 K memory size, and 9.3 sec total recycle time. Measurements were performed with 64 scans for a total time close to 10 min 30 sec. Resonances of the obtained spectra were integrated and metabolites concentrations were calculated using the ERETIC2 NMR quantification Bruker program. To confirm complex spectra and the presence of hydroxyglutarate in some samples, H-NMR spectra were performed at 800 MHz on a Bruker Avance spectrometer at the MetaToul Platform (<https://www6.toulouse.inrae.fr/metatoul>).

## REFERENCES

- Albisetti, A., Florimond, C., Landrein, N., Vidilaseris, K., Eggenspieler, M., Lesigang, J., Dong, G., Robinson, D.R., Bonhivers, M., 2017. Interaction between the flagellar pocket collar and the hook complex via a novel microtubule-binding protein in *Trypanosoma brucei*. PLOS Pathog. 13, e1006710. <https://doi.org/10.1371/journal.ppat.1006710>
- Alexander, K., Parsons, M., 1993. Characterization of a divergent glycosomal microbody phosphoglycerate kinase from *Trypanosoma brucei*. Mol. Biochem. Parasitol. 60, 265–272. [https://doi.org/10.1016/0166-6851\(93\)90137-M](https://doi.org/10.1016/0166-6851(93)90137-M)
- Allmann, S., Morand, P., Ebikeme, C., Gales, L., Biran, M., Hubert, J., Brennand, A., Mazet, M., Franconi, J.-M., Michels, P.A.M., Portais, J.-C., Boshart, M., Bringaud, F., 2013. Cytosolic NADPH Homeostasis in Glucose-starved Procyclic *Trypanosoma brucei* Relies on Malic Enzyme and the Pentose Phosphate Pathway Fed by Gluconeogenic Flux. J. Biol. Chem. 288, 18494–18505. <https://doi.org/10.1074/jbc.M113.462978>
- Allmann, S., Bringaud, F., 2017. Glycosomes: A comprehensive view of their metabolic roles in *T. brucei*. Int. J. Biochem. Cell Biol. 85, 85–90. <https://doi.org/10.1016/j.biocel.2017.01.015>
- Allmann, S., Wargnies, M., Cahoreau, E., Biran, M., Plazolles, N., Morand, P., Pineda, E., Kulyk, H., Asencio, C., Villafraz, O., Rivière, L., Tétaud, E., Rotureau, B., Mourier, A., Portais, J.-C., Bringaud, F., 2019. “Metabolic contest”, a new way to control carbon source preference (preprint). Microbiology. <https://doi.org/10.1101/800839>
- Al-Saryi, N.A., Al-Hejjaj, M.Y., van Roermund, C.W.T., Hulmes, G.E., Ekal, L., Payton, C., Wanders, R.J.A., Hettema, E.H., 2017a. Two NAD-linked redox shuttles maintain the peroxisomal redox balance in *Saccharomyces cerevisiae*. Sci. Rep. 7, 11868. <https://doi.org/10.1038/s41598-017-11942-2>
- Al-Saryi, N.A., Hutchinson, J.D., Al-hejjaj, M.Y., Sedelnikova, S., Baker, P., Hettema, E.H., 2017b. Pnc1 piggy-back import into peroxisomes relies on Gpd1 homodimerisation. Sci. Rep. 7, 42579. <https://doi.org/10.1038/srep42579>
- Aranda, A., Maugeri, D., Uttaro, A.D., Opperdoes, F., Cazzulo, Juan.J., Nowicki, C., 2006. The malate dehydrogenase isoforms from *Trypanosoma brucei*: Subcellular localisation and differential expression in bloodstream and procyclic forms. Int. J. Parasitol. 36, 295–307. <https://doi.org/10.1016/j.ijpara.2005.09.013>
- Aslett, M., Aurrecochea, C., Berriman, M., Brestelli, J., Brunk, B.P., Carrington, M., Depledge, D.P., Fischer, S., Gajria, B., Gao, X., Gardner, M.J., Gingle, A., Grant, G., Harb, O.S., Heiges, M., Hertz-Fowler, C., Houston, R., Innamorato, F., Iodice, J., Kissinger, J.C., Kraemer, E., Li, W., Logan, F.J., Miller, J.A., Mitra, S., Myler, P.J., Nayak, V., Pennington, C., Phan, I., Pinney, D.F., Ramasamy, G., Rogers, M.B., Roos, D.S., Ross, C., Sivam, D., Smith, D.F., Srinivasamoorthy, G., Stoeckert, C.J., Subramanian, S., Thibodeau, R., Tivey, A., Treatman, C., Velarde, G., Wang, H., 2010. TriTrypDB: a functional genomic resource for the Trypanosomatidae. Nucleic Acids Res. 38, D457–D462. <https://doi.org/10.1093/nar/gkp851>
- Balogun, R.A., 1974. Studies on the amino acids of the tsetse fly, *Glossina morsitans*, maintained on in vitro and in vivo feeding systems. Comp. Biochem. Physiol. A Physiol. 49, 215–222. [https://doi.org/10.1016/0300-9629\(74\)90110-8](https://doi.org/10.1016/0300-9629(74)90110-8)
- Bandini, G., Mariño, K., Güther, M.L.S., Wernimont, A.K., Kuettel, S., Qiu, W., Afzal, S., Kelner, A., Hui, R., Ferguson, M.A.J., 2012. Phosphoglucomutase is absent in *Trypanosoma brucei* and redundantly substituted by phosphomannomutase and phospho-N-acetylglucosamine mutase: PMM, PAGM and phosphoglucomutase activity in *T. brucei*. Mol. Microbiol. 85, 513–534. <https://doi.org/10.1111/j.1365-2958.2012.08124.x>
- Bandini, G., Damerow, S., Sampaio Güther, M.L., Mehlert, A., Guo, H., Beverley, S.M., Ferguson, M.A.J., 2019. An essential GDP-Fuc:  $\beta$ -D-Gal  $\alpha$ -1,2-fucosyltransferase is located in the mitochondrion of *Trypanosoma brucei*. bioRxiv 726117. <https://doi.org/10.1101/726117>
- Banerjee, S.K., Kessler, P.S., Saveria, T., Parsons, M., 2005. Identification of trypanosomatid PEX19: Functional characterization reveals impact on cell growth and glycosome size and number. Mol. Biochem. Parasitol. 142, 47–55. <https://doi.org/10.1016/j.molbiopara.2005.03.008>
- Banerjee, H., Knoblich, B., Rachubinski, R.A., 2019. The early-acting glycosome biogenic protein Pex3 is essential for trypanosome viability. Life Sci. Alliance 2, e201900421. <https://doi.org/10.26508/lsa.201900421>
- Bard, F., Chia, J., 2016. Cracking the Glycome Encoder: Signaling, Trafficking, and Glycosylation. Trends Cell Biol. 26, 379–388. <https://doi.org/10.1016/j.tcb.2015.12.004>

- Barrett, M., 1998. Trypanosome glucose transporters. *Mol. Biochem. Parasitol.* 91, 195–205. [https://doi.org/10.1016/S0166-6851\(97\)00192-8](https://doi.org/10.1016/S0166-6851(97)00192-8)
- Bartossek, T., Jones, N.G., Schäfer, C., Cvitković, M., Glogger, M., Mott, H.R., Kuper, J., Brennich, M., Carrington, M., Smith, A.-S., Fenz, S., Kisker, C., Engstler, M., 2017. Structural basis for the shielding function of the dynamic trypanosome variant surface glycoprotein coat. *Nat. Microbiol.* 2, 1523–1532. <https://doi.org/10.1038/s41564-017-0013-6>
- Bauer, S., Morris, J.C., Morris, M.T., 2013. Environmentally regulated glycosome protein composition in the African trypanosome. *Eukaryot. Cell* 12, 1072–1079. <https://doi.org/10.1128/EC.00086-13>
- Bauer, S., Morris, M.T., 2017. Glycosome biogenesis in trypanosomes and the de novo dilemma. *PLoS Negl. Trop. Dis.* 11, e0005333. <https://doi.org/10.1371/journal.pntd.0005333>
- Bedzhov, I., Stemmler, M.P., 2015. Applying the Proximity Ligation Assay (PLA) to Mouse Preimplantation Embryos for Identifying Protein-Protein Interactions In Situ, in: Germano, S. (Ed.), *Receptor Tyrosine Kinases: Methods and Protocols*. Springer New York, New York, NY, pp. 57–64. [https://doi.org/10.1007/978-1-4939-1789-1\\_6](https://doi.org/10.1007/978-1-4939-1789-1_6)
- Beneke, T., Madden, R., Makin, L., Valli, J., Sunter, J., Gluenz, E., 2017. A CRISPR Cas9 high-throughput genome editing toolkit for kinetoplastids. *R. Soc. Open Sci.* 4, 170095. <https://doi.org/10.1098/rsos.170095>
- Bernstein, B.E., Michels, P.A., Kim, H., Petra, P.H., Hol, W.G., 1998. The importance of dynamic light scattering in obtaining multiple crystal forms of *Trypanosoma brucei* PGK. *Protein Sci. Publ. Protein Soc.* 7, 504–507. <https://doi.org/10.1002/pro.5560070232>
- Berriman, M., Ghedin, E., Hertz-Fowler, C., Blandin, G., Renauld, H., Bartholomeu, D.C., Lennard, N.J., Caler, E., Hamlin, N.E., Haas, B., Böhme, U., Hannick, L., Aslett, M.A., Shallom, J., Marcello, L., Hou, L., Wickstead, B., Alsmark, U.C.M., Arrowsmith, C., Atkin, R.J., Barron, A.J., Bringaud, F., Brooks, K., Carrington, M., Cherevach, I., Chillingworth, T.-J., Churcher, C., Clark, L.N., Corton, C.H., Cronin, A., Davies, R.M., Doggett, J., Djikeng, A., Feldblyum, T., Field, M.C., Fraser, A., Goodhead, I., Hance, Z., Harper, D., Harris, B.R., Hauser, H., Hostettler, J., Ivens, A., Jagels, K., Johnson, D., Johnson, J., Jones, K., Kerhornou, A.X., Koo, H., Larke, N., Landfear, S., Larkin, C., Leech, V., Line, A., Lord, A., MacLeod, A., Mooney, P.J., Moule, S., Martin, D.M.A., Morgan, G.W., Mungall, K., Norbertczak, H., Ormond, D., Pai, G., Peacock, C.S., Peterson, J., Quail, M.A., Rabbinowitsch, E., Rajandream, M.-A., Reitter, C., Salzberg, S.L., Sanders, M., Schobel, S., Sharp, S., Simmonds, M., Simpson, A.J., Tallon, L., Turner, C.M.R., Tait, A., Tivey, A.R., Van Aken, S., Walker, D., Wanless, D., Wang, S., White, B., White, O., Whitehead, S., Woodward, J., Wortman, J., Adams, M.D., Embley, T.M., Gull, K., Ullu, E., Barry, J.D., Fairlamb, A.H., Opperdoes, F., Barrell, B.G., Donelson, J.E., Hall, N., Fraser, C.M., Melville, S.E., El-Sayed, N.M., 2005. The Genome of the African Trypanosome *Trypanosoma brucei*. *Science* 309, 416. <https://doi.org/10.1126/science.1112642>
- Besteiro, S., Biran, M., Biteau, N., Coustou, V., Baltz, T., Canioni, P., Bringaud, F., 2002. Succinate Secreted by *Trypanosoma brucei* Is Produced by a Novel and Unique Glycosomal Enzyme, NADH-dependent Fumarate Reductase. *J. Biol. Chem.* 277, 38001–38012. <https://doi.org/10.1074/jbc.M201759200>
- Beyer, H.M., Gonschorek, P., Samodelov, S.L., Meier, M., Weber, W., Zurbriggen, M.D., 2015. AQUA Cloning: A Versatile and Simple Enzyme-Free Cloning Approach. *PLOS ONE* 10, e0137652. <https://doi.org/10.1371/journal.pone.0137652>
- Biebinger, S., Elizabeth Wirtz, L., Lorenz, P., Christine Clayton, 1997. Vectors for inducible expression of toxic gene products in bloodstream and procyclic *Trypanosoma brucei*. *Mol. Biochem. Parasitol.* 85, 99–112. [https://doi.org/10.1016/S0166-6851\(96\)02815-0](https://doi.org/10.1016/S0166-6851(96)02815-0)
- Bienen, E.J., Meturi, Raj.K., Pollakis, G., Clarkson, A.B., 1993. Non-cytochrome mediated mitochondrial ATP production in bloodstream form *Trypanosoma brucei brucei*. *Eur. J. Biochem.* 216, 75–80. <https://doi.org/10.1111/j.1432-1033.1993.tb18118.x>
- Bochud-Allemann, N., Schneider, A., 2002. Mitochondrial Substrate Level Phosphorylation Is Essential for Growth of Procyclic *Trypanosoma brucei*. *J. Biol. Chem.* 277, 32849–32854. <https://doi.org/10.1074/jbc.M205776200>
- Bringaud, F., Baltz, D., Baltz, T., 1998. Functional and molecular characterization of a glycosomal PP<sub>i</sub>-dependent enzyme in trypanosomatids: Pyruvate, phosphate dikinase. *Proc. Natl. Acad. Sci.* 95, 7963. <https://doi.org/10.1073/pnas.95.14.7963>
- Bringaud, F., Robinson, D.R., Barradeau, S., Biteau, N., Baltz, D., Baltz, T., 2000. Characterization and disruption of a new *Trypanosoma brucei* repetitive flagellum protein, using double-stranded RNA inhibition. *Mol. Biochem. Parasitol.* 111, 283–297. [https://doi.org/10.1016/S0166-6851\(00\)00319-4](https://doi.org/10.1016/S0166-6851(00)00319-4)

- Bringaud, F., Rivière, L., Coustou, V., 2006. Energy metabolism of trypanosomatids: Adaptation to available carbon sources. *Mol. Biochem. Parasitol.* 149, 1–9. <https://doi.org/10.1016/j.molbiopara.2006.03.017>
- Bringaud, F., Ebikeme, C., Boshart, M., 2010. Acetate and succinate production in amoebae, helminths, diplomonads, trichomonads and trypanosomatids: common and diverse metabolic strategies used by parasitic lower eukaryotes. *Parasitology* 137, 1315–1331. <https://doi.org/10.1017/S0031182009991843>
- Bringaud F, Barrett MP, Zilberstein D., 2012. Multiple roles of proline transport and metabolism in trypanosomatids. *Front Biosci (Landmark Ed)*. 17:349–74. doi: 10.2741/3931. PMID: 22201748.
- Bringaud, F., Biran, M., Millerioux, Y., Wargnies, M., Allmann, S., Mazet, M., 2015. Combining reverse genetics and nuclear magnetic resonance-based metabolomics unravels trypanosome-specific metabolic pathways. *Mol. Microbiol.* 96, 917–926. <https://doi.org/10.1111/mmi.12990>
- Brocard, C., Hartig, A., 2006. Peroxisome targeting signal 1: Is it really a simple tripeptide? *Biochim. Biophys. Acta BBA - Mol. Cell Res.* 1763, 1565–1573. <https://doi.org/10.1016/j.bbamcr.2006.08.022>
- Brown, E.D., Wood, J.M., 1993. Conformational change and membrane association of the PutA protein are coincident with reduction of its FAD cofactor by proline. *J. Biol. Chem.* 268, 8972–8979.
- Brun, R., Schönenberger, null, 1979. Cultivation and in vitro cloning or procyclic culture forms of *Trypanosoma brucei* in a semi-defined medium. Short communication. *Acta Trop.* 36, 289–292.
- Bursell, E., 1981. The Role of Proline in Energy Metabolism, in: Downer, R.G.H. (Ed.), *Energy Metabolism in Insects*. Springer US, Boston, MA, pp. 135–154. [https://doi.org/10.1007/978-1-4615-9221-1\\_5](https://doi.org/10.1007/978-1-4615-9221-1_5)
- Büscher, P., Gilman, Q., Lejon, V., 2013. Rapid Diagnostic Test for Sleeping Sickness. *N. Engl. J. Med.* 368, 1069–1070. <https://doi.org/10.1056/NEJMc1210373>
- Büscher, P., Mertens, P., Leclipteux, T., Gilman, Q., Jacquet, D., Mumba-Ngoyi, D., Pyana, P.P., Boelaert, M., Lejon, V., 2014. Sensitivity and specificity of HAT Sero-K-SeT, a rapid diagnostic test for serodiagnosis of sleeping sickness caused by *Trypanosoma brucei gambiense*: a case-control study. *Lancet Glob. Health* 2, e359–e363. [https://doi.org/10.1016/S2214-109X\(14\)70203-7](https://doi.org/10.1016/S2214-109X(14)70203-7)
- Büscher, P., Cecchi, G., Jamonneau, V., Priotto, G., 2017. Human African trypanosomiasis. *The Lancet* 390, 2397–2409. [https://doi.org/10.1016/S0140-6736\(17\)31510-6](https://doi.org/10.1016/S0140-6736(17)31510-6)
- Büscher, P., Bart, J.-M., Boelaert, M., Bucheton, B., Cecchi, G., Chitnis, N., Courtin, D., Figueiredo, L.M., Franco, J.-R., Grébaut, P., Hasker, E., Ilboudo, H., Jamonneau, V., Koffi, M., Lejon, V., MacLeod, A., Masumu, J., Matovu, E., Mattioli, R., Noyes, H., Picado, A., Rock, K.S., Rotureau, B., Simo, G., Thévenon, S., Trindade, S., Truc, P., Van Reet, N., 2018. Do Cryptic Reservoirs Threaten Gambiense-Sleeping Sickness Elimination? *Trends Parasitol.* 34, 197–207. <https://doi.org/10.1016/j.pt.2017.11.008>
- Butenko, A., Opperdoes, F.R., Flegontova, O., Horák, A., Hampl, V., Keeling, P., Gawryluk, R.M.R., Tikhonenkov, D., Flegontov, P., Lukeš, J., 2020. Evolution of metabolic capabilities and molecular features of diplomonids, kinetoplastids, and euglenids. *BMC Biol.* 18. <https://doi.org/10.1186/s12915-020-0754-1>
- Bütikofer, P., Ruepp, S., Boschung, M., Roditi, I., 1997. 'GPEET' procyclin is the major surface protein of procyclic culture forms of *Trypanosoma brucei brucei* strain 427. *Biochem. J.* 326, 415–423. <https://doi.org/10.1042/bj3260415>
- Caldas, R.A., Araújo, E.F., Felix, C.R., Roitman, I., Araujo, E.F., 1980. Incorporation of Ammonium in Amino Acids by *Trypanosoma cruzi*. *J. Parasitol.* 66, 213. <https://doi.org/10.2307/3280806>
- Caljon, G., Van Reet, N., De Trez, C., Vermeersch, M., Pérez-Morga, D., Van Den Abbeele, J., 2016. The Dermis as a Delivery Site of *Trypanosoma brucei* for Tsetse Flies. *PLOS Pathog.* 12, e1005744. <https://doi.org/10.1371/journal.ppat.1005744>
- Camara, Mariame, Soumah, A.M., Ilboudo, H., Travaillé, C., Clucas, C., Cooper, A., Kuispond Swar, N.-R., Camara, O., Sadissou, I., Calvo Alvarez, E., Crouzols, A., Bart, J.-M., Jamonneau, V., Camara, Mamadou, MacLeod, A., Bucheton, B., Rotureau, B., 2020. Extravascular Dermal Trypanosomes in Suspected and Confirmed Cases of gambiense Human African Trypanosomiasis. *Clin. Infect. Dis.* <https://doi.org/10.1093/cid/ciaa897>
- Capewell, P., Cren-Travaillé, C., Marchesi, F., Johnston, P., Clucas, C., Benson, R.A., Gorman, T.-A., Calvo-Alvarez, E., Crouzols, A., Jouvion, G., Jamonneau, V., Weir, W., Stevenson, M.L., O'Neill, K., Cooper, A., Swar, N.K., Bucheton, B., Ngoyi, D.M., Garside, P., Rotureau, B., MacLeod, A., 2016. The skin is a significant but overlooked anatomical reservoir for vector-borne African trypanosomes. *eLife* 5, e17716. <https://doi.org/10.7554/eLife.17716>



- Capewell, P., Atkins, K., Weir, W., Jamonneau, V., Camara, M., Clucas, C., Swar, N.-R.K., Ngoyi, D.M., Rotureau, B., Garside, P., Galvani, A.P., Bucheton, B., MacLeod, A., 2019. Resolving the apparent transmission paradox of African sleeping sickness. *PLOS Biol.* 17, e3000105. <https://doi.org/10.1371/journal.pbio.3000105>
- Casareno, R.L.B., Waggoner, D., Gitlin, J.D., 1998. The Copper Chaperone CCS Directly Interacts with Copper/Zinc Superoxide Dismutase. *J. Biol. Chem.* 273, 23625–23628. <https://doi.org/10.1074/jbc.273.37.23625>
- Casas-Sánchez, A., Perally, S., Ramaswamy, R., Haines, L.R., Rose, C., Yunta, C., Aguilera-Flores, M., Lehane, M.J., Almeida, I.C., Boulanger, M.J., Acosta-Serrano, A., 2018. The crystal structure and localisation of *Trypanosoma brucei* invariant surface glycoproteins suggest a more permissive VSG coat in the tsetse-transmitted metacyclic stage (preprint). *Microbiology*. <https://doi.org/10.1101/477737>
- Cayla, M., Rojas, F., Silvester, E., Venter, F., Matthews, K.R., 2019. African trypanosomes. *Parasit. Vectors* 12. <https://doi.org/10.1186/s13071-019-3355-5>
- Cazzulo, J.J., de Cazzulo, B.M.F., Higa, A.I., Segura, E.L., 1979. NAD-linked glutamate dehydrogenase in *Trypanosoma cruzi*. *Comp. Biochem. Physiol. Part B Comp. Biochem.* 64, 129–131. [https://doi.org/10.1016/0305-0491\(79\)90197-4](https://doi.org/10.1016/0305-0491(79)90197-4)
- Chambers, J.K., Macdonald, L.E., Sarau, H.M., Ames, R.S., Freeman, K., Foley, J.J., Zhu, Y., McLaughlin, M.M., Murdock, P., McMillan, L., Trill, J., Swift, A., Aiyar, N., Taylor, P., Vawter, L., Naheed, S., Szekeres, P., Hervieu, G., Scott, C., Watson, J.M., Murphy, A.J., Duzic, E., Klein, C., Bergsma, D.J., Wilson, S., Livi, G.P., 2000. A G Protein-coupled Receptor for UDP-glucose. *J. Biol. Chem.* 275, 10767–10771. <https://doi.org/10.1074/jbc.275.15.10767>
- Chanez, A.-L., Hehl, A.B., Engstler, M., Schneider, A., 2006. Ablation of the single dynamin of *T. brucei* blocks mitochondrial fission and endocytosis and leads to a precise cytokinesis arrest. *J. Cell Sci.* 119, 2968. <https://doi.org/10.1242/jcs.03023>
- Chen, M., Qiu, T., Wu, J., Yang, Y., Wright, G.D., Wu, M., Ge, R., 2018. Extracellular anti-angiogenic proteins augment an endosomal protein trafficking pathway to reach mitochondria and execute apoptosis in HUVECs. *Cell Death Differ.* 25, 1905–1920. <https://doi.org/10.1038/s41418-018-0092-9>
- Chitanga, S., Marcotty, T., Namangala, B., Van den Bossche, P., Van Den Abbeele, J., Delespau, V., 2011. High Prevalence of Drug Resistance in Animal Trypanosomes without a History of Drug Exposure. *PLoS Negl. Trop. Dis.* 5, e1454. <https://doi.org/10.1371/journal.pntd.0001454>
- Clarkson, A.B., Bienen, E.J., Pollakis, G., Grady, R.W., 1989. Respiration of bloodstream forms of the parasite *Trypanosoma brucei brucei* is dependent on a plant-like alternative oxidase. *J. Biol. Chem.* 264, 17770–17776.
- Clayton, C., Michaeli, S., 2011. 3' processing in protists: 3' processing in protists. *Wiley Interdiscip. Rev. RNA* 2, 247–255. <https://doi.org/10.1002/wrna.49>
- Clayton, C., 2019. Regulation of gene expression in trypanosomatids: living with polycistronic transcription. *Open Biol.* 9, 190072. <https://doi.org/10.1098/rsob.190072>
- Colasante, C., Ellis, M., Ruppert, T., Voncken, F., 2006. Comparative proteomics of glycosomes from bloodstream form and procyclic culture form *Trypanosoma brucei brucei*. *PROTEOMICS* 6, 3275–3293. <https://doi.org/10.1002/pmic.200500668>
- Colasante, C., Robles, A., Li, C.-H., Schwede, A., Benz, C., Voncken, F., Guilbride, D.L., Clayton, C., 2007. Regulated expression of glycosomal phosphoglycerate kinase in *Trypanosoma brucei*. *Mol. Biochem. Parasitol.* 151, 193–204. <https://doi.org/10.1016/j.molbiopara.2006.11.003>
- Costello, J.L., Castro, I.G., Hacker, C., Schrader, T.A., Metz, J., Zeuschner, D., Azadi, A.S., Godinho, L.F., Costina, V., Findeisen, P., Manner, A., Islinger, M., Schrader, M., 2017. ACBD5 and VAPB mediate membrane associations between peroxisomes and the ER. *J. Cell Biol.* 216, 331–342. <https://doi.org/10.1083/jcb.201607055>
- Costello, J.L., Schrader, M., 2018. Unloosing the Gordian knot of peroxisome formation. *Cell Archit.* 50, 50–56. <https://doi.org/10.1016/j.ceb.2018.02.002>
- Courtin, F., Camara, M., Rayaisse, J.-B., Kagbadouno, M., Dama, E., Camara, O., Traoré, I.S., Rouamba, J., Peylhard, M., Somda, M.B., Leno, M., Lehane, M.J., Torr, S.J., Solano, P., Jamonneau, V., Bucheton, B., 2015. Reducing Human-Tsetse Contact Significantly Enhances the Efficacy of Sleeping Sickness Active Screening Campaigns: A Promising Result in the Context of Elimination. *PLoS Negl. Trop. Dis.* 9, e0003727. <https://doi.org/10.1371/journal.pntd.0003727>
- Coustou, V., Besteiro, S., Biran, M., Diolez, P., Bouchaud, V., Voisin, P., Michels, P.A.M., Canioni, P., Baltz, T., Bringaud, F., 2003. ATP generation in the *Trypanosoma brucei* Procyclic Form:

- cytosolic substrate level phosphorylation is essential, but not oxidative phosphorylation. *J. Biol. Chem.* 278, 49625–49635. <https://doi.org/10.1074/jbc.M307872200>
- Coustou, V., Besteiro, S., Rivière, L., Biran, M., Biteau, N., Franconi, J.-M., Boshart, M., Baltz, T., Bringaud, F., 2005. A Mitochondrial NADH-dependent Fumarate Reductase Involved in the Production of Succinate Excreted by Procyclic *Trypanosoma brucei*. *J. Biol. Chem.* 280, 16559–16570. <https://doi.org/10.1074/jbc.M500343200>
- Coustou, V., Biran, M., Besteiro, S., Rivière, L., Baltz, T., Franconi, J.-M., Bringaud, F., 2006. Fumarate Is an Essential Intermediary Metabolite Produced by the Procyclic *Trypanosoma brucei*. *J. Biol. Chem.* 281, 26832–26846. <https://doi.org/10.1074/jbc.M601377200>
- Coustou, V., Biran, M., Breton, M., Guegan, F., Rivière, L., Plazolles, N., Nolan, D., Barrett, M.P., Franconi, J.-M., Bringaud, F., 2008. Glucose-induced Remodeling of Intermediary and Energy Metabolism in Procyclic *Trypanosoma brucei*. *J. Biol. Chem.* 283, 16342–16354. <https://doi.org/10.1074/jbc.M709592200>
- Creek, D.J., Chokkathukalam, A., Jankevics, A., Burgess, K.E.V., Breitling, R., Barrett, M.P., 2012. Stable Isotope-Assisted Metabolomics for Network-Wide Metabolic Pathway Elucidation. *Anal. Chem.* 84, 8442–8447. <https://doi.org/10.1021/ac3018795>
- Creek, D.J., Mazet, M., Achcar, F., Anderson, J., Kim, D.-H., Kamour, R., Morand, P., Millerioux, Y., Biran, M., Kerkhoven, E.J., Chokkathukalam, A., Weidt, S.K., Burgess, K.E.V., Breitling, R., Watson, D.G., Bringaud, F., Barrett, M.P., 2015. Probing the Metabolic Network in Bloodstream-Form *Trypanosoma brucei* Using Untargeted Metabolomics with Stable Isotope Labelled Glucose. *PLOS Pathog.* 11, e1004689. <https://doi.org/10.1371/journal.ppat.1004689>
- Cross, G.A.M., Klein, R.A., Linstead, D.J., 1975. Utilisation of amino acids by *Trypanosoma brucei* in culture: L-threonine as a precursor for acetate. *Parasitology* 71, 311–326. <https://doi.org/10.1017/S0031182000046758>
- Cross, G.A.M., Kim, H.-S., Wickstead, B., 2014. Capturing the variant surface glycoprotein repertoire (the VSGnome) of *Trypanosoma brucei* Lister 427. *Mol. Biochem. Parasitol.* 195, 59–73. <https://doi.org/10.1016/j.molbiopara.2014.06.004>
- Cull, B., Prado Godinho, J.L., Fernandes Rodrigues, J.C., Frank, B., Schurigt, U., Williams, R.A., Coombs, G.H., Mottram, J.C., 2014. Glycosome turnover in *Leishmania major* is mediated by autophagy. *Autophagy* 10, 2143–2157. <https://doi.org/10.4161/auto.36438>
- Damerow, S., Lamerz, A.-C., Haselhorst, T., Fühling, J., Zarnovican, P., von Itzstein, M., Routier, F.H., 2010. *Leishmania* UDP-sugar Pyrophosphorylase: The missing link in galactose salvage? *J. Biol. Chem.* 285, 878–887. <https://doi.org/10.1074/jbc.M109.067223>
- Damerow, S., 2010. Identification and Characterization of *Leishmania major* UDP-sugar Pyrophosphorylase and Determination of its Impact on UDP-galactose Metabolism. Hannover : Gottfried Wilhelm Leibniz Universität, Diss., 2010, 94 S. <https://doi.org/10.15488/7378>
- Damerow, M., Rodrigues, J.A., Wu, D., Güther, M.L.S., Mehlert, A., Ferguson, M.A.J., 2014. Identification and Functional Characterization of a Highly Divergent N-Acetylglucosaminyltransferase I (TbGnTI) in *Trypanosoma brucei*. *J. Biol. Chem.* 289, 9328–9339. <https://doi.org/10.1074/jbc.M114.555029>
- Damerow, S., Hoppe, C., Bandini, G., Zarnovican, P., Buettner, F.F.R., Ferguson, M.A.J., Routier, F.H., 2015a. *Leishmania major* UDP-sugar pyrophosphorylase salvages galactose for glycoconjugate biosynthesis. *Int. J. Parasitol.* 45, 783–790. <https://doi.org/10.1016/j.ijpara.2015.06.004>
- Damerow, S., Hoppe, C., Bandini, G., Zarnovican, P., Buettner, F.R., Lüder, C.G.K., Ferguson, M.A.J., Routier, F.H., 2015b. Depletion of UDP-Glucose and UDP-Galactose Using a Degron System Leads to Growth Cessation of *Leishmania major*. *PLoS Negl. Trop. Dis.* 9, e0004205. <https://doi.org/10.1371/journal.pntd.0004205>
- Damerow, M., Graalfs, F., Güther, M.L.S., Mehlert, A., Izquierdo, L., Ferguson, M.A.J., 2016. A Gene of the  $\beta$ 3-Glycosyltransferase Family Encodes N-Acetylglucosaminyltransferase II Function in *Trypanosoma brucei*. *J. Biol. Chem.* 291, 13834–13845. <https://doi.org/10.1074/jbc.M116.733246>
- Dawidowski, M., Emmanouilidis, L., Kalel, V.C., Tripsianes, K., Schorpp, K., Hadian, K., Kaiser, M., Mäser, P., Kolonko, M., Tanghe, S., Rodriguez, A., Schliebs, W., Erdmann, R., Sattler, M., Popowicz, G.M., 2017. Inhibitors of PEX14 disrupt protein import into glycosomes and kill *Trypanosoma* parasites. *Science* 355, 1416. <https://doi.org/10.1126/science.aal1807>
- Dean, S., Sunter, J., Wheeler, R.J., Hodgkinson, I., Gluenz, E., Gull, K., 2015. A toolkit enabling efficient, scalable and reproducible gene tagging in trypanosomatids. *Open Biol.* 5, 140197–140197. <https://doi.org/10.1098/rsob.140197>

- Dean, S., Sunter, J.D., Wheeler, R.J., 2017. TrypTag.org: A Trypanosome Genome-wide Protein Localisation Resource. *Trends Parasitol.* 33, 80–82. <https://doi.org/10.1016/j.pt.2016.10.009>
- Decker, D., Meng, M., Gornicka, A., Hofer, A., Wilczynska, M., Kleczkowski, L.A., 2012. Substrate kinetics and substrate effects on the quaternary structure of barley UDP-glucose pyrophosphorylase. *Phytochemistry* 79, 39–45. <https://doi.org/10.1016/j.phytochem.2012.04.002>
- Decker, D., Kleczkowski, L., 2019. UDP-Sugar Producing Pyrophosphorylases: Distinct and Essential Enzymes With Overlapping Substrate Specificities, Providing de novo Precursors for Glycosylation Reactions. *Front. Plant Sci.* 9, 1822. <https://doi.org/10.3389/fpls.2018.01822>
- Delespaulx, V., Geysen, D., Van den Bossche, P., Geerts, S., 2008. Molecular tools for the rapid detection of drug resistance in animal trypanosomes. *Trends Parasitol.* 24, 236–242. <https://doi.org/10.1016/j.pt.2008.02.006>
- Delille, H.K., Agricola, B., Guimaraes, S.C., Borta, H., Lüers, G.H., Fransen, M., Schrader, M., 2010. Pex11p $\beta$ -mediated growth and division of mammalian peroxisomes follows a maturation pathway. *J. Cell Sci.* 123, 2750. <https://doi.org/10.1242/jcs.062109>
- DeLoache, W.C., Russ, Z.N., Dueber, J.E., 2016. Towards repurposing the yeast peroxisome for compartmentalizing heterologous metabolic pathways. *Nat. Commun.* 7, 11152. <https://doi.org/10.1038/ncomms11152>
- Denton, H., Fyffe, S., Smith, T.K., 2010. GDP-mannose pyrophosphorylase is essential in the bloodstream form of *Trypanosoma brucei*. *Biochem. J.* 425, 603–614. <https://doi.org/10.1042/BJ20090896>
- Deschamps, P., Lara, E., Marande, W., Lopez-Garcia, P., Ekelund, F., Moreira, D., 2011. Phylogenomic Analysis of Kinetoplastids Supports That Trypanosomatids Arose from within Bodonids. *Mol. Biol. Evol.* 28, 53–58. <https://doi.org/10.1093/molbev/msq289>
- Dewar, C.E., MacGregor, P., Cooper, S., Gould, M.K., Matthews, K.R., Savill, N.J., Schnauffer, A., 2018. Mitochondrial DNA is critical for longevity and metabolism of transmission stage *Trypanosoma brucei*. *PLOS Pathog.* 14, e1007195. <https://doi.org/10.1371/journal.ppat.1007195>
- Dias, A.F., Rodrigues, T.A., Pedrosa, A.G., Barros-Barbosa, A., Francisco, T., Azevedo, J.E., 2017. The peroxisomal matrix protein translocon is a large cavity-forming protein assembly into which PEX5 protein enters to release its cargo. *J. Biol. Chem.* 292, 15287–15300. <https://doi.org/10.1074/jbc.M117.805044>
- Dickie, E.A., Giordani, F., Gould, M.K., Mäser, P., Burri, C., Mottram, J.C., Rao, S.P.S., Barrett, M.P., 2020. New Drugs for Human African Trypanosomiasis: A Twenty First Century Success Story. *Trop. Med. Infect. Dis.* 5, 29. <https://doi.org/10.3390/tropicalmed5010029>
- Dolezelova, Eva; Taleva, Gergana; Panicucci, Brian; Hierro-Yap, Carolina; Husova, Michaela; Pineda, Erika; Bringaud, Frederic; Zíková, Alena. 2019. The *Trypanosoma brucei* infectious form mitochondrion is capable of ATP generation. Paper presented at the 8th Kinetoplastid Molecular Cell Biology Meeting, Woods Hole, USA. Retrieved from <https://www.mbl.edu/conferences/2019/04/19/kinetoplastid-molecular-cell-biology-2019-abstract-book/>
- Doleželová, E., Kunzová, M., DeJung, M., Levin, M., Panicucci, B., Regnault, C., Janzen, C.J., Barrett, M.P., Butter, F., Zíková, A., 2020. Cell-based and multi-omics profiling reveals dynamic metabolic repurposing of mitochondria to drive developmental progression of *Trypanosoma brucei*. *PLOS Biol.* 18, e3000741. <https://doi.org/10.1371/journal.pbio.3000741>
- Duschak, V.G., Cazzulo, J.J., 1991. Subcellular localisation of glutamate dehydrogenases and alanine aminotransferase in epimastigotes of *Trypanosoma cruzi*. *FEMS Microbiol. Lett.* 83, 131–136. <https://doi.org/10.1111/j.1574-6968.1991.tb04429.x>
- Ebrecht, A.C., Asención Diez, M.D., Piattoni, C.V., Guerrero, S.A., Iglesias, A.A., 2015. The UDP-glucose pyrophosphorylase from *Giardia lamblia* is redox regulated and exhibits promiscuity to use galactose-1-phosphate. *Biochim. Biophys. Acta BBA - Gen. Subj.* 1850, 88–96. <https://doi.org/10.1016/j.bbagen.2014.10.002>
- Effelsberg, D., Cruz-Zaragoza, L.D., Tonillo, J., Schliebs, W., Erdmann, R., 2015. Role of Pex21p for Piggyback Import of Gpd1p and Pnc1p into Peroxisomes of *Saccharomyces cerevisiae*. *J. Biol. Chem.* 290, 25333–25342. <https://doi.org/10.1074/jbc.M115.653451>
- El Magraoui, F., Bäumer, B.E., Platta, H.W., Baumann, J.S., Girzalsky, W., Erdmann, R., 2012. The RING-type ubiquitin ligases Pex2p, Pex10p and Pex12p form a heteromeric complex that displays enhanced activity in an ubiquitin conjugating enzyme-selective manner. *FEBS J.* 279, 2060–2070. <https://doi.org/10.1111/j.1742-4658.2012.08591.x>
- Elgersma, Y., Vos, A., van den Berg, M., van Roermund, C.W.T., van der Sluijs, P., Distel, B., Tabak, H.F., 1996. Analysis of the Carboxyl-terminal Peroxisomal Targeting Signal 1 in a Homologous

- Context in *Saccharomyces cerevisiae*. J. Biol. Chem. 271, 26375–26382. <https://doi.org/10.1074/jbc.271.42.26375>
- Engqvist, M.K.M., Eßer, C., Maier, A., Lercher, M.J., Maurino, V.G., 2014. Mitochondrial 2-hydroxyglutarate metabolism. Mitochondrion 19, 275–281. <https://doi.org/10.1016/j.mito.2014.02.009>
- Erdmann, R., Schliebs, W., 2005. Peroxisomal matrix protein import: the transient pore model. Nat. Rev. Mol. Cell Biol. 6, 738–742. <https://doi.org/10.1038/nrm1710>
- Ersfeld, K., 2011. Nuclear architecture, genome and chromatin organisation in *Trypanosoma brucei*. Res. Microbiol. 162, 626–636. <https://doi.org/10.1016/j.resmic.2011.01.014>
- Estévez, A.M., Kierszenbaum, F., Wirtz, E., Bringaud, F., Grunstein, J., Simpson, L., 1999. Knockout of the glutamate dehydrogenase gene in bloodstream *Trypanosoma brucei* in culture has no effect on editing of mitochondrial mRNAs. Mol. Biochem. Parasitol. 100, 5–17. [https://doi.org/10.1016/S0166-6851\(99\)00024-9](https://doi.org/10.1016/S0166-6851(99)00024-9)
- Fairlamb, A.H., Horn, D., 2018. Melarsoprol Resistance in African Trypanosomiasis. Trends Parasitol. 34, 481–492. <https://doi.org/10.1016/j.pt.2018.04.002>
- Fang, J., Beattie, D.S., 2002. Novel FMN-Containing Rotenone-Insensitive NADH Dehydrogenase from *Trypanosoma brucei* Mitochondria: Isolation and Characterization. Biochemistry 41, 3065–3072. <https://doi.org/10.1021/bi015989w>
- Faria, J., Glover, L., Hutchinson, S., Boehm, C., Field, M.C., Horn, D., 2019. Monoallelic expression and epigenetic inheritance sustained by a *Trypanosoma brucei* variant surface glycoprotein exclusion complex. Nat. Commun. 10. <https://doi.org/10.1038/s41467-019-10823-8>
- Fatarova, M., Bellvert, F., Cahoreau, E., Bringaud, F., Portais, J.-C., 2016. Methods to Investigate Metabolic Systems in *Trypanosoma*, in: Müller, S., Cerdan, R., Radulescu, O. (Eds.), Comprehensive Analysis of Parasite Biology: From Metabolism to Drug Discovery. Wiley-VCH Verlag GmbH & Co. KGaA, Weinheim, Germany, pp. 295–320. <https://doi.org/10.1002/9783527694082.ch13>
- Ferguson, M., Homans, S., Dwek, R., Rademacher, T., 1988. Glycosyl-phosphatidylinositol moiety that anchors *Trypanosoma brucei* variant surface glycoprotein to the membrane. Science 239, 753. <https://doi.org/10.1126/science.3340856>
- Ferguson, M.A., Murray, P., Rutherford, H., McConville, M.J., 1993. A simple purification of procyclic acidic repetitive protein and demonstration of a sialylated glycosyl-phosphatidylinositol membrane anchor. Biochem. J. 291, 51–55. <https://doi.org/10.1042/bj2910051>
- Ferguson, M.A.J., 1997. The surface glycoconjugates of trypanosomatid parasites. Philos. Trans. R. Soc. B Biol. Sci. 352, 1295–1302. <https://doi.org/10.1098/rstb.1997.0113>
- Ferguson, M.A.J., 2000. Glycosylphosphatidylinositol biosynthesis validated as a drug target for African sleeping sickness. Proc. Natl. Acad. Sci. 97, 10673–10675. <https://doi.org/10.1073/pnas.97.20.10673>
- Field, M.C., Menon, A.K., Cross, G.A., 1991. A glycosylphosphatidylinositol protein anchor from procyclic stage *Trypanosoma brucei*: lipid structure and biosynthesis. EMBO J. 10, 2731–2739. <https://doi.org/10.1002/j.1460-2075.1991.tb07821.x>
- Flynn, I.W., Bowman, I.B.R., 1973. The metabolism of carbohydrate by pleomorphic African trypanosomes. Comp. Biochem. Physiol. Part B Comp. Biochem. 45, 25–42. [https://doi.org/10.1016/0305-0491\(73\)90281-2](https://doi.org/10.1016/0305-0491(73)90281-2)
- Forchhammer, K., Selim, K.A., 2020. Carbon/nitrogen homeostasis control in cyanobacteria. FEMS Microbiol. Rev. 44, 33–53. <https://doi.org/10.1093/femsre/fuz025>
- Franco, J.R., Cecchi, G., Priotto, G., Paone, M., Diarra, A., Grout, L., Simarro, P.P., Zhao, W., Argaw, D., 2020. Monitoring the elimination of human African trypanosomiasis at continental and country level: Update to 2018. PLoS Negl. Trop. Dis. 14, e0008261. <https://doi.org/10.1371/journal.pntd.0008261>
- Freitas, M.O., Francisco, T., Rodrigues, T.A., Alencastre, I.S., Pinto, M.P., Grou, C.P., Carvalho, A.F., Fransen, M., Sá-Miranda, C., Azevedo, J.E., 2011. PEX5 protein binds monomeric catalase blocking its tetramerization and releases it upon binding the N-terminal domain of PEX14. J. Biol. Chem. 286, 40509–40519. <https://doi.org/10.1074/jbc.M111.287201>
- Freitas, M.O., Francisco, T., Rodrigues, T.A., Lismont, C., Domingues, P., Pinto, M.P., Grou, C.P., Fransen, M., Azevedo, J.E., 2015. The peroxisomal protein import machinery displays a preference for monomeric substrates. Open Biol. 5, 140236–140236. <https://doi.org/10.1098/rsob.140236>
- Fühling, J., Cramer, J.T., Routier, F.H., Lamerz, A.-C., Baruch, P., Gerardy-Schahn, R., Fedorov, R., 2013. Catalytic Mechanism and Allosteric Regulation of UDP-Glucose Pyrophosphorylase from *Leishmania major*. ACS Catal. 3, 2976–2985. <https://doi.org/10.1021/cs4007777>

- Fühning, J.I., Cramer, J.T., Schneider, J., Baruch, P., Gerardy-Schahn, R., Fedorov, R., 2015. A Quaternary Mechanism Enables the Complex Biological Functions of Octameric Human UDP-glucose Pyrophosphorylase, a Key Enzyme in Cell Metabolism. *Sci. Rep.* 5. <https://doi.org/10.1038/srep09618>
- Furuya, T., Kessler, P., Jardim, A., Schnauffer, A., Crudder, C., Parsons, M., 2002. Glucose is toxic to glycosome-deficient trypanosomes. *Proc. Natl. Acad. Sci. U. S. A.* 99, 14177–14182. <https://doi.org/10.1073/pnas.222454899>
- Galland, N., Michels, P.A.M., 2010. Comparison of the peroxisomal matrix protein import system of different organisms. Exploration of possibilities for developing inhibitors of the import system of trypanosomatids for anti-parasite chemotherapy. *Eur. J. Cell Biol.* 89, 621–637. <https://doi.org/10.1016/j.ejcb.2010.04.001>
- Ghozlane, A., Bringaud, F., Soueidan, H., Dutour, I., Jourdan, F., Thébault, P., 2012. Flux Analysis of the *Trypanosoma brucei* Glycolysis Based on a Multiobjective-Criteria Bioinformatic Approach. *Adv. Bioinforma.* 2012, 159423–159423. <https://doi.org/10.1155/2012/159423>
- Gibson, W., 2016. Kinetoplastea, in: Archibald, J.M., Simpson, A.G.B., Slamovits, C.H., Margulis, L., Melkonian, M., Chapman, D.J., Corliss, J.O. (Eds.), *Handbook of the Protists*. Springer International Publishing, Cham, pp. 1–50. [https://doi.org/10.1007/978-3-319-32669-6\\_7-1](https://doi.org/10.1007/978-3-319-32669-6_7-1)
- Giordani, F., Morrison, L.J., Rowan, T.G., De Koning, H.P., Barrett, M.P., 2016. The animal trypanosomiasis and their chemotherapy: a review. *Parasitology* 143, 1862–1889. <https://doi.org/10.1017/S0031182016001268>
- Girard, R.M.B.M., Crispim, M., Alencar, M.B., Silber, A.M., 2018. Uptake of L-Alanine and Its Distinct Roles in the Bioenergetics of *Trypanosoma cruzi*. *mSphere* 3, e00338-18. <https://doi.org/10.1128/mSphereDirect.00338-18>
- Glover, J.R., Andrews, D.W., Rachubinski, R.A., 1994. *Saccharomyces cerevisiae* peroxisomal thiolase is imported as a dimer. *Proc. Natl. Acad. Sci.* 91, 10541–10545. <https://doi.org/10.1073/pnas.91.22.10541>
- Grunfelder, C.G., Engstler, M., Weise, F., Schwarz, H., Stierhof, Y.-D., Boshart, M., Overath, P., 2002. Accumulation of a GPI-Anchored Protein at the Cell Surface Requires Sorting at Multiple Intracellular Levels. *Traffic* 3, 547–559. <https://doi.org/10.1034/j.1600-0854.2002.30805.x>
- Gualdrón-López, M., Brennand, A., Hannaert, V., Quiñones, W., Cáceres, A.J., Bringaud, F., Concepción, J.L., Michels, P.A.M., 2012a. When, how and why glycolysis became compartmentalised in the Kinetoplastea. A new look at an ancient organelle. *Int. J. Parasitol.* 42, 1–20. <https://doi.org/10.1016/j.ijpara.2011.10.007>
- Gualdrón-López, M., Vapola, M.H., Miinalainen, I.J., Hiltunen, J.K., Michels, P.A.M., Antonenkov, V.D., 2012b. Channel-Forming Activities in the Glycosomal Fraction from the Bloodstream Form of *Trypanosoma brucei*. *PLoS ONE* 7, e34530. <https://doi.org/10.1371/journal.pone.0034530>
- Gualdrón-López, M., Brennand, A., Avilan, L., Michels, P.A.M., 2013a. Translocation of solutes and proteins across the glycosomal membrane of trypanosomes; possibilities and limitations for targeting with trypanocidal drugs. *Parasitology* 140, 1–20. <https://doi.org/10.1017/S0031182012001278>
- Gualdrón-López, M., Chevalier, N., Van Der Smissen, P., Courtoy, P.J., Rigden, D.J., Michels, P.A.M., 2013b. Ubiquitination of the glycosomal matrix protein receptor PEX5 in *Trypanosoma brucei* by PEX4 displays novel features. *Biochim. Biophys. Acta BBA - Mol. Cell Res.* 1833, 3076–3092. <https://doi.org/10.1016/j.bbamcr.2013.08.008>
- Guerra, D.G., Decottignies, A., Bakker, B.M., Michels, P.A.M., 2006. The mitochondrial FAD-dependent glycerol-3-phosphate dehydrogenase of Trypanosomatidae and the glycosomal redox balance of insect stages of *Trypanosoma brucei* and *Leishmania spp.* *Mol. Biochem. Parasitol.* 149, 155–169. <https://doi.org/10.1016/j.molbiopara.2006.05.006>
- Gullberg, M., Andersson, A.-C., 2010. Visualization and quantification of protein-protein interactions in cells and tissues. *Nat. Methods* 7, v–vi. <https://doi.org/10.1038/nmeth.f.306>
- Günzl, A., Bruderer, T., Laufer, G., Schimanski, B., Tu, L.-C., Chung, H.-M., Lee, P.-T., Lee, M.G.-S., 2003. RNA Polymerase I Transcribes Procyclin Genes and Variant Surface Glycoprotein Gene Expression Sites in *Trypanosoma brucei*. *Eukaryot. Cell* 2, 542–551. <https://doi.org/10.1128/EC.2.3.542-551.2003>
- Günzl, A., 2010. The Pre-mRNA Splicing Machinery of Trypanosomes: Complex or Simplified? *Eukaryot. Cell* 9, 1159–1170. <https://doi.org/10.1128/EC.00113-10>
- Gurvitz, A., Mursula, A.M., Yagi, A.I., Hartig, A., Ruis, H., Rottensteiner, H., Hiltunen, J.K., 1999. Alternatives to the Isomerase-dependent Pathway for the  $\beta$ -Oxidation of Oleic Acid Are Dispensable in *Saccharomyces cerevisiae*: Identification of YOR180c/DCI1 encoding

- peroxisomal  $\Delta 3,5$  - $\Delta 2,4$  -dienoyl-CoA isomerase. *J. Biol. Chem.* 274, 24514–24521. <https://doi.org/10.1074/jbc.274.35.24514>
- Güther, M.L.S., Urbaniak, M.D., Tavendale, A., Prescott, A., Ferguson, M.A.J., 2014. High-confidence glycosome proteome for procyclic form *Trypanosoma brucei* by epitope-tag organelle enrichment and SILAC proteomics. *J. Proteome Res.* 13, 2796–2806. <https://doi.org/10.1021/pr401209w>
- Haanstra, J.R., van Tuijl, A., Kessler, P., Reijnders, W., Michels, P.A.M., Westerhoff, H.V., Parsons, M., Bakker, B.M., 2008. Compartmentation prevents a lethal turbo-explosion of glycolysis in trypanosomes. *Proc. Natl. Acad. Sci.* 105, 17718. <https://doi.org/10.1073/pnas.0806664105>
- Haanstra, J.R., Bakker, B.M., Michels, P.A.M., 2014. In or out? On the tightness of glycosomal compartmentalization of metabolites and enzymes in *Trypanosoma brucei*. *Mol. Biochem. Parasitol.* 198, 18–28. <https://doi.org/10.1016/j.molbiopara.2014.11.004>
- Haanstra, J.R., González-Marcano, E.B., Gualdrón-López, M., Michels, P.A.M., 2016. Biogenesis, maintenance and dynamics of glycosomes in trypanosomatid parasites. *Biochim. Biophys. Acta BBA - Mol. Cell Res.* 1863, 1038–1048. <https://doi.org/10.1016/j.bbamcr.2015.09.015>
- Hagen, S., Drepper, F., Fischer, S., Fodor, K., Passon, D., Platta, H.W., Zenn, M., Schliebs, W., Girzalsky, W., Wilmanns, M., Warscheid, B., Erdmann, R., 2015. Structural insights into cargo recognition by the yeast PTS1 receptor. *J. Biol. Chem.* 290, 26610–26626. <https://doi.org/10.1074/jbc.M115.657973>
- Hager, K.M., Pierce, M.A., Moore, D.R., Tytler, E.M., Esko, J.D., Hajduk, S.L., 1994. Endocytosis of a cytotoxic human high density lipoprotein results in disruption of acidic intracellular vesicles and subsequent killing of African trypanosomes. *J. Cell Biol.* 126, 155–167. <https://doi.org/10.1083/jcb.126.1.155>
- Hajduk, S., Ochsenreiter, T., 2010. RNA editing in kinetoplastids. *RNA Biol.* 7, 229–236. <https://doi.org/10.4161/rna.7.2.11393>
- Hall, R.J., Flanagan, L.A., Bottery, M.J., Springthorpe, V., Thorpe, S., Darby, A.C., Wood, A.J., Thomas, G.H., 2019. A Tale of Three Species: Adaptation of *Sodalis glossinidius* to Tsetse Biology, *Wigglesworthia* Metabolism, and Host Diet. *mBio* 10, e02106-18. <https://doi.org/10.1128/mBio.02106-18>
- Harden, T.K., Sesma, J.I., Fricks, I.P., Lazarowski, E.R., 2010. Signalling and pharmacological properties of the P2Y<sub>14</sub> receptor. *Acta Physiol.* 199, 149–160. <https://doi.org/10.1111/j.1748-1716.2010.02116.x>
- Heise, N., Opperdoes, F.R., 1999. Purification, localisation and characterisation of glucose-6-phosphate dehydrogenase of *Trypanosoma brucei*. *Mol. Biochem. Parasitol.* 99, 21–32. [https://doi.org/10.1016/S0166-6851\(98\)00176-5](https://doi.org/10.1016/S0166-6851(98)00176-5)
- Hemphill, A., Lawson, D., Seebeck, T., 1991. The Cytoskeletal Architecture of *Trypanosoma brucei*. *J. Parasitol.* 77, 603. <https://doi.org/10.2307/3283167>
- Herman, M., Pérez-Morga, D., Schtickzelle, N., Michels, P.A.M., 2008. Turnover of glycosomes during life-cycle differentiation of *Trypanosoma brucei*. *Autophagy* 4, 294–308. <https://doi.org/10.4161/auto.5443>
- Hirumi, H., Hirumi, K., 1989. Continuous Cultivation of *Trypanosoma brucei* Blood Stream Forms in a Medium Containing a Low Concentration of Serum Protein without Feeder Cell Layers. *J. Parasitol.* 75, 985. <https://doi.org/10.2307/3282883>
- Hoare, C.A., 1966. The classification of mammalian trypanosomes, in: Henle, W., Kikuth, W., Meyer, K.F., Nauck, E.G., Tomcsik, J. (Eds.), *Ergebnisse Der Mikrobiologie Immunitätsforschung Und Experimentellen Therapie: Fortsetzung Der Ergebnisse Der Hygiene Bakteriologie · Immunitätsforschung Und Experimentellen Therapie Begründet von Wolfgang Weichardt*. Springer Berlin Heidelberg, Berlin, Heidelberg, pp. 43–57. [https://doi.org/10.1007/978-3-662-38353-7\\_3](https://doi.org/10.1007/978-3-662-38353-7_3)
- Hoepfner, D., Schildknecht, D., Braakman, I., Philippsen, P., Tabak, H.F., 2005. Contribution of the Endoplasmic Reticulum to Peroxisome Formation. *Cell* 122, 85–95. <https://doi.org/10.1016/j.cell.2005.04.025>
- Horiguchi, H., Yurimoto, H., Goh, T.-K., Nakagawa, T., Kato, N., Sakai, Y., 2001. Peroxisomal Catalase in the Methylophilic Yeast *Candida boidinii*: Transport Efficiency and Metabolic Significance. *J. Bacteriol.* 183, 6372–6383. <https://doi.org/10.1128/JB.183.21.6372-6383.2001>
- Horn, D., 2014. Antigenic variation in African trypanosomes. *Mol. Biochem. Parasitol.* 195, 123–129. <https://doi.org/10.1016/j.molbiopara.2014.05.001>
- Horváth, A., Horáková, E., Dunajčíková, P., Verner, Z., Pravdová, E., Šlapetová, I., Cuninková, L., Lukeš, J., 2005. Downregulation of the nuclear-encoded subunits of the complexes III and IV

- disrupts their respective complexes but not complex I in procyclic *Trypanosoma brucei*. *Mol. Microbiol.* 58, 116–130. <https://doi.org/10.1111/j.1365-2958.2005.04813.x>
- Hua, R., Cheng, D., Coyaoud, É., Freeman, S., Di Pietro, E., Wang, Y., Vissa, A., Yip, C.M., Fairn, G.D., Braverman, N., Brumell, J.H., Trimble, W.S., Raught, B., Kim, P.K., 2017. VAPs and ACBD5 tether peroxisomes to the ER for peroxisome maintenance and lipid homeostasis. *J. Cell Biol.* 216, 367–377. <https://doi.org/10.1083/jcb.201608128>
- Huergo, L.F., Dixon, R., 2015. The Emergence of 2-Oxoglutarate as a Master Regulator Metabolite. *Microbiol. Mol. Biol. Rev. MMBR* 79, 419–435. <https://doi.org/10.1128/MMBR.00038-15>
- Hughes, L., Borrett, S., Towers, K., Starborg, T., Vaughan, S., 2017. Patterns of organelle ontogeny through a cell cycle revealed by whole-cell reconstructions using 3D electron microscopy. *J. Cell Sci.* 130, 637. <https://doi.org/10.1242/jcs.198887>
- Hulpia, F., Mabile, D., Campagnaro, G.D., Schumann, G., Maes, L., Roditi, I., Hofer, A., de Koning, H.P., Caljon, G., Van Calenbergh, S., 2019. Combining tubercidin and cordycepin scaffolds results in highly active candidates to treat late-stage sleeping sickness. *Nat. Commun.* 10, 5564. <https://doi.org/10.1038/s41467-019-13522-6>
- Hunt, M., Köhler, P., 1995. Purification and characterization of phosphoenolpyruvate carboxykinase from *Trypanosoma brucei*. *Biochim. Biophys. Acta BBA - Protein Struct. Mol. Enzymol.* 1249, 15–22. [https://doi.org/10.1016/0167-4838\(95\)00061-X](https://doi.org/10.1016/0167-4838(95)00061-X)
- Huybrechts, S.J., Van Veldhoven, P.P., Brees, C., Mannaerts, G.P., Los, G.V., Fransen, M., 2009. Peroxisome Dynamics in Cultured Mammalian Cells. *Traffic* 10, 1722–1733. <https://doi.org/10.1111/j.1600-0854.2009.00970.x>
- Igoillo-Esteve, M., Mazet, M., Deumer, G., Wallemacq, P., Michels, P.A.M., 2011. Glycosomal ABC transporters of *Trypanosoma brucei*: Characterisation of their expression, topology and substrate specificity. *Int. J. Parasitol.* 41, 429–438. <https://doi.org/10.1016/j.ijpara.2010.11.002>
- Imanaka, T., Shimozaawa, N. (Eds.), 2019. Peroxisomes: Biogenesis, Function, and Role in Human Disease. Springer Singapore, Singapore. <https://doi.org/10.1007/978-981-15-1169-1>
- Intlekofer, A.M., Wang, B., Liu, H., Shah, H., Carmona-Fontaine, C., Rustenburg, A.S., Salah, S., Gunner, M.R., Chodera, J.D., Cross, J.R., Thompson, C.B., 2017. L-2-Hydroxyglutarate production arises from noncanonical enzyme function at acidic pH. *Nat. Chem. Biol.* 13, 494–500. <https://doi.org/10.1038/nchembio.2307>
- Islinger, M., Li, K.W., Seitz, J., Völkl, A., Lüers, G.H., 2009. Hitchhiking of Cu/Zn Superoxide Dismutase to Peroxisomes - Evidence for a Natural Piggyback Import Mechanism in Mammals. *Traffic* 10, 1711–1721. <https://doi.org/10.1111/j.1600-0854.2009.00966.x>
- Izquierdo, L., Atrih, A., Rodrigues, J.A., Jones, D.C., Ferguson, M.A.J., 2009a. *Trypanosoma brucei* UDP-Glucose:Glycoprotein Glucosyltransferase Has Unusual Substrate Specificity and Protects the Parasite from Stress. *Eukaryot. Cell* 8, 230–240. <https://doi.org/10.1128/EC.00361-08>
- Izquierdo, L., Nakanishi, M., Mehlert, A., Machray, G., Barton, G.J., Ferguson, M.A.J., 2009b. Identification of a glycosylphosphatidylinositol anchor-modifying  $\beta$ 1-3 N-acetylglucosaminyl transferase in *Trypanosoma brucei*. *Mol. Microbiol.* 71, 478–491. <https://doi.org/10.1111/j.1365-2958.2008.06542.x>
- Izquierdo, L., Mehlert, A., Ferguson, M.A.J., 2012. The lipid-linked oligosaccharide donor specificities of *Trypanosoma brucei* oligosaccharyltransferases. *Glycobiology* 22, 696–703. <https://doi.org/10.1093/glycob/cws003>
- Izquierdo, L., Acosta-Serrano, A., Mehlert, A., Ferguson, M.A., 2015. Identification of a glycosylphosphatidylinositol anchor-modifying  $\beta$ 1-3 galactosyltransferase in *Trypanosoma brucei*. *Glycobiology* 25, 438–447. <https://doi.org/10.1093/glycob/cwu131>
- Jackson, A.P., Otto, T.D., Aslett, M., Armstrong, S.D., Bringaud, F., Schlacht, A., Hartley, C., Sanders, M., Wastling, J.M., Dacks, J.B., Acosta-Serrano, A., Field, M.C., Ginger, M.L., Berriman, M., 2016. Kinetoplastid Phylogenomics Reveals the Evolutionary Innovations Associated with the Origins of Parasitism. *Curr. Biol.* 26, 161–172. <https://doi.org/10.1016/j.cub.2015.11.055>
- Jacobs, R.T., Nare, B., Wring, S.A., Orr, M.D., Chen, D., Sligar, J.M., Jenks, M.X., Noe, R.A., Bowling, T.S., Mercer, L.T., Rewerts, C., Gaukel, E., Owens, J., Parham, R., Randolph, R., Beaudet, B., Bacchi, C.J., Yarlett, N., Plattner, J.J., Freund, Y., Ding, C., Akama, T., Zhang, Y.-K., Brun, R., Kaiser, M., Scandale, I., Don, R., 2011. SCYX-7158, an Orally-Active Benzoxaborole for the Treatment of Stage 2 Human African Trypanosomiasis. *PLoS Negl. Trop. Dis.* 5, e1151. <https://doi.org/10.1371/journal.pntd.0001151>
- Jafari, F., Ganjalikhany, M.R., Moradi, A., Hemati, M., Jafari, S., 2019. Novel Peptide Inhibitors for Lactate Dehydrogenase A (LDHA): A Survey to Inhibit LDHA Activity via Disruption of Protein-Protein Interaction. *Sci. Rep.* 9, 4686. <https://doi.org/10.1038/s41598-019-38854-7>

- Jamonneau, V., Camara, O., Ilboudo, H., Peylhard, M., Koffi, M., Sakande, H., N'Dri, L., Sanou, D., Dama, E., Camara, M., Lejon, V., 2015. Accuracy of Individual Rapid Tests for Serodiagnosis of Gambiense Sleeping Sickness in West Africa. *PLoS Negl. Trop. Dis.* 9, e0003480. <https://doi.org/10.1371/journal.pntd.0003480>
- Janse van Rensburg, H.C., Van den Ende, W., 2018. UDP-Glucose: A Potential Signaling Molecule in Plants? *Front. Plant Sci.* 8, 2230. <https://doi.org/10.3389/fpls.2017.02230>
- Johnston, K., Kim, D.-H., Kerkhoven, E.J., Burchmore, R., Barrett, M.P., Achcar, F., 2019. Mapping the metabolism of five amino acids in bloodstream form *Trypanosoma brucei* using U-(13)C-labelled substrates and LC-MS. *Biosci. Rep.* 39, BSR20181601. <https://doi.org/10.1042/BSR20181601>
- Jones, T.W., Dávila, A.M.R., 2001. *Trypanosoma vivax* – out of Africa. *Trends Parasitol.* 17, 99–101. [https://doi.org/10.1016/S1471-4922\(00\)01777-3](https://doi.org/10.1016/S1471-4922(00)01777-3)
- Kalel, V.C., Schliebs, W., Erdmann, R., 2015. Identification and functional characterization of *Trypanosoma brucei* peroxin 16. *Biochim. Biophys. Acta BBA - Mol. Cell Res.* 1853, 2326–2337. <https://doi.org/10.1016/j.bbamcr.2015.05.024>
- Kalel, V.C., Li, M., Gaussmann, S., Delhommel, F., Schäfer, A.-B., Tippler, B., Jung, M., Maier, R., Oeljeklaus, S., Schliebs, W., Warscheid, B., Sattler, M., Erdmann, R., 2019. Evolutionary divergent PEX3 is essential for glycosome biogenesis and survival of trypanosomatid parasites. *Biochim. Biophys. Acta BBA - Mol. Cell Res.* 1866, 118520. <https://doi.org/10.1016/j.bbamcr.2019.07.015>
- Käll, L., Canterbury, J.D., Weston, J., Noble, W.S., MacCoss, M.J., 2007. Semi-supervised learning for peptide identification from shotgun proteomics datasets. *Nat. Methods* 4, 923–925. <https://doi.org/10.1038/nmeth1113>
- Kataya, A.R.A., Heidari, B., Hagen, L., Kommedal, R., Slupphaug, G., Lillo, C., 2015. Protein Phosphatase 2A Holoenzyme Is Targeted to Peroxisomes by Piggybacking and Positively Affects Peroxisomal  $\beta$ -Oxidation. *Plant Physiol.* 167, 493–506. <https://doi.org/10.1104/pp.114.254409>
- Kaufer, A., Ellis, J., Stark, D., Barratt, J., 2017. The evolution of trypanosomatid taxonomy. *Parasit. Vectors* 10. <https://doi.org/10.1186/s13071-017-2204-7>
- Kaur, B., Záhonová, K., Valach, M., Faktorová, D., Prokopchuk, G., Burger, G., Lukeš, J., 2020. Gene fragmentation and RNA editing without borders: eccentric mitochondrial genomes of diplonemids. *Nucleic Acids Res.* 48, 2694–2708. <https://doi.org/10.1093/nar/gkz1215>
- Kieft, R., Zhang, Y., Marand, A.P., Moran, J.D., Bridger, R., Wells, L., Schmitz, R.J., Sabatini, R., 2019. Identification of a Novel Base J Binding Protein Complex Involved in RNA Polymerase II Transcription Termination in Trypanosomes. *bioRxiv* 753004. <https://doi.org/10.1101/753004>
- Kleczkowski, L.A., Kunz, S., Wilczynska, M., 2010. Mechanisms of UDP-Glucose Synthesis in Plants. *Crit. Rev. Plant Sci.* 29, 191–203. <https://doi.org/10.1080/07352689.2010.483578>
- Kleczkowski, L.A., Decker, D., 2015. Sugar Activation for Production of Nucleotide Sugars as Substrates for Glycosyltransferases in Plants. *J. Appl. Glycosci.* 62, 25–36. [https://doi.org/10.5458/jag.jag.JAG-2015\\_003](https://doi.org/10.5458/jag.jag.JAG-2015_003)
- Knoblach, B., Sun, X., Coquelle, N., Fagarasanu, A., Poirier, R.L., Rachubinski, R.A., 2013. An ER-peroxisome tether exerts peroxisome population control in yeast. *EMBO J.* 32, 2439–2453. <https://doi.org/10.1038/emboj.2013.170>
- Koch, H., Raabe, M., Urlaub, H., Bindereif, A., Preußner, C., 2016. The polyadenylation complex of *Trypanosoma brucei*: Characterization of the functional poly(A) polymerase. *RNA Biol.* 13, 221–231. <https://doi.org/10.1080/15476286.2015.1130208>
- Kolev, N.G., Ramey-Butler, K., Cross, G.A.M., Ullu, E., Tschudi, C., 2012. Developmental Progression to Infectivity in *Trypanosoma brucei* Triggered by an RNA-Binding Protein. *Science* 338, 1352–1353. <https://doi.org/10.1126/science.1229641>
- Kovářová, J., Nagar, R., Faria, J., Ferguson, M.A.J., Barrett, M.P., Horn, D., 2018. Gluconeogenesis using glycerol as a substrate in bloodstream-form *Trypanosoma brucei*. *PLOS Pathog.* 14, e1007475. <https://doi.org/10.1371/journal.ppat.1007475>
- Králová, I., Rigden, D.J., Oppendoes, F.R., Michels, P.A.M., 2000. Glycerol kinase of *Trypanosoma brucei*. *Eur. J. Biochem.* 267, 2323–2333. <https://doi.org/10.1046/j.1432-1327.2000.01238.x>
- Kuettel, S., Wadum, M.C.T., Güther, M.L.S., Mariño, K., Riemer, C., Ferguson, M.A.J., 2012. The *de novo* and salvage pathways of GDP-mannose biosynthesis are both sufficient for the growth of bloodstream-form *Trypanosoma brucei*: Pathway of GDP-mannose biosynthesis in *T. brucei*. *Mol. Microbiol.* 84, 340–351. <https://doi.org/10.1111/j.1365-2958.2012.08026.x>
- Kumar, S., Singh, R., Williams, C.P., van der Klei, I.J., 2016. Stress exposure results in increased peroxisomal levels of yeast Pnc1 and Gpd1, which are imported via a piggy-backing



- mechanism. *Biochim. Biophys. Acta BBA - Mol. Cell Res.* 1863, 148–156. <https://doi.org/10.1016/j.bbamcr.2015.10.017>
- Lacomble, S., Vaughan, S., Gadelha, C., Morphew, M.K., Shaw, M.K., McIntosh, J.R., Gull, K., 2009. Three-dimensional cellular architecture of the flagellar pocket and associated cytoskeleton in trypanosomes revealed by electron microscope tomography. *J. Cell Sci.* 122, 1081–1090. <https://doi.org/10.1242/jcs.045740>
- Lamerz, A.-C., Haselhorst, T., Bergfeld, A.K., von Itzstein, M., Gerardy-Schahn, R., 2006. Molecular Cloning of the *Leishmania major* UDP-glucose Pyrophosphorylase, Functional Characterization, and Ligand Binding Analyses Using NMR Spectroscopy. *J. Biol. Chem.* 281, 16314–16322. <https://doi.org/10.1074/jbc.M600076200>
- Lamour, N., Riviere, L., Coustou, V., Coombs, G.H., Barrett, M.P., Bringaud, F., 2005. Proline Metabolism in Procyclic *Trypanosoma brucei* Is Down-regulated in the Presence of Glucose. *J. Biol. Chem.* 280, 11902–11910. <https://doi.org/10.1074/jbc.M414274200>
- Langousis, G., Hill, K.L., 2014. Motility and more: the flagellum of *Trypanosoma brucei*. *Nat. Rev. Microbiol.* 12, 505–518. <https://doi.org/10.1038/nrmicro3274>
- Lazarowski, E.R., Harden, T.K., 2015. UDP-Sugars as Extracellular Signaling Molecules: Cellular and Physiologic Consequences of P2Y<sub>14</sub> Receptor Activation. *Mol. Pharmacol.* 88, 151. <https://doi.org/10.1124/mol.115.098756>
- Lee, M., Mullen, R.T., Trelease, R.N., 1997. Oilseed Isocitrate Lyases Lacking Their Essential Type 1 Peroxisomal Targeting Signal Are Piggybacked to Glyoxysomes 13.
- Lehane, M.J., 1997. Peritrophic matrix structure and function. *Annu. Rev. Entomol.* 42, 525–550. <https://doi.org/10.1146/annurev.ento.42.1.525>
- Leiper, M., Oatey, P.B., Danpure, C.J., 1996. Inhibition of Alanine:Glyoxylate Aminotransferase 1 Dimerization Is a Prerequisite for Its Peroxisome-to-Mitochondrion Mistargeting in Primary Hyperoxaluria Type I 13.
- L'Hostis, C., Geindre, M., Deshusses, J., 1993. Active transport of L-proline in the protozoan parasite *Trypanosoma brucei brucei*. *Biochem. J.* 291 (Pt1), 297–301. <https://doi.org/10.1042/bj2910297>
- Linstead, D.J., Klein, R.A., Cross, G.A.M., 1977. Threonine Catabolism in *Trypanosoma brucei*. *J. Gen. Microbiol.* 101, 243–251. <https://doi.org/10.1099/00221287-101-2-243>
- Liu, F., Lu, Y., Pieuchot, L., Dhavale, T., Jedd, G., 2011. Import Oligomers Induce Positive Feedback to Promote Peroxisome Differentiation and Control Organelle Abundance. *Dev. Cell* 21, 457–468. <https://doi.org/10.1016/j.devcel.2011.08.004>
- Liu, L., Xu, Y.-X., Caradonna, K.L., Kruzel, E.K., Burleigh, B.A., Bangs, J.D., Hirschberg, C.B., 2013. Inhibition of Nucleotide Sugar Transport in *Trypanosoma brucei* Alters Surface Glycosylation. *J. Biol. Chem.* 288, 10599–10615. <https://doi.org/10.1074/jbc.M113.453597>
- Lobo-Rojas, Á.E., González-Marciano, E.B., Valera-Vera, E.A., Acosta, H.R., Quiñones, W.A., Burchmore, R.J.S., Concepción, J.L., Cáceres, A.J., 2016. *Trypanosoma cruzi* contains two galactokinases; molecular and biochemical characterization. *Parasitol. Int.* 65, 472–482. <https://doi.org/10.1016/j.parint.2016.06.008>
- Lorenz, P., Maier, A.G., Baumgart, E., Erdmann, R., Clayton, C., 1998. Elongation and clustering of glycosomes in *Trypanosoma brucei* overexpressing the glycosomal Pex11p. *EMBO J.* 17, 3542–3555. <https://doi.org/10.1093/emboj/17.13.3542>
- Lukeš, J., Lys Guilbride, D., Votýpka, J., Zíková, A., Benne, R., Englund, P.T., 2002. Kinetoplast DNA Network: Evolution of an Improbable Structure. *Eukaryot. Cell* 1, 495–502. <https://doi.org/10.1128/EC.1.4.495-502.2002>
- Lukeš, J., Wheeler, R., Jirsová, D., David, V., Archibald, J.M., 2018. Massive mitochondrial DNA content in diplomid and kinetoplastid protists. *IUBMB Life* 70, 1267–1274. <https://doi.org/10.1002/iub.1894>
- Lumbala, C., Biéler, S., Kayembe, S., Makabuza, J., Ongarello, S., Ndung'u, J.M., 2018. Prospective evaluation of a rapid diagnostic test for *Trypanosoma brucei gambiense* infection developed using recombinant antigens. *PLoS Negl. Trop. Dis.* 12, e0006386. <https://doi.org/10.1371/journal.pntd.0006386>
- MacRae, J.I., Obado, S.O., Turnock, D.C., Roper, J.R., Kierans, M., Kelly, J.M., Ferguson, M.A.J., 2006. The suppression of galactose metabolism in *Trypanosoma cruzi* epimastigotes causes changes in cell surface molecular architecture and cell morphology. *Mol. Biochem. Parasitol.* 147, 126–136. <https://doi.org/10.1016/j.molbiopara.2006.02.011>
- Mahamat, M.H., Peka, M., Rayaisse, J.-B., Rock, K.S., Toko, M.A., Darnas, J., Brahim, G.M., Alkatib, A.B., Yoni, W., Tirados, I., Courtin, F., Brand, S.P.C., Nersy, C., Alfaroukh, I.O., Torr, S.J., Lehane, M.J., Solano, P., 2017. Adding tsetse control to medical activities contributes to

- decreasing transmission of sleeping sickness in the Mandoul focus (Chad). *PLoS Negl. Trop. Dis.* 11, e0005792. <https://doi.org/10.1371/journal.pntd.0005792>
- Maier, A., Lorenz, P., Voncken, F., Clayton, C., 2001. An essential dimeric membrane protein of trypanosome glycosomes. *Mol. Microbiol.* 39, 1443–1451. <https://doi.org/10.1046/j.1365-2958.2001.02333.x>
- Manthri, S., Güther, M.L.S., Izquierdo, L., Acosta-Serrano, A., Ferguson, M.A.J., 2008. Deletion of the TbALG3 gene demonstrates site-specific N-glycosylation and N-glycan processing in *Trypanosoma brucei*. *Glycobiology* 18, 367–383. <https://doi.org/10.1093/glycob/cwn014>
- Mantilla, B.S., Marchese, L., Casas-Sánchez, A., Dyer, N.A., Ejeh, N., Biran, M., Bringaud, F., Lehane, M.J., Acosta-Serrano, A., Silber, A.M., 2017. Proline Metabolism is Essential for *Trypanosoma brucei* Survival in the Tsetse Vector. *PLOS Pathog.* 13, e1006158. <https://doi.org/10.1371/journal.ppat.1006158>
- Mariño, K., Güther, M.L.S., Wernimont, A.K., Amani, M., Hui, R., Ferguson, M.A., 2010. Identification, subcellular localisation, biochemical properties, and high-resolution crystal structure of *Trypanosoma brucei* UDP-glucose pyrophosphorylase. *Glycobiology* 20, 1619–1630. <https://doi.org/10.1093/glycob/cwq115>
- Mariño, K., Güther, M.L.S., Wernimont, A.K., Qiu, W., Hui, R., Ferguson, M.A.J., 2011. Characterization, Localisation, Essentiality, and High-Resolution Crystal Structure of Glucosamine 6-Phosphate N-Acetyltransferase from *Trypanosoma brucei*. *Eukaryot. Cell* 10, 985. <https://doi.org/10.1128/EC.05025-11>
- Martínez, L.I., Piattoni, C.V., Garay, S.A., Rodríguez, D.E., Guerrero, S.A., Iglesias, A.A., 2011. Redox regulation of UDP-glucose pyrophosphorylase from *Entamoeba histolytica*. *Biochimie* 93, 260–268. <https://doi.org/10.1016/j.biochi.2010.09.019>
- Maslov, D.A., Oppenheimer, F.R., Kostygov, A.Y., Hashimi, H., Lukeš, J., Yurchenko, V., 2019. Recent advances in trypanosomatid research: genome organization, expression, metabolism, taxonomy and evolution. *Parasitology* 146, 1–27. <https://doi.org/10.1017/S003182018000951>
- Matsuzaki, T., Fujiki, Y., 2008. The peroxisomal membrane protein import receptor Pex3p is directly transported to peroxisomes by a novel Pex19p- and Pex16p-dependent pathway. *J. Cell Biol.* 183, 1275–1286. <https://doi.org/10.1083/jcb.200806062>
- Matthews, K.R., Gull, K., 1994. Evidence for an interplay between cell cycle progression and the initiation of differentiation between life cycle forms of African trypanosomes. *J. Cell Biol.* 125, 1147–1156. <https://doi.org/10.1083/jcb.125.5.1147>
- Mayor, S., Menon, A.K., Cross, G.A., 1992. Galactose-containing glycosylphosphatidylinositols in *Trypanosoma brucei*. *J. Biol. Chem.* 267, 754–761.
- Mazet, M., Morand, P., Biran, M., Bouyssou, G., Courtois, P., Daulouède, S., Millerioux, Y., Franconi, J.-M., Vincendeau, P., Moreau, P., Bringaud, F., 2013. Revisiting the Central Metabolism of the Bloodstream Forms of *Trypanosoma brucei*: Production of Acetate in the Mitochondrion Is Essential for Parasite Viability. *PLoS Negl. Trop. Dis.* 7, e2587. <https://doi.org/10.1371/journal.pntd.0002587>
- Mazhari-Tabrizi, R., Eckert, V., Blank, M., Müller, R., Mumberg, D., Funk, M., Schwarz, R.T., 1996. Cloning and functional expression of glycosyltransferases from parasitic protozoans by heterologous complementation in yeast: the dolichol phosphate mannose synthase from *Trypanosoma brucei*. *Biochem. J.* 316 (Pt3), 853–858. <https://doi.org/10.1042/bj3160853>
- McCoy, J.G., Bitto, E., Bingman, C.A., Wesenberg, G.E., Bannen, R.M., Kondrashov, D.A., Phillips, G.N., 2007. Structure and Dynamics of UDP-Glucose Pyrophosphorylase from *Arabidopsis thaliana* with Bound UDP-Glucose and UTP. *J. Mol. Biol.* 366, 830–841. <https://doi.org/10.1016/j.jmb.2006.11.059>
- McNew, J.A., Goodman, J.M., 1994. An oligomeric protein is imported into peroxisomes in vivo. *J. Cell Biol.* 127, 1245–1257. <https://doi.org/10.1083/jcb.127.5.1245>
- Mehlert, A., 1998. The glycosylation of the variant surface glycoproteins and procyclic acidic repetitive proteins of *Trypanosoma brucei*. *Mol. Biochem. Parasitol.* 91, 145–152. [https://doi.org/10.1016/S0166-6851\(97\)00187-4](https://doi.org/10.1016/S0166-6851(97)00187-4)
- Mehlert, A., Wormald, M.R., Ferguson, M.A.J., 2012. Modeling of the N-Glycosylated Transferrin Receptor Suggests How Transferrin Binding Can Occur within the Surface Coat of *Trypanosoma brucei*. *PLoS Pathog.* 8, e1002618. <https://doi.org/10.1371/journal.ppat.1002618>
- Meinecke, M., Cizmowski, C., Schliebs, W., Krüger, V., Beck, S., Wagner, R., Erdmann, R., 2010. The peroxisomal importomer constitutes a large and highly dynamic pore. *Nat. Cell Biol.* 12, 273–277. <https://doi.org/10.1038/ncb2027>

- Mesu, V.K.B.K., Kalonji, W.M., Bardonneau, C., Mordt, O.V., Blesson, S., Simon, F., Delhomme, S., Bernhard, S., Kuziena, W., Lubaki, J.-P.F., Vuvu, S.L., Ngima, P.N., Mbembo, H.M., Ilunga, M., Bonama, A.K., Heradi, J.A., Solomo, J.L.L., Mandula, G., Badibabi, L.K., Dama, F.R., Lukula, P.K., Tete, D.N., Lumbala, C., Scherrer, B., Strub-Wourgaft, N., Tarral, A., 2018. Oral fexinidazole for late-stage African *Trypanosoma brucei gambiense* trypanosomiasis: a pivotal multicentre, randomised, non-inferiority trial. *The Lancet* 391, 144–154. [https://doi.org/10.1016/S0140-6736\(17\)32758-7](https://doi.org/10.1016/S0140-6736(17)32758-7)
- Michels, P.A.M., Bringaud, F., Herman, M., Hannaert, V., 2006. Metabolic functions of glycosomes in trypanosomatids. *Peroxisomes Morphol. Funct. Biog. Disord.* 1763, 1463–1477. <https://doi.org/10.1016/j.bbamcr.2006.08.019>
- Millerioux, Y., Morand, P., Biran, M., Mazet, M., Moreau, P., Wargnies, M., Ebikeme, C., Deramchia, K., Gales, L., Portais, J.-C., Boshart, M., Franconi, J.-M., Bringaud, F., 2012. ATP Synthesis-coupled and -uncoupled Acetate Production from Acetyl-CoA by Mitochondrial Acetate:Succinate CoA-transferase and Acetyl-CoA Thioesterase in *Trypanosoma*. *J. Biol. Chem.* 287, 17186–17197. <https://doi.org/10.1074/jbc.M112.355404>
- Millerioux, Y., Ebikeme, C., Biran, M., Morand, P., Bouyssou, G., Vincent, I.M., Mazet, M., Riviere, L., Franconi, J.-M., Burchmore, R.J.S., Moreau, P., Barrett, M.P., Bringaud, F., 2013. The threonine degradation pathway of the *Trypanosoma brucei* procyclic form: the main carbon source for lipid biosynthesis is under metabolic control: Metabolic adaptation for acetate production. *Mol. Microbiol.* n/a-n/a. <https://doi.org/10.1111/mmi.12351>
- Millerioux, Y., Mazet, M., Bouyssou, G., Allmann, S., Kiema, T.-R., Bertiaux, E., Fouillen, L., Thapa, C., Biran, M., Plazolles, N., Dittrich-Domergue, F., Crouzols, A., Wierenga, R.K., Rotureau, B., Moreau, P., Bringaud, F., 2018. De novo biosynthesis of sterols and fatty acids in the *Trypanosoma brucei* procyclic form: Carbon source preferences and metabolic flux redistributions. *PLoS Pathog.* 14, e1007116–e1007116. <https://doi.org/10.1371/journal.ppat.1007116>
- Misset, O., Bos, O.J.M., Opperdoes, F.R., 1986. Glycolytic enzymes of *Trypanosoma brucei*. *Eur. J. Biochem.* 157, 441–453. <https://doi.org/10.1111/j.1432-1033.1986.tb09687.x>
- Mochizuki, K., Inaoka, D.K., Mazet, M., Shiba, T., Fukuda, K., Kurasawa, H., Millerioux, Y., Boshart, M., Balogun, E.O., Harada, S., Hirayama, K., Bringaud, F., Kita, K., 2020. The ASCT/SCS cycle fuels mitochondrial ATP and acetate production in *Trypanosoma brucei*. *Biochim. Biophys. Acta BBA - Bioenerg.* 1861, 148283. <https://doi.org/10.1016/j.bbabi.2020.148283>
- Morales, J., Hashimoto, M., Williams, T.A., Hirawake-Mogi, H., Makiuchi, T., Tsubouchi, A., Kaga, N., Taka, H., Fujimura, T., Koike, M., Mita, T., Bringaud, F., Concepción, J.L., Hashimoto, T., Embley, T.M., Nara, T., 2016. Differential remodelling of peroxisome function underpins the environmental and metabolic adaptability of diplomonads and kinetoplastids. *Proc. R. Soc. B Biol. Sci.* 283, 20160520. <https://doi.org/10.1098/rspb.2016.0520>
- Moreira, D., 2004. An updated view of kinetoplastid phylogeny using environmental sequences and a closer outgroup: proposal for a new classification of the class Kinetoplastea. *Int. J. Syst. Evol. Microbiol.* 54, 1861–1875. <https://doi.org/10.1099/ijs.0.63081-0>
- Morgan, G.W., Goulding, D., Field, M.C., 2004. The Single Dynamin-like Protein of *Trypanosoma brucei* Regulates Mitochondrial Division and Is Not Required for Endocytosis. *J. Biol. Chem.* 279, 10692–10701. <https://doi.org/10.1074/jbc.M312178200>
- Morris, M.T., DeBruin, C., Yang, Z., Chambers, J.W., Smith, K.S., Morris, J.C., 2006. Activity of a Second *Trypanosoma brucei* Hexokinase Is Controlled by an 18-Amino-Acid C-Terminal Tail. *Eukaryot. Cell* 5, 2014–2023. <https://doi.org/10.1128/EC.00146-06>
- Mowatt, M.R., Clayton, C.E., 1987. Developmental regulation of a novel repetitive protein of *Trypanosoma brucei*. *Mol. Cell. Biol.* 7, 2838–2844. <https://doi.org/10.1128/MCB.7.8.2838>
- Mowatt, M.R., Wisdom, G.S., Clayton, C.E., 1989. Variation of tandem repeats in the developmentally regulated procyclic acidic repetitive proteins of *Trypanosoma brucei*. *Mol. Cell. Biol.* 9, 1332–1335. <https://doi.org/10.1128/MCB.9.3.1332>
- Moyersoen, J., Choe, J., Kumar, A., Voncken, F.G.J., Hol, W.G.J., Michels, P.A.M., 2003. Characterization of *Trypanosoma brucei* PEX14 and its role in the import of glycosomal matrix proteins. *Eur. J. Biochem.* 270, 2059–2067. <https://doi.org/10.1046/j.1432-1033.2003.03582.x>
- Moyersoen, J., Choe, J., Fan, E., Hol, W.G.J., Michels, P.A.M., 2004. Biogenesis of peroxisomes and glycosomes: trypanosomatid glycosome assembly is a promising new drug target. *FEMS Microbiol. Rev.* 28, 603–643. <https://doi.org/10.1016/j.femsre.2004.06.004>
- Muchut, R.J., Calloni, R.D., Herrera, F.E., Garay, S.A., Arias, D.G., Iglesias, A.A., Guerrero, S.A., 2018. Elucidating paramylon and other carbohydrate metabolism in *Euglena gracilis*: Kinetic

- characterization, structure and cellular localisation of UDP-glucose pyrophosphorylase. *Biochimie* 154, 176–186. <https://doi.org/10.1016/j.biochi.2018.09.006>
- Müller, M., Mentel, M., van Hellemond, J.J., Henze, K., Woehle, C., Gould, S.B., Yu, R.-Y., van der Giezen, M., Tielens, A.G.M., Martin, W.F., 2012. Biochemistry and evolution of anaerobic energy metabolism in eukaryotes. *Microbiol. Mol. Biol. Rev.* MMBR 76, 444–495. <https://doi.org/10.1128/MMBR.05024-11>
- Nagamune, K., Nozaki, T., Maeda, Y., Ohishi, K., Fukuma, T., Hara, T., Schwarz, R.T., Sutterlin, C., Brun, R., Riezman, H., Kinoshita, T., 2000. Critical roles of glycosylphosphatidylinositol for *Trypanosoma brucei*. *Proc. Natl. Acad. Sci.* 97, 10336–10341. <https://doi.org/10.1073/pnas.180230697>
- Navarro, M., Gull, K., 2001. A pol I transcriptional body associated with VSG mono-allelic expression in *Trypanosoma brucei*. *Nature* 414, 759–763. <https://doi.org/10.1038/414759a>
- N'Djetchi, M.K., Ilboudo, H., Koffi, M., Kaboré, J., Kaboré, J.W., Kaba, D., Courtin, F., Coulibaly, B., Fauret, P., Kouakou, L., Ravel, S., Deborggraeve, S., Solano, P., De Meeüs, T., Bucheton, B., Jamonneau, V., 2017. The study of trypanosome species circulating in domestic animals in two human African trypanosomiasis foci of Côte d'Ivoire identifies pigs and cattle as potential reservoirs of *Trypanosoma brucei gambiense*. *PLoS Negl. Trop. Dis.* 11, e0005993. <https://doi.org/10.1371/journal.pntd.0005993>
- Ngô, H., Tschudi, C., Gull, K., Ullu, E., 1998. Double-stranded RNA induces mRNA degradation in *Trypanosoma brucei*. *Proc. Natl. Acad. Sci. U. S. A.* 95, 14687–14692. <https://doi.org/10.1073/pnas.95.25.14687>
- Niemann, M., Wiese, S., Mani, J., Chanfon, A., Jackson, C., Meisinger, C., Warscheid, B., Schneider, A., 2013. Mitochondrial outer membrane proteome of *Trypanosoma brucei* reveals novel factors required to maintain mitochondrial morphology. *Mol. Cell. Proteomics MCP* 12, 515–528. <https://doi.org/10.1074/mcp.M112.023093>
- Nolan, D.P., Voorheis, H.P., 1992. The mitochondrion in bloodstream forms of *Trypanosoma brucei* is energized by the electrogenic pumping of protons catalysed by the F1F0-ATPase. *Eur. J. Biochem.* 209, 207–216. <https://doi.org/10.1111/j.1432-1033.1992.tb17278.x>
- Nolan, D.P., Jackson, D.G., Biggs, M.J., Brabazon, E.D., Pays, A., Van Laethem, F., Paturiaux-Hanocq, F., Elliot, J.F., Voorheis, H.P., Pays, E., 2000. Characterization of a Novel Alanine-rich Protein Located in Surface Microdomains in *Trypanosoma brucei*. *J. Biol. Chem.* 275, 4072–4080. <https://doi.org/10.1074/jbc.275.6.4072>
- Nwagwu, M., Oppendoes, F., 1982. Regulation of glycolysis in *Trypanosoma brucei*: hexokinase and phosphofructokinase activity. *Acta Trop.* 39, 61–72.
- O'Brien, J., Wilson, I., Orton, T., Pognan, F., 2000. Investigation of the Alamar Blue (resazurin) fluorescent dye for the assessment of mammalian cell cytotoxicity. *Eur. J. Biochem.* 267, 5421–5426. <https://doi.org/10.1046/j.1432-1327.2000.01606.x>
- Obungu, V.H., Kiara, J.K., Njogu, R.M., Olembu, N.K., 1999. Catabolism of proline by procyclic culture forms of *Trypanosoma congolense*. *Comp. Biochem. Physiol. B Biochem. Mol. Biol.* 123, 59–65. [https://doi.org/10.1016/S0305-0491\(99\)00040-1](https://doi.org/10.1016/S0305-0491(99)00040-1)
- Ogbadoyi, E., Ersfeld, K., Robinson, D., Sherwin, T., Gull, K., 2000. Architecture of the *Trypanosoma brucei* nucleus during interphase and mitosis. *Chromosoma* 108, 501–513. <https://doi.org/10.1007/s004120050402>
- Ogbadoyi, E.O., Robinson, D.R., Gull, K., 2003. A High-Order *Trans* -Membrane Structural Linkage Is Responsible for Mitochondrial Genome Positioning and Segregation by Flagellar Basal Bodies in Trypanosomes. *Mol. Biol. Cell* 14, 1769–1779. <https://doi.org/10.1091/mbc.e02-08-0525>
- Oppendoes, F.R., Borst, P., 1977a. Localisation of nine glycolytic enzymes in a microbody-like organelle in *Trypanosoma brucei*: The glycosome. *FEBS Lett.* 80, 360–364. [https://doi.org/10.1016/0014-5793\(77\)80476-6](https://doi.org/10.1016/0014-5793(77)80476-6)
- Oppendoes, F.R., Borst, P., Baker, S., Leene, W., 1977b. Localisation of Glycerol-3-Phosphate Oxidase in the Mitochondrion and Particulate NAD<sup>+</sup>-Linked Glycerol-3-Phosphate Dehydrogenase in the Microbodies of the Bloodstream Form of *Trypanosoma brucei*. *Eur. J. Biochem.* 76, 29–39. <https://doi.org/10.1111/j.1432-1033.1977.tb11567.x>
- Oppendoes, F.R., Baudhuin, P., Coppens, I., De Roe, C., Edwards, S.W., Weijers, P.J., Misset, O., 1984. Purification, morphometric analysis, and characterization of the glycosomes (microbodies) of the protozoan hemoflagellate *Trypanosoma brucei*. *J. Cell Biol.* 98, 1178–1184. <https://doi.org/10.1083/jcb.98.4.1178>
- Oppendoes, F.R., Szikora, J.-P., 2006. In silico prediction of the glycosomal enzymes of *Leishmania major* and trypanosomes. *Mol. Biochem. Parasitol.* 147, 193–206. <https://doi.org/10.1016/j.molbiopara.2006.02.010>

- Osinga, K.A., Swinkels, B.W., Gibson, W.C., Borst, P., Veeneman, G.H., Van Boom, J.H., Michels, P.A., Opperdoes, F.R., 1985. Topogenesis of microbody enzymes: a sequence comparison of the genes for the glycosomal (microbody) and cytosolic phosphoglycerate kinases of *Trypanosoma brucei*. *EMBO J.* 4, 3811–3817. <https://doi.org/10.1002/j.1460-2075.1985.tb04152.x>
- Otera, H., Fujiki, Y., 2012. Pex5p Imports Folded Tetrameric Catalase by Interaction with Pex13p: Oligomeric Import of Human Catalase. *Traffic* 13, 1364–1377. <https://doi.org/10.1111/j.1600-0854.2012.01391.x>
- Overath, P., Engstler, M., 2004. Endocytosis, membrane recycling and sorting of GPI-anchored proteins: *Trypanosoma brucei* as a model system: The endocytic system of *T. brucei*. *Mol. Microbiol.* 53, 735–744. <https://doi.org/10.1111/j.1365-2958.2004.04224.x>
- Panicucci, B., Gahura, O., Zíková, A., 2017. *Trypanosoma brucei* TbIF1 inhibits the essential F1-ATPase in the infectious form of the parasite. *PLoS Negl. Trop. Dis.* 11, e0005552. <https://doi.org/10.1371/journal.pntd.0005552>
- Pays, E., Vanhollebeke, B., Vanhamme, L., Paturiaux-Hanocq, F., Nolan, D.P., Pérez-Morga, D., 2006. The trypanolytic factor of human serum. *Nat. Rev. Microbiol.* 4, 477–486. <https://doi.org/10.1038/nrmicro1428>
- Pedrosa, A.G., Francisco, T., Bicho, D., Dias, A.F., Barros-Barbosa, A., Hagmann, V., Dodt, G., Rodrigues, T.A., Azevedo, J.E., 2018. Peroxisomal monoubiquitinated PEX5 interacts with the AAA ATPases PEX1 and PEX6 and is unfolded during its dislocation into the cytosol. *J. Biol. Chem.* 293, 11553–11563. <https://doi.org/10.1074/jbc.RA118.003669>
- Persat, F., Azzar, G., Martel, M.-B., Got, R., 1984. Evidence for coupling between transport of UDP-glucose and its synthesis by membrane-bound pyrophosphorylase in golgi apparatus of cat liver. *Biochim. Biophys. Acta BBA - Biomembr.* 769, 377–380. [https://doi.org/10.1016/0005-2736\(84\)90320-1](https://doi.org/10.1016/0005-2736(84)90320-1)
- Pineda, E., Thonnus, M., Mazet, M., Mourier, A., Cahoreau, E., Kulyk, H., Dupuy, J.-W., Biran, M., Masante, C., Allmann, S., Rivière, L., Rotureau, B., Portais, J.-C., Bringaud, F., 2018. Glycerol supports growth of the *Trypanosoma brucei* bloodstream forms in the absence of glucose: Analysis of metabolic adaptations on glycerol-rich conditions. *PLOS Pathog.* 14, e1007412. <https://doi.org/10.1371/journal.ppat.1007412>
- Pinger, J., Nešić, D., Ali, L., Aresta-Branco, F., Lilic, M., Chowdhury, S., Kim, H.-S., Verdi, J., Raper, J., Ferguson, M.A.J., Papavasiliou, F.N., Stebbins, C.E., 2018. African trypanosomes evade immune clearance by O-glycosylation of the VSG surface coat. *Nat. Microbiol.* 3, 932–938. <https://doi.org/10.1038/s41564-018-0187-6>
- Platta, H.W., Grunau, S., Rosenkranz, K., Girzalsky, W., Erdmann, R., 2005. Functional role of the AAA peroxins in dislocation of the cycling PTS1 receptor back to the cytosol. *Nat. Cell Biol.* 7, 817–822. <https://doi.org/10.1038/ncb1281>
- Poon, S.K., Peacock, L., Gibson, W., Gull, K., Kelly, S., 2012. A modular and optimised single marker system for generating *Trypanosoma brucei* cell lines expressing T7 RNA polymerase and the tetracycline repressor. *Open Biol.* 2, 110037. <https://doi.org/10.1098/rsob.110037>
- Priest, J.W., Hajduk, S.L., 1994. Developmental regulation of mitochondrial biogenesis in *Trypanosoma brucei*. *J. Bioenerg. Biomembr.* 26, 179–191. <https://doi.org/10.1007/BF00763067>
- Qiu, Y., Milanes, J.E., Jones, J.A., Noorai, R.E., Shankar, V., Morris, J.C., 2018. Glucose Signaling Is Important for Nutrient Adaptation during Differentiation of Pleomorphic African Trypanosomes 3, 18.
- Rico, E., Jeacock, L., Kovářová, J., Horn, D., 2018. Inducible high-efficiency CRISPR-Cas9-targeted gene editing and precision base editing in African trypanosomes. *Sci. Rep.* 8, 7960. <https://doi.org/10.1038/s41598-018-26303-w>
- Rivière, L., van Weelden, S.W.H., Glass, P., Vegh, P., Coustou, V., Biran, M., van Hellemond, J.J., Bringaud, F., Tielens, A.G.M., Boshart, M., 2004. Acetyl:Succinate CoA-transferase in Procyclic *Trypanosoma brucei*: gene identification and role in carbohydrate metabolism. *J. Biol. Chem.* 279, 45337–45346. <https://doi.org/10.1074/jbc.M407513200>
- Rivière, L., Moreau, P., Allmann, S., Hahn, M., Biran, M., Plazolles, N., Franconi, J.-M., Boshart, M., Bringaud, F., 2009. Acetate produced in the mitochondrion is the essential precursor for lipid biosynthesis in procyclic trypanosomes. *Proc. Natl. Acad. Sci. U. S. A.* 106, 12694–12699. <https://doi.org/10.1073/pnas.0903355106>
- Robertson, D.A., 1985. A Review of Ichthyobodo Necator (Henneguy, 1883) an Important and Damaging Fish Parasite, in: Muir, J.F., Roberts, R.J. (Eds.), *Recent Advances in Aquaculture: Volume 2*. Springer US, Boston, MA, pp. 1–30. [https://doi.org/10.1007/978-1-4684-8736-7\\_1](https://doi.org/10.1007/978-1-4684-8736-7_1)

- Robinson, D.R., Gull, K., 1991. Basal body movements as a mechanism for mitochondrial genome segregation in the trypanosome cell cycle. *Nature* 352, 731–733. <https://doi.org/10.1038/352731a0>
- Robinson, D.R., Sherwin, T., Ploubidou, A., Byard, E.H., Gull, K., 1995. Microtubule polarity and dynamics in the control of organelle positioning, segregation, and cytokinesis in the trypanosome cell cycle. *J. Cell Biol.* 128, 1163–1172. <https://doi.org/10.1083/jcb.128.6.1163>
- Roditi, I., Carrington, M., Turner, M., 1987. Expression of a polypeptide containing a dipeptide repeat is confined to the insect stage of *Trypanosoma brucei*. *Nature* 325, 272–274. <https://doi.org/10.1038/325272a0>
- Rodrigues, T.A., Alencastre, I.S., Francisco, T., Brites, P., Fransen, M., Grou, C.P., Azevedo, J.E., 2014. A PEX7-Centered Perspective on the Peroxisomal Targeting Signal Type 2-Mediated Protein Import Pathway. *Mol. Cell. Biol.* 34, 2917. <https://doi.org/10.1128/MCB.01727-13>
- Rodrigues, J.A., Acosta-Serrano, A., Aebi, M., Ferguson, M.A.J., Routier, F.H., Schiller, I., Soares, S., Spencer, D., Titz, A., Wilson, I.B.H., Izquierdo, L., 2015. Parasite Glycobiology: A Bittersweet Symphony. *PLOS Pathog.* 11, e1005169. <https://doi.org/10.1371/journal.ppat.1005169>
- Rojas, F., Silvester, E., Young, J., Milne, R., Tetley, M., Houston, D.R., Walkinshaw, M.D., Pérez-Pi, I., Auer, M., Denton, H., Smith, T.K., Thompson, J., Matthews, K.R., 2019. Oligopeptide Signaling through TbGPR89 Drives Trypanosome Quorum Sensing. *Cell* 176, 306–317.e16. <https://doi.org/10.1016/j.cell.2018.10.041>
- Roper, J.R., Guthrie, M.L.S., Milne, K.G., Ferguson, M.A.J., 2002. Galactose metabolism is essential for the African sleeping sickness parasite *Trypanosoma brucei*. *Proc. Natl. Acad. Sci.* 99, 5884–5889. <https://doi.org/10.1073/pnas.092669999>
- Roper, J.R., Güther, M.L.S., MacRae, J.I., Prescott, A.R., Hallyburton, I., Acosta-Serrano, A., Ferguson, M.A.J., 2005. The Suppression of Galactose Metabolism in Procyclic Form *Trypanosoma brucei* Causes Cessation of Cell Growth and Alters Procyclin Glycoprotein Structure and Copy Number. *J. Biol. Chem.* 280, 19728–19736. <https://doi.org/10.1074/jbc.M502370200>
- Rose, C., Casas-Sánchez, A., Dyer, N.A., Solórzano, C., Beckett, A.J., Middlehurst, B., Marcello, M., Haines, L.R., Lisack, J., Engstler, M., Lehane, M.J., Prior, I.A., Acosta-Serrano, Á., 2020. *Trypanosoma brucei* colonizes the tsetse gut via an immature peritrophic matrix in the proventriculus. *Nat. Microbiol.* 5, 909–916. <https://doi.org/10.1038/s41564-020-0707-z>
- Rotureau, B., Subota, I., Bastin, P., 2011. Molecular bases of cytoskeleton plasticity during the *Trypanosoma brucei* parasite cycle: Plasticity of *Trypanosoma brucei*. *Cell. Microbiol.* 13, 705–716. <https://doi.org/10.1111/j.1462-5822.2010.01566.x>
- Rucktäschel, R., Girzalsky, W., Erdmann, R., 2011. Protein import machineries of peroxisomes. *Spec. Sect. Protein Translocat. Inser. Membr.* 1808, 892–900. <https://doi.org/10.1016/j.bbamem.2010.07.020>
- Ryan, D.G., Murphy, M.P., Frezza, C., Prag, H.A., Chouchani, E.T., O'Neill, L.A., Mills, E.L., 2019. Coupling Krebs cycle metabolites to signalling in immunity and cancer. *Nat. Metab.* 1, 16–33. <https://doi.org/10.1038/s42255-018-0014-7>
- Ryley, J., 1962. Studies on the metabolism of the protozoa. 9. Comparative metabolism of blood-stream and culture forms of *Trypanosoma rhodesiense*. *Biochem. J.* 85, 211–223. <https://doi.org/10.1042/bj0850211>
- Rzem, R., Vincent, M.-F., Van Schaftingen, E., Veiga-da-Cunha, M., 2007. L-2-Hydroxyglutaric aciduria, a defect of metabolite repair. *J. Inherit. Metab. Dis.* 30, 681. <https://doi.org/10.1007/s10545-007-0487-0>
- Sambrook, J., 1989. Molecular cloning: a laboratory manual. Third edition. Cold Spring Harbor, N.Y.: Cold Spring Harbor Laboratory Press.
- Saveria, T., Halbach, A., Erdmann, R., Volkmer-Engert, R., Landgraf, C., Rottensteiner, H., Parsons, M., 2007. Conservation of PEX19-Binding Motifs Required for Protein Targeting to Mammalian Peroxisomal and Trypanosome Glycosomal Membranes. *Eukaryot. Cell* 6, 1439. <https://doi.org/10.1128/EC.00084-07>
- Schliebs, W., Saidowsky, J., Agianian, B., Dodt, G., Herberg, F.W., Kunau, W.-H., 1999. Recombinant Human Peroxisomal Targeting Signal Receptor PEX5: Structural basis for interaction of PEX5 with PEX14. *J. Biol. Chem.* 274, 5666–5673. <https://doi.org/10.1074/jbc.274.9.5666>
- Schnauffer, A., Clark-Walker, G.D., Steinberg, A.G., Stuart, K., 2005. The F1-ATP synthase complex in bloodstream stage trypanosomes has an unusual and essential function. *EMBO J.* 24, 4029–4040. <https://doi.org/10.1038/sj.emboj.7600862>
- Schueren, F., Lingner, T., George, R., Hofhuis, J., Dickel, C., Gärtner, J., Thoms, S., 2014. Peroxisomal lactate dehydrogenase is generated by translational readthrough in mammals. *eLife* 3, e03640. <https://doi.org/10.7554/eLife.03640>

- Schuldiner, M., Zalckvar, E., 2017. Incredibly close-A newly identified peroxisome-ER contact site in humans. *J. Cell Biol.* 216, 287–289. <https://doi.org/10.1083/jcb.201701072>
- Schulz, D., Zaringhalam, M., Papavasiliou, F.N., Kim, H.-S., 2016. Base J and H3.V Regulate Transcriptional Termination in *Trypanosoma brucei*. *PLOS Genet.* 12, e1005762. <https://doi.org/10.1371/journal.pgen.1005762>
- Shapiro, T.A., Englund, P., 1995. The Structure and Replication of Kinetoplast DNA. *Annu. Rev. Microbiol.* 117–43.
- Siegel, T.N., Hekstra, D.R., Kemp, L.E., Figueiredo, L.M., Lowell, J.E., Fenyo, D., Wang, X., Dewell, S., Cross, G.A.M., 2009. Four histone variants mark the boundaries of polycistronic transcription units in *Trypanosoma brucei*. *Genes Dev.* 23, 1063–1076. <https://doi.org/10.1101/gad.1790409>
- Simpson, A.G.B., Stevens, J.R., Lukeš, J., 2006. The evolution and diversity of kinetoplastid flagellates. *Trends Parasitol.* 22, 168–174. <https://doi.org/10.1016/j.pt.2006.02.006>
- Smith, T.L., Rutter, J., 2007. Regulation of Glucose Partitioning by PAS Kinase and Ugp1 Phosphorylation. *Mol. Cell* 26, 491–499. <https://doi.org/10.1016/j.molcel.2007.03.025>
- Smith, J.J., Aitchison, J.D., 2013. Peroxisomes take shape. *Nat. Rev. Mol. Cell Biol.* 14, 803–817. <https://doi.org/10.1038/nrm3700>
- Smith, T.K., Bringaud, F., Nolan, D.P., Figueiredo, L.M., 2017. Metabolic reprogramming during the *Trypanosoma brucei* life cycle. *F1000Research* 6, F1000 Faculty Rev-683. <https://doi.org/10.12688/f1000research.10342.2>
- Söderberg, O., Gullberg, M., Jarvius, M., Ridderstråle, K., Leuchowius, K.-J., Jarvius, J., Wester, K., Hydbring, P., Bahram, F., Larsson, L.-G., Landegren, U., 2006. Direct observation of individual endogenous protein complexes in situ by proximity ligation. *Nat. Methods* 3, 995–1000. <https://doi.org/10.1038/nmeth947>
- Sokolova, A.Y., Wyllie, S., Patterson, S., Oza, S.L., Read, K.D., Fairlamb, A.H., 2010. Cross-Resistance to Nitro Drugs and Implications for Treatment of Human African Trypanosomiasis. *Antimicrob. Agents Chemother.* 54, 2893–2900. <https://doi.org/10.1128/AAC.00332-10>
- Sousa, M., Parodi, A.J., 1995. The molecular basis for the recognition of misfolded glycoproteins by the UDP-Glc:glycoprotein glucosyltransferase. *EMBO J.* 14, 4196–4203.
- Souza Bombaça, A.C., de Oliveira, L.G.F., Almeida-Amaral, E.E., Menna-Barreto, R.F.S., 2019. The Biological Impact of Oxidative Metabolism in Trypanosomatid Parasites: What Is the Perfect Balance Between Reactive Species Production and Antioxidant Defenses?, in: Chakraborti, S., Chakraborti, T., Chattopadhyay, D., Shaha, C. (Eds.), *Oxidative Stress in Microbial Diseases*. Springer Singapore, Singapore, pp. 127–173. [https://doi.org/10.1007/978-981-13-8763-0\\_8](https://doi.org/10.1007/978-981-13-8763-0_8)
- Spitznagel, D., Ebikeme, C., Biran, M., Nic a' Bháird, N., Bringaud, F., Hennehan, G.T.M., Nolan, D.P., 2009. Alanine aminotransferase of *Trypanosoma brucei*—a key role in proline metabolism in procyclic life forms. *FEBS J.* 276, 7187–7199. <https://doi.org/10.1111/j.1742-4658.2009.07432.x>
- Stephens, N.A., Kieft, R., MacLeod, A., Hajduk, S.L., 2012. Trypanosome resistance to human innate immunity: targeting Achilles' heel. *Trends Parasitol.* 28, 539–545. <https://doi.org/10.1016/j.pt.2012.09.002>
- Steverding, D., 2008. The history of African trypanosomiasis. *Parasit. Vectors* 1, 3. <https://doi.org/10.1186/1756-3305-1-3>
- Stokes, M.J., Güther, M.L.S., Turnock, D.C., Prescott, A.R., Martin, K.L., Alphey, M.S., Ferguson, M.A.J., 2008. The Synthesis of UDP- *N*-acetylglucosamine Is Essential for Bloodstream Form *Trypanosoma brucei* *in Vitro* and *in Vivo* and UDP- *N*-acetylglucosamine Starvation Reveals a Hierarchy in Parasite Protein Glycosylation. *J. Biol. Chem.* 283, 16147–16161. <https://doi.org/10.1074/jbc.M709581200>
- Stuart, K.D., Schnaufer, A., Ernst, N.L., Panigrahi, A.K., 2005. Complex management: RNA editing in trypanosomes. *Trends Biochem. Sci.* 30, 97–105. <https://doi.org/10.1016/j.tibs.2004.12.006>
- Šubrtová, K., Panicucci, B., Zíková, A., 2015. ATPaseTb2, a Unique Membrane-bound FoF1-ATPase Component, Is Essential in Bloodstream and Dyskinetoplastic Trypanosomes. *PLOS Pathog.* 11, e1004660. <https://doi.org/10.1371/journal.ppat.1004660>
- Sugiura, A., Mattie, S., Prudent, J., McBride, H.M., 2017. Newly born peroxisomes are a hybrid of mitochondrial and ER-derived pre-peroxisomes. *Nature* 542, 251–254. <https://doi.org/10.1038/nature21375>
- Surve, S.V., Jensen, B.C., Heestand, M., Mazet, M., Smith, T.K., Bringaud, F., Parsons, M., Schnaufer, A., 2017. NADH dehydrogenase of *Trypanosoma brucei* is important for efficient acetate production in bloodstream forms. *Mol. Biochem. Parasitol.* 211, 57–61. <https://doi.org/10.1016/j.molbiopara.2016.10.001>

- Sykes, S.E., Hajduk, S.L., 2013. Dual Functions of  $\alpha$ -Ketoglutarate Dehydrogenase E2 in the Krebs Cycle and Mitochondrial DNA Inheritance in *Trypanosoma brucei*. *Eukaryot. Cell* 12, 78–90. <https://doi.org/10.1128/EC.00269-12>
- Szöör, B., Silvester, E., Matthews, K.R., 2020. A Leap Into the Unknown – Early Events in African *Trypanosome* Transmission. *Trends Parasitol.* 36, 266–278. <https://doi.org/10.1016/j.pt.2019.12.011>
- Tanifuji, G., Cenci, U., Moog, D., Dean, S., Nakayama, T., David, V., Fiala, I., Curtis, B.A., Sibbald, S.J., Onodera, N.T., Colp, M., Flegontov, P., Johnson-MacKinnon, J., McPhee, M., Inagaki, Y., Hashimoto, T., Kelly, S., Gull, K., Lukeš, J., Archibald, J.M., 2017. Genome sequencing reveals metabolic and cellular interdependence in an amoeba-kinetoplastid symbiosis. *Sci. Rep.* 7, 11688. <https://doi.org/10.1038/s41598-017-11866-x>
- ten Asbroek, A.L.M.A., Ouellette, M., Borst, P., 1990. Targeted insertion of the neomycin phosphotransferase gene into the tubulin gene cluster of *Trypanosoma brucei*. *Nature* 348, 174–175. <https://doi.org/10.1038/348174a0>
- Tetaud, E., Barrett, M.P., Bringaud, F., Baltz, T., 1997. Kinetoplastid glucose transporters. *Biochem. J.* 325, 569–580. <https://doi.org/10.1042/bj3250569>
- Tetley, L., Vickerman, K., 1985. Differentiation in *Trypanosoma brucei*: host-parasite cell junctions and their persistence during acquisition of the variable antigen coat. *J. Cell Sci.* 74, 1.
- Thoms, S., Debelyy, M.O., Nau, K., Meyer, H.E., Erdmann, R., 2008. Lpx1p is a peroxisomal lipase required for normal peroxisome morphology. *FEBS J.* 275, 504–514. <https://doi.org/10.1111/j.1742-4658.2007.06217.x>
- Thoms, S., Hofhuis, J., Thöing, C., Gärtner, J., Niemann, H.H., 2011. The unusual extended C-terminal helix of the peroxisomal  $\alpha/\beta$ -hydrolase Lpx1 is involved in dimer contacts but dispensable for dimerization. *J. Struct. Biol.* 175, 362–371. <https://doi.org/10.1016/j.jsb.2011.06.008>
- Thoms, S., 2015. Import of proteins into peroxisomes: piggybacking to a new home away from home. *Open Biol.* 5, 150148. <https://doi.org/10.1098/rsob.150148>
- Tielens, A.G.M., van Hellemond, J.J., 2009. Surprising variety in energy metabolism within Trypanosomatidae. *Trends Parasitol.* 25, 482–490. <https://doi.org/10.1016/j.pt.2009.07.007>
- Tirados, I., Esterhuizen, J., Kovacic, V., Mangwiro, T.N.C., Vale, G.A., Hastings, I., Solano, P., Lehane, M.J., Torr, S.J., 2015. Tsetse Control and Gambian Sleeping Sickness; Implications for Control Strategy. *PLoS Negl. Trop. Dis.* 9, e0003822. <https://doi.org/10.1371/journal.pntd.0003822>
- Titorenko, V.I., Nicaud, J.-M., Wang, H., Chan, H., Rachubinski, R.A., 2002. Acyl-CoA oxidase is imported as a heteropentameric, cofactor-containing complex into peroxisomes of *Yarrowia lipolytica*. *J. Cell Biol.* 156, 481–494. <https://doi.org/10.1083/jcb.200111075>
- Torreele, E., Bourdin Trunz, B., Tweats, D., Kaiser, M., Brun, R., Mazué, G., Bray, M.A., Pécou, B., 2010. Fexinidazole – A New Oral Nitroimidazole Drug Candidate Entering Clinical Development for the Treatment of Sleeping Sickness. *PLoS Negl. Trop. Dis.* 4, e923. <https://doi.org/10.1371/journal.pntd.0000923>
- Trapani, S., Linss, J., Goldenberg, S., Fischer, H., Craievich, A.F., Oliva, G., 2001. Crystal structure of the dimeric phosphoenolpyruvate carboxykinase (PEPCK) from *Trypanosoma cruzi* at 2 Å resolution. 1 Edited by R. Huber. *J. Mol. Biol.* 313, 1059–1072. <https://doi.org/10.1006/jmbi.2001.5093>
- Trindade, S., Rijo-Ferreira, F., Carvalho, T., Pinto-Neves, D., Guegan, F., Aresta-Branco, F., Bento, F., Young, S.A., Pinto, A., Van Den Abbeele, J., Ribeiro, R.M., Dias, S., Smith, T.K., Figueiredo, L.M., 2016. *Trypanosoma brucei* Parasites Occupy and Functionally Adapt to the Adipose Tissue in Mice. *Cell Host Microbe* 19, 837–848. <https://doi.org/10.1016/j.chom.2016.05.002>
- Turnock, D.C., Ferguson, M.A.J., 2007. Sugar Nucleotide Pools of *Trypanosoma brucei*, *Trypanosoma cruzi*, and *Leishmania major*. *Eukaryot. Cell* 6, 1450–1463. <https://doi.org/10.1128/EC.00175-07>
- Turnock, D.C., Izquierdo, L., Ferguson, M.A.J., 2007. The *de Novo* Synthesis of GDP-fucose Is Essential for Flagellar Adhesion and Cell Growth in *Trypanosoma brucei*. *J. Biol. Chem.* 282, 28853–28863. <https://doi.org/10.1074/jbc.M704742200>
- Turnquist, R.L., Hansen, R.G., 1973. 2 Uridine Diphosphoryl Glucose Pyrophosphorylase, in: Boyer, P.D. (Ed.), *The Enzymes*. Academic Press, pp. 51–71. [https://doi.org/10.1016/S1874-6047\(08\)60062-1](https://doi.org/10.1016/S1874-6047(08)60062-1)
- Turrens, J.F., 1989. The role of succinate in the respiratory chain of *Trypanosoma brucei* procyclic trypomastigotes. *Biochem. J.* 259, 363–368. <https://doi.org/10.1042/bj2590363>
- Uzureau, P., Uzureau, S., Lecordier, L., Fontaine, F., Tebabi, P., Homblé, F., Grélard, A., Zhendre, V., Nolan, D.P., Lins, L., Crowet, J.-M., Pays, A., Felu, C., Poelvoorde, P., Vanhollebeke, B., Moestrup, S.K., Lyngsø, J., Pedersen, J.S., Mottram, J.C., Dufourc, E.J., Pérez-Morga, D.,



- Pays, E., 2013. Mechanism of *Trypanosoma brucei gambiense* resistance to human serum. *Nature* 501, 430–434. <https://doi.org/10.1038/nature12516>
- Van Hellemond, J.J., Opperdoes, F.R., Tielens, A.G.M., 1998. Trypanosomatidae produce acetate via a mitochondrial acetate:succinate CoA transferase. *Proc. Natl. Acad. Sci.* 95, 3036. <https://doi.org/10.1073/pnas.95.6.3036>
- van Weelden, S.W.H., Fast, B., Vogt, A., van der Meer, P., Saas, J., van Hellemond, J.J., Tielens, A.G.M., Boshart, M., 2003. Procyclic *Trypanosoma brucei* Do Not Use Krebs Cycle Activity for Energy Generation. *J. Biol. Chem.* 278, 12854–12863. <https://doi.org/10.1074/jbc.M213190200>
- van Weelden, S.W.H., van Hellemond, J.J., Opperdoes, F.R., Tielens, A.G.M., 2005. New Functions for Parts of the Krebs Cycle in Procyclic *Trypanosoma brucei*, a Cycle Not Operating as a Cycle. *J. Biol. Chem.* 280, 12451–12460. <https://doi.org/10.1074/jbc.M412447200>
- Van Xong, H., Vanhamme, L., Chamekh, M., Chimfwembe, C.E., Van Den Abbeele, J., Pays, A., Van Meirvenne, N., Hamers, R., De Baetselier, P., Pays, E., 1998. A VSG Expression Site–Associated Gene Confers Resistance to Human Serum in *Trypanosoma rhodesiense*. *Cell* 95, 839–846. [https://doi.org/10.1016/S0092-8674\(00\)81706-7](https://doi.org/10.1016/S0092-8674(00)81706-7)
- Vassella, E., Oberle, M., Urwyler, S., Renggli, C.K., Studer, E., Hemphill, A., Fragoso, C., Bütikofer, P., Brun, R., Roditi, I., 2009. Major Surface Glycoproteins of Insect Forms of *Trypanosoma brucei* Are Not Essential for Cyclical Transmission by Tsetse. *PLoS ONE* 4, e4493. <https://doi.org/10.1371/journal.pone.0004493>
- Verner, Z., Čermáková, P., Škodová, I., Kriegová, E., Horváth, A., Lukeš, J., 2011. Complex I (NADH:ubiquinone oxidoreductase) is active in but non-essential for procyclic *Trypanosoma brucei*. *Mol. Biochem. Parasitol.* 175, 196–200. <https://doi.org/10.1016/j.molbiopara.2010.11.003>
- Verner, Z., Škodová, I., Poláková, S., Ďurišová-Benkovičová, V., Horváth, A., Lukeš, J., 2013. Alternative NADH dehydrogenase (NDH2): intermembrane-space-facing counterpart of mitochondrial complex I in the procyclic *Trypanosoma brucei*. *Parasitology* 140, 328–337. <https://doi.org/10.1017/S003118201200162X>
- Vickerman, K., 1965. Polymorphism and Mitochondrial Activity In Sleeping Sickness Trypanosomes. *Nature* 208, 762–766. <https://doi.org/10.1038/208762a0>
- Vickerman, K., 1985. Developmental cycles and biology of pathogenic trypanosomes. *Br. Med. Bull.* 41, 105–114. <https://doi.org/10.1093/oxfordjournals.bmb.a072036>
- Vigneron, A., O'Neill, M.B., Weiss, B.L., Savage, A.F., Campbell, O.C., Kamhawi, S., Valenzuela, J.G., Aksoy, S., 2020. Single-cell RNA sequencing of *Trypanosoma brucei* from tsetse salivary glands unveils metacyclogenesis and identifies potential transmission blocking antigens. *Proc. Natl. Acad. Sci.* 117, 2613–2621. <https://doi.org/10.1073/pnas.1914423117>
- Visser, N., Opperdoes, F.R., 1980. Glycolysis in *Trypanosoma brucei*. *Eur. J. Biochem.* 103, 623–632. <https://doi.org/10.1111/j.1432-1033.1980.tb05988.x>
- Walshe, D.P., Ooi, C.P., Lehane, M.J., Haines, L.R., 2009. Chapter 3 The Enemy Within, in: *Advances in Insect Physiology*. Elsevier, pp. 119–175. [https://doi.org/10.1016/S0065-2806\(09\)37003-4](https://doi.org/10.1016/S0065-2806(09)37003-4)
- Walton, P.A., Hill, P.E., Subramani, S., 1995. Import of stably folded proteins into peroxisomes. *Mol. Biol. Cell* 6, 675–683. <https://doi.org/10.1091/mbc.6.6.675>
- Wan, J., Liu, H., Chu, J., Zhang, H., 2019. Functions and mechanisms of lysine crotonylation. *J. Cell. Mol. Med.* 23, 7163–7169. <https://doi.org/10.1111/jcmm.14650>
- Wang, X., Inaoka, D.K., Shiba, T., Balogun, E.O., Allmann, S., Watanabe, Y., Boshart, M., Kita, K., Harada, S., 2017. Expression, purification, and crystallization of type 1 isocitrate dehydrogenase from *Trypanosoma brucei brucei*. *Protein Expr. Purif.* 138, 56–62. <https://doi.org/10.1016/j.pep.2017.06.011>
- Wargnies, M., Bertiaux, E., Cahoreau, E., Ziebart, N., Crouzols, A., Morand, P., Biran, M., Allmann, S., Hubert, J., Villafranz, O., Millerioux, Y., Plazolles, N., Asencio, C., Rivière, L., Rotureau, B., Boshart, M., Portais, J.-C., Bringaud, F., 2018. Gluconeogenesis is essential for trypanosome development in the tsetse fly vector. *PLOS Pathog.* 14, e1007502. <https://doi.org/10.1371/journal.ppat.1007502>
- Welburn, S.C., Arnold, K., Maudlin, I., Gooday, G.W., 1993. Rickettsia-like organisms and chitinase production in relation to transmission of trypanosomes by tsetse flies. *Parasitology* 107, 141–145. <https://doi.org/10.1017/S003118200006724X>
- Wells, E.A., 1972. The importance of mechanical transmission in the epidemiology of nagana: A review. *Trop. Anim. Health Prod.* 4, 74–89. <https://doi.org/10.1007/BF02359739>
- Wheeler, R.J., Gull, K., Sunter, J.D., 2019. Coordination of the Cell Cycle in Trypanosomes. *Annu. Rev. Microbiol.* 73, 133–154. <https://doi.org/10.1146/annurev-micro-020518-115617>

- Wickstead, B., Ersfeld, K., Gull, K., 2002. Targeting of a tetracycline-inducible expression system to the transcriptionally silent minichromosomes of *Trypanosoma brucei*. *Mol. Biochem. Parasitol.* 125, 211–216. [https://doi.org/10.1016/S0166-6851\(02\)00238-4](https://doi.org/10.1016/S0166-6851(02)00238-4)
- Williams, C., van den Berg, M., Panjikar, S., Stanley, W.A., Distel, B., Wilmanns, M., 2012. Insights into ubiquitin-conjugating enzyme/ co-activator interactions from the structure of the Pex4p:Pex22p complex. *EMBO J.* 31, 391–402. <https://doi.org/10.1038/emboj.2011.411>
- Wirtz, E., Clayton, C., 1995. Inducible gene expression in trypanosomes mediated by a prokaryotic repressor. *Science* 268, 1179–1183. <https://doi.org/10.1126/science.7761835>
- Wirtz, E., Leal, S., Ochatt, C., Cross, George A.M., 1999. A tightly regulated inducible expression system for conditional gene knock-outs and dominant-negative genetics in *Trypanosoma brucei*. *Mol. Biochem. Parasitol.* 99, 89–101. [https://doi.org/10.1016/S0166-6851\(99\)00002-X](https://doi.org/10.1016/S0166-6851(99)00002-X)
- Wolfe, A.J., 2005. The acetate switch. *Microbiol. Mol. Biol. Rev.* MMBR 69, 12–50. <https://doi.org/10.1128/MMBR.69.1.12-50.2005>
- World Health Organization, 2019. WHO interim guidelines for the treatment of gambiense human African trypanosomiasis.
- Wright, J.R., Siegel, T.N., Cross, G.A.M., 2010. Histone H3 trimethylated at lysine 4 is enriched at probable transcription start sites in *Trypanosoma brucei*. *Mol. Biochem. Parasitol.* 172, 141–144. <https://doi.org/10.1016/j.molbiopara.2010.03.013>
- Yang, J., Pieuchot, L., Jedd, G., 2018. Artificial import substrates reveal an omnivorous peroxisomal importomer. *Traffic* 19, 786–797. <https://doi.org/10.1111/tra.12607>
- Yang, T., Bar-Peled, M., 2010. Identification of a novel UDP-sugar pyrophosphorylase with a broad substrate specificity in *Trypanosoma cruzi*. *Biochem. J.* 429, 533–543. <https://doi.org/10.1042/BJ20100238>
- Yang, X., Edward Purdue, P., Lazarow, P.B., 2001. Eci1p uses a PTS1 to enter peroxisomes: either its own or that of a partner, Dci1p. *Eur. J. Cell Biol.* 80, 126–138. <https://doi.org/10.1078/0171-9335-00144>
- Yernaux, C., Fransen, M., Brees, C., Stephan Lorenzen, L., Michels, P.A.M., 2006. *Trypanosoma brucei* glycosomal ABC transporters: identification and membrane targeting. *Mol. Membr. Biol.* 23, 157–172. <https://doi.org/10.1080/09687860500460124>
- Zamze, S.E., Wooten, E.W., Ashford, D.A., Ferguson, M.A.J., Dwek, R.A., Rademacher, T.W., 1990. Characterisation of the asparagine-linked oligosaccharides from *Trypanosoma brucei* type-I variant surface glycoproteins. *Eur. J. Biochem.* 187, 657–663. <https://doi.org/10.1111/j.1432-1033.1990.tb15350.x>
- Zamze, S.E., Ashford, D.A., Wooten, E.W., Rademacher, T.W., Dwek, R.A., 1991. Structural characterization of the asparagine-linked oligosaccharides from *Trypanosoma brucei* type II and type III variant surface glycoproteins. *J. Biol. Chem.* 266, 20244–20261.
- Zhang, N., Jiang, N., Zhang, K., Zheng, L., Zhang, D., Sang, X., Feng, Y., Chen, R., Yang, N., Wang, X., Cheng, Z., Suo, X., Lun, Z., Chen, Q., 2020. Landscapes of Protein Posttranslational Modifications of African *Trypanosoma* Parasites. *iScience* 23, 101074–101074. <https://doi.org/10.1016/j.isci.2020.101074>
- Ziegelbauer, K., Overath, P., 1992. Identification of invariant surface glycoproteins in the bloodstream stage of *Trypanosoma brucei*. *J. Biol. Chem.* 267, 10791–10796.
- Zíková, A., Schnauffer, A., Dalley, R.A., Panigrahi, A.K., Stuart, K.D., 2009. The F<sub>0</sub>F<sub>1</sub>-ATP Synthase Complex Contains Novel Subunits and Is Essential for Procyclic *Trypanosoma brucei*. *PLOS Pathog.* 5, e1000436. <https://doi.org/10.1371/journal.ppat.1000436>
- Zíková, A., Verner, Z., Nenarokova, A., Michels, P.A.M., Lukeš, J., 2017. A paradigm shift: The mitoproteomes of procyclic and bloodstream *Trypanosoma brucei* are comparably complex. *PLOS Pathog.* 13, e1006679. <https://doi.org/10.1371/journal.ppat.1006679>